University of Technology, Sydney

School of Civil and Environmental Engineering

Faculty of Engineering and Information Technology

Investigation of a Proposed Long Span Timber Floor for Non-Residential Applications

By

Zhinus Zabihi

BEng, MEngSc (From BIHE)

Thesis submitted in fulfilment of

requirements for the degree of

Doctor of Philosophy

October 2014

CERTIFICATE OF AUTHORSHIP/ORIGINALITY

I certify that the work in this thesis has not previously been submitted for any degree nor has it been submitted as part of requirements for a degree except as fully acknowledged within the text.

I also certify that the thesis has been written by me and help that I have received in my research work and the preparation of the thesis itself has been acknowledged. In addition, I certify that all information sources and literature used are indicated in the thesis.

Zhinus Zabihi
October 2014

ACKNOWLEDGMENTS

ABSTRACT

Design of floor systems for commercial and multi-residential buildings in many parts of the world is currently dominated by the use of structural materials other than timber, such as reinforced concrete systems. Recent research in Australia has shown that the major barriers to using timber in non-residential buildings are the fire performance and the lack of designer confidence in commercial and industrial timber-based constructions. In this regard, significant research initiatives have commenced in Australia and New Zealand with the aim of developing timber and timber hybrid systems for large span commercial and industrial applications. This PhD research provides a detailed procedure for designing and investigating the short term static behaviour of a proposed long span timber floor system for non-residential applications that meets serviceability and ultimate limit design criteria, with the use of timber as the only structural load bearing part of the system. The specimen's responses to long-term loading, in-plane loading, dynamic excitation, cyclic loading and loading history are outside the scope of this PhD research. Moreover, other aspects of performance such as assessment of acoustic performance, dynamic performance and the possible interconnection systems alongside floor modules are not covered in the scope of this research project.

In this study the behaviour of two types of LVL are investigated through a number of experimental and analytical tests. As a result of the tension and compression tests, a suitable constitutive law is developed which can accurately capture the stress-strain relationship and the failure behaviour of LVL, and it can also be incorporated into FE analysis of any LVL beam with similar structural features to the tested specimens. Further, the results of the full scale four point bending tests on LVL sections are used to identify the behaviour of LVL up to the failure point and to develop a finite element model to capture the behaviour and failure of LVL.

Moreover, after investigating the long span timber floors, one system is proposed to be fabricated for the extensive experimental and numerical investigation. The experimental investigation involved subjecting the full scale proposed floor modules (6m and 8m

clear span LVL modules) to both serviceability and ultimate limit state static loading to assess the strength and serviceability performance of the proposed system. A continuum-based finite element model is also developed to capture the behaviour and failure of the long span LVL modules and to adequately predict the serviceability and ultimate limit performance of the proposed floor system.

To evaluate the partially-composite strength and serviceable performance of LVL floor system, a series of push-out tests are conducted on the fabricated timber connections using normal screws as the shear connectors, and the stiffness of the connections are assessed at serviceability and ultimate limit state. A number of LVL beams (3.5m "T" shaped beams) were also fabricated using only normal screws as the load bearing shear connectors at the interfaces, and are tested under serviceability and ultimate limit state loads with different screw spacing. Furthermore, a closed-form prediction analysis is conducted to calculate the partially-composite ultimate load of the beams. A comparison between the experimental results and the closed-from predicted results is undertaken, and the results are used for predicting the partially-composite behaviour of long span 6m and 8m LVL modules.

The results of the full scale experimental tests together with the numerical investigation provide a robust model for predicting the performance of any timber beams with similar structural features to the proposed system while the dimensions and spans can be varied according to special requirements such as dynamic performance or fire resistance requirements.

TABLE OF CONTENTS

LIST OF FIGURES

LIST OF TABLES

LIST OF PUBLICATIONS BASED ON THIS THESIS

Zabihi, Z., Samali, B., and Crews, K. (2010), "Modern trends in long span timber flooring systems", *Proceedings, 21st Australasian Conference on the Mechanics of Structures and Materials, ACMSM 21,* Melbourne, Australia, 7-10 December.

Zabihi, Z., Samali, B., Shrestha, R., Gerber, C. and Crews, K. (2012), "Serviceability and Ultimate Performance of Long Span Timber Floor Modules", *Proceedings, Twelfth World Conference on Timber Engineering, WCTE 2012,* Auckland, New Zealand, 16-19 July.

Zabihi, Z., Samali, B., Shrestha, R., and Crews, K. (2012), "Ultimate Performance of Timber Connection with Normal Screws", *Proceedings, 22nd Australasian Conference on the Mechanics of Structures and Materials, ACMSM 22,* Sydney, Australia, 11-14 December.

LIST OF NOTATIONS

α	modification factor in Glos model
α_{tf}	distance between point of zero bending moment to centroid of top flange
α_{bf}	distance between point of zero bending moment to centroid of bottom flange
α_{tf}	distance between point of zero bending moment to centroid of web
γ_{tf}	partial factor for material properties of the top flange
γ_{bf}	partial factor for material properties of the bottom flange
γ_{web}	partial factor for material properties of the web
δ_{max}	maximum mid span deflection
δ_{Mid}	measurements of LVDTs under mid-span
δ_{Trd}	measurements of LVDTs under third-span
ε_t	tensile strain
ε_c	compressive strain
ε_0	strain coefficient
ϕ	Capacity factor for imposed load as per AS1720.1 (2010)
ϕN	axial design capacity of the timber cross-section
ϕM	bending design capacity of the timber cross-section
ϕN_p	bearing design capacity of the timber cross-section
$\phi\sigma_{tf,axial}$	top flange axial stress design capacity
$\phi\sigma_{bf,axial}$	bottom flange axial stress design capacity
$\phi\sigma_{tf,bending}$	top flange bending stress design capacity
$\phi\sigma_{bf,bending}$	bottom flange bending stress design capacity
ρ	density
$\sigma^*_{tf,axial}$	axial stress in top flange due to design action
$\sigma^*_{bf,axial}$	axial stress in bottom flange due to design action

$\sigma^*_{tf,bending}$	bending stress in top flange due to design action
$\sigma^*_{bf,bending}$	bending stress in bottom flange due to design action
$\sigma_{f,t,\max}$	tensile design stress of the extreme fiber of flange
$\sigma_{f,t}$	mean tensile design stress of the flange
υ	Poisson's ratio
v	relative slip of timer connections
Ψ	coefficient for long term load combination
$\Delta F/\Delta e$	linear elastic slope of the load-displacement graph
Δ_{vib}	mid span deflection of the floor beams as a result of impact loading
Δ_b	mid span flexural deflection of the floor beams
1-D	one-dimensional
2-D	two-dimensional
3-D	three-dimensional
A_{tf}	top flange area
A_{bf}	bottom flange area
A_w	web area
b	width (breadth) of the timber cross section
b_{tf}	top flange width
b_{bf}	bottom flange width
b_w	web width
CoV	coefficient of variation
d	total depth of the timber cross section
d_{tf}	top flange depth
d_{tf}	bottom flange depth
d_w	web depth
E_{tf}	top flange modulus of elasticity
E_{bf}	bottom flange modulus of elasticity
E_w	web modulus of elasticity
E	modulus of elasticity
E_t	modulus of elasticity in tension
E_c	modulus of elasticity in compression

EI	flexural stiffness
$(EI)_{eff, LT}$	long term effective flexural stiffness
$(EI)_{eff}$	effective flexural stiffness
$(EI)_{Mid}$	flexural stiffness at mid-span
$(EI)_{Trd}$	Flexural stiffness at third-span
F, P	point load
F_{est}	peak load
F_{max}	Ultimate/failure load
F_{ave}	average reading of load cells 1 and 2
F_{bf}	shear load on a single screw in bottom flange
F_{tf}	shear load on a single screw in bottom flange
f'_b	characteristic strength in bending (bending design capacity)
f'_c	characteristic strength in compression (compression design capacity)
f'_s	characteristic strength in shear (shear design capacity)
$f'_{s,glue}$	shear strength (shear design capacity) of glue
f'_t	characteristic strength in tension (tensile design capacity)
$f'_{b,tf}$	top flange bending strength (design capacity)
$f'_{b,bf}$	bottom flange bending strength (design capacity)
$f'_{b,w}$	web bending strength (design capacity)
$f'_{t,tf}$	top flange tension strength (parallel to grain) (design capacity)
$f'_{t, bf}$	bottom flange tension strength (design capacity) parallel to grain
$f'_{t,w}$	web tension strength (design capacity) parallel to grain
$f'_{c,tf}$	top flange compression strength(design capacity) parallel to grain
$f'_{c,bf}$	bottom flange compression strength (design capacity) parallel to grain
$f'_{c,w}$	web compression strength (design capacity) parallel to grain
$f'_{s,tf}$	top flange shear strength(design capacity)
$f'_{s,bf}$	bottom flange shear strength (design capacity)
$f'_{s,w}$	web shear strength (design capacity)
f_1	fundamental frequency (first natural frequency of the structure)
f^*_s	shear stress due to loading (design action)
f'_p	bearing strength of the bottom flange
f_b	mean bending strength
f_c	mean compression strength

f_t	mean tension strength
$f_{c,y}$	yielding compression strength
f_t	mean tensile strength
f_v	mean shear strength
G	self-weight & permanent loading
g	acceleration due to gravity (9.81 m/s^2)
G_s	shear modulus; Modulus of rigidity
h_{tf}	distance between the neutral axis of the cross section and the centroid of htop flange
h_w	distance between the neutral axis of the cross section and the centroid of webs
h_{bf}	distance between the neutral axis of the cross section and the centroid of botom flanges flange
I	moment of inertia
I_{eff}	effective moment of area
j_2	creep factor (stiffness modification factor)
K	stiffness
K_{Mid}	stiffness at third-span of the beam
K_{Trd}	stiffness at mid-span of the beam
K_i	initial stiffness of the connection
$K_{s,0.4}$	serviceability stiffness
$K_{s,0.6}$	ultimate stiffness
$K_{s,08}$	near collapse
K_p	the strain-hardening stiffness in Richard-Abbott model
K_0	initial stiffness in Richard-Abbott model
k_1	duration of load (timber)
k_{12}	stability factor (timber)
k_4	moisture condition factor (timber)
k_6	temperature factor (timber)
k_7	length and position of bearing factor (timber)
k_9	strength sharing between parallel members factor (timber)
$K_{(11)}$	coefficient factor in Glos model

$K_{(22)}$	coefficient factor in Glos model
$K_{(33)}$	coefficient factor in Glos model
$K_{(44)}$	coefficient factor in Glos model
$(K_{(11)})_{mod}$	modified coefficient factor in Glos model
L	span of the floor modules or length of the timber beams
LL	live Load
$LVDT$	Linear Variable Differential Transformers
m	mass of the floor ; mass per unit area (kg/m^2)
M^*	maximum bending moment due to design action
MC	moisture content
M_0	oven dried mass
M_i	initial mass
$N.A.$	neutral axis
N	power in Glos model (chapter 4)
N^*	maximum axial force due to design action
N^*_p	bearing load due to design action
n	a parameter associated with the sharpness of the curve in Richard-Abbott
n_w	modular ratios for web of the LVL modules (Chapter 3)
n_{bf}	modular ratios for bottom flange of the LVL models (Chapter 3)
P_0	reference shear force in in Richard-Abbott model
Q_{tf}	first moment of area of top flange about the neutral axis
Q_{bf}	first moment of area of bottom flange about the neutral axis
Q_{max}	maximum first moment of area
Q	imposed loading
R^2	coefficient of determination
S	joist spacing
SDL	superimposed permanent load
S_s	screw spacing
S_{tf}	screw spacing in top flange interface
S_{bf}	screw spacing in bottom flange interface
V^*	maximum acting shear force (shear force due to design action)

$\bar{y}_c$, y_c	neutral axis of the LVL floor module
$\bar{y}_{tf}$	location of centroid of top flange from the base of the cross section
$\bar{y}_w$	location of centroid of web from the base of the cross section
y_{bf}, $\bar{y}_{bf}$	location of centroid of bottom flange from the base of the cross section
$y_{bf/2}$	the distance between the half of the depth of bottom flange and the centroid of the section

University of Technology, Sydney

CHAPTER 1
INTRODUCTION

1   INTRODUCTION

1.1   Background

The application of timber for floor systems was very common in the last century, but with the advent of other types of floor systems utilizing stronger materials with higher performance, timber floor systems have been mainly restricted to domestic applications. This is due in part to the fact that traditional timber floor systems are often susceptible to excessive vibrations, poor fire rating and unacceptable acoustic performance. Consequently, design of floor systems for commercial and multi-residential buildings in many parts of the world is currently dominated by the use of reinforced and / or prestressed concrete construction, and usually supported by steel or concrete beams and frames.

However, the advent of engineered wood products (EWP's) such as laminated veneer lumber (LVL), cross laminated timber (CLT), plywood and glulam with similar structural properties to that of steel or concrete in the same applications, has provided the means to fabricate large section and long spanning structural members. Also, recent developments in timber construction methods such as prestressed timber structures, and the advent of the new generation of adhesives and materials make it possible to produce large sections and long spanning timber structural members which are also able to satisfy strict serviceability design criteria and are suitable for multi-storey/ commercial timber buildings.

The inherent characteristics unique to wood make this natural material in many cases superior to other construction materials. From an environmental perspective, timber extracts the "main contributor to the greenhouse effect", the carbon dioxide, from the atmosphere. The processing of raw structural materials such as concrete, clay bricks and steel requires huge amounts of energy with enormous CO_2 emission into the atmosphere. However, timber extracts carbon dioxide from the atmosphere through the process of photosynthesis, using just solar energy, natural soil and rain (Boughton and Crews 1998). At the end of its life cycle, timber building components can be recycled

for their materials, and once it is no longer feasible to recover the materials, they can be burnt to produce energy, and the carbon dioxide released during burning will be offset by managed forest re-planting (Kolb 2008). Every cubic meter of timber used in buildings instead of concrete, reduces the CO_2 emission in the atmosphere by an average of 1.1 tonne of CO_2 and if this is added to 0.9 tonne CO_2 which is stored in the wood, the total saving from using one cubic metre of timber is 2 tonnes of CO_2 (KAUFMANN 2010). Therefore, beside the engineering perspective, the use of timber can greatly reduce environmental impacts since timber is the only structural material that is truly renewable with significantly lower CO_2 emissions to the environment compared to other materials such as brick and concrete.

Moreover, consuming only as much resources as nature can reproduce, or "sustainable development", is the inevitable way of future productions. By applying the simple principle of sustainability to the forests which is "more trees are replanted than are harvested", and through proper management practices of supervised logging and forest replanting, timber is the only building material which complies with the principle of sustainability (Kolb 2008). These features of timber make it a viable alternative to other construction materials such as steel and concrete.

Despite the many benefits of using timber, several studies undertaken in Canada, the USA, Australia and New Zealand have highlighted the lack of timber used in non-residential buildings. For example, McKeever and Adair (1995) found that 51% by value of all non-residential projects in America could have been built with timber. Recent research in Australia has shown that there are two major barriers to using timber in non-residential buildings in Australia, one being the fire performance and the other, the lack of overall designer confidence in commercial and industrial timber-based constructions (Bayne & Taylor 2006). In this regards, significant research initiatives have commenced since 2007 in Australia and New Zealand with the aim of developing timber and timber hybrid systems for large span commercial and industrial applications and since January 2009, these researched initiatives have been consolidated into a collaborative program being undertaken through the Structural Timber Innovation Company (STIC).

1.2   Structural Timber Innovation Company (STIC)

STIC is a research consortium whose purpose is to develop the construction of large numbers of innovative and sustainable commercial and industrial multi-storey timber buildings in Australia and New Zealand and other export markets, with positive impact on environment.

STIC was registered in New Zealand and its seven shareholders are Carter Holt Harvey Ltd, Nelson Pine Industries Ltd, Wesbeam Pty Ltd, Building Research Association New Zealand Inc., NZ Pine Manufacturers Association, University of Auckland and University of Canterbury. In addition, it has two major financial stakeholders, Forest and Wood Products Australia (FWPA), and Foundation for Research Science and Technology (FRST).

SITC research programme is being carried out in three Universities with three parallel objectives, that is, single storey timber roofs, portal frames and connection systems (at University of Auckland), timber floors for multi-storey timber buildings (at University of Technology Sydney) and timber frames for multi-storey timber buildings (at University of Canterbury).   Moreover, design guidelines, analysis packages, recommendations and supporting data sets have been developed for architects, engineers, fabricators and constructors which provide the information they need to design and construct long span multi-storey timber buildings with confidence and minimal inconvenience. Figure 1.1 shows a summary of the detailed objective of STIC research program. The focus of this research topic however, is to develop and investigate the performance of a long span "timber only" floor system (the highlighted topic in Figure 1.1) and will be discussed in the following sections.

1.3   Scope of Research Topic

As shown in Figure 1.1, extensive research projects have been conducted at University of Technology Sydney to thoroughly assess the performance of long span timber and timber hybrid floor systems.
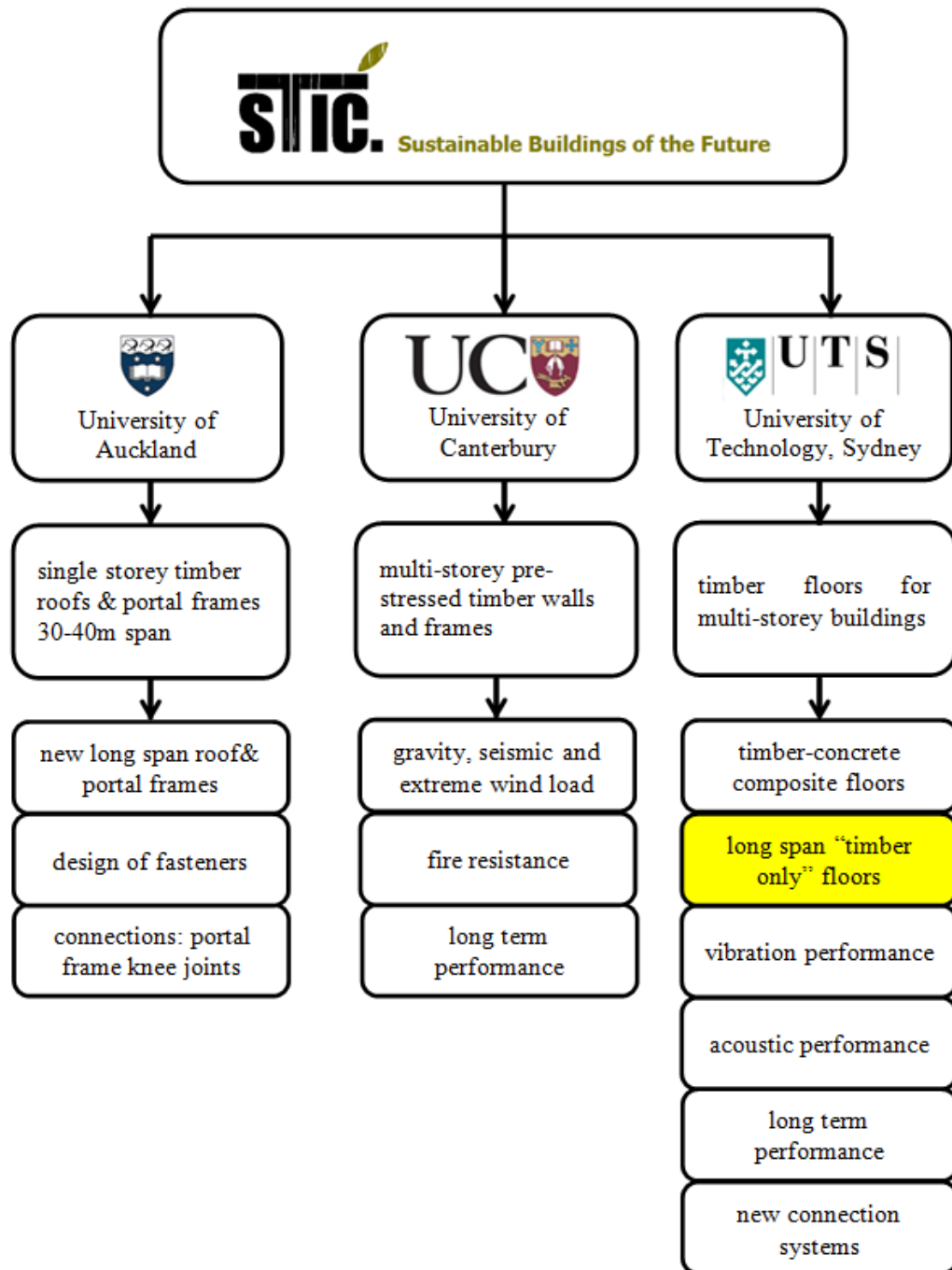
Figure 1.1 Summary of STIC's objectives

Although timber has a significant strength to weight ratio, many timber floor systems are susceptible to excessive vibration and show poor acoustic performance due to their light-weight and insufficient stiffness. To address these problems a layer of concrete can be used in timber floor systems (timber-concrete composite or TCC) to improve their performance since the combination of timber and concrete produces improved strength

and stiffness, more thermal mass and better acoustic separation, and the system is also less susceptible to vibration (Crews et al. 2007). However, the use of concrete, as a load bearing part of the system, makes the fabrication and performance of the system more complex as the shear connectors need to be accurately designed and modelled, the level of composite behaviour of the system must be clearly assessed, and they are not as easy and fast to be prefabricated and erected as the "timber only" systems.

The focus of this research topic is to propose a long span timber floor system with the use of timber as the only structural load bearing material of the system (beside the shear connector at the interfaces such as screws and glue), while addressing and satisfying the serviceability and ultimate design criteria for long span multi-storey/commercial timber buildings. As shown in Figure 1.1, the scope of this research project is to investigate the short term behaviour of the proposed floor system under static loading. Other aspects of performance such as long term behaviour, fire performance, dynamic performance and acoustic performance of the floor system are undertaken by other members of the UTS team and they are not covered in this research topic (Rijal 2013; Khorsandnia 2013). Also, the possible interconnection systems alongside floor modules are not investigated in this project. The specimen's responses to long-term loading, in-plane loading, dynamic excitation, cyclic loading and loading history are outside the scope of this PhD research. The scope of this topic is limited to investigate the short term static behavior, but will address broader issues where relevant, by drawing from other research which is undertaken by other members of the UTS team (e.g. long term behavior and dynamic performance of the system).

Laminated veneer lumber (LVL) was used as the only structural material of the proposed system and the main reason for utilizing LVL in this study is the ready availability of LVL in Australia and New-Zealand and its inherent reliability as a structural material, whereas alternative structural products such as glue laminated timber or cross laminated timber (CLT) are not as readily available in Australia and New-Zealand. As shown in Figure 1.2, the experimental investigation includes assessing the properties of LVL, investigating the performance of the proposed long span modules under service and ultimate limit state loads, and investigating the partially -composite behaviour of LVL beams. All experimental results in all phases of

investigation are compared with analytically predicted results. Also, experimental results of the tested long span LVL modules (under four point bending loads) are compared with the numerical results of the developed finite element model, and the FE model is calibrated against the experimental results. The details of experimental and numerical investigation in each phase are further explained in section 1.5.

1.4   Research Objectives

The main objective of this research project is to propose a long span (6-10m) timber floor system for commercial, industrial and multi-storey residential applications, which meets both strength and serviceability design criteria. Short term behaviour of such system is studied through extensive full scale serviceability and ultimate limit state tests and a comprehensive numerical analysis. The broad objectives of the research can be sub-divided into a number of goals as below:

- Experimental and analytical investigation of LVL sections under tension, shear bending and compression loads (investigation of the material properties of LVL) and development of a suitable constitutive law for LVL which can be used for modelling the behaviour of any composite LVL beams.
- Proposal of a technique for FE modelling of LVL beams based on the preliminary experimental results of four-point bending tests of LVL section, using the proposed constitutive law.
- Proposal of long span (6m and 8m) LVL floor modules to be fabricated and tested under four-point bending loads, and extensive experimental investigation on the performance of the LVL floor modules through serviceability and ultimate limit tests.
- Interpretation of structural behaviour of the LVL modules through experimental data analysis and experimental observations. Some of the features which will be specifically focused on are as follows:
  - Clearly identifying the failure modes of the system (whether that will be in the flanges or in the web through web buckling, or in the connections and interfaces).

- To evaluate the stiffness of the system by assessing the deflection of the system versus load and to interpret the serviceable and ultimate behaviour of the system.
- To assess the linear characteristics of the system up to the failure point
- To assess the strain distribution over the depth of the section and to identify the composite behaviour of the section (composite action between the webs and flanges).

- Development of a technique for FE modelling of the behaviour and failure of the LVL floor modules (6m and 8m single unites) and verification and calibration against the tests results, and development of the FE modelling of the full floor system by considering an assembly of the individual modules side by side and in a composite manner.

- Experimental and numerical investigation on the fabricated timber connections (using just normal screws as the shear connectors) which are tested under push – out loads at serviceability and ultimate state in order to assess the partially-composite behaviour of LVL modules.

- Investigation of partially-composite behaviour of LVL modules by conducting the experimental and numerical investigation on fabricated LVL beams (using only screws as the shear connectors), and by assessing their performance under four point bending loads at serviceability and ultimate limit state.

- Development of a model to predict the serviceability and ultimate limit performance of any LVL beams with similar structural features to the proposed LVL modules, irrespective of different cross sectional dimensions and spans.

- Favourable comparison between all the experimental and numerical results and development of practical design guidelines and recommendations.

1.5   Research Methodology

To achieve the objectives of the research, the following research methodology was adopted:

a) **Literature review:** The "timber only" options with the ability to meet the design criteria for large span timber floor systems (6-10m) were reviewed and a comparison of structural timber materials and systems (I beams, box beams,

CLT timber panels, Stressed Skin Panels, etc.) was presented. Moreover, the current claims for structural floor spans (available Load Span Tables) were reviewed. The structural performance of composite timber floor systems was investigated. The numerical investigations of timber floors were reviewed .After an investigation on the options of long span timber floors, one system was proposed to be tested for the experimental and numerical investigation.

b) **Experimental investigation:** Figure 1.2 shows the extensive research plan for experimental study which includes four phases.

For the first phase, the properties of LVL were assessed through a series of tests conducted on LVL sections, including tension and compression tests, shear tests and bending tests. As the second phase of experimental study, the performance of the proposed 6m and 8m modules were investigated under service and ultimate limit state loads. The 6m and 8m modules were subjected to "four point bending" loading to quantify the serviceability behaviour of the system such as deflection, stiffness and strength of the modules, and to evaluate strain distribution over the depth of the section to identify the composite action between the webs and the flanges. The loading was increased up to ultimate limit stage to assess the ultimate limit state behaviour of the system and to identify the failure modes of the section and the structural properties of the system at that stage.

The third and fourth phase of the experimental study dealt with assessing the partially-composite behavior of LVL modules through a series of push out tests conducted on timber connections, and a series of four point bending tests conducted on LVL beams (which are fabricated using only normal screws at the interfaces). The major items needed for the experimental tests were as follows:
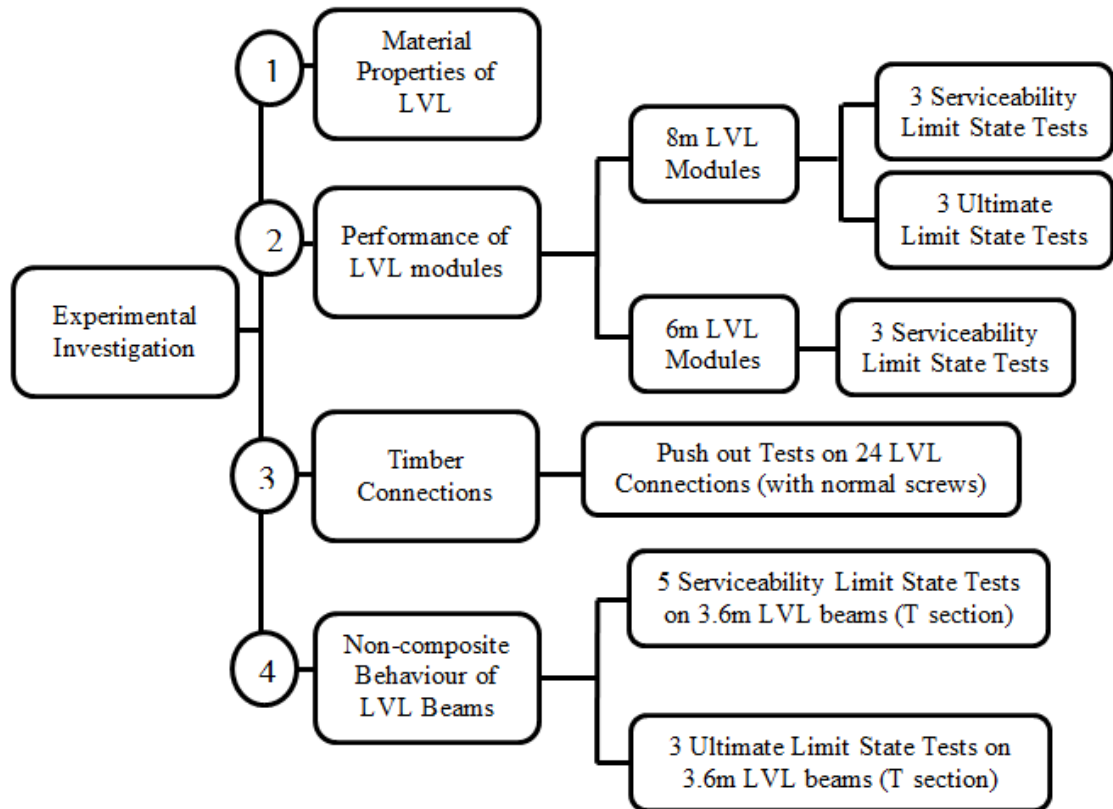
Figure 1.2 Research plan for experimental study

- **Materials for fabrication**: The 6m and 8m LVL modules were fabricated with laminated veneer lumber (LVL) with different stress grades. The interlayer connections were made with screw-gluing technique using PURBOND® as the adhesive. The adhesives could be spread manually with as much consistency as possible, and then the flanges were located on the webs. Type 17 normal screws were also used to ensure the full attachment of flanges and webs.

- **Strain Gauges:** Strain gauges were used for assessing the composite action between the webs and the flanges and will be located on joists as well as interior and exterior faces of the flanges (extreme fibers) to measure critical strains. Type PL-60-11 strain gauges with the gauge length of 60mm are used in this study.

- **Linear Variable Differential Transducer (LVTD):** a number of LVDTs were used to measure the deflection at mid span and around one-third span (from each end) of the beams, they were also used to measure any possible slip between the flanges and the webs, and they can be within the range of 50-300 mm.

- **Loading System:** The reaction frame consisted of two main load frames and a connecting beam used for applying loads. The loads were applied through the hydraulic jackets and the load cells. The type of the hydraulic jackets and the load cells depended on the value of ultimate loads needed for the experimental tests.

- **Data processing centre:** the data processing centre consisted of the terminal blocks, the data acquisition and a computer. All the instrumentation was connected to the terminal blocks through cables, which in turn were connected to the data acquisition system. The experimental data were transferred from the data acquisition system to a computer where they were recorded and saved.

c) **Data Analysis and Numerical study:** All the experimental results were analysed and interpreted, and a numerical study needed to be developed in order to predict/simulate the behaviour of the system at the serviceable and ultimate limit states, and to assess the influence of different materials and geometric properties. ANSYS (which is a finite Element software package) was used in this study which has rigorous structural features and able to model the structural systems in details.

d) **Design recommendation:** a set of recommendations were developed to ensure a safe design procedure for serviceability and ultimate limit state design.

1.6   Research Significance

The enhanced reliability and load-bearing capacity of engineered wood products (EWPs) together with using new construction methods for timber structures make them attractive to engineers, and provide a lot of new opportunities for the use of timber in multi-storey residential, industrial and commercial buildings. However, in Australia, the insufficient design guidelines and the lack of overall confidence in designing commercial and industrial timber-based constructions is a major barrier to using timber in non-residential applications.

This PhD research contributes towards a better understanding of the performance of a proposed long span timber floor system for non-residential applications, and develops a detailed procedure for designing and investigating the behaviour of the proposed long span timber floor system, through extensive experimental tests and numerical analysis. An analytical model is also developed to predict the behaviour and failure of the proposed system which offers a robust technique to model any floor system with similar structural features to that of the proposed system, irrespective of different cross sectional dimensions and spans, whilst minimising the need for additional costly experiments.

1.7   Layout of the Thesis

This thesis is organised into eight chapters as follows:

Chapter 1: An introduction and background to the research topic, objectives of the study and the research methodology, significance of the work and contribution to knowledge are described in this chapter.

Chapter 2: This chapter provides a review of literature on long span timber floor systems, their design requirements and criteria, and the structural timber materials and their properties. It also looks at the experimental and numerical research studies and analytical models conducted on timber floors

Chapter 3: This chapter presents the proposed floor system to be fabricated for the experimental and numerical investigation. Its material properties, geometry and fabrication process are also specified. The serviceability and ultimate design criteria including the maximum deflection limits, the bending stress, axial stress, the flexural shear stress and the shear capacity of the interfaces are evaluated. Also, the static and dynamic responses of the system are analytically predicted at serviceability and ultimate limit state and they are reported in this chapter.

Chapter 4: In this chapter, the behaviour of LVL is assessed through a series of tests conducted on LVL sections, and its behaviour and properties are investigated under tension, compression, shear and bending loads. Moreover, a suitable constitutive law is developed in this chapter which can accurately capture the stress-strain relationship and the failure behaviour of LVL, and it can also be incorporated into FE analysis of any LVL beam.

Chapter 5: This chapter provides the detailed experimental test procedure and experimental results of the destructive and non-destructive tests conducted on 6m and 8m LVL timber modules. Furthermore, a closed-form prediction analysis is conducted to calculate the ultimate load of the system and a comparison between the experimental results and the closed-from predicted results are reported in this chapter.

Chapter 6: This chapter presents the results of a series of push-out tests which were conducted on the fabricated timber connections, and a series of destructive and non-destructive four point bending tests conducted on LVL beams (which are fabricated using only normal screws at the interfaces). Furthermore, a closed-form prediction analysis of the response of the system, and a comparison between the experimental results and the closed-from predicted results is reported in this chapter.

Chapter 7: This chapter provides a technique for finite element modelling of timber beams, and the results of the FE model are verified against the experimental results. An analytical model of predicting the performance of any timber beams with similar structural features to the proposed long span LVL modules is also presented in this chapter.

Chapter 8: A summary of the main contributions and conclusions of this research, and the recommendations for future research are highlighted in this chapter.

References to literature referred in this study and appendices are presented at the end of this dissertation.

University of Technology, Sydney

CHAPTER 2

LITERATURE REVIEW

2 LITERATURE REVIEW

2.1 Introduction

In this chapter the structural timber materials and systems for long span timber floors are reviewed and their advantages and disadvantages are investigated. The research studies conducted on composite and partially-composite floor systems are studied and their structural performance and design criteria are investigated and reported in this chapter. Whilst the scope of this dissertation is primarily limited to strength and deflection behaviour, it is important to recognise that other considerations such as dynamic, acoustic and fire behaviour will often influence the final design solution for a long spanning timber floor. As such, some discussion of these broader issues is presented in this chapter.

2.2 Materials in Timber Structures

Since sawn timber sections are limited in size and quality, Engineered Wood Products (EWPs), with similar structural properties to that of steel or concrete, have been developed to overcome the limitations of sawn timber. They are often stronger than equivalent solid timbers and they can be manufactured to satisfy specific performance requirements and to meet special applications. They are not limited in size and quality, and large sections or panels in long lengths can be manufactured from small logs with defects being removed or dispersed. Some of the important wood products which have been used in timber structures are summarised below.

Glued-laminated Timber (or Glulam) can be fabricated from several layers of dried planks of wood (called laminates) which are bonded together with adhesives with all grains directed along the longitudinal axis (Figure 2.1a). The first patents for glued laminated timber were issued in Switzerland and Germany in the late 1890s (Nagaraj 2005). The fascinating feature of glulam is its flexibility to be formed into almost any shape while maintaining its high load-bearing capacity. Cross-Laminated Timber or CLT has evolved first in Switzerland in the 1970s as one of the most exciting and innovative engineered wood panels available (Wood Naturally Better 2010). Cross-

laminated timber (CLT) is a panel-shaped engineered wood product assembled of layers of lamellas (mostly softwood) with grain direction perpendicular to each other (Steiger et al. 2008). Stacking the layers crosswise (alternating layers, as illustrated in the Figure 2.1b) increases the structural and dimensional stability of the product. FPInnovations (2012) presents a comprehensive manual about properties and design of CLT panels.

(a)

(b)

(c)

(d)
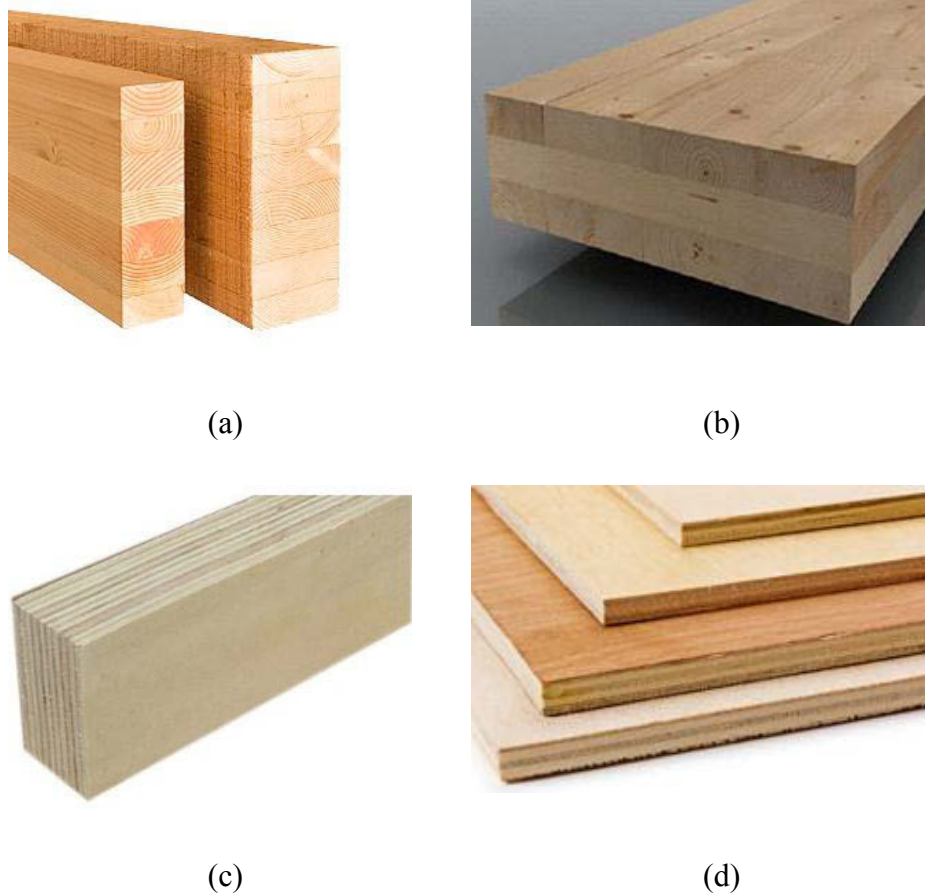
Figure 2.1 Engineered wood products (a) Glulam (BoiseCascade 2013), (b) CLT (APA 2013), (c) LVL (CarterHoltHarvey 2013) and (d) Plywood (Harper Timber 2013)

Laminated Veneer Lumbers or LVL was first produced around 40 years ago in which thin veneer layers with thickness of 3-4mm are peeled off the logs and are bonded together with adhesives to make the LVL (Figure 2.1c). The entire veneer layers are generally oriented in one direction, which gives LVL similar orthotropic properties to those in sawn timber. The structural LVL in Australia and New Zealand is manufactured using pine species (Radiata and Maritime) and should comply with Australian and New Zealand Standard for Structural Laminated Veneer Lumber (AS/NZS 4357.1:2005) in which the minimum requirement for determination of

mechanical properties and its verification is set out. LVL manufactured to AS/NZS 4367 has a type A phenolic bond which is made out of phenol or resorcinol formaldehyde and they can provide durable and permanent performance in open conditions (weather exposure) as well as long term stress. (Mcdowall 2007).

Moreover, plywood is commonly used in Australia and New Zealand (Figure 2.1d). The structural plywood in Australia and New Zealand is manufactured from either hardwood or softwood timber veneers or combination of both and they are mainly from pine plantation (Radiata, hoop or Slash). Their properties should comply with structural plywood standard (AS/NZS 2269:1994). The stress grades for structural plywood are listed in AS 1720.1 (2010), and the thicknesses and their identification codes are also mentioned in AS/NZS 2269. Other EWPs with more popularity in smaller scale applications (mostly in residential sector) are also common for structural use. For example, chipped wood in different sizes can be bonded together by exterior type adhesives (comprising 95% wood and 5% resin and wax) to produce fibreboards, chipboards or oriented strand boards (OSB). OSB for example, which belongs to the group of the particle boards with modest load carrying capacity, is composed of long and thin chips, orthogonally directed during the composition of the panel. Engineering Strand Lumber (ESL), parallel strand lumber (PSL) known as Parallam® _ or laminated strand lumber (LSL) known as TimberStrand® are made out of different form of sliced wood. There are other products also available from different manufactures however they are not generally being used in the non-residential building sector.

2.3 Performance Requirements of Timber Floors

In considering the development of long span floor systems, there are a number of performance requirements that must be satisfied (Crews et al. 2007):

- Resistance to gravity load (strength limit state for out-of-plane loading)
- Resistance to lateral load, particularly in earthquake areas (strength limit state for in-plane loading)
- Control of vibration and deflection due to gravity load (serviceability limit state)
- Control of deflection due to lateral load (serviceability limit state)
- Fire resistance

- Acoustic separation

- Thermal insulation

Stiffness of the floors is the main contributor to the short term deflection, long term deflection (creep) and vibration of the system. Generally, these serviceability criteria (deflection and vibration) govern the design of floors more than strength. Concerning structural safety, timber floors have never shown any problems throughout history and the load bearing performance of timber floors has always been satisfactory (Jorissen 2006). The structural performance and load bearing behaviour of timber floors are further discussed in section 2.5. In this section some general information about vibration, fire resistance and acoustic performance of floor systems is presented.

Kolb (2008) recommended that a natural fundamental frequency of over 8 Hz should be aimed for a timber floors system in order to satisfy the comfort design criteria. Extensive research programs have been conducted to evaluate the vibration of timber floors. Hamm et al. (2010) provide new results on timber floor vibrations and how to construct a timber floor in the two categories, namely, low demand and high demand. The results of the research project provide a flowchart for design and construction of timber floors, and how to construct a timber floor without any annoying vibrations. Hu et al. (2001 and 2006) found that the annoying vibrations due to normal walking can be effectively controlled through a design approach that accounts for stiffness and mass for wood-framed floors. For heavyweight floors, an approach must be taken which considers frequency, damping and acceleration of the movement. Other investigations such as research by Weckendorf et al. (2006), Mohr (1999), Dolan et al (1999), and Onsysko (1998) assess the requirements and performance of timber floors. Major findings of these researchs are summarised below. In general there are three main factors that influence the perception of movement in floor systems, which include the vibration frequency, damping and acceleration of the movement. In most timber floors, frequency and acceleration are more important and are also related to each other. Natural frequencies of around 3 Hz can lead to resonance with walking traffic. Frequencies in the range 5 Hz to 8 Hz should also be avoided because they coincide with resonant frequencies in human organs and can be very uncomfortable. In order to increase frequencies, span or mass of floor systems can be reduced, and stiffness of the system can be increased. However, if mass of a floor system is reduced, the

accelerations of the motion will increase which result in more perceptible vibrations. Therefore, an acceptable solution is to balance the span, stiffness and mass of the floor systems.

Vibrations in timber floors can be reduced by increasing joist size or by using stiffer floor materials. Also increasing the two-way action in floor systems by connecting the joists transversely with suitable connecters or by using transverse beams can result in significant vibration reduction. In general, frequencies greater than 10 Hz and accelerations less than 0.375 m/s^2 perform adequately (Buchanan 2007).

Timber has good thermal insulation behaviour, and when a timber section is exposed to fire the char-layer protects the remaining uncharred residual cross-section against heat. However, the combustibility of wood and the fire performance of timber structures are the main reasons why many building codes limit the use of timber as a building material, particularly in multi-storey applications (Östman and Rydholm 2002). Fire safety has to be considered the main precondition for the use of timber for multi-storey timber buildings, and fire safety design of the timber structures is as important as the load bearing behaviour of the structure. Fire reduces the cross-section, stiffness and strength of the heated timber close to the burning surface (König and Walleij 200). The stiffness and strength of wood significantly decrease with increasing temperature (Källsner 2000). In order to design the structural timber members exposed to fire, the loss in cross-section due to charring and the reduction in strength and stiffness near the charred layer due to elevated temperatures need to be considered (Frangi et al. 2008 and 2010; Moss et al. 2009 ; Erchinger et al. 2010; Buchanan 2000 and 2001).

Some decades ago, the acoustic performance of timber floor systems was not considered a problem, but after introducing other floor types, such as reinforced concrete floors with much better performance in acoustics, timber floors gained a bad reputation in this regard (Jorissen 2006). Research has shown that most floor systems have potential problems with acoustic insulation (Crews et al. 2007). In the acoustic design of timber floors, two types of noise transmission need to be considered; the airborne noise and impact noise. In multi-storey buildings and most other occupancies it is important that floors and walls have resistance to airborne and impact sound transmission. The airborne noise is measured in terms of Sound Transmission Class (STC) and can be

reduced by increasing the mass of the floor, providing a number of different layers, and by reducing paths for sound to travel. The impact noise is measured in terms of Impact Insulation Class (IIC) and it can be decreased with floor coverings such as thick carpet and a high quality underlay. Further improvement can be achieved by putting a non-structural layer of flooring such as a light weight concrete or gypsum plaster about 35 mm thick over an insulating layer of rubber or soft board. Also, small openings and gaps can be sealed by polythene membranes which can significantly reduce sound transmission. Other approaches such as using a suspended ceiling or placing fibreglass batts in the cavity will also result in better acoustic performance of timber floors (Buchanan 2007).

2.4   An Overview of Various Types of Timber Floor Systems

As shown in Figure 2.2, a typical timber flooring system consists of three parts; the floor core which is the structural part of the floor and governs the structural strength and serviceability of the system. The upper part of the system which is on top of the floor core, which serves as the floor finish and may include different layers, and lastly the lower part of the system to make a ceiling (Kolb 2008). In the following sections, different possible types of structural floors (the floor core) will be introduced.
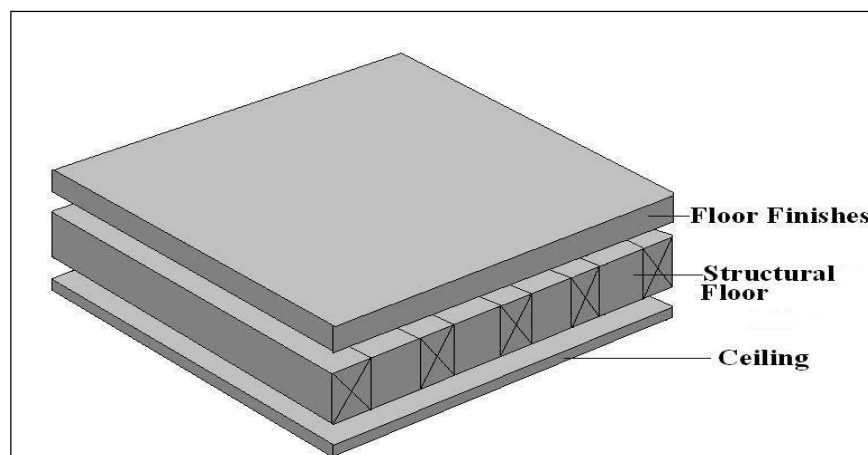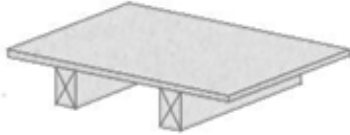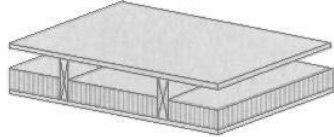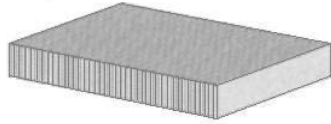
Figure 2.2 A typical timber flooring system (Kolb 2008)

Different literatures have classified the flooring systems in different ways but all use the same basic concept. According to Kolb (2008) the floor systems can be broken down into the following types:

Linear systems: timber joists floors, beams, trusses. This traditional form of construction is made up of linear components (joists) which can be nailed or screwed to a wood-base panel. The joists can be a solid sawn timber or a glued laminated timber that forms the structural load bearing part of the floor. It has been well known over the centuries and still is extensively being used for the new construction.	
Timber composite systems: ribbed-panel and hollow-box floors (open section stressed skin panels and box sections stressed skin panels). They have a similar structure to timber joist floors but with top and/or bottom sheathing rigidly glued to the joists to create a structural composite cross section (like an I or a T section).	
Solid timber system: solid timber sections. They can be made from solid timber sections, lamination, glued laminated timber sections or individual glulam sections which are connected together through dowels or nails to form a solid slab floor, or they can be butt-jointed together or they are prefabricated with tongue and grooves profiles.	
Solid timber floors: board type, glued floors. Large size panels which are made up of boards in various layers, and glued floors consisting of cross-laminated timber, cross-banded, parallel board or veneer plies can make a panelised flooring system.	
Timber –concrete composite floors: In TCC floor system, a reinforced concrete topping is placed over the timber elements in order to provide a better insulation and vibration behaviour than that of timber alone. The concrete layer is connected to the underneath timber elements through shear connections.	

In another way of classification (Sigrist and Gerber 2002) the floor systems are classified into massif, light floors and heavy floors potentially in composite action with concrete on top (Figure 2.3).
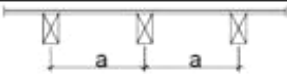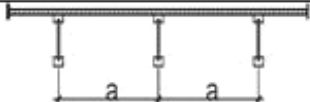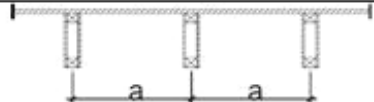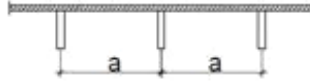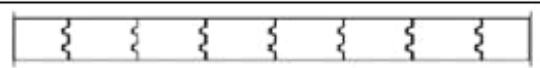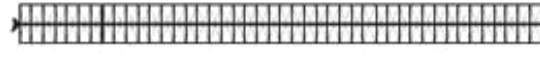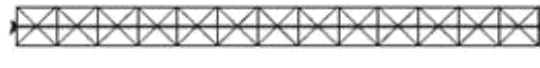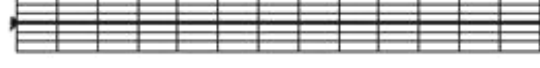
1) **Massif**	
	Traditional floor system

2) **light floors:**		
	I joists	Hollow-Sections
Boxes	Stress Skin Open	Stress Skin Box

3) **Heavy floors**		
	solid	massive
	glued	
	board	
	glulam	
	block-panel	
	board	Massive pre-stressed
	logs	
	glulam	

Figure 2.3 "Timber only" flooring systems (Sigrist & Gerber 2002)

Also, in the work done by the University of Technology Eindhoven in Netherlands (Jorissen 2006) the timber floors can be divided into two general types: plate floors and beam floors. In this section the "timber only" floor systems will be explored and their advantages and disadvantages are discussed.
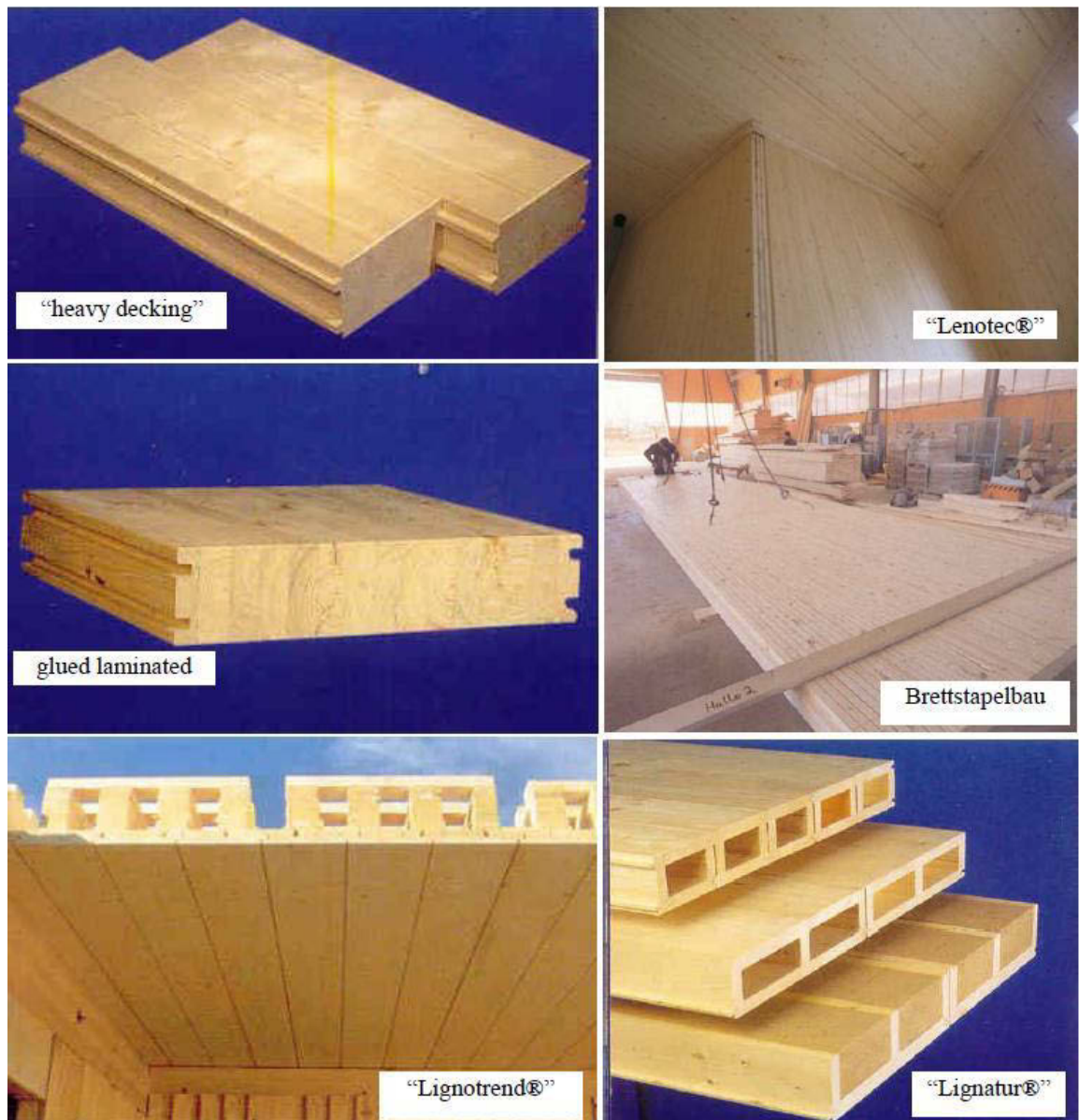
Figure 2.4 "Modern" plate floor systems (Jorissen 2006)

2.4.1   Joist Floor Systems

In timber joist floors, the floor system is made up of linear components (joists) which can be nailed or screwed to a wood-based panel such as particleboard or plywood as the superimposed sheathing of the system. Traditional joist floors are vastly used for single- or two-storey houses (Buchanan 2007). They are light weight, low cost, easy to construct, and well known over the centuries. They are easily adapted to various levels of loading and building functions such as fire resistance and sound insulations but because of their limited load carrying capacity, a considerable structural depth is usually required. Due to available log sizes and natural defects, the available sawn sections of softwood are limited in size and quality (Kolb 2008).

Because of the inherent flexibility of timber, the linear timber floor systems show poor performance in terms of vibration and deflection. Excessive deflection and vibrations are usually observed in medium to large spans (spans exceeding 4.5-5.5m), and also an effective level of acoustic performance, which is very important in inter-tenancy residential buildings, is hard to achieve with using only wood based floor panels (Crews et al. 2007). Chung et al. (2005) offered possible solutions such as using layers of sand above the flooring and expensive proprietary panels suspended under the floor.

2.4.1.1   Timber Joists

Solid timber joists can be sawn timber joists, glued laminated (Glulam) timber joists or Laminated Veneer Lumber (LVL) joists. As mentioned earlier, sawn timber joists with particleboard sheathing above, is the most common flooring solution in Australia and New Zealand. Sawn timber is produced by sawing logs longitudinally to create pieces of sawn timber, each with a square or rectangular cross section. The sizes vary from those used in domestic construction up to those used in heavy engineering constructions which include the large sizes used in structures such as bridges, wharves, warehouses, factories and railway lines. In Australia, they can be MGP stress graded timber (Machined Stress Grade) or F graded timber (either visually or mechanically graded) which is mentioned in AS 1720.1 (2010).

However, longer floor spans can be achieved by using Glulam joists. They can be shaped into curves (curved glulam has no structural role in floor system) and they can

be left visible in order to provide an aesthetically pleasing timber look Glulam joists are also available in different standard grades, for example GL8 with a stiffness performance similar to that of higher sawn timber grades, and higher Glulam grades for special applications (Grant 2010).

Laminated Veneer Lumbers (LVL) are also increasingly being used in joist floor system instead of sawn timber, as LVL offers increased strength, better dimensional stability, longer and deeper product dimensions, thus allowing longer traditional style floor spans to be achieved (Grant 2010).

2.4.1.2   I joist and webbed box beams

The use of I sections goes back to the early 1920's where I sections were used for stringers, ribs and longerons in wooden aircraft (Robins 1987). By the mid-1930s, composite I-beams with hardboard webs were used in European building structures (McNatt 1980). The researchers of Forest Products Laboratory (FPL) first recognised the efficiency of the I-shaped sections while studying web buckling in composite assemblies (Lewis and Dawley 1943). Afterwards, the use of I-beams in structural applications has been investigated by researchers such as   Koehl (1976), Keil (1977) and Germer (1986). The design of composite sections were thoroughly treated by design guides such as APA design guide (1982), Hoyle (1973a, 1986), Wood Handbook (USDA 1987) and ASTM (1986).

When using composite sections such as I shape beams, lower quality trees could also be fully utilized as 50 precent of wood fiber can be saved by using wood composite structural shapes (Nelson 1975; Tang and Leichti 1984). I joists are structurally sound and they provide the best use of their material properties since, in general, flanges are designed to provide the moment capacity and webs are designed to take the shear forces. The suitable span-to-depth ratio for most floor applications is about 15:1 whereas this ratio can increase to 25:1 for roof applications (Leichti et el. 1990). Different materials can be used for an I section. For example, LVL can be used for flanges whereas OSB (Oriented Strand Board) or plywood can be used as a web. Flange-web interfaces can be fabricated by mechanical fasteners and/or adhesives.

Using adhesives for the flange-web joist interfaces will result in eliminating the shear slip at the joint, and simplifying the design procedure.

Moreover, thin webbed box beams (Figure 2.5) can be used in wide variety of applications from beams in residential applications, to rafters, columns, purlins, girts and box beam portal frames in industrial buildings. They can also be designed and shaped to suit a particular application as tapered, curved or pitched beams (Mcdowall 2007). They consist of LVL flanges, plywood webs and web stiffener which are usually made out of the same material as flanges (Figure 2.5). A deep section is required if longer spans need to be achieved (EWPA 2008).
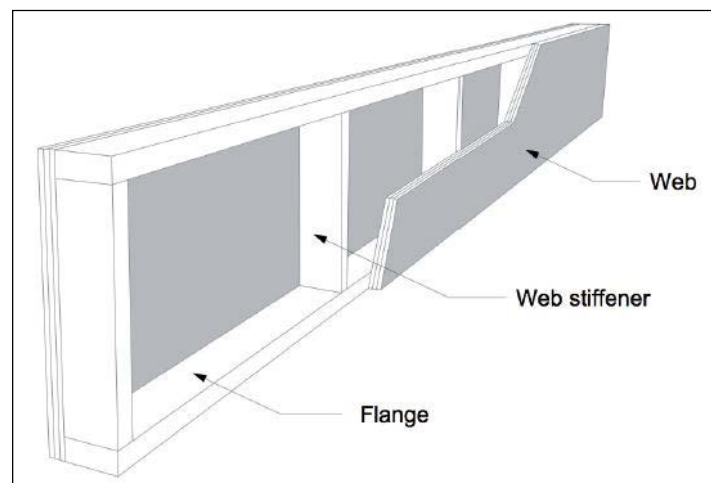
Figure 2.5 Plywood webbed box beams (EWPA 2008)(the thickness of flanges and webs are schematic)

2.4.2   Stressed Skin Panels

To address the deficiencies of the joist floor system mentioned earlier (section 2.4.1) , other innovative flooring systems such as stressed skin panels, solid timber slabs made from cross-laminated sections and timber concrete composite systems are developed to overcome the limitations of the timber joist floor systems.

Stressed Skin Panels (SSP) were first developed in the early 1930's by the researchers of the USDA, Forest Service, Forest Products Laboratory. According to Heyer and Blomquist (1964), the first structural application of SSP panels goes back to 1937 when a prefabricated house was built in USA using stressed skin panels (KURT 2005).

Many researchers described SSP panels in different ways. According to Stalnaker and Harris (1989), Baird and Ozelton (1984), and Hoyle and Woeste (1989), SSP panels consists of a plywood sheets attached to stringers, either by glue (usually nail-glued joints) or mechanical fasteners (usually nails or staples) so that the units acts compositely. However, other than plywood, the use of other materials such as OSB (Bach and Cheng 1996), particleboard (Henry 1971; Kliger and Pellicane 1996), hardboard (Henry, 1971), plaster, plastics, and steel tension flange (Kliger 1996; Kliger and Pellicane 1997) have also been investigated for skin. Laminated Veneer Lumber (LVL), three-ply glulam, laminated strand lumber (LSL) can be used as stringers (Merz 1996).

The stressed skin system, in theory, is one of the most efficient structural systems (Henry 1971). In general, Stressed skin panel systems have a similar structure to timber joist floors but with top and/or bottom sheathing rigidly glued to the joists to create a structural composite cross section which can behave like an I or a T section (Figure 2.6). Therefore, compared to conventional floor systems which have no or few composite properties, SSPs can perform as fully composite sections capable of improving the structural properties of the system such as strength, stiffness and the bending capacity of the system (Gerber 2006). To make shear resistant connections and ensure that there is no slip between the interconnections (skin-to-joist), the ribs and the sheathings are glued together in an industrial process, or by using adhesives together with screws where the roles of screws are to apply pressure until the adhesive sets and therefore, they do not have a structural role (Kolb 2008). As there is no slip between the interconnections (skin-to-joist), the strain distribution over the depth of the cross-section is linear, and the fundamental static principles such as Single Beam Theory (Amana & Booth 1967) and the transformed section (Gere & Timoshenko 1999) can be applied and therefore, and the optimum uses of the material properties of all structural members is achieved (Gerber 2006).

(a) T section SSP   (b) Upside-down T sections SSP   (c) Box sections SSP
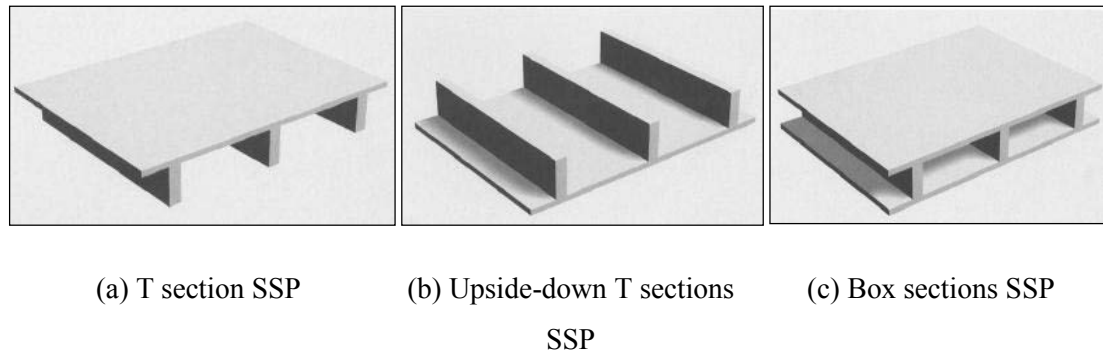
Figure 2.6 Stressed Skin Panels Systems (Kolb 2008)

Stressed Skin panels are light weight and they require low structural depth with higher load bearing behaviour since both the joists and the sheathing have structural load bearing role (Kolb 2008). The bottom sheathing can be left visible as a ceiling. SSPs are easy to construct by a few ordinary carpenter tools (Vick and Wittenberg 1971), or they can be factory fabricated to reduce site work and speed up the assembly process (Wardle and Peek 1970; Baird and Ozelton 1984).

Since the stressed skin panels are light weight, they are still prone to excessive vibrations for long-span floors and also cannot normally provide an effective acoustic separation (Crews et al. 2007). The acoustic performance can be improved by the use of low density concrete flooring panels and the research undertaken in this area has shown the improvements in acoustic performance, although the interaction between timber and concrete was not as significant as originally expected (Crews et al. 2005). Some of the stressed skin panel systems which developed recently will be introduced in the following paragraphs.

2.4.3 Plate Floor Systems

Cross-banded laminated veneer lumber and glued laminated timber sections can be assembled together to form a solid slab floor system for relatively long spans and/or high floor loads. Although solid timber floors are sometimes used in domestic construction, they are more common in commercial or industrial buildings. As illustrated in Figure 2.7, solid timber sections or individual glulam sections can be glued together, or can be connected with tongue and groove profiles as shown in Figure 2.8 (Kolb 2008).
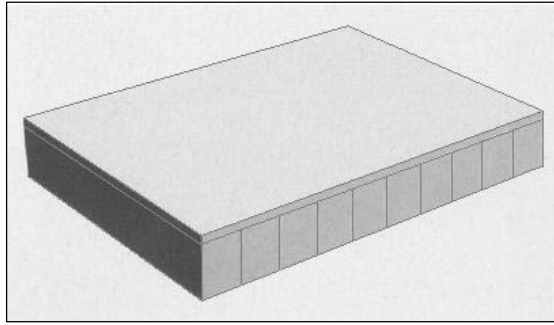
Figure 2.7 Butt-jointed solid timber joists (Kolb 2008)
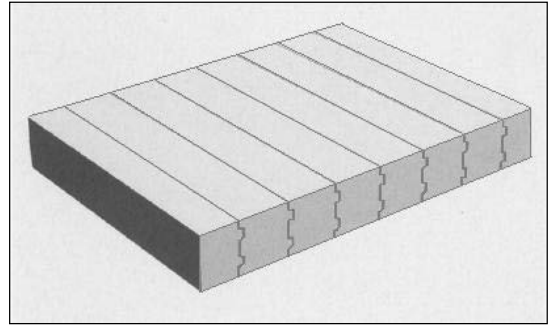
Figure 2.8 Solid timber joists with double tongue and groove (Kolb 2008)

In the Edge-fixed timber floors, the individual timber elements are placed together side by side and fixed in the factory using dowels (Figure 2.9) or nails (Figure 2.10) to form the prefabricated solid sections. These solid sections are then joined together using special connectors (Figure 2.11) to make solid slab floors. The nails or dowels connecting the individual timber elements transfer the shear forces in the transverse direction and ensure the transverse distribution of the concentrated loads. If the connecting material is pre-stressed transversally, the load carrying capacity is improved in this direction. (Kolb 2008).
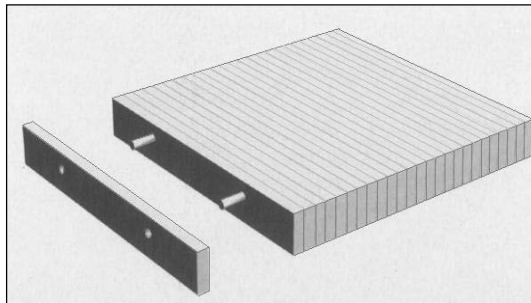
Figure 2.9 Edge-fixed floor elements, dowelled (Kolb 2008)
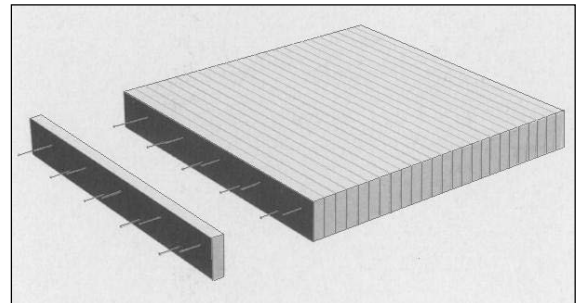
Figure 2.10 Edge-fixed floor elements, nailed (Kolb 2008)
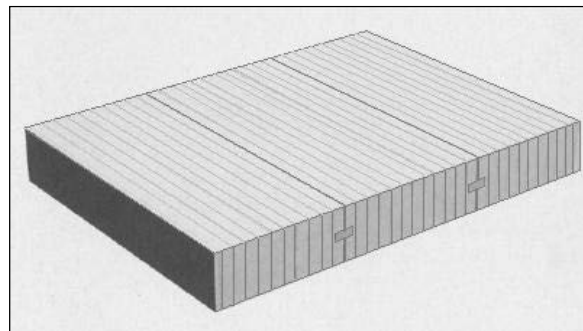
Figure 2.11 Edge-fixed timber floors (glued, with loose tongue joints) (Kolb 2008)

The solid timber systems are fast to erect as they can be prefabricated, and problems such as ineffective acoustic performance and excessive deflections and vibrations can be addressed by using slabs of sufficient thickness. However, the high timber consumption may make the system less convenient or cost effective in some countries when compared with traditional reinforced concrete floors (Crews et al. 2007) and also in comparison to the large quantity of wood required for this system, the load-carrying capacity is only moderate. Moreover, the problems such as high shrinkage and swelling effects must also be considered (Kolb 2008).

2.4.4   Timber Concrete Composite System

Although Timber has significant strength to weight ratio, timber floor systems are susceptible to excessive vibration and show poor acoustic performance due to their light weight. To address these problems an upper layer of concrete can be used in timber floor systems (timber-concrete composite or TCC) to improve their performance since the combination of timber and concrete produces improved strength and stiffness, more thermal mass and better acoustic separation and the system is also less susceptible to vibration (Crews et al. 2007). In this way, the bending and tensile forces induced by gravity loads are resisted by timber and the compression forces by the concrete topping.

In the last 50 years, TCC system has gained a great deal of renewed interest and many buildings and bridges in different part of the word (United States, New Zealand, Australia and European countries) were constructed using TCC system, and the existing timber floors were up- graded in Europe (Natterer et al. 1996). Since the early 1990s, the use of TCC system in structural applications has significantly increased in Europe (Turrini and Piazza 1983a, b). Although the TCC system provides an improved acoustic performance and increases the stiffness of the floor, the design of the system is more complicated than timber only floors as the transformed section method from the conventional principals of structural analysis cannot be used in design. The shear connecter of the system must be designed strong and stiff enough to transfer the shear force. The partial composite behaviour of the system can be designed by the linear-elastic method which is based on the assumption that all the material of the section remains within the linear elastic range, until the timber beam fails (Möhler

1956; Ceccotti 2002). If the failure of TCC system occurs when the connectors are in the plastic range, the design of the system should be followed by elastoplastic method (Frangi and Fontana 2003). Further, the time-dependent properties of the component of the TCC system should be designed, and several studies have been conducted in this regards (Fragiacomo 2006; Schänzlin 2003; Schänzlin and Fragiacomo 2007).

The type of shear connectors plays an important role in behaviour and composite performance of TCC system. The early research conducted on shear connectors goes back to 1940s (McCullough 1943; Richart and Williams 1943) and 1970s (Pincus 1970; Pillai and Ramakrishnan 1977). Notches cut in the timber beam and reinforced with a steel screw or dowel can provide very strong and stiff connectors but may not be very economical (Kuhlmann and Schänzlin 2001; Van der Linden 1999; Deam et al. 2007).The length of the notch, the presence of a lag screw (which improves the ductility) and the penetration depth of screw into the timber have important effect on behaviour and performance of notch timber-concrete connections (Yeoh et al. 2009b, 2011) Other types of connections such as nailplates (Aicher et al. 2003), screws and dowels (Pillai and Ramakrishnan 1977; Meierhofer 1993; Steinberg et al. 2003; Grantham et al. 2004) have also been investigated by different researchers. Moreover, recent development such as using glue and epoxy resin in the connection system (Brunner et al. 2007; Miotto and Dias (2008); Kuhlmann and Aldi 2008) and prefabricated demountable composite systems (Lukaszewska et al. 2008) have attracted a lot of interest among researchers.

A number of short term and long terms experimental tests have been conducted on TCC beams including the experimental investigation by Ceccotti et al. (2006) who tested a double 6m span glulam T-beam with 18 corrugated rebars glued to each beam with epoxy resin, Gutkowski et al. (2008) who investigated multiple timber-concrete layered beams connected with notch shear/key anchor and tested under four-point bending loads, and Yeoh et al. (2009a ; 2010) who investigated 11 LVL-concrete composite T-beams under four-point bending loads with 8m and 10m span, 600 and 1,200 mm widths and different types of shear connectors. Moreover, Lukaszewska et al. (2010) conducted short term investigation on five 4.8m span full-scale TCC floors under four –point bending loads, and a 1 year long term test on two TCC beams which were

subjected to sustained load evaluated as 13% of the failure load in the short-term collapse test. All the investigations resulted in a better understanding of the behaviour and performance of the TCC beams and different types of timber-concrete connections.

2.5 Structural Performance of Composite Floor Systems

2.5.1 Interaction between the Floor Members

Structural performance of timber floor systems depends on the mechanical properties of the floor members and the connections between them. Therefore, the interlayers have an important role in the serviceability and ultimate strength and stiffness of the floor unit (Foschi 1982; Vanderbilt, Goodman and Criswell 1974; Corder and Jordan 1975). The superimposed panels in a multi-layer floor systems can have structural or functional (insulating, acoustic, aesthetic, etc.) roles. The connection between different members of a floor system can vary from mechanical only (nail, screws, etc.) to connections which provide a full bond. Depending on the type of bond that the shear connectors provide, three types of composite performance can be encountered:

- No composite action: no interaction between the floor members (in which the floor members act independently)
- Partially composite action: limited interaction between the floor members (in which the floor members have limited composite action as a result of mechanical fasteners)
- Fully composite action: the floor members act like one solid section (fully composite action can be provided by screw-gluing technique)

The level of composite action affects the stiffness and strength performance of floor assemblies, and also affects the load-bearing capacity of the system (Goodman et al. 1974; Vanderbilt, Goodman and Criswell 1974, wolfe 1990). In general, higher shear strength and slip modulus of the interlayers will result in higher load-bearing performance and lower deflection in the floor assembly (Moody and McCutcheon 1984).

Extensive research have been carried out to identify the behaviour and properties of shear connectors such as nails, screws and bolts, to assess the load slip response of the

joints under lateral load and to develop theoretical methods of design analysis (Kuenzi 1955; Patterson 1973; Wilkinson 1971, 1972; Stluka 1960). Also, many codes present design methods for assessing the structural performance of wood-to-wood connections with mechanical fasteners (such as AS 1720.1 (2010) and EC5 (2004)).

Moreover, the use of glue at the interfaces improves the properties of floor system by increasing the first and second moment of area of the floor section. Stiffness of the floors manufactured with a screw or nail and gluing technique increase significantly compare to screwing or nailing alone, and the shear transfer between the joists and the skins (or flanges) improves considerably (Corder and Jordan 1975; Liu and Bulleit 1995). The new generation of adhesives complies with the short term and long term requirement of floor structures and they can provide infinite stiffness at the interfaces (Raadschelders and Blass 1995).

2.5.2 Fully Composite Action

When there is no slip at the interfaces, a linear strain distribution over the depth of the floor section can be assumed (Raadschelders & Blass 1995). Figure 2.12 shows the strain and stress distribution over the depth of section with no slip in the interlayers
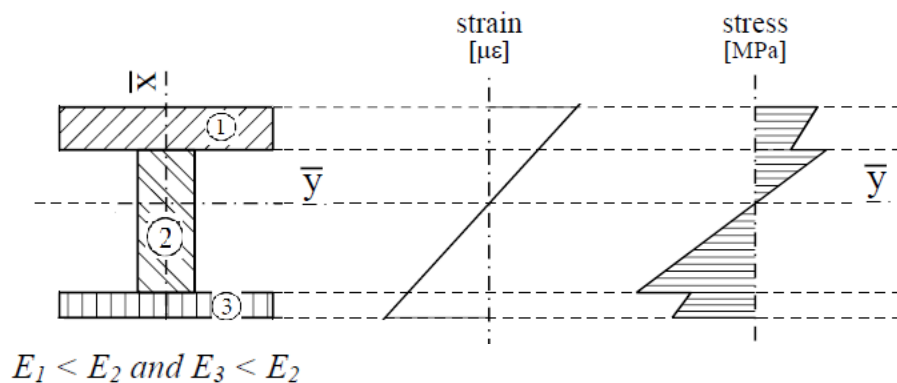
Figure 2.12 The strain and stress distribution over the depth of section with no slip in the interlayers

Because there is no slip at the interfaces, the transformed-section method is applicable. This method is well-known and described in numerous literature such as Beer and Johnston (1992), Gere (2004) and Gere and Timoshenko (1999). In this method the neutral axis is determined with Equation 2.1 to 2.3.

$$\int_1 y_1 dA_1 + n_2 \int_2 y_2 dA_2 + ... + n_n \int_n y_n dA_n = 0 \qquad \text{Eq.2.1}$$

In which A_n is the area of the nth section component and y_n is the y axis vertical distance and n is the modular ratio as follows:

$$n_1 = \frac{E_1}{E_1} = 1 \ , \ n_2 = \frac{E_2}{E_1} \ , \ ... \ , \ n_n = \frac{E_n}{E_1} \qquad \text{Eq.2.2}$$

$$\bar{y} = \frac{\int_1 y_1 dA_1 + n_2 \int_2 y_2 dA_2 + ... n_n \int_n y_n dA_n}{\int_1 dA_1 + \int_2 dA_2 + ... \int_n dA_n} \qquad \text{Eq.2.3}$$

Where $\bar{y}$ is the neutral axis of a composite section. The section properties of the composite section can be calculated as follows:

$$A_T = \sum_{i=1}^{n} n_i \int dA_i \qquad \text{Eq.2.4}$$

$$Q_T = \sum_{i=1}^{n} n_i \int y_i dA_i \qquad \text{Eq.2.5}$$

$$I_T = \sum_{i=1}^{n} n_i \int y_i^2 dA_i \qquad \text{Eq.2.6}$$

$$S_{T,upper} = \frac{I_T}{\bar{y}_{upper}} \qquad \text{Eq.2.7}$$

$$S_{T,lower} = \frac{I_T}{\bar{y}_{lower}} \qquad \text{Eq.2.8}$$

In which A_T is the area of the composite section, Q_T is the first moment of area of a composite section, I_T is the second moment of area of a composite section, and $S_{T,upper}$ and $S_{T,lower}$ are the section moduli of a composite section.

2.5.3 The Effects of Shear lag and plate buckling on Effective Flange Width

In fully composite floor systems such as glued thin-webbed beams and SSP systems, the concept of effective width of flange is an important aspect of the structural performance. It corresponds to the portions of the skin/flange that contribute to the stiffness of the structure and act compositely with the joist. The occurrence of shear deformations and plate buckling affect the stress distributions in the unsupported part of the flange/skin

(between the joists) and hence, limit the portion of the flange/skin that acts compositely with the joists. When joist spacing increases, the contribution of the panel(s) decreases, the stress peaks become larger and the serviceability and load-bearing capacity of the floor system reduce. This concept is described as the "shear lag".

Early studies on shear lag behaviour focused on isotropic materials (von Karman 1924) and later, on orthotropic materials such as plywood (Amana 1967; Smith 1966a, 1966b). Foschi (1969b), Ozelton and Baird (2002) proposed that the normal stresses reach a maximum at the intersection of the joists and the skins, and a minimum in the middle between the joists (Figure 2.13). Raadschelders and Blass (1995) proposed that the magnitude of the stress diminution depends on the ratios of (joist spacing)/(floor span) and (modulus of elasticity)/(shear modulus), that is, with increasing these ratios the effective width of the skin(s) decreases.
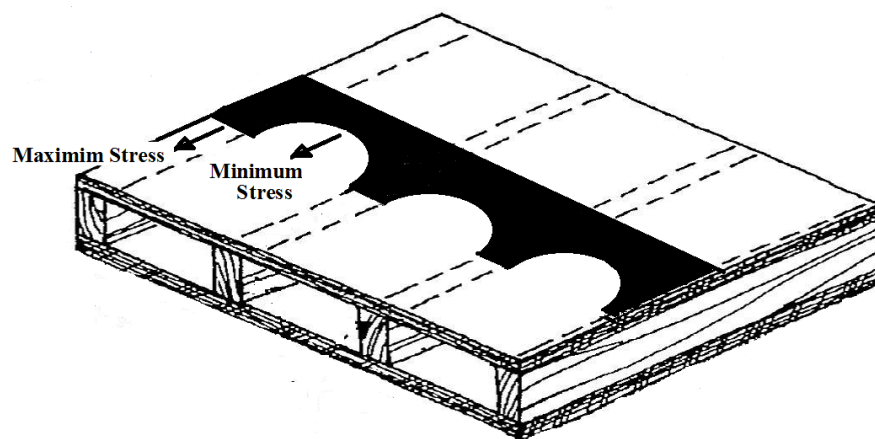
Figure 2.13 The effect of shear lag on stress distribution

Considerable researches have been carried out to quantify the behaviour of shear lag and effective flange width. Möhler, Abdel-Sayed and Ehlbeck (1963) for example, proposed a mathematical expression to calculate the shear lag (Equations 2.9 and 2.10) and the effective flange width (Equations 2.17 and 2.18) of the elastic orthotropic flanges/skins.

For interior joists:

$$b_{ef,i} = 2L \frac{(\lambda_1 \tanh\varphi_1 - \lambda_2 \tanh\varphi_2)}{\pi(\lambda_1^2 - \lambda_2^2)}$$

Eq.2.9

For exterior joists:

$$b_{ef,e} = L \frac{(\lambda_1 \tanh\varphi_1 - \lambda_2 \tanh\varphi_2)}{\pi(\lambda_1^2 - \lambda_2^2)}$$

Eq.2.10

in which the coefficients are:

$$\varphi_1 = \frac{\lambda_1 \pi b_f}{2L}$$

Eq.2.11

$$\varphi_2 = \frac{\lambda_2 \pi b_f}{2L}$$

Eq.2.12

$$\lambda_1 = \sqrt{\beta + \sqrt{\beta^2 - c}}$$

Eq.2.13

$$\lambda_1 = \sqrt{\beta - \sqrt{\beta^2 - c}}$$

Eq.2.14

$$\beta = \frac{E_y}{2G} - \upsilon_{xy}$$

Eq.2.15

$$c = \frac{E_y}{E_x}$$

Eq.2.16

and the effective flange width can be calculated as follows:

For interior joists:

$$w_{ef,i} = b_w + b_{ef,i}$$

Eq.2.17

For exterior joists:

$$w_{ef,e} = b_w + b_{ef,e}$$
Eq.2.18

Where w is the effective width [mm], b_{ef} is the shear lag , b_w is the joist width, L is span

of the structure [mm], υ_{xy} is Poisson's ratio of the panel, subscripts x relates to parallel to

the joist's longitudinal axis and y is related to perpendicular to the joist's longitudinal

axis, E_y and E_x are modulus of elasticity of the panel [MPa] and G is the shear modulus

[MPa]. The buckling of flanges under compression may also limit the portions of the skin/flange that contribute to the stiffness of the structure. Many studies have been carried out in which the critical buckling load is assessed (Foschi 1969a, 1969b; Mansour 1976; von Halász and Cziesielski 1966). Also, the theory of plate buckling and stability of structures can be found in many books such as Girkmann (1954), Timoshenko and Woinowsky-Krieger (1959), Timoshenko and Gere (1961), Timoshenko and Goodier (1987), etc. Similar to what was shown in Möhler's formulas (Equations 2.14 to 2.19), accurate calculation of shear lag and plate buckling is commonly tedious and involves too many parameters. Therefore most of the codes consider an approximation for calculating the shear lag, plate buckling and the effective width of flange. For example EC5 (2004), SIA 164 (1992), APA (APA – The Engineered Wood Association 1990) and methods and guidelines such as guidelines proposed by Desler (2002) and McLain (1999) present an approximation for evaluating the effective width of flange which are adequately accurate for a safe design, and easy to calculate. In this project, the method by EC5 (2004) is used to estimate the effective width of the flange (chapter 3).

2.5.4   Partially Composite Action

The procedure of partially composite action for evaluating the properties of a floor system is applicable when the interlayer's stiffness is much lower than that of the structural wood members (flanges and webs) and therefore, slip occurs at the interfaces. Strain and stress distribution over the depth of the section is shown schematically in Figure 2.14 with free slip at the interfaces.

$E_1 < E_2$ and $E_3 < E_2$
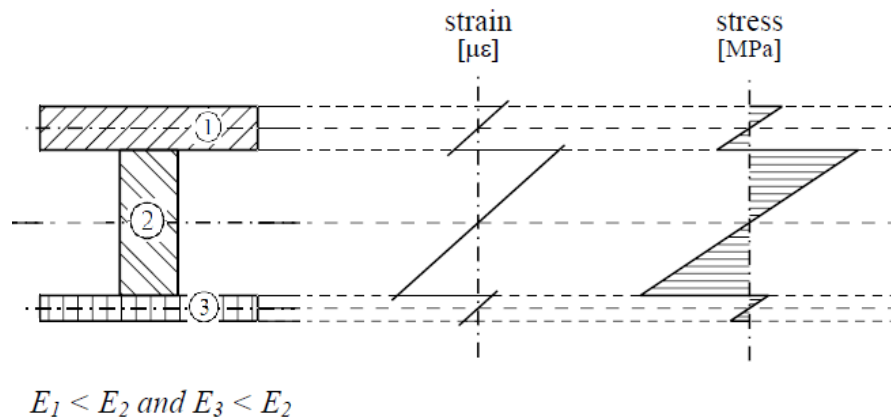
Figure 2.14 Strain and stress distribution across the floor section – free slip at the interfaces

To account for non-linearity of the strain distribution over the depth of section (caused by the free slip at the interfaces), the axial stiffness (direction parallel to the joists) of the sheathing shall be modified (McCutcheon 1986). Equation 2.19 shows the modification in the axial stiffness of flanges.

$$\overline{EA}_f = \frac{EA_f}{1+10\dfrac{EA_f}{SL_f^2}}$$ Eq.2.19

where $\overline{EA}_f$ is the transformed axial stiffness of the flange (width of panel acting compositely to the joist) [N], EA_f is the actual axial stiffness of the flange [N], S is the interlayer stiffness [N/m^2], and L_f is the distance between gaps in the flange [m]. Moreover, McCutcheon (1986) proposed the weighted modulus of elasticity in order to evaluate the section properties of a partially composite section. Equation 2.20 shows the weighted stiffness for T-beam composite sections and Equation 2.21 and Equation 2.22 show the weighted stiffness for I-beam composite sections:

$$EI = EI_u + \frac{(\overline{EA}_f)(EA_w)}{\overline{EA}_f + EA_w}h^2$$ Eq.2.20

$$EI = EI_u + EA_w\bar{y}^2 + \overline{EA}_{f,1}(h_1 - \bar{y})^2 + \overline{EA}_{f,2}(h_2 + \bar{y})^2$$ Eq.2.21

$$EI = EI_u + EA_w\bar{y}^2 + \overline{EA}_{f,1}(h_1 + \bar{y})^2 + \overline{EA}_{f,2}(h_2 - \bar{y})^2$$ Eq.2.22

where EI is the flexural stiffness of the partially composite section [Nm^2], EI_u is the flexural stiffness if the joist and flange are fully unconnected [Nm^2], EA_w is the axial stiffness of the joist [N], h is the distance between centroids of the joist and flange [m], and $\bar{y}$ is the distance of the neutral axis from the top of the partially composite section (Equation 2.21) or from the bottom of the partially composite section (Equation 2.22). Other researchers such as Kliger and Pellicane (1997; 1998) have also proposed similar methods which can produce good estimates of the stiffness of the composite beams. EC5 (2004) offers the following approach for calculating the effective stiffness of the partially composite I beams or box beams:

$$EI_{ef} = \sum_{i=1}^{3} (E_i I_i + \gamma_i E_i A_i a_i^2)$$

<div align="right">Eq2.23</div>

$$A_i = b_i h_i$$

<div align="right">Eq 2.24</div>

$$I_i = \frac{b_i h_i^3}{12}$$

<div align="right">Eq 2.25</div>

for $i=1$ and $i=3$: $\gamma_i = [1 + \pi^2 E_i A_i S_i / (K_i l^2)]^{-1}$

<div align="right">Eq 2.26a</div>

for $i=2$: $\gamma_2 = 1$

<div align="right">Eq 2.26b</div>

$$a_2 = \frac{\gamma_1 E_1 A_1 (h_1 + h_2) - \gamma_3 E_3 (h_2 + h_3)}{2 \sum_{i=1}^{3} \gamma_i E_i A_i}$$

<div align="right">Eq 2.27</div>

$$a_1 = 0.5(h_1 + h_2) - a_2$$

<div align="right">Eq 2.28</div>

$$a_1 = 0.5(h_1 + h_2) + a_2$$

<div align="right">Eq 2.29</div>

$$\bar{y} = h_3 + 0.5 h_2 + a_2$$

<div align="right">Eq 2.30</div>

Where E_i is the modulus of elasticity of each section component (bottom flange, web(s) and top flange), h_i is the height of each section component, A_i is the height of each section component, I_i is the second moment of area of each section component, b_i is the width of each section component, γ_i is the connection coefficient, $\bar{y}$ is the neutral axis of the partially composite section and l is the span of the section. For serviceability limit state calculations $K_i = K_{ser,i}$ and for ultimate limit state calculations $K_i = K_{u,i}$. This method is used in the subject research (chapter 6).

2.5.5   Verification of the Serviceability and Ultimate Limit State

In composite floor systems (such as I beams or stressed skin panels), the flanges are commonly designed to provide the moment capacity of the beam and the webs to predominantly carry the shear force. According to EC5 (2004) the flanges should satisfy the requirements of axial stresses at the center fiber of the flanges, and the extreme fibers of flanges should satisfy the requirements bending stresses. Also, AS 1720.1 (2010), SIA 256 (2003) and the APA method (Desler 2002; McLain 1999) require that the extreme fiber of the flanges should be designed to resist bending stresses. The

requirements of shear stresses should be satisfied at the neutral axis, and the interfaces should be designed to resist the rolling shear stresses. Table 2.1 shows a summary of stress verification for I beams, double I beams and box beams (which are used for the full scale experimental test in this research project) for simply supported single span.

Table 2.1 stress verification for I beams, double I beams or box beams

Section component	Type and location of Stress to be verified
Upper flange	Bending stress should be verified at the extreme fiber Compression stress should be verified at the center fiber
Upper web-to-flange interlayer	Roller shear stress should be verified at the interface
Web(s)	Bending stress should be verified at upper extreme fiber Shear stress should be verified at neutral axis Bending stress should be verified at lower extreme fiber
Lower web-to-flange interlayer	Roller shear stress should be verified at the interface
Lower flange	Bending stress should be verified at the extreme fiber Tension stress should be verified at center fiber

Typical values of the uniformly distributed permanent actions, G, are 1.5 kPa for domestic housing, 3.0 kPa for offices, classrooms and lecture theatres, and 4.0 kPa for shops and general industrial floors as per AS/NZS 1170.1 (2002). There is corresponding concentrated imposed action for each application listed in AS/NZS 1170.1 (2002) ranging from 1.8 kN for a domestic house to 4.5 kN for general industrial floors. Specific cases and the combinations of actions for serviceability and ultimate limit state are also provided in AS/NZS 1170.0 (2002).

For the serviceability requirement, many codes and guidelines provide guidance on maximum deflection at mid-span, which is often expressed as ratios of span. The maximum deflection limit of L/300 to L/500 is usually recommended (L is the span length of the system).For example, AS/NZS 1170.0 (2002) imposes a limitation coefficient of 300 in order to control the sagging of the floor structure. The deflection under any point alongside the beam can be calculated using principle of virtual work (Carpinteri 1997; Ghali and Neville 1989; Timoshenko and Young 1968). Equation 2.31 shows the maximum deflection of the beam at mid-span under four point bending load

(Figure 2.15) which is used in this study for the experimental investigations, to simulate the uniform distributed load.
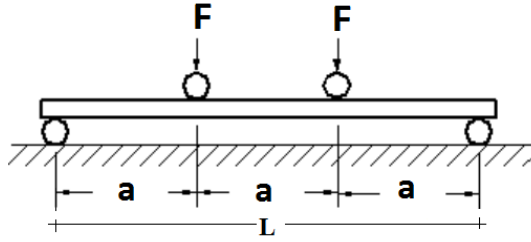
Figure 2.15 Four point bending load

$$u_{max} = \frac{23FL^3}{648(EI)_T} + k\frac{FL}{6GA_T}$$ Eq. 2.31

where u_{max} is maximum deflection at mid-span, F is load, L is the span, $(EI)_T$ is the effective stiffness of the transformed-section and A_T is the area of the transformed-section. Also, the short term and the long term deflections should be multiplied by the modification factor (creep factor) which can be found in the Australian (AS 1720.1 2010) and New Zealand design code (NZS 3603:1993).

 Many structural timber codes such as DIN 1052 (2008), DIN 1055 (2003), EC5 (2004), SIA 256 (2003) and other non-timber codes such as steel design guide series (Murray 2003), SCI design guide (Wyatt 1989) and SCI Guide P354 (Smith 2007) deal with the vibration of floors. The following are specified in EC5 (2004):

$f_1 \geq 8Hz$ Eq.2.32

$\frac{w}{f} \leq a$ mm/kN Eq.2.33

$v \leq b^{(f_1 \cdot \zeta - 1)}$ [m/(Ns²)] Eq.2.34

Where f_1 is fundamental frequency of the floor, w is the maximum instantaneous vertical deflection caused by a vertical concentrated static force F applied at any point on the floor, taking account of load distribution, v is the unit impulse velocity response and ζ is the modal damping ratio. Values for a and b are given in Figure 2.16.
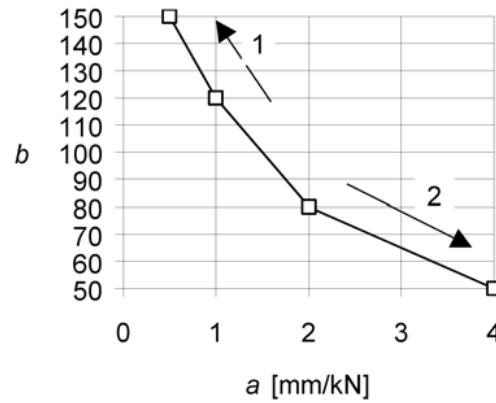
Figure 2.16 Interrelation between the values a and b taken from Eurocode 5 [3]: Direction 1 means better performance, direction 2 means poorer performance

DIN 1052 (2008) specifies a limit of deflection. The deflection due to a quasi permanent load should be less than 6 mm (Equation 2.35).

$$\delta_{q.perm} \leq 6mm$$ Eq.2.35

$$w_{q.perm} = w_{perm.load} + \varphi_2 w_{live.load}$$ Eq.2.36

The "quasi permanent load" means that a certain part of the live load (defined in DIN 1055(2003)) should be added to the permanent load (Equation 2.36). φ_2 is the combination factor taken from DIN 1055 (2003). The vibration performance of the full scale experimental specimens of this research is investigated and assessed by Rijal (2013).

2.6   Numerical Investigations on Timber Floor Systems

The developed numerical models can generally be classified as frame FE models (Mungava and Kenmou 1993; Fragiacomo 2005; Amadio et al.2000; Fragiacomo and Ceccotti 2006) and continuum-based FE models (Fortino and Toratti 2010; Bou Said, Jullien and Ceccotti 2004). In general, the behaviour of wood is classified as nonlinear anisotropic, with different properties along the grain and perpendicular to the grain direction. Its properties also depend on its density, moisture content and natural defects like knots (Franke et al 2012; Yeoh et al.2011). Since the short-term and long term

response of timber beams depends strongly on the behaviour of timber, a suitable constitutive law is needed in order to model timber behaviour and to capture the strain-stress relationship and failure of timber (Qudjene and Khelifa 2009). Several constitutive laws have been developed over the last three decades for modelling the behaviour of timber. They can be classified into 1D, 2D and 3D models. The stress-strain relationship in 1D constitutive laws were typically used within the framework of frame FE models (Glos 1981; Conners and Appleton 1989; Bazan 1980; Fragiacomo 2005; Fragiacomo and Ceccotti 2006) while the 2D and 3D models were used in a continuum-based FE model (Dias 2007; Schmidt 2009).

The alternative classification of the existing constitutive laws can be the empirical models (Glos 1981; Conners and Appleton 1989), elasticity-based models (equivalent uniaxial and invariant-based models) and plasticity-based models (classical plasticity, bounding surface plasticity and multi-surface plasticity) (Mackenzie et al. 2005; Guan 2009), models based on progressive damage such as fracture-based models (Yasumura and Daudeville 2000; Serrano and Gustafsson 2007), continuum damage models and combination of plasticity with damage and fracture models.

Besides a suitable constitutive law for capturing the state of stress under any given load, a suitable failure model is also required to determine whether the failure happened or not. One class of failure criteria are those which are based on the progressive damage, using fracture mechanics (Yasumura and Daudeville 2000; Serrano and Gustafsson 2007). These techniques can be used when the crack is described using oversized plastic strains in the elements (Fleischmann 2005; Grosse 2005) or when a crack is described by releasing the degrees of freedom between adjacent elements (Parrod 2002; Reichert 2008; Snow 2006).

Another group of failure criteria are those which use a failure envelope such as Hashin failure criteria (Hashin 1980), Tsai and Wu model (Tsai and Wu 1971) and other failure envelopes (Eberhardsteiner and Gingerl 1999; Nahas 1986; Rowlands 1985). In its simplest form, and for the isotropic materials, the failure occurs when the principal stress (or strain) exceeds the maximum stress and maximum strain in that direction. For isotropic material, the maximum values for stress and strain are similar in all directions,

however, for orthotropic materials, different values should be considered for longitudinal, perpendicular and radial directions.

Among available orthotropic failure criteria implemented in the commercial softwares, Hashin damage model (Hashin 1980) is describes in this section. The Hashin model was originally developed as failure criteria for unidirectional polymeric composites (Hashin 1980; Hashin & Rotem 1973). Therefore, applying the Hashin model to other laminate types or non-polymeric composites has a significant approximation. Hashin damage model (Hashin 1980) can be calibrated using seven input parameters and has the potential to be used for practical non-linear analysis of timber beams. The Hashin damage model uses the interaction between stress components (shear and normal) to evaluate different failure modes. The damage evolution law is based on the energy dissipated during the damage process and linear material softening (Hashin 1980; Sun et al. 1996). The Hashin criteria consider four different damage initiation mechanisms expressed in terms of effective stress components as $\hat{\sigma}_{ij}$ $(i,j=1,2)$ follows :

$$
\begin{cases}
F_f^t = \left(\dfrac{\hat{\sigma}_{11}}{X^T}\right)^2 + a\left(\dfrac{\hat{\sigma}_{12}}{S^L}\right) & \text{Tensile failure of fibres} \quad \text{Eq.2.37} \\[3ex]
F_f^c = \left(\dfrac{\hat{\sigma}_{11}}{X^C}\right)^2 & \text{Compression failure of fibres} \quad \text{Eq.2.38} \\[3ex]
F_m^t = \left(\dfrac{\hat{\sigma}_{22}}{Y^T}\right)^2 + \alpha\left(\dfrac{\hat{\sigma}_{12}}{S^L}\right)^2 & \text{Tensile failure of matrix} \quad \text{Eq.2.39} \\[3ex]
F_m^c = \left(\dfrac{\hat{\sigma}_{22}}{2S^T}\right)^2 + \left[\left(\dfrac{Y^C}{2S^T}\right)^2 - 1\right]\left(\dfrac{\hat{\sigma}_{22}}{Y^C}\right) + \left(\dfrac{\hat{\sigma}_{12}}{S^L}\right)^2 &
\end{cases}
$$

Compression failure of matrix Eq.2.40

where X^T and Y^T are the tensile strength of timber along the grains and perpendicular to grains, respectively, X^c and Y^c are the compressive strength of timber along the grains and perpendicular to grains, respectively, S^L and S^T represents the shear strength along the grain and perpendicular to grains, respectively, and α is a coefficient that determines the contribution of the shear stress to the fibre tensile initiation criterion.

The effective stress vector $\hat{\sigma} = \left[\hat{\sigma}_{11}, \hat{\sigma}_{22}, \hat{\sigma}_{12}\right]^T$ is related to stress vector $\sigma = \left[\sigma_{11}, \sigma_{22}, \sigma_{12}\right]^T$ by $\hat{\sigma} = \omega\sigma$ in which:

$$\omega = \begin{bmatrix} \dfrac{1}{1-\omega_f} & 0 & 0 \\ 0 & \dfrac{1}{1-\omega_m} & 0 \\ 0 & 0 & \dfrac{1}{1-\omega_s} \end{bmatrix}$$

where ω_f and ω_m are scalar damage variables along the grains and perpendicular to grains, respectively, and ω_s is shear damage variable expressed as a function of ω_f and ω_m (ABAQUS 2011; Hashin 1980).

However, in this research project, the effect of features influencing perpendicular to grain behaviour is considered to be negligible because there are no defects (such as hole or notch) or connections along the length of LVL modules (see chapter 3 and 5) and the behaviour of LVL beams is dominated by bending in the longitudinal direction (see the experimental results in chapter 5). Therefore, a uniaxial material model can well describe the behaviour of the beams tested in this project. The available uniaxial material model in ANSYS (ANSYS 2013) is a model which is capable of defining the state of stress of materials with different behaviour in tension and compression. The model is isotropic elastic with the same elastic behaviour in tension and compression. The yield strength and isotropic hardening behaviour may be different in tension and in compression. Different yield criteria are used for tension and compression. A composite yield surface is used to model different yield behaviour in tension and compression. The tension behaviour is pressure-dependent and the Rankine maximum stress criterion is used as follows (ANSYS 2013):

$$f_t(\sigma, \sigma_y^t) = \frac{2}{3}\cos(\beta)\sigma_e + \frac{1}{3}trace(\sigma) - \sigma_y^t = 0 \qquad\qquad \text{Eq.2.41}$$

Where σ_y^t is the uniaxial tensile yield stress, and β is the load angle:

$$\beta(J_2, J_3) = -\frac{1}{3}\sin^{-1}\left(\frac{3\sqrt{3}J_3}{2J_2^{3/2}}\right) \qquad\qquad \text{Eq.2.42}$$

Where J_2 and J_3 are the stress invariants:

$$J_2 = \frac{1}{2} s : s \quad , \quad J_3 = \det(s)$$ Where s is the deviatoric stress.

In compression, the pressure-independent von Mises yield criterion is used. The von Mises yield criterion is commonly used in plasticity models for a wide range of materials. The criterion is isotropic and independent of hydrostatic pressure. The von Mises yield criteria is:

$$f_c(\sigma, \sigma^c{}_y) = \sigma_e - \sigma^c{}_y = 0 \tag{Eq.2.43}$$

Where σ_e is the von Mises effective stress, also known as the von Mises equivalent stress:

$$\sigma_e = \sqrt{\frac{3}{2}\left(\sigma : \sigma - \frac{1}{3} tr(\sigma)^2\right)} \tag{Eq.2.44}$$

And $\sigma^c{}_y$ is the yield strength and corresponds to the yield in uniaxial stress loading.

In principal stress space, the yield surface is a cylinder with the axis along the hydrostatic line $\sigma_1 = \sigma_2 = \sigma_3$ and gives a yield criterion that is independent of the hydrostatic stress, as shown in the Figure 2.17:
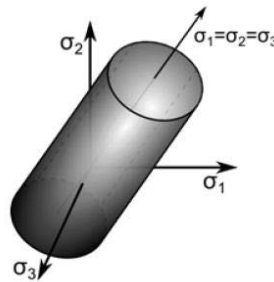
Figure 2.17 Yield Surface for von Mises Yield Criterion

More details about the uniaxial material model and the yield surfaces are presented in chapter 7.

There are several failure criteria and material models for wood based materials such as LVL, however they are usually used for research purposes only and are very difficult to be used in practical design, simply because of too many input parameters and

limitations, and there is a need for a simplified material model and a simplified constitutive law (especially when the behaviour of beams are dominated by bending in the longitudinal direction) which can adequately capture the behaviour and the failure of LVL.

2.7   Long Span Timber Floors

There are many long span (more than 6m) floor systems available in the industry and some of them are presented in this section.

The Finnjoist (FJI) is a well-known I joist which consists of the Kerto flange and high quality OSB3 web. Finnjoist I beams makes a strong, stable and lightweight floor system with quick and easy installation and fast erection (Figure 2.18). Finnjoists are the first product on the market to gain the European Technical Approval (ETA). The standard Finnjoist sizes are illustrated in Figure 2.18b. term deflections, respectively (Finnforest 2010a). SoundBar® system is an acoustic floor solution for compartment floors with utilizing Finnjoist as its structural loadbearing part (Finnforest 2010b).

(a)
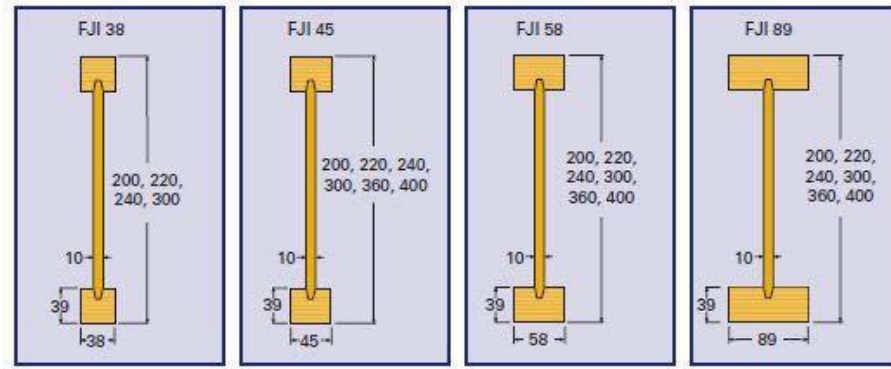
(b)

Figure 2.18:Finnjoist® Systems (a) I beams (Finnforest 2010a), (b) standard Finnjoist sizes(Finnforest 2010a)

Table 2.2 presents the load bearing capacity of the system under 1.5 kPa superimposed action and 0.8 kN/m. Finnjoists floor system provides a lowest natural frequency of more than 8Hz with a maximum deflection of L/350 and L/250 for short term and long TECBEAM beam joists, is a composite structural beam (manufactured in Australia) consisting of a continuous, light gauge galvanised steel plate web, with press formed stiffening ribs and uniformly spaced service (Figure 2.19). Most services can be installed through these web holes, including air conditioning ducts and large waste pipes. The structural timber flanges are fixed by nails and/or spikes to each side of the continuous steel web and they are made of MGP10, MGP12 or LVL13 (*Tecbeam* 2010). Table 2.2 presents the load bearing capacity of the system under 3 kPa superimposed action.

Figure 2.19:Tecbeam system (*Tecbeam* 2010)

There are many I joist systems available in Australia and New Zeeland (with similar features to Tecbeams or Finnjoist, and with similar structural performance) such as TECslab® (Figure 2.20a), HyJOIST® (Figure 2.20b), SmartJoist (Figure 2.20c), and Lumberworx® (Figure 2.20d). Table 2.2 presents a typical the load bearing capacity of these systems under different superimposed actions. The details of the load bearing behaviour and the other characterises of these systems are provided by their manufacturer.
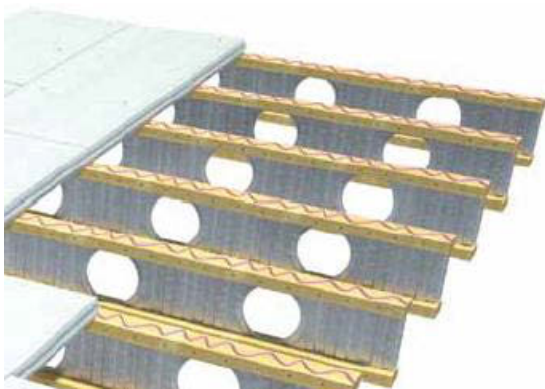
(a)   (b)

(c)   (d)

Figure 2.20 I joist systems (a) TECslab® (2013), (b) HyJoist® (2013), (C) SmartJoist (2013) and (d) Lumberworx® (2013)

Truss systems can also act as the load bearing joist beams. There are a number of products available worldwide such as GITTERBJELKER from Norway (Figure 2.21a),

Pryda from Australia and New Zealand (Figure 2.21b) and Posi-STRUT^{TM} which is a product of UK. The structural details of these systems are provided by their manufacturer and Table 2.2 presents a typical load bearing capacity of these systems under different superimposed actions. GITTERBJELKER for example, is a truss beams made of structural timber members with punched metal plate fasteners (Figure 2.21). Depending on the project, the dimensions of beams can vary from case to case but a common dimension is 148 mm x 48 mm (flat wise) and depths of the beams can vary from 400 mm up to 1,200 mm (Paevere & Mackenzie 2006). This system can provide a high quality floor, good sound insulation and high fire resistance (REI60). The elements of the floor can be pre-fabricated and the truss webs can provide proper locations for the services and plumbing and wiring. (Paevere & Mackenzie 2006).

(a)   (b)

Figure 2.21: Truss Systems (a) Gitterbjelker System (2013), (b) Pryda (2013)

In General, the joist floor systems are light weight, low cost and easy to construct. However, they show poor performance in terms of vibration and deflection. Excessive deflection and vibrations are usually observed in medium to large spans (spans exceeding 4.5-5.5m), and also an effective level of acoustic performance is hard to achieve with using only wood based floor panels (Crews et al. 2007).

To address the deficiencies and limitations of the joist floor system, other innovative floor systems such as stressed skin panels are developed.Finnforest is a well-known manufacturer of Stressed Skin Panels, the Kerto-Ripa®. All structural details such as the load bearing behaviour and the fire resistance of the system are provided by the

manufacturer (Finnforest 2010c) . They can be produced as a T section SSP or a box section SSP (Figure 2.22). The top and/or bottom skins are rigidly glued to the ribs to make a T and/or I composite cross section in order to increase the stiffness of the system. The skins are made from Kerto-Q panels whereas the ribs are made from Kerto-S. The depth of the standard element items are 200-500 mm. Based on 2.5 kN/m^2 permanent action and 3 kN/m^2 superimposed action, the system can have a maximum span of 8m and 9m for the depth of 500 mm and 550 mm, respectively. Table 2.2 presents a typical load bearing capacity of this system. They can have a diaphragm action, short installation time, enough room for the services such as plumbing and acoustic materials, high load bearing and fire resistance behaviour. (Finnforest 2010b)
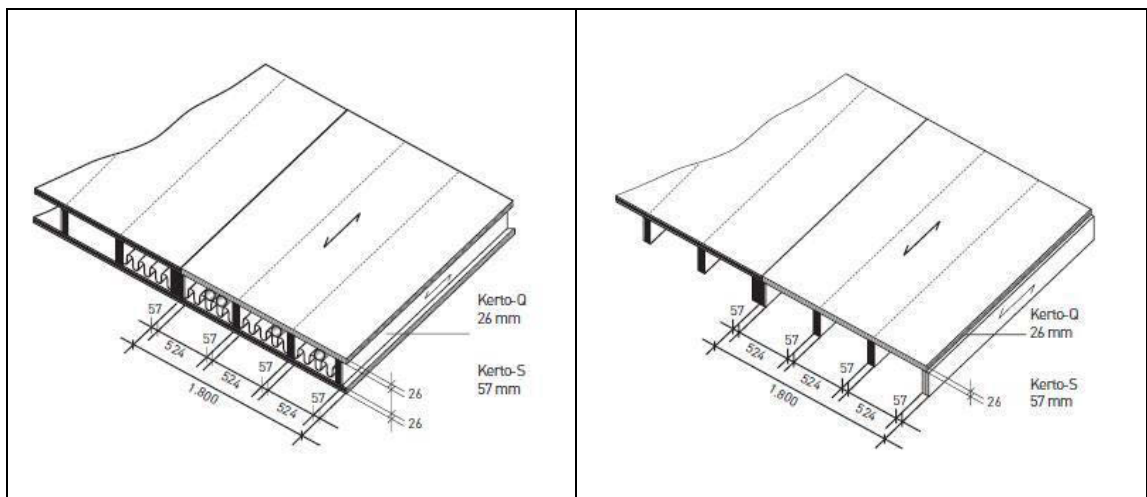
Figure 2.22 Kerto-Ripa®, T section and Box section SSPs

In Eindhoven (TU/e) and SHR Timber Research in the Netherlands, a research on design of an "upside-down" SSP system has been undertaken. All dimensions of the floor system are illustrated in Figure 2.23. This SSP system can be used in residential and commercial constructions, and it is also designed to be suitable for all types of use in high-rise structures whether concrete, steel or wood (Jorissen 2006; Koop 2005). The system is made up of glued laminated timber joists with LVL-Q bottom plate. During normal use, the "covering floor" load is transferred to the upside down T beams. The modal mass of one floor element is about 1,400 kg which results in f_e = 8 Hz and puts the floor in comfort class D (Jorissen 2006).
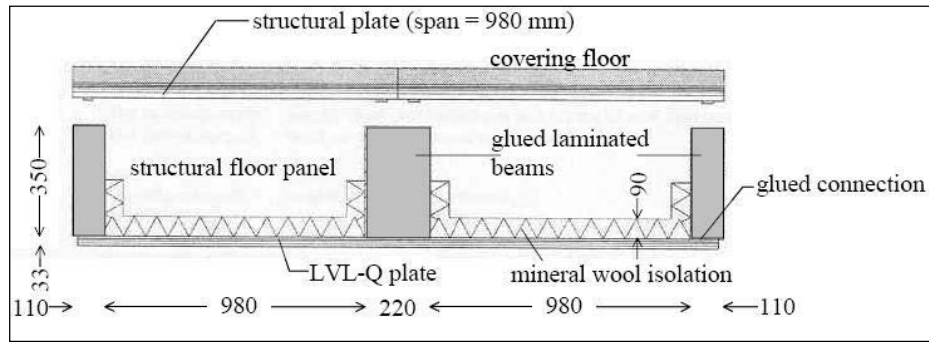
Figure 2.23 Cross section of the floor elements (André Jorissen 2006)

In September 2007, Potius Building Systems Ltd started developing a structural floor and roof system in New Zealand (Potius[TM] 2010). They use locally grown pine to make the LVL to make structural panels. The LVL panels are glued together using the adhesives to make Potius floor system (Figure 2.24). Structural floor panels can span up to 8m with 2.5 kPa superimposed actions, and the roof span panels can go up to 11m.
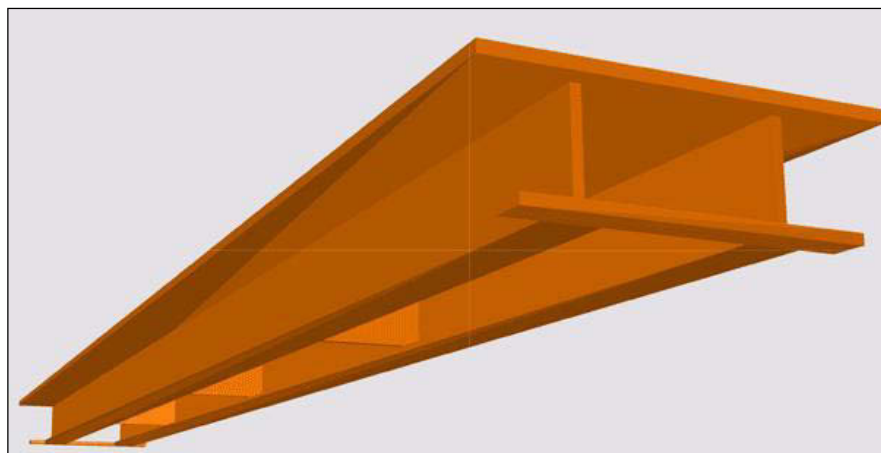
Figure 2.24 Potius floor system (Potius[TM] 2010)

SST systems are light weight, easy to construct and fast to erect. However, they are still prone to excessive vibrations for long-span floors and also cannot provide an effective acoustic separation.

Lignatur is a product of Germany and Switzerland which can be used in floor and roof systems. They are factory fabricated and all the design details such as load bearing behaviour, fire rating and the level of sound and thermal insulation are provided by the

manufacturer. Lignatur is one of the manufacturer's products which satisfy all the design criteria and comfort criteria (mainly acoustic insulation), with the aim of gaining back the market of timber floor systems after world war II. Lignatur can be manufactured in three elements, Lignatur box beam elements (Figure 2.25a), Lignatur surface elements (Figure 2.25b) and Lignatur shell elements (Figure 2.25c).

(a)

(b)

(c)

Figure 2.25 Lignatur flooring systems, (a) box beam elements, (b)surface beam elements, (c) shell beam elements

The Lignatur box elements with the web dimension of 200 mm and a length up to 12m can be manufactured in different heights (120 mm up to 320 mm). They can be used for floors and roofs with a fire protection of REI60. Lignatur surface elements can also be

manufactured in different heights (120 mm up to 320 mm) with standard width of 514 mm and 1,000 mm and maximum length of up to 16m. They can provide a fire protection up to REI90. Lignatur shell elements can be provided in 514 mm and 1,000 mm widths, with a length of up to 12 m and standard heights of 200 mm and 240 mm. They can provide fire protection of up to REI30. All the technical details are provide by the manufacturer (Lignatur 2010). Table 2.2 presents a typical load bearing capacity of this system.

KLH floor system is a panel shape floor which is made from cross-laminated timber. KLH is produced from spruce strips that are stacked crosswise on top of each other and glued to each other (Figure 2.26). The crosswise arrangement of lamellas reduces the swelling and shrinkage to a minimum, and increases the static strength and shape retention considerably. They can provide a maximum span length up to 16.50 m, maximum width up to 2.95 m and maximum depth of 0.50 m (Massiveholz KLH 2010). This system is used in many projects such as the well-known 9 storey residential building in Hackney, London. Table 2.2 presents a typical load bearing capacity of KLH floor panels.

Figure 2.26 (KLH) Cross-laminated timber panels

There are other manufacturers which produce CLT panels with similar properties to KLH such as Finnforest (Finnforest 2010d), Moelven (Moelven 2010), MHM (MHM 2010) and KAUFMANN (KAUFMANN 2010), and the technical information about the properties of CLT are provided by the manufacturers. Table 2.2 presents the load bearing capacity of the floor systems described in this section.
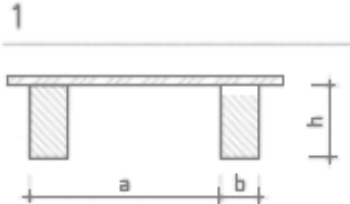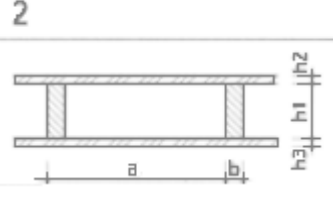
Table 2.2 Load bearing capacity of floor systems

*The deflection limits are in the range of L/400 to L/300 (L is the span of the systems)

Floor type	Section (dimensions in mm)	Load		Span (m)
		Superimposed action	Permanent load	
Finnjoist®	Joist depth: 400mm Flange Width: 89mm joist spacing :400mm	1.5 (kPa) (for residential applications)	0.8 kN/m	7.0
TECBEAM	Joist depth: 345mm Flange Width: 71mm joist spacing :400mm	3.0 (kPa)	Joist self-weight	7.50
HyJoist®	Joist depth: 400mm Flange Width: 90mm joist spacing :450mm	1.5 (kPa) (for residential applications)	Joist self-weight	7.2
Lumberworx®	Joist depth: 360mm Flange Width: 88mm joist spacing :400mm	1.5 (kPa) (for residential applications)	40 (kg/m^2)	6.6
TECSLAB™	Joist depth: 354mm Flange Width: 71mm joist spacing :400mm	2.0(kPa)	1.0(kPa) and Joist self-weight	7.3
PRYDA	Joist depth: 420mm Flange Width: 90mm joist spacing :400mm	3.0 (kPa)	0.8(kPa) and self-weight	6.6
Posi-STRUT	Joist depth: 413mm Flange Width: 140mm joist spacing :400mm	3.0 (kPa)	Joist self-weight	6.2
Kerto-Ripa® (Box sections)	Joist depth: 300mm Flange depth: 26mm joist spacing :400mm	3 kPa	1kPa and self-weight	7.9m
Lignatur	Section depth: 320mm	3 kPa	1kPa and self-weight	8.2m
KLH (CLT panels)	Panel depth :230mm	3 kPa	1kPa and self-weight	8m

Below is a summary of the possible dimensions of different floor systems suggested by Kolb (2008) for superimposed action of 3kPa (for non-residential buildings), 1.8 kPa permanent load and the self-weight. The maximum deflection is limited to l/500 (L is the span of the systems). Also, the advantages and disadvantages of each system is summarised in the table.

Table 2.3 Comparison between timber floor systems

 Span = 7.5 m a=500 mm , b=160, h=400 mm Timber joist grade C24/GL24	Joist floor systems: They are light weight, low cost, easy to construct and easy to adapt to various levels building functions. However, They have limited load carrying capacity and are limited in size and quality. They show poor performance in vibration, deflection and acoustic separation.
 Span=7.5m a=500 mm, b=80 mm,h_1=360, h_2=27, h_3=27 Stringers of grade C24/GL24 Sheathings made of plywood	Stressed Skin Panel : They are structurally very efficient (can provide the best use of material) and they are structurally very sound. They provide higher stiffness and load bearing capacity than the conventional joist floor systems and they allow various degrees of prefabrication. They are still prone to excessive deflection and vibrations for long spans and they have poor acoustic performance.
 Edge fixed floor elements made from dowelled, nailed or glued sections, Elements are 1,000 mm wide. **Span=6m** h= 240 mm	Plate floor systems: They are fast to erect and problems such as ineffective acoustic performance and excessive deflections and vibrations can be addressed by using slabs of sufficient thickness. However, the high timber consumption may make the system less convenient or cost effective compared with traditional reinforced concrete floors, and also in comparison to the large quantity of wood required for this system, the load-carrying capacity is moderate. Moreover, the problems such as high shrinkage and swelling effects must also be considered.

	Timber-Concrete composite systems:
 Timber-Concrete composite systems: **Span=7.5m** h_1=160 mm, h_2=140 mm	They can provide an improved strength and stiffness, more thermal mass and better acoustic separation, and the system is also less susceptible to vibration. They are not as easy and fast to be prefabricated and erected as the "timber only" systems. The shear connector needs to be accurately designed.

For the proposed section to be tested in this research, LVL is utilized as the only wood-based material of the section. The reason for utilizing LVL in this study (and not other alternatives such as CLT) is the ready availability of LVL in Australia and New-Zealand and its inherent reliability as a structural material, whereas alternative structural products such as Cross Laminated Timber (CLT) is not as readily available in Australia and New-Zealand. CarterHoltHarvey (2013) is the supplier of LVL for this project.

Floor systems with I or box shape (composite I beams, composite box beams, SSP systems) are structurally very efficient as the flanges are commonly designed to provide the moment capacity of the beam and the webs to predominantly carry the shear force. They have a high stiffness and can carry a high load for a minimum self-weight, and they allow various degrees of prefabrication which leads to less on-site work. In general, box beams provide a higher stiffness and load bearing capacity than I beams and they can provide a ready-to-use platform for the subsequent stages of the building construction. However, if there is a void between flanges, the insulations and other services can be fit into it and it is beneficial. With considering the above factors, Figure 2.27 schematically shows the proposed section to be investigated in this research. The proposed section was investigated in this study to provide a "safe" solution for a long span floor system for non-residential applications which can meet short term and long term design criteria and was used to develop a parametric model that would permit optimisation for design purposes. Therefore, development of an optimised section was not an objective to be tested in this research project. However, optimising the proposed section by changing the spacing between webs or changing the width of the top and bottom flanges, or changing the material properties can be easily done through the verified FE model (please chapter 7 of the thesis), whilst minimising the need for additional costly experiments.
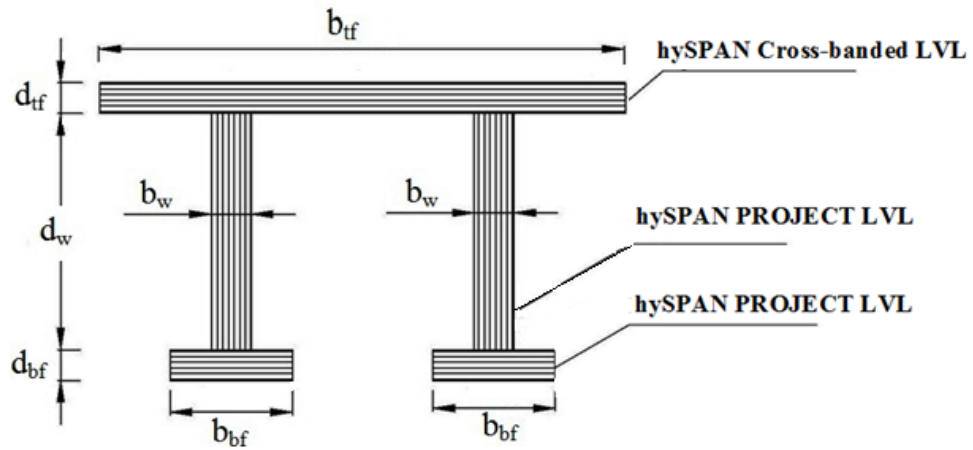
Figure 2.27 The proposed section for the experimental and analytical investigation

The dimensions and design of the system were based on 1 kPa permanent action and 3 kPa imposed action for non-residential buildings (AS/NZ 1170.1:2002) and the long term and short term deflection limits of span/400 and span/300, respectively (AS/NZS 1720.1) and to negate any shear lag in the system. 3kPa was chosen from Tables 3.1 of AS/NZS 1170.1(2002) for non-residential applications such as classrooms, lecture theatres, laboratories, offices for general use, laundries, utility rooms, commercial/institutional kitchen, etc. The details of the design check requirements of the system are presented in the following chapter.

University of Technology, Sydney

CHAPTER 3

THE PROPOSED TIMBER FLOOR SYSTEM

3 THE PROPOSED TIMBER FLOOR SYSTEM

3.1 Introduction

In this chapter the long span timber floor system for non-residential/commercial buildings is introduced and its properties and advantages are assessed. The reasons of "why this system?" are described; and the details of the system, including the material properties, the geometry and its fabrication process are specified. The serviceability and ultimate design criteria including the maximum deflection limits, the bending stress, axial stress, the flexural shear stress and the shear capacity of the interfaces are thoroughly investigated. Finally, the static and dynamic responses of the system are analytically predicted at serviceability and ultimate limit state and all the calculations and results are reported in this chapter.

3.2 The Proposed Long Span Timber Floor Modules

The most common types of sections with low structural depth while being structurally sound are the composite I and composite box beams (Porteous and Kermani 2007). They have a high stiffness and can carry a high load for a minimum self-weight. Moreover, they can provide a void between flanges so that the insulations as well as some other services (plumbing and wiring) can be installed into the floor system. In the previous chapter the performance requirement of timber floors are investigated, and the advantages and disadvantages of them were reviewed. Also, one system was proposed to provide a "safe" solution for a long span floor system for non-residential applications which can meet short term and long term design criteria and could be used to develop a parametric model that would permit optimisation for design purposes.

The dimensions of the system was designed and fabricated with the span of 6m and 8m and they were planned to be subjected to a number of destructive and non-destructive tests. Laminated Veneer Lumber (LVL) was used as the only structural material for the 6m and 8m timber modules. The main reason for utilizing LVL in this study is the ready availability of LVL in Australia and New-Zealand and its inherent reliability as a structural material, whereas alternative structural products such as glue laminated

timber or Cross Laminated Timber (CLT) are not as readily available in Australia and New-Zealand. The dimensions and design of the system were based on 1 kPa permanent action and 3 kPa imposed action for non-residential buildings (AS/NZ 1170.1:2002) and the long term and short term deflection limits of span/400 and span/300, respectively (AS/NZS 1720.1). 3kPa was chosen from Tables 3.1 of AS/NZS 1170.1(2002) for non-residential applications such as classrooms, lecture theatres, laboratories, offices for general use, laundries, utility rooms, commercial/institutional kitchen, etc. The proposed section was investigated to be a safe answer for a wide range of non-residential applications which can meet short term and long term design criteria. Optimising the proposed section by changing the spacing between webs or changing the width of the top and bottom flanges can be easily done through the verified FE model (please chapter 7 of the thesis), whilst minimising the need for additional costly experiments.

The details of the design of the system are presented in the following section. Figure 3.1 and Figure 3.2 show the cross-sectional dimensions of the 8m and 6m span modules, respectively.
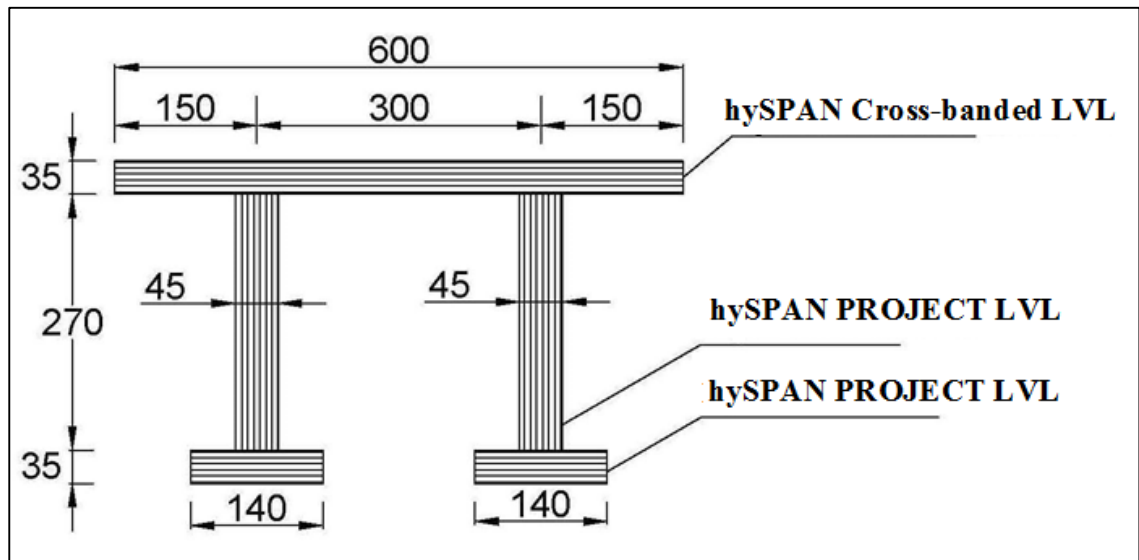
Figure 3.1 Dimensions of 8m modules
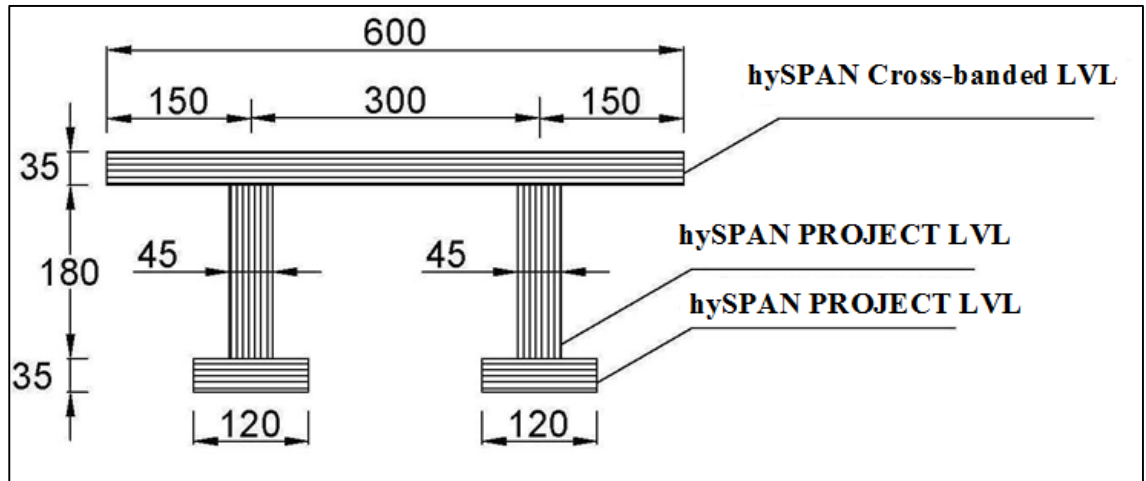
Figure 3.2 Dimensions of 6m modules

For 6m span modules, the top flange was 600 mm wide and 35mm deep, while the bottom flanges has a width of 120 mm and a depth of 35 mm. The webs were 180 mm deep with the widths of 45 mm. The 8m span modules had an identical top flange to the 6 m span beams, however; the bottom flanges were 140 mm wide and the webs were 270 mm deep with 45mm thickness. The bond between flanges and the webs for all modules was provided by the glue and screws. Type 17 normal screws were used for the interfaces where the dimensions are shown in Figure 3.3.
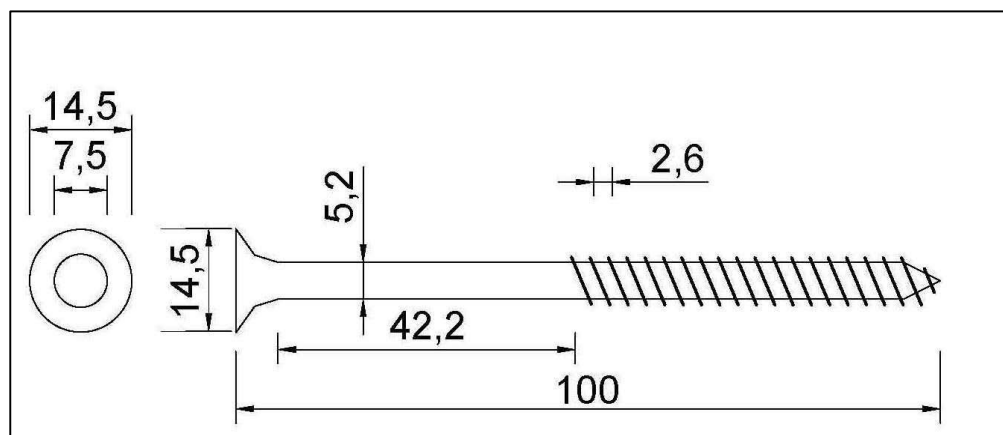
Figure 3.3 The Dimensions of the type 17 normal screws

The screws were installed at nominal 400mm spacing on each web (at an equal spacing of 375mm and 385mm for 6 m and 8 m span beams, respectively) and their role was to help the glue to set properly, while the actual bond between the flanges and the webs is provided by the glue. The type of adhesive used in gluing flanges and webs together is PURBOND, a polyurethane adhesive which can provide a structural bond between the flanges and the webs. PURBOND is a single pot adhesive so that doesn't require mixing, whereas other types of adhesives such as resorcinol are a two part mix, which can result in significant wastage as it can set prematurely due to the start/stop nature of the fabrication process. The bond between the flanges and the webs is assumed to be fully composite – an assumption which was to be investigated during the experimental testing.

The two types of LVL (hySPAN Cross-banded LVL and hySPAN PROJECT LVL), which form the structural section of the modules, were supplies by CHH (CarterHoltHarvey 2010) and Table 3.1 shows the material properties which is provided by the manufacturer. In the next chapter (chapter 4), the properties and the behaviour of two types of LVL is investigated in depth, however in this chapter the values of Table 3.1 is used to predict the response of the system.

Table 3.1 The Properties of LVL provided by the manufacturer CHH

Brand	Characteristic Strength MPa				Modulus of Elasticity MPa (E)	Modulus of Rigidity MPa (G_s)
	Bending $(f'_b)^1$	Tension Parallel to Grain $(f'_t)^2$	Shear in Beams (f'_s)	Compression Parallel to Grain (f'_c)		
hySPAN	$(50)(95/d)^{0.154}$	25	4.6	42	13200	660
hySpan+F17	$(50)(95/d)^{0.154}$	25	4.6	42	14000	700

1. f'_b is the design characteristic value in bending for beams of depth d(mm) where d>95mm, for depth less than 95mm f'_b=50MPa

2. The tension strength above applied for tension members with depth d(mm) not greater than 150mm .for depth greater 150mm the design characteristic values are obtained by multiplying $(150/d)^{0.167}$ where d is the largest dimension of the cross section

In summary, some of the key features of the proposed system are as follows:

• Significant low structural depth while being structurally very sound.

- Can provide a void between flanges in order to fit the insulations and other services.

- Can be prefabricated so they can be under high quality controlled processes.

- Can provide good vibration performance (Rijal 2013).

- Has high stiffness to weight ratio

- Non-structural layers (such as concrete topping) can be applied on top or bottom of system, in case of special dynamic performance or fire resistance requirements

3.3   Serviceability and Ultimate Design Criteria

As mentioned in previous section, the bond between the flanges and the webs is assumed to be fully composite with no slip at the interfaces, and this assumption was investigated during the experimental study in chapter 5. Therefore, to get the predicted serviceability and ultimate response of system, the "transformed section method" is used for calculation of the effective cross-section characteristics of the LVL modules. In this method the timber cross-section can be can be represented by a transformed section based on the modulus of elasticity of the LVL presented in Table 3.1. This method is also in compliance with the current design codes and practices in Australia.

3.3.1   Design Requirement and Procedure

The structural design of LVL modules must satisfy the strength (normative) and serviceability (advisory or informative) limit states requirements. Table 3.2 and Table 3.3 summarise the load combination and the deflection limit, for serviceability and ultimate limit state design criteria, respectively. Load type and intensity, load combinations and modification factors for both the serviceability and the ultimate limit states are in accordance to the AS/NZS 1170.0 (2002).

Table 3.2 Load combinations and deflection limit for serviceability limit state design

Serviceability limit state		
Load combination		Deflection Criteria
1.SLS combination: G	self-weight & permanent loading	Span/400
2.SLS combination: G+Q	imposed loading (instantaneous)	Span/300
3.SLS combination: G+ 0.7Q	imposed loading (short-term)	Span/300
4.SLS combination: G+0.4Q	imposed loading (long-term)	Span/400
5. SLS combination: 1.0 kN	imposed *impact* loading (vibration)	1mm-2mm

Table 3.3 Load combinations for ultimate limit state design

Ultimate limit state	
Load combination	
1.ULS combination: 1.35G	self-weight & permanent loading(permanent)
2.ULS combination: $1.2G + (1.5\Psi) Q$ $\Psi=0.4$	imposed loading (long-term)
3.ULS combination: 1.2G + 1.5Q	imposed loading (short-term)

Therefore, the serviceability and ultimate design requirement for LVL floor system are as follows:

- Short-term serviceability limit state which corresponds to the instantaneous response of the structure to an imposed load.

- Long-term serviceability limit state which corresponds to the service life behaviour of the system and the time-dependent variations of the material properties; in particular creep.

- Short-term ultimate limit state which identifies the short term reaction of the structure to the maximum load.

- Long-term ultimate limit state which corresponds to the response of the structure to a quasi permanent loading to avoid failure due to long term deflection of the timber member in particular.

- 1.0-kN serviceability limit state which represents the dynamic behaviour of the system and corresponds to the instantaneous response of the structure to an imposed load of 1.0 kN at mid-span

- Additional design criteria include fire resistance requirement, special dynamic performance requirement and acoustic performance requirements

The first step in design procedure of LVL modules is to identify the cross-sectional characteristics of the system. As mentioned previously, the effective (apparent) stiffness of the cross-section is calculated using transformed section method. Figure 3.4a shows the dimension of the section and Figure 3.4b show the dimensions of the equivalent transformed section.

As shown in Figure 3.4b, the timber cross-section is represented by an equivalent section, in which the modulus of elasticity of the entire section is the same as for top flange while the webs and bottom flanges widths are transformed into the equivalent widths based on the modular ratios, n_w and n_{bf}, respectively. The calculation of modular ratios is in shown Table 3.4. Moreover, Table 3.4 and Equation 3.1 show the procedure to calculate the neutral axis of the LVL floor module ($\bar{y}_c$) step by step. $\bar{y}_c$ is calculated from the bottom flange. The second moment of area for the webs (I_w), top flange (I_{tf}) and bottom flanges (I_{bf}) are calculated about the neutral axis (Table 3.5) and Equations 3.2 and 3.3 shows the final calculation for moment of area $(I)_{eff}$ and the effective flexural stiffness $(EI)_{eff}$, respectively.

As calculated in Tables 3.4 and 3.5 , $\bar{y}_{tf}$, $\bar{y}_w$ and $\bar{y}_{bf}$ represent the location of centroid of top flange, webs and bottom flanges from the base of the cross section, respectively. h_{tf}, h_w and h_{bf} represent the distance between the neutral axis of the cross section and the centroid of top flange, webs and botom flanges, respectively
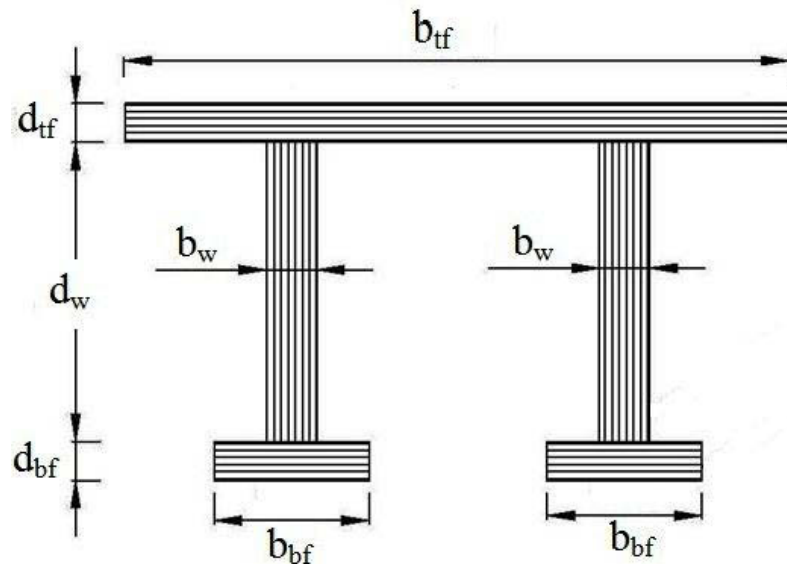
(a)
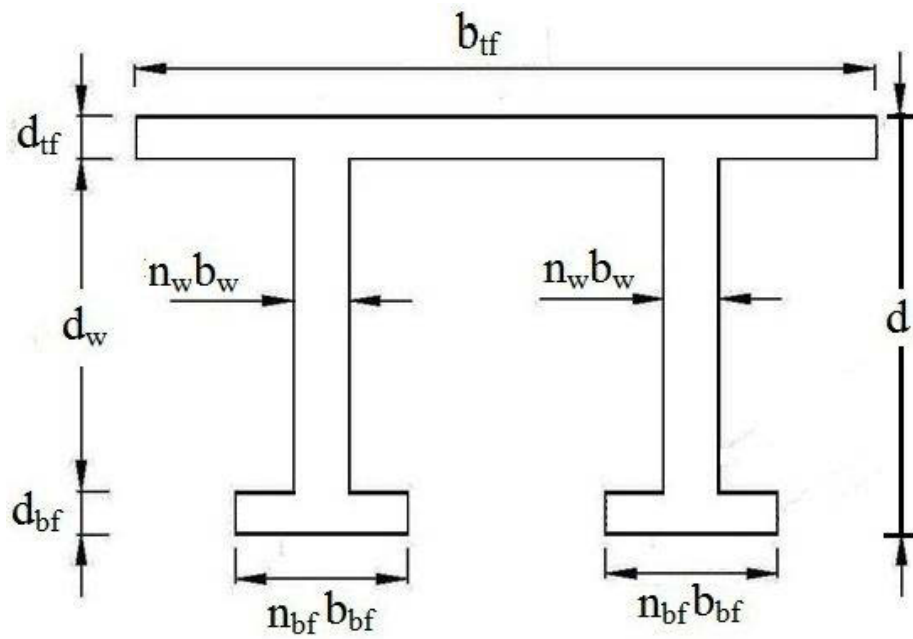
(b)

Figure 3.4 Geometry of timber floor module (a) Cross-section geometry, (b) Transformed cross-section geometry

Table 3.4 Calculation of neutral axis in step by step procedure

Calculating of Neutral Axis Location					
	Step 1	Step 2	Step 3	Step 4	Step 5
	MOE (Mpa)	n (modular ratios)	A (area)	$\bar{y}$ (mm)	$A_* \bar{y}$
Top Flange	E_{tf}	$n_{tf}=1$	$A_{tf}=(n_{tf})(b_{tf})(d_{tf})$	$\bar{y}_{tf}=d_{bf}+d_w+(d_{tf}/2)$	$(A_{tf})(\bar{y}_{tf})$
Webs	E_w	$n_w=E_w/E_{tf}$	$A_w=(n_w)(2b_w)(d_w)$	$\bar{y}_w=d_{bf}+(d_w/2)$	$(A_w)(\bar{y}_w)$
Bottom Flanges	E_{bf}	$n_{bf}=E_{bf}/E_{tf}$	$A_{bf}=(n_{bf})(2b_{bf})(d_{bf})$	$\bar{y}_{bf}=d_{bf}/2$	$(A_{bf})(\bar{y}_{bf})$

$$\bar{y}_c = (A_{tf}\,\bar{y}_{tf} + A_w\,\bar{y}_w + A_{bf}\,\bar{y}_{bf})/(A_{tf}+A_w+A_{bf}) \qquad \text{Eq.3.1}$$

Table 3.5 Calculation of the effective flexural stiffness in step by step procedure

Calculating the I and EI			
	Step 1	Step 2	Step 3
	I	h	$I+Ah^2$
Top Flange	$I_{tf}=(n_{tf})(b_{tf})(d_{tf}^3)/12$	$h_{tf}=d_{bf}+d_w+(d_{tf}/2)-\bar{y}_c$	$I_{tf}+A_{tf}\,h^2_{tf}$
Webs	$I_w=(n_w)(2b_w)(d_w^3)/12$	$h_w=\bar{y}_c-d_{bf}+(d_w/2)$	$I_w+A_w\,h^2_w$
Bottom Flanges	$I_{bf}=(n_{bf})(2b_{bf})(d_{bf}^3)/12$	$h_{bf}=\bar{y}_c-(d_{bf}/2)$	$I_{bf}+A_{bf}\,h^2_{bf}$

$$I_{eff} = I_{tf} + A_{tf}h_{tf}^2 + I_w + A_w h_w^2 + I_{bf} + A_{bf}h_{bf}^2 \qquad \text{Eq.3.2}$$

$$(EI)_{eff} = E_{tf}I_{eff} \qquad \text{Eq.3.3}$$

Where I_{eff} is the moment of area, and $(EI)_{eff}$ is the effective flexural stiffness of the floor modules. The effective flexural stiffness will be used for calculating the mid-span deflection for serviceability or deflection limit checks.

3.3.2   Serviceability – Deflection

Serviceability of the timber floor is assessed by checking the deflections against the limits defined to suit the functional requirements of the building being designed. The serviceability load combinations and deflection limits were presented in Table 3.2 in previous section. Therefore, the following serviceability checks are recommended:

- Long term deflection check as a result of self-weight and permanent loading

$$\Delta_b = \frac{5GL^4}{384(EI)_{eff}} \leq Span/400$$

Eq.3.4

- Short term deflection check as a result of short term the imposed loading

$$\Delta_b = \frac{5(G+0.7Q)L^4}{384(EI)_{eff}} \leq Span/300$$

Eq.3.5

- Long term deflection check as a result of long term the imposed loading

Eq.3.6

$$\Delta_b = \frac{5(G+0.4Q)L^4}{384(EI)_{eff}} \leq Span/400$$

- Short term deflection check as a result of impact loading (point load)

$$\Delta_{vib} = \frac{P^*L^3}{48(EI)_{eff}} \leq 1mm\ to\ 2mm$$

Eq.3.7

Equations 3.4 to 3.6 calculate the mid-span deflection under uniformly distributed load and Equation 3.7 calculates the mid span deflection under a point load (1kN), and L is the span of the modules. Other components of Equations 3.4 to 3.7 are defined in Table 3.2 and Table 3.3.

In order to consider the long term deformation of a structure to satisfy a specific serviceability limit state, an appropriate modification factor for creep (see Table 3.6) should be applied to the deformation (1720.1 (2010)). To consider the creep deformation of the LVL modules, the creep factor is applied for the portion of the serviceability load that is permanently applied (see Equation 3.8a and 3.8b).

$$\Delta_b = \frac{5(j_2 G + 0.7Q)L^4}{384(EI)_{eff}} \leq Span / 300 \qquad \text{Eq.3.8a}$$

$$\Delta_b = \frac{5 j_2 (G + 0.4Q)L^4}{384(EI)_{eff}} \leq Span / 400 \qquad \text{Eq. 3.8b}$$

Table 3.6 Recommended values of the creep factor j2 according to AS 1720.1 (2010)

Instantaneous Live load	1.0
Long-term loads for initial moisture content ≤ 15	2.0
Long-term loads for initial moisture content ≥ 25	3.0

3.3.3   Serviceability - Dynamic behaviour

Another fundamental serviceably criteria is the first natural frequency which represents the dynamic performance of the floor system. The first natural frequency of the floor systems is generally recommended to be more than 10Hz, whilst natural frequencies below 3Hz and between 5Hz to 8Hz should be avoided, in order to prevent the walking resonance and human discomfort, respectively (Hasns 1970). There are several prediction formulas proposed to calculate the first natural frequency of the structure. In this chapter the proposed formula in Eurocode 5 (EN 1995-1-1 2004+A1:2008) is used to predict the dynamic behaviour of the LVL floor modules (Eq.3.9).

$$f_1 = \frac{\pi}{2L^2} \sqrt{\frac{(EI)_{eff}}{m}} \qquad \text{Eq.3.9}$$

where f_1 is the fundamental frequency of the floor modules, $(EI)_{eff}$ is the equivalent bending stiffness of the floor modules in the perpendicular to the beam direction

(Nm^2/m), L is the floor span (m) and m is the mass per unit area (kg/m^2). The mass includes self-weight of the floor and other permanent actions, such as imposed dead load.

3.3.4 Strength of the LVL floor modules

The load combinations and factors for the ultimate limit states (ULS) were presented in Table 3.3 which is according to AS/NZS 1170.0 (2002). However, the design capacities need to be checked under flexural action and flexural and axial actions and are described in sections 3.2 and 3.5 of AS 1720.1 (2010).

3.3.4.1 Bending Strength

According to AS 1720.1 (2010), Equation 3.10 must be satisfied when the system is subjected to a combined bending and axial actions.

$$\frac{N^*}{(\phi N)} + \frac{M^*}{(\phi M)} \leq 1.0$$

Eq.3.10

Where N^* and M^* are the axial force and bending moment due to the design action and ϕN and ϕM are the axial design capacity and bending design capacity of the timber cross-section, respectively. Equation 3.10 can be rearranged in terms of the axial and bending stress (Eq.3.11). According to the fundamental theories of mechanics of solids principal theories of structural analysis, the extreme fibres at the top and bottom flanges experience the most compression and tension stresses as a result of bending and axial actions and need to be checked. Table 3.8 and Table 3.9 show the components of Equation 3.11, where the modification factors for strength (ϕ, k_1, k_4, k_6, k_9, and k_{12}) are based on AS1720.1(2010) and are introduced in Table 3.7. M* and N* are the maximum bending and axial force that are acting on the LVL modules, and h$_{tf}$ and h$_{bf}$ are the distance between the centroid of the top and bottom flange to the neutral axis, respectively (were calculated in Table 3.5). d, d_{tf} and d_{bf} are the depth of the cross section, top flange and bottom flange, respectively. y_c is the neutral axis of the section from the bottom fibre. $f'_{b,tf}$ and $f'_{b,bf}$ are the bending design capacity of the materials used for top and bottom flange, respectively whereas $f'_{c,tf}$ and $f'_{t,bf}$ are the compression and tension design capacities of the materials used for top and bottom flange,

respectively. Equation 3.11, which is inferred from Equation 3.2 (3) of AS 1720.1 (2010), must be satisfied:

$$\frac{\sigma^*_{axial}}{\phi\sigma_{axial}} + \frac{\sigma^*_{bending}}{\phi\sigma_{bending}} \leq 1$$

Eq.3.11

Table 3.7 Modification Factors

Modification Factor Symbol	Modification Factor Description
ϕ	Capacity factor as per AS1720.1 (2010)
j_2	stiffness modification factor – load duration
k_1	duration of load (timber)
k_{12}	stability factor (timber)
k_4	moisture condition (timber)
k_6	temperature (timber)
k_7	length and position of bearing (timber)
k_9	strength sharing between parallel members (timber)

Table 3.8 Axial components of Equation 3.11

Axial Stress	Axial stress due to design action (due to bending moment)	Axial stress due to design action (due to axial force)	Axial stress capacity of the timber cross-section
Top Flange	$\sigma^*_{tf,axial} = \dfrac{E_{tf}M^*}{(EI)_{eff}}h_{tf}$	$\sigma^*_{tf,axial} = \dfrac{N^*}{b_{tf}d_{tf}}$	$\phi\sigma_{tf,axial} = \phi k_1 k_4 k_6 k_{12}[f'_{c,tf}]$
Bottom Flanges	$\sigma^*_{bf,axial} = \dfrac{E_{bf}M^*}{(EI)_{eff}}h_{bf}$	$\sigma^*_{bf,axial} = \dfrac{N^*}{b_{bf}d_{bf}}$	$\phi\sigma_{bf,axial} = \phi k_1 k_4 k_6 k_{12}[f'_{t,bf}]$

Table 3.9 Bending components of Equation 3.11

Bending Stress	Stress due to design action	bending stress capacity of the timber cross-section
Top Flange	$\sigma^*_{tf,bending} = \dfrac{E_{tf}M^*}{(EI)_{eff}}(d - y_c)$	$\phi\sigma_{tf,bending} = \phi k_1 k_4 k_6 k_9 k_{12}[f'_{b,tf}]$
Bottom Flanges	$\sigma^*_{bf,bending} = \dfrac{E_{bf}M^*}{(EI)_{eff}}y_c$	$\phi\sigma_{bf,bending} = \phi k_1 k_4 k_6 k_9 k_{12}[f'_{b,bf}]$

3.3.4.2 Flexural Shear Strength

Equation 3.12 must be satisfied to check the flexural shear strength in LVL modules and to ensure a safe design:

$$\phi f_s \geq f^*_s \qquad \text{Eq.3.12}$$

Equation 3.13 shows the calculation of ϕf_s in which $f'_{s,w}$ is the shear design capacity of the material used for web which needs to be modified by the modification factors given in Equation 3.13. f^*_s on the other hand, is the shear stress due to loading which can be calculated using Equation 3.14.

$$\phi f_s = \phi k_1 k_4 k_6 [f'_{s,w}]$$

Eq.3.13

$$f^*_s = \frac{V^* Q_{max}}{I(2b_w)}$$

Eq.3.14

(V^*) is the acting shear force at the distance of 1.5d from the supports of the LVL modules and Q_{max} is the maximum fist moment of area of the LVL cross section which can be calculated by Equation 3.15.

$$Q_{max} = [n_{tf} b_{bf} d_{tf} [d - \bar{y}_c - (d_{tf}/2)]] + [n_w d_w (d - d_{tf} - \bar{y}_c)^2/2] \qquad \text{Eq.3.15}$$

3.3.4.3 Shear Strength at Glue Line

To ensure there is no failure in the glue line at the interfaces of LVL modules, the shear stress at the interfaces between top flange and the webs, and bottom flanges and webs must be checked according to Equations 3.16 and 3.17:

$$\frac{V^* Q_{tf}}{I(2b_w)} \leq \min[f'_s, f'_{s,glue}] \qquad \text{Eq.3.16}$$

$$\frac{V^* Q_{bf}}{I(2b_w)} \leq \min[f'_s, f'_{s,glue}] \qquad \text{Eq.3.17}$$

Where, Q_{tf} and Q_{bf} are first moment of areas of top and bottom flanges about the neutral axis which can be calculated by Equations 3.18 and 3.19, respectively. f'_s and $f'_{s,glue}$ are the shear design capacity LVL and glue, respectively.

$$Q_{tf} = n_{tf} b_{tf} d_{tf} [d_{bf} + d_w + (d_{tf}/2) - \bar{y}_c]$$
Eq.3.18

$$Q_{bf} = 2n_{bf} b_{bf} d_{bf} [\bar{y}_c - (d_{bf}/2)]$$
Eq.3.19

n_{tf} and n_{bf} are the modular ratios as defined in Table 3.4 and $\bar{y}_c$ is the neutral axis of the section.

3.3.4.4 Bearing Strength

The design capacity in bearing must satisfy the condition given in Equation 3.20 and 3.21:

$$(\phi N_p) \geq N_p^*$$
Eq.3.20

$$(\phi N_p) = \phi k_1 k_4 k_6 k_7 f'_p A_p$$
Eq.3.21

Where, N_p^* is the design load in bearing, f'_p is the bearing strength of the bottom flange, and A_p is the bearing area.

3.4   Analytically Predicted Response of the System

In this section the serviceability and ultimate response of the system are analytically predicted and reported. As shown in Figure 3.1 and Figure 3.2, hySPAN cross-banded LVL was used for top flange while hySPAN Project LVL was used for the web and bottom flanges. The different stages of analysis are summarised in the following sections.

3.4.1   Material Properties Input

In the next chapter (chapter 4) a comprehensive study is undertaken to investigate the material properties of LVL utilised as the structural part of the modules. However, in this chapter, the published material properties which are provided by the manufacturer

(CHH), are used for the prediction response of the system. Material Properties of the web and flanges are based on manufacturer's data are as given below:

Timber Density:	ρ = 601 kg/m^3
Top Flange Modulus of Elasticity :	E_{tf}= 10.5 GPa
Web Modulus of Elasticity :	E_w= 13.2GPa
Bottom Flange Modulus of Elasticity :	E_{bf}= 13.2 GPa
Top Flange Bending Strength :	f'$_{b,tf}$= 40MPa
Web Bending Strength :	f'$_{b,w}$= 50 MPa
Bottom Flange Bending Strength :	f'$_{b,bf}$= 50MPa
Top Flange Tension Strength (parallel to grain):	f'$_{t,tf}$ = 20 MPa
Web Tension Strength(parallel to grain):	f'$_{t,w}$= 25 MPa
Bottom Flange Tension Strength(parallel to grain):	f'$_{t,bf}$ = 25 MPa
Top Flange Compression Strength (parallel to grain):	f'$_{c,tf}$= 34 MPa
Web Compression Strength(parallel to grain):	f'$_{c,w}$ = 42 MPa
Bottom Flange Compression Strength(parallel to grain):	f'$_{c,bf}$= 42 MPa
Top Flange Shear Strength :	f'$_{s,tf}$ =4 MPa
Web Shear Strength :	$f_{s,w}$= 4.6 MPa
Bottom Flange Shear Strength :	$f_{s,bf}$ = 4.6 MPa

Note: The material properties of hySPAN PROJECT are
provided in Chh website.
 For Cross-banded LVL, 80% of the values of hySPAN
PROJECT were considered

3.4.2   Effective Bending Stiffness and the Second Moment of Inertia

The geometry of the 8m LVL modules which are based on Figure 3.1 are as given below:

Beam Span (Overall):	8.4m
Beam Span (support to support):	8m
Top Flange width:	b_{tf}= 600mm
Web Width :	b_w= 45mm
Bottom Flange width:	b_{bf}= 140mm
Joist Spacing	S=300mm
Top Flange depth:	d_{tf}= 35mm
Web depth :	d_w= 270mm
Bottom Flange depth:	d_{bf}= 35mm
Beam total depth	d=340mm

The maximum effective flange width needs to be checked to assess the shear lag and plate buckling in the section and to make sure if the entire section in contributing to the

effective bending stiffness of the timber cross-section. In order to check these considerations, it is appropriate to use EC5 (2004). In this regard Equations 3.22 and 3.23 should be satisfied:

$$Min[(b_w + 0.1L),(b_w + 20d_{bf})] = 745mm \geq S = 300mm \longrightarrow Ok$$ Eq.3.22

$$(b_w + 0.1L) = 845 \geq S = 300 \longrightarrow Ok$$ Eq.3.23

Where S is the spacing between webs. Therefore, Top and bottom flanges fully participate in carrying the load. The neutral axis, the effective bending stiffness (EI)$_{eff}$ and the second moment of area (I)$_{eff}$ are calculated according to Table 3.4 and Table 3.5 and the Equations 3.1 to 3.3, and the results are as follows:

Neutral axis: y_c = 190.7mm

I_{eff} = 9.36E+08 mm^4

$(EI)_{eff}$ = 9.8e+12 MPa.mm^4= 9832704.64 Pa.m^4

3.4.3   Loading Input

The loading input is according to AS/NZ 1170 (2002) and it includes 1kPa permanent action, 3kPa superimposed action and the self-weight. Table 3.10 shows the input loading of the LVL modules.

Table 3.10 Input loading of the LVL modules

Load Type	Loading Input
Permanent Load (allows concrete topping and the flooring)	1(kPa)(b$_{tf}$) =0.6 kN/m
Self –Weight	[(b$_{tf}$)(d$_{tf}$) + 2(b$_w$)(d$_w$) + 2(b$_{bf}$)(d$_{bf}$)] x(601 kg/m3)= 0.331 kN/m
Live Load	3(kPa)(b$_{tf}$) = 1.8 kN/m

3.4.4   Serviceability Check

The load combinations and the deflection criteria for serviceability check were presented in Table 3.2. Since the moisture of content of LVLs were less than 15% , the

creep factor (or the duration of load factor) is equal to 1 and 2 for short term and long term serviceability check, respectively (Table 3.6). Considering the effect of creep factor, the short term and long term deflection of the 8m LVL modules (Equations 3.5 and 3.6) are equal to 17mm and 18mm respectively, which are smaller than Span/300 (or 27.6mm) and Span/400 (or 20mm), respectively. The deflection check for 1kN point load (Equation 3.7) is also equal to 1mm which is smaller than the deflection limit (2mm). For the dynamic performance of the LVL modules, the first natural frequency of the system is calculated according to Equation 3.9 and it is about 13Hz which is in the safe frequency zone (more than 8Hz).

3.4.5   Strength Check

Maximum bending moment (M_d) will be at the mid-span and given by $\dfrac{wL^2}{8}$ .However, the critical section for shear will be located at a distance of 1.5d from the face of the support, and here it is conservatively given by $\dfrac{wL}{2}$. Table 3.11 shows the load combination and the maximum bending and shear force. The required modification factors are presented in Table 3.12 and Table 3.13 which are based on AS 1720.1 (2010).

Table 3.11 The maximum bending moment and shear force at ultimate limit state

	Combination		Load (kN/m)	Bending moment M^* (kNm)	Shear force V^* (kN)
1	Permanent	1.35G	1.26	10.06	5.03
2	Short Term	1.2G + 1.5Q	3.82	30.54	15.27
3	Long Term	1.2G + (1.5Ψ)Q Ψ=0.4 for office buildings	2.19	17.58	8.79

Table 3.12. The modification factors

	Φ	k_4	k_6	k_9	k_{12}
Tension	0.9	1	1	-	-
Compression	0.9	1	1	-	1

Shear	0.9	1	1	-	-
Bending	0.9	1	1	1	1

Table 3.13 k1 modification factors

	k_1	Comment
Permanent	0.57	50+ years
Long term	0.8	5 months
Short term	0.97	5 hours

With substituting the values of material properties and the dimensions of the system into Equation 3.11 (the component of Equation 3.11 are precisely described in Tables 3.8 and 3.9) and with considering the values of Table 3.11, Table 3.12 and Table 3.13, the bending strength ratio for top flange and for permanent, long term and short term loading will be 0.16, 0.20 and 0.28, respectively which are all well below a value of 1.0 and indicates a safe design. The bending strength checks for the bottom flange also ensure a safe design with 0.29, 0.35 and 0.51 strength ratio for permanent, long term and short term load combination, respectively.

As mentioned previously in section 3.3.4.2, Equation 3.12 should also be satisfied to check the flexural stiffness of the system. With using Equations 3.12 to 3.15, the values of shear stress ratio for permanent, long term and short term load combination are 0.16, 0.20 and 0.28, respectively. The shear capacity of the glue line is also checked according to Equations 3.16 to 3.19 and the results of the shear stress ratio for top and bottom flanges interfaces are reported in Table 3.14.

Table 3.14 Shear Stress ratios at the interfaces

Load-Combination Types	Top Flange Interface	Bottom Flanges Interfaces
Permanent	0.07≤1 Ok	0.06≤1 Ok
Long-Term	0.13≤1 Ok	0.10≤1 Ok
Short-Term	0.22≤1 OK	0.17≤1 Ok

The details of the calculations of stress ratios for both the strength and serviceability checks are presented in Appendix A in which, all of the calculations are reported in

detail. All the results of the checks are summarised in Tables 3.15 and 3.16 for 8m modules and 6m modules respectively.

Table 3.15 Stress ratio checks for 8m modules

Bending Strength check		
Load-Combination Types	Top Flange Interface	Bottom Flanges Interfaces
Permanent	0.16≤1 Ok	0.28≤1 Ok
Long-Term	0.20≤1 Ok	0.35≤1 Ok
Short-Term	0.28≤1 Ok	0.50≤1 Ok
Shear Strength check		
	At the glue line	
Load-Combination Types	Top Flange Interface	Bottom Flanges Interfaces	Max Flexural Shear
Permanent	0.07≤1 Ok	0.06≤1 Ok	0.16≤1 Ok
Long-Term	0.13≤1 Ok	0.10≤1 Ok	0.20≤1 Ok
Short-Term	0.22≤1 OK	0.17≤1 Ok	0.28≤1 Ok

Table 3.16 Stress ratio checks for 6m modules

Bending Strength check		
Load-Combination Types	Top Flange Interface	Bottom Flanges Interfaces
Permanent	0.24≤1 Ok	0.47≤1 Ok
Long-Term	0.30≤1 Ok	0.60≤1 Ok
Short-Term	0.44≤1 Ok	0.88≤1 Ok
Shear Strength check		
	At the glue line	
Load-Combination Types	Top Flange Interface	Bottom Flanges Interfaces	Max Flexural Shear
Permanent	0.10≤1 Ok	0.10≤1 Ok	0.22≤1 Ok
Long-Term	0.19≤1 Ok	0.14≤1 Ok	0.28≤1 Ok
Short-Term	0.33≤1 Ok	0.25≤1 Ok	0.40≤1 Ok

3.5   Conclusions

As a result of a thorough investigation on best possible options of long span timber floor systems, a number of composite cross sections were designed and proposed. After considering the cost and performance of each of them, one system was finalised and chosen to be fabricated for the extensive laboratory investigation. Laminated veneer lumber (LVL) is used as the only structural load bearing part of the system and the experimental investigation involved subjecting the LVL floor modules (6m and 8m span) to both destructive and non-destructive static loading to assess the strength and serviceability performance of the proposed system. However, in this chapter, the proposed long span timber floor system for non-residential/commercial buildings was introduced and its advantages and properties were assessed. The serviceability and ultimate design procedure of the system were investigated and all of the design criteria including the maximum deflection limits, the bending stress, the axial stress, the flexural shear stress and the shear capacity of the interfaces were evaluated. The results show that the maximum deflection of the system under serviceability loads (stiffness of the system) governs the design of the section. The first fundamental frequency of the system was also predicted to be around 13Hz which indicates a safe design. All responses of the system including the serviceability and ultimate performance and dynamic behaviour of the system were analytically calculated and reported in this chapter, and the results ensured a safe design of the proposed LVL modules.

University of Technology, Sydney

CHAPTER 4

EXPERIMENTAL AND ANALYTICAL

INVESTIGATION ON SHORT TERM

BEHAVIOUR OF LVL

4 EXPERIMENTAL AND ANALYTICAL INVESTIGATION ON SHORT TERM BEHAVIOUR OF LVL

4.1 Introduction

Prediction of the short term response of the 6m and 8m long span LVL modules and development of their preliminary FE model necessitated a thorough understanding of the behaviour of LVL. In this regard, and prior to the extensive laboratory investigation on 6m and 8m modules, the relevant characteristic properties of LVL under tension, compression and bending loads were assessed through a series of tests conducted on LVL sections.

Since the short-term and long term response of timber beams depend on the material behaviour of timber, a suitable constitutive law is also needed in order to model timber behaviour and to capture the strain-stress relationship and failure mode (s) of timber (Qudjene and Khelifa 2009). Several constitutive laws have been developed over the last three decades for modelling the behaviour of timber in 1D, 2D and 3D, where the 2D and 3D models were used in continuum-based FE model (Glos 1981; Conners and Appleton 1989; Dias 2007; Schmidt 2009). Although several criteria and material models have been developed which can be applicable to orthotropic materials such as wood, but they are very difficult to be used in practical design, simply because of too many input parameters and limitations. Therefore, there is a need for a simplified material model and a constitutive law, which can adequately capture the behaviour and the failure of wood in general, and Engineered Wood Products (EWPs) such as LVL in particular.

In this chapter the behaviour of two types of LVL, that is hySPAN cross-banded LVL and hySPAN Project LVL, are investigated through a number of experimental and analytical tests. As a result of the tension and compression tests, a suitable constitutive law is developed which can accurately capture the stress-strain relationship and the

failure behaviour of LVL, and it can also be incorporated into FE analysis of any LVL beam. A number of three point bending and four-point bending tests were conducted on LVL sections in both edge-wise and flat-wise directions. The results of the full scale four point bending tests are used to investigate the material properties of LVL and to identify the behaviour of LVL up to the failure point. Furthermore, a closed-form prediction analysis was also conducted and a comparison between the experimental results and the closed-form predicted results is undertaken and reported in this chapter.

4.2   Experimental Program

The tests conducted on hySPAN Cross-banded LVL and hySPAN PROJECT LVL (which form the structural material of 6m and 8m modules) were:

- Tension and compression strength parallel to the grain
- Bending strength (in both edge-wise and flat- wise directions)
- The flexural modulus of elasticity (MoE) (in both edge-wise and flat- wise directions)
- Axial MoE
- Flexural shear strength
- Shear modulus

The general approach for testing the mechanical properties of LVL should comply with Australasian Standard AS/NZS4063.1 (AS/NZS 4063.1 2010). The details of each test and the experimental results and observations are reported in the following sections.

4.2.1   Tension and Compression Test Specimens

In manufacturing of LVL, thin veneer layers with thickness of 3mm are peeled from logs and are bonded together with adhesives, and the entire veneer layers are generally oriented in one direction. As a result, the natural growth characteristics (or natural defects) of wood are randomised and so effectively removed and the structural properties of LVL become basically uniform alongside the section. In this study, the adopted lengths for LVL samples were 900mm and 200mm for tension and compression tests, respectively, which are shorter than what is specified for natural

wood. A total number of 36 LVL samples were tested under tension and compression load (18 tension and 18 compression tests); the dimensions as well as the number of tests for each types of LVL are summarised in Table 4.1 and Table 4.2.

The difference between the two types of LVL used in this study is that in hySpan Cross-Banded LVL two laminations (or veneers) of the cross section are running perpendicular to the longitudinal axis which enhances the load distribution capacity and LVL properties across the panel. However, in hySpan Project LVL all veneers are oriented along the longitudinal axis.

Table 4.1 Dimensions and number of samples for tension test

		Section Dimension		
Section Name	Number of tests	L (Length)	b (breadth)	d (depth)
		(mm)	(mm)	(mm)
hySpan Cross-Banded LVL (CB)35mmX90mm	6	900	35	90
hySpan Project LVL 45mmX90mm	6	900	45	90
hySpan Project LVL 35mmX90mm	6	900	35	90

Table 4.2 Dimensions and number of samples for compression test

		Section Dimension		
Section Name	Number of tests	L (Length)	b (breadth)	d (depth)
		(mm)	(mm)	(mm)
hySpan Cross-Banded LVL (CB)35mmX90mm	6	200	35	90
hySpan Project LVL 45mmX90mm	6	200	45	90
hySpan Project LVL 35mmX90mm	6	200	35	90

As shown in Table 4.1 and Table 4.2, six samples of hySpan Cross-Banded LVL with depth of 35mm and width of 90mm were tested under tension and compression loads, whereas twelve samples of hySpan Project LVL with different depths of 35mm and 45mm (6 sample of each) and width of 90mm were tested under tension and compression load. Figure 4.1 shows the dimensions and test set up for tension tests. As shown in the figure, the clear length of the specimens between grips is 500mm, while 200mm from each end is gripped, therefore, the total length of the specimens are 900mm for tension tests. However, the length of the samples for compression test is only 200mm in order to avoid any possible buckling under compression load (Figure 4.2). One or two strain gauges are attached at the centre of the test pieces to measure the strain responses verses load, and the axial load (compression or tension load) was applied at a uniform load rate until failure occurred.
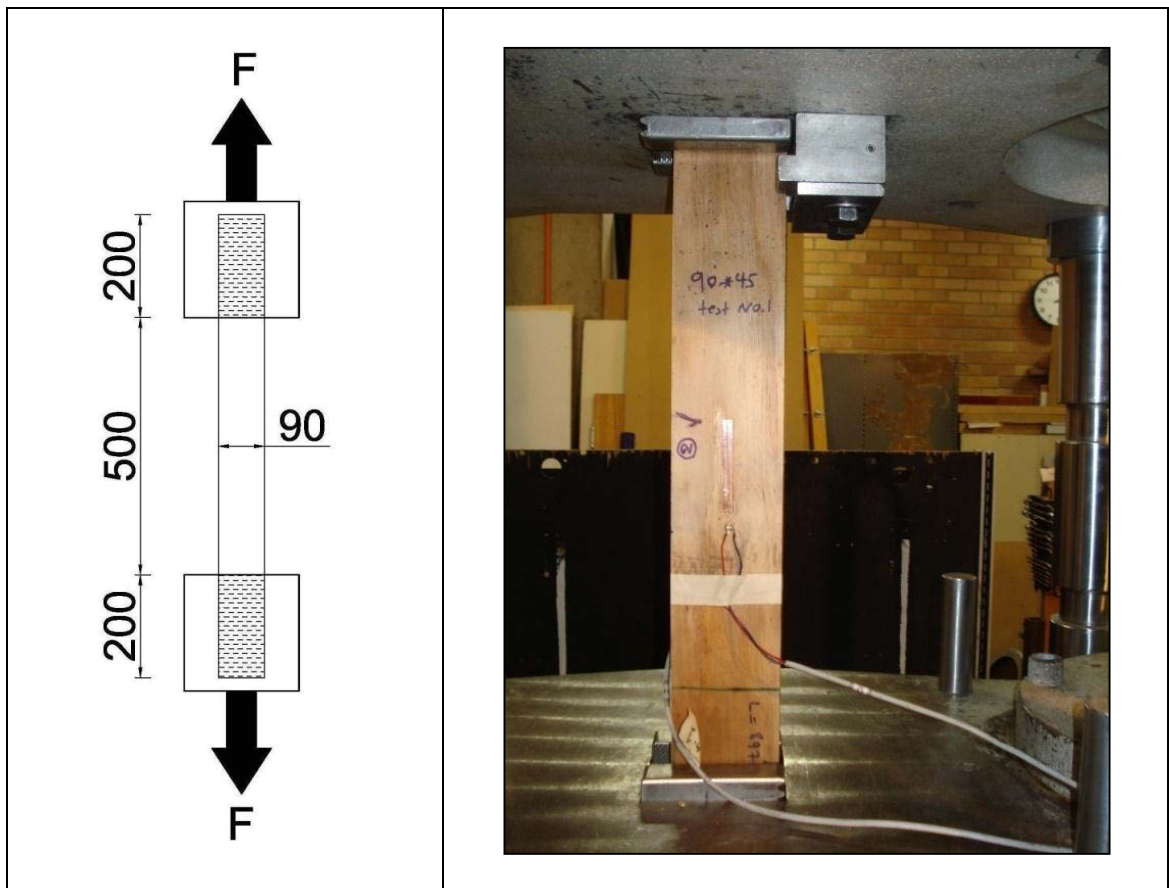
Figure 4.1 Dimensions and test set up for tension test
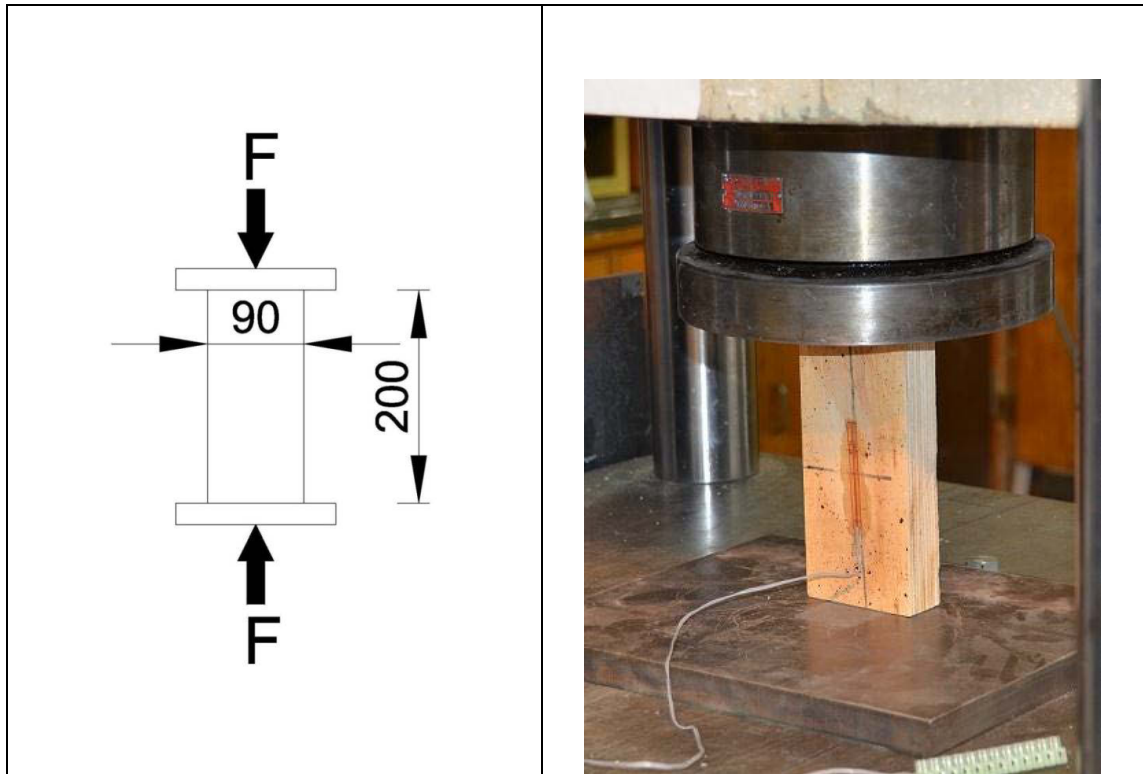
Figure 4.2 Dimensions and test set up for compression test

4.2.2 Proposed Constitutive Law for LVL

In this section the results of the compression and tension tests of LVL are presented and a material model for capturing the stress-strain relationship and failure of LVL is developed. All the results of the tests including the true modulus of elasticity and the compressive and tensile strength with their associated strains are presented in Table 4.3.

Table 4.3 The compression and tension test results

	Cross-Banded LVL	CoV	hySpan Project LVL	CoV
True MoE	10690 (MPa)		13660 (Mpa)	
Tensile strength (f_t)	34 (MPa)	7%	37.4 (MPa)	9%
Tensile Strain (ε_t)	0.0032		0.00275	
Compressive strength (f_c)	42 (MPa)	8%	51.4 (Mpa)	8%
Compressive Strain (ε_c)	0.0045		0.0046	

Figure 4.3 shows the stress-strain graphs for hySpan Cross-Banded LVL for tension tests. As shown in the figure, all graphs display a linear behaviour and the linear characteristics of the specimens are preserved up to about 25-28kN. By using MATLAB 2012 ®, which is technical computing software for data analysis and mathematical modelling, a least squared regression line for all test data was developed for each tests series (Figure 4.4). The correlation among the data is identified by the coefficient R^2 of the regression line. If R^2 equals to 1, there is a perfect correlation among the data, and if R^2 equals to 0, it shows no correlation among the data. Moreover, the slope of stress-strain curve represents the true modulus of elasticity (MoE) of the material. Therefore, as shown in Figure 4.3, the correlation among the data is about 92% and the indicative MoE is equal to 10,690 MPa or 10.7GPa for hySpan Cross-Banded LVL. With a similar approach, but more number of samples (described in Table 4.1), the coefficient of determination R^2 and MoE for hySpan Project LVL are equal to 97% and 13.7GPa, respectively. Figure 4.5 shows the stress-strain graphs as well as the regression line for the tension tests for hySpan Project LVL.
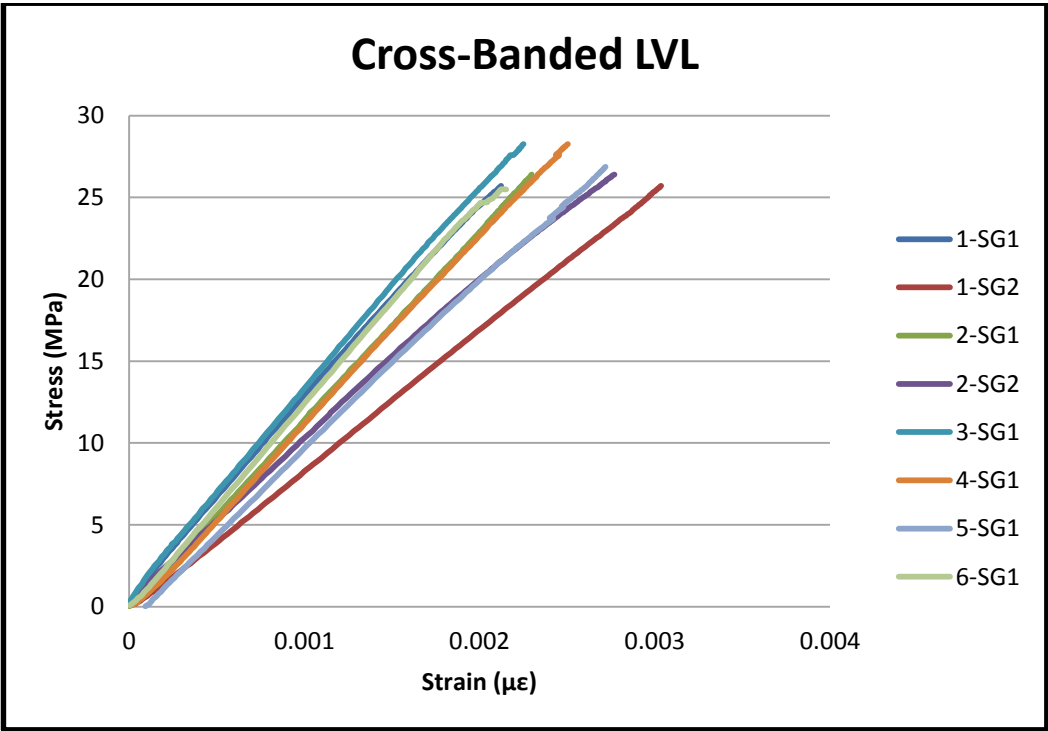
Figure 4.3 Stress-Strain graphs for tension tests for hySpan Cross-Banded LVL
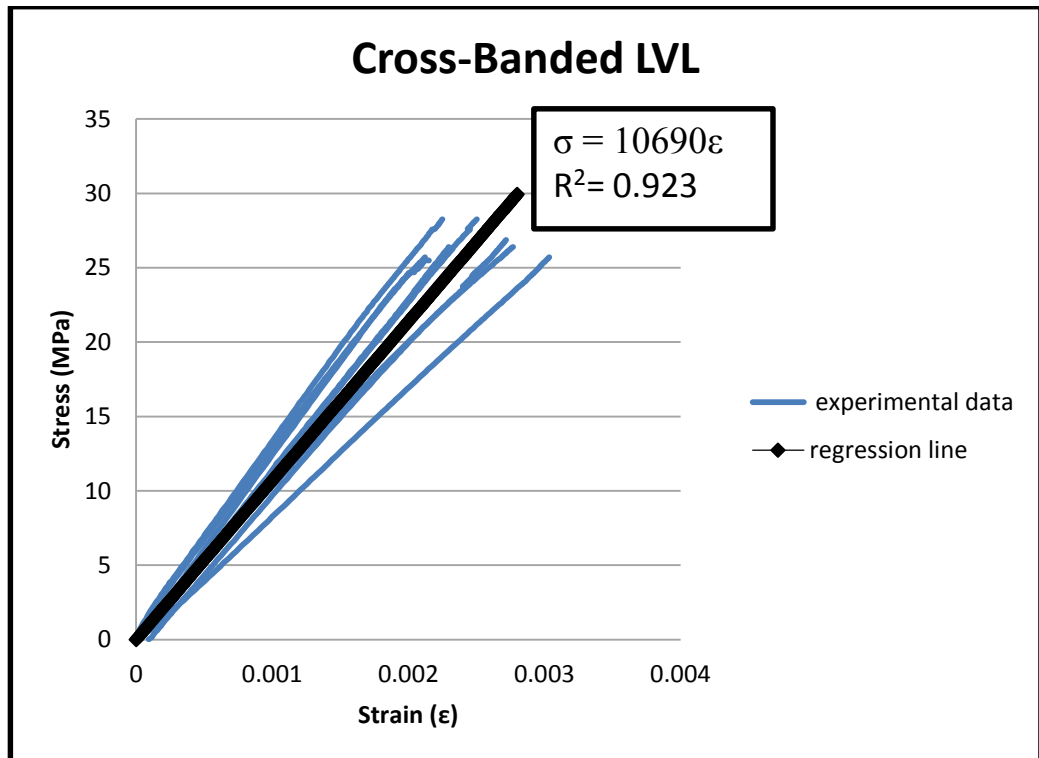
Figure 4.4 The regression line for the tension tests for hySpan Cross-Banded LVL
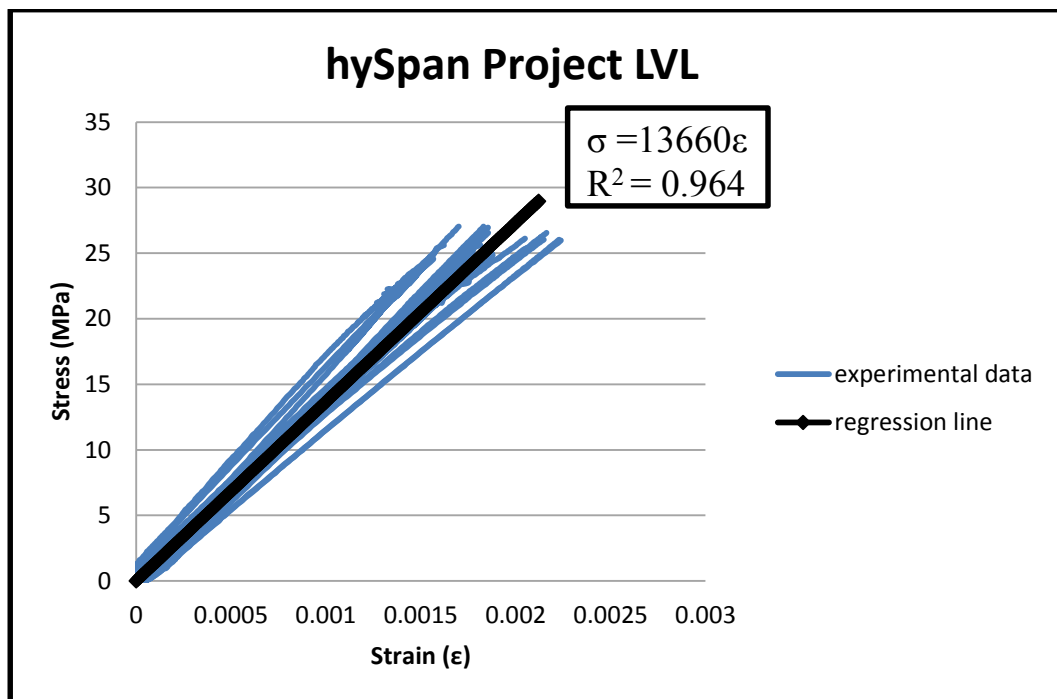
Figure 4.5 The regression line for the tension tests for hySpan Project LVL

Although the failure behaviour of LVL is brittle in tension, it demonstrates ductile behaviour in compression. Figure 4.6 and Figure 4.7 depict the stress-strain graphs for compression tests for hySpan Cross-Banded LVL and hySpan Project LVL, respectively. The stress-strain response for compression tests can be divided into two stages (Figs 4.6 and 4.7). The first stage of the response shows a linear behaviour and the slope of the lines represent the MoE of LVL, and the linear characteristics of LVL are preserved up to the peak load. After the peak load, the strain softening occurs which is associated with a gradual decrease of the stress while the strain still increases.
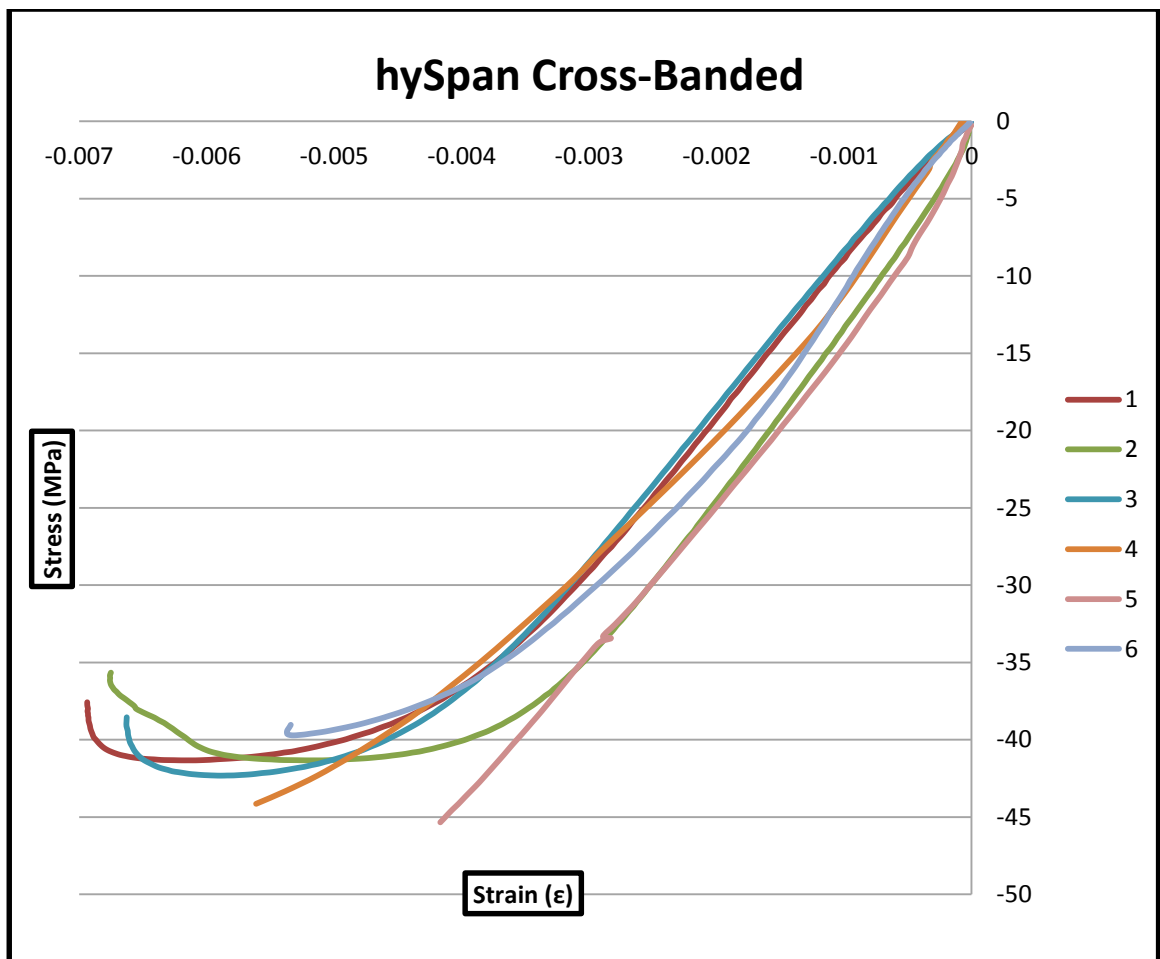
Figure 4.6 Stress-Strain graphs for compression tests of hySpan hySpan Project LVL
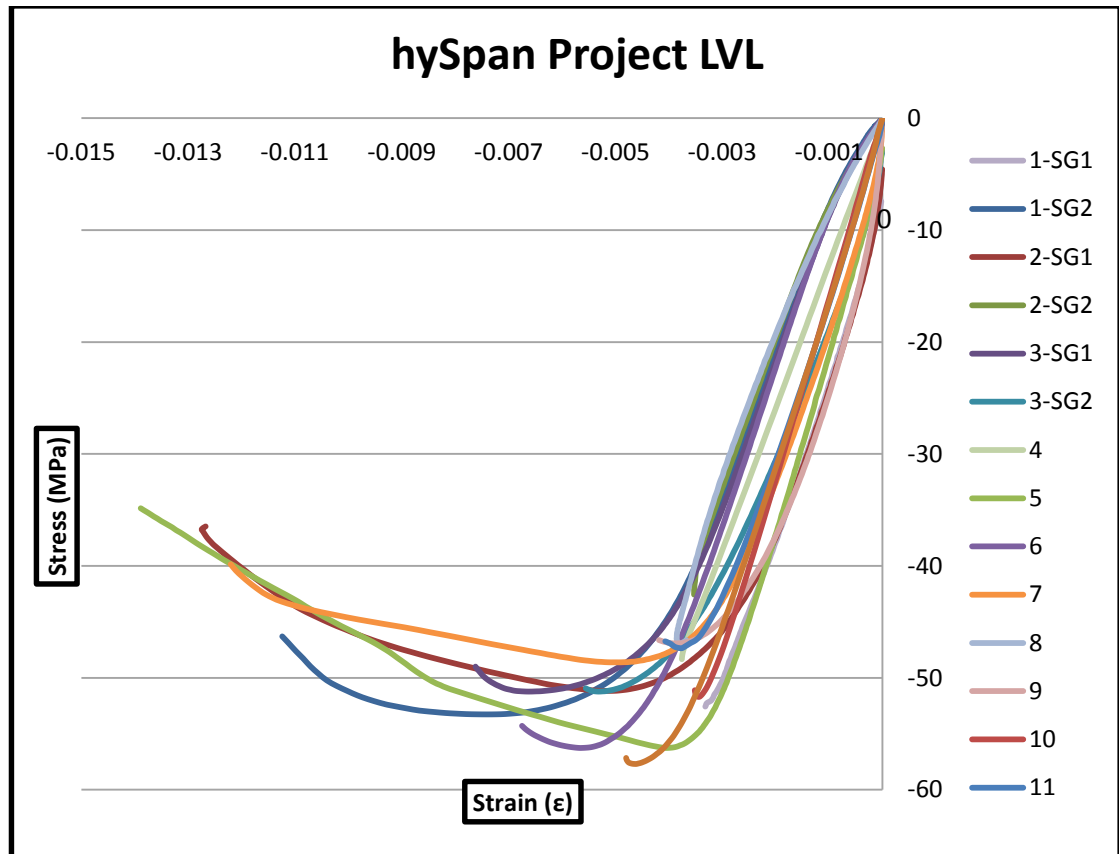
Figure 4.7 Stress-Strain graphs for compression tests for hySpan Project LVL
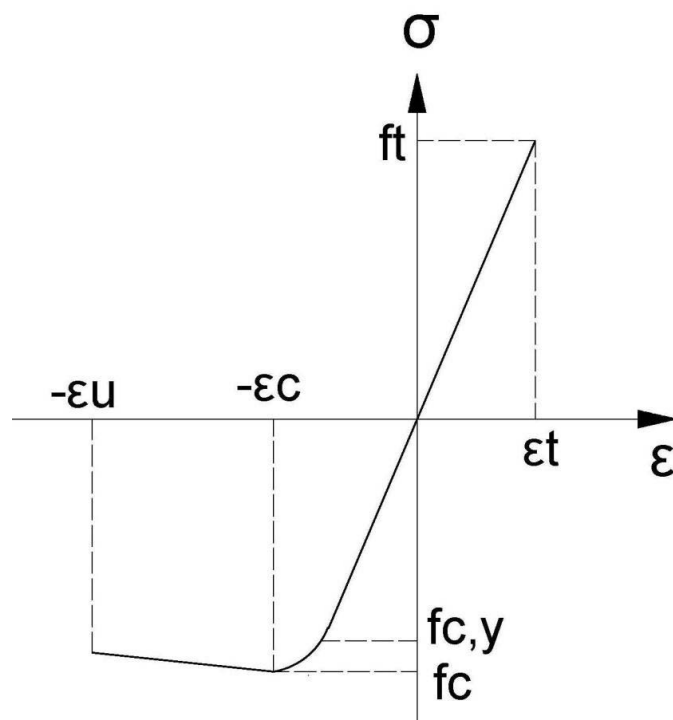
Figure 4.8 Stress-Strain relation according to Glos Model (Glos 1981)

The Glos model (Glos 1981) can be adopted to represent the behaviour of LVL in compression. As shown in Figure 4.8, The stress-strain relation is described by the initial modulus of elasticity (Ec), the maximum compression strength (fc), the yielding compression strength (fc,y), the strain (εc) at maximum compression stress (fc) and the ultimate strain (εu) . The empirical relation is presented in Equation 4.1:

$$\sigma(\varepsilon) = \begin{cases} \dfrac{\varepsilon + k_{(11)}\varepsilon^N}{k_{(22)} + k_{(33)}\varepsilon + k_{(44)}\varepsilon^N} & , \quad -\varepsilon_u \leq \varepsilon \leq 0 \\ \\ E_t\varepsilon & , \quad 0 \leq \varepsilon \leq \varepsilon_t \end{cases} \qquad \text{Eq.4.1}$$

Where coefficients k(11) to k(44) are defined as follows:

$$k_{(11)} = \dfrac{f_{c,y}}{(N-1).E_c.\varepsilon_c^{(N-1)}(1-\dfrac{f_{c,y}}{f_c})} \qquad \text{Eq.4.2}$$

$$k_{(22)} = \dfrac{1}{E_c} \qquad \text{Eq.4.3}$$

$$k_{(33)} = \dfrac{1}{f_c} - \dfrac{N}{(N-1).E_c.\varepsilon_c} \qquad \text{Eq.4.4}$$

$$k_{(44)} = \dfrac{k_{(11)}}{f_{c,y}} \qquad \text{Eq.4.5}$$

Conditions for Equation 4.1 are:

$$\varepsilon \geq \dfrac{N}{(N-1)}\dfrac{f_c}{E_c} \qquad \text{Eq.4.6}$$

$$f_{c,y} \leq f_c - 1 \text{ [MPa]} \qquad \text{Eq.4.7}$$

The typical parameters suggested by Glos (Glos 1981) are:

$$\varepsilon_c = 0.008 \text{ to } 0.0012 \text{ ,} \qquad \varepsilon_u = 3\varepsilon_c \text{ ,} \qquad \frac{f_{c,y}}{f_c} \approx 0.8 \text{ ,} \qquad N=7$$

It is specified that the typical parameters and the stress-strain relation (Equation 4.1) can be different and modified for the structural timber (such as LVL). It is important to note that in the Glos model, point $(\varepsilon_c, \sigma_c)$ will form the maximum point of the curve only if ε_c is equal to 0.01, or in other words, the differential of equation 1 will be zero at $(\varepsilon_c, \sigma_c)$ only if ε_c is equal to 0.01. Therefore, the Glos model works well when ε_c is around 0.01, otherwise a modification factor is needed in Equation 4.2 for $k_{(11)}$. However, for LVL, ε_c is around 0.005 (See Figure 4.6 and Figure 4.7) and as a result, a modification factor, α, is needed to be introduced in Equation 4.2 as follows:

$$(k_{(11)})_{mod} = \frac{\alpha f_{c,y}}{(N-1).E_c.\varepsilon_c^{(N-1)}(1-\frac{f_{c,y}}{f_c})} \qquad\qquad \text{Eq.4.8}$$

By using MATLAB 2012 and developing the best regression curve among the experimental data, α is equal to 200 and the best ratio for $\frac{f_{c,y}}{f_c}$ is equal to 0.9. Finally, with substituting the values of E_c, σ_c, ε_c from Table 4.3 into Equations 4.3, 4.4, 4.5 and 4.8, and with considering $\alpha=200$, $\frac{f_{c,y}}{f_c} = 0.9$ and N=7, the following mathematical model represents the behaviour of hySpan Cross-Banded LVL (Equation 4.9 and Figure 4.9) and hySpan project LVL (Equation 4.10 and Figure 4.10), respectively, where R^2 coefficient shows the difference between the experimental results and the proposed equations:

$$\sigma(\varepsilon) = \begin{cases} -\dfrac{\left||\varepsilon| + (1.24*10^{14})|\varepsilon^7|\right|}{(9.35*10^{-5})+(8.42*10^{-5})|\varepsilon|+(3.29*10^{12})|\varepsilon^7|} \text{ ,} & -\varepsilon_u \leq \varepsilon \leq 0 \quad (\text{R}^2=0.97) \\[20pt] (10.7*10^3)\varepsilon \text{ ,} & 0 \leq \varepsilon \leq \varepsilon_t \qquad (\text{R}^2=0.92) \end{cases}$$

Eq.4.9

$$\sigma(\varepsilon) = \begin{cases} -\dfrac{|\varepsilon| + (1.35 * 10^{14})|\varepsilon^7|}{(7.32 * 10^{-5}) + (6.28 * 10^{-4})|\varepsilon| + (2.94 * 10^{12})|\varepsilon^7|} & , \quad -\varepsilon_u \le \varepsilon \le 0 \qquad (R^2 = 0.91) \\[3em] (13.7 * 10^3)\,\varepsilon & , \quad 0 \le \varepsilon \le \varepsilon_t \qquad (R^2 = 0.97) \end{cases}$$

Eq.4.10

Figure 4.9 The comparison between the experimental data and the modified Glos model for hySpan Cross-Banded LVL
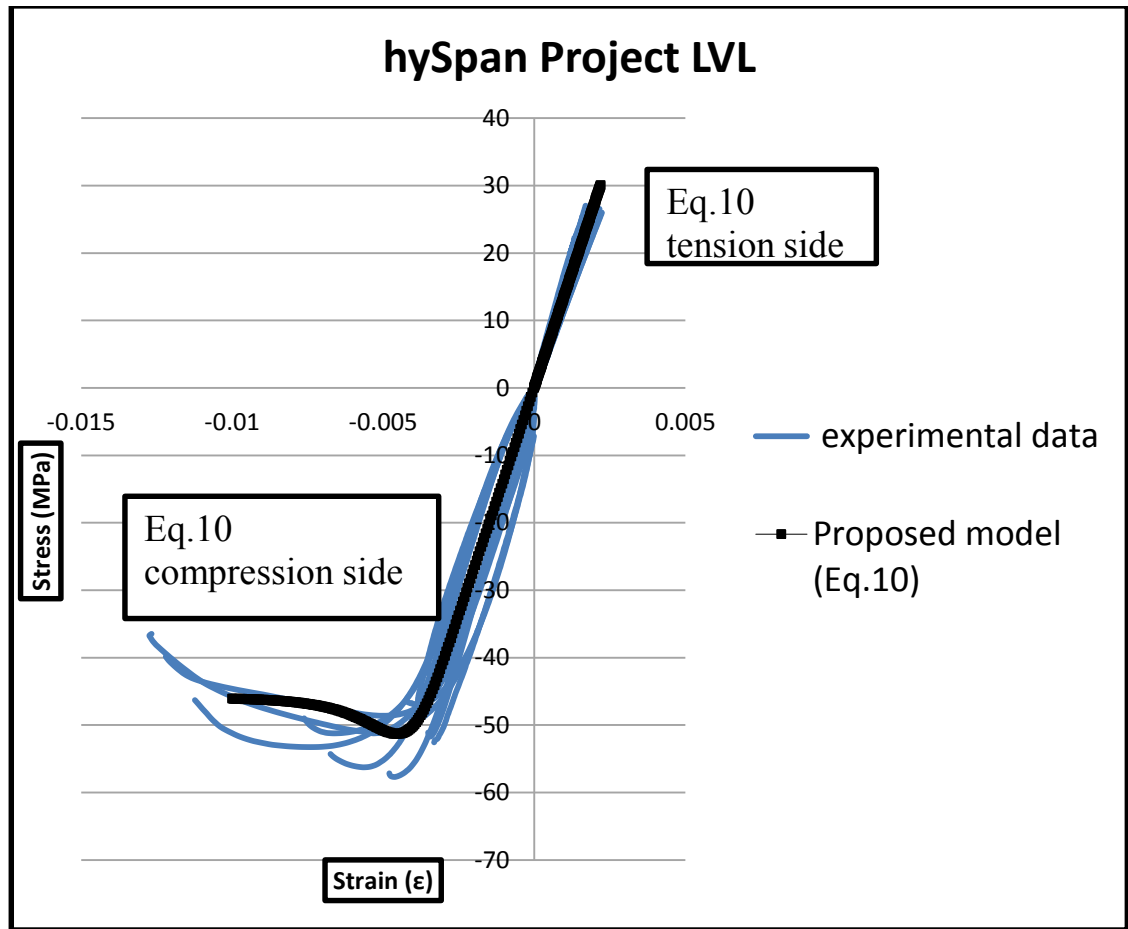
Figure 4.10 The comparison between the experimental data and the modified Glos model for hySpan Project LVL

Figures 4.9 and 4.10 show that all experimental data of the tension and compression tests can be well represented by Equations 4.9 and 4.10, and it is noteworthy that in the mathematical model (Eq 4.9 and 4.10) the slope of the compression and tension curves is equal, which confirms the adequacy of the proposed mathematical expression.

Moreover, Equation 4.11, which is a simplified quadratic model in the shape of a parabola, can also represent the behaviour of LVL in compression. However, as shown in Figure 4.11 and Figure 4.12, the adopted parabolic model cannot capture the behaviour of LVL at ultimate load, and the maximum stress (f_c) with the associated strain (ε_c) cannot be obtained as accurately as in modified Glos model and therefore, the modified Glos model is a better and more rigorous mathematical expression for the behaviour of LVL in compression. Equation 4.11 shows the adopted parabolic model as follows:

$$\sigma(\varepsilon) = -f_c \left[2 * \left(\frac{|\varepsilon|}{\varepsilon_0} \right) - \left(\frac{\varepsilon}{\varepsilon_0} \right)^2 \right] \qquad , \qquad -\varepsilon_u \leq \varepsilon \leq 0$$

Eq.4.11

Where f_c represents the maximum compression stress, and by using MATLAB 2012, the values of ε_0 are equal to 0.006 and 0.0066 with R^2 of 0.97 and 0.87 for hySpan Cross-Banded LVL and hySpan Project LVL, respectively.
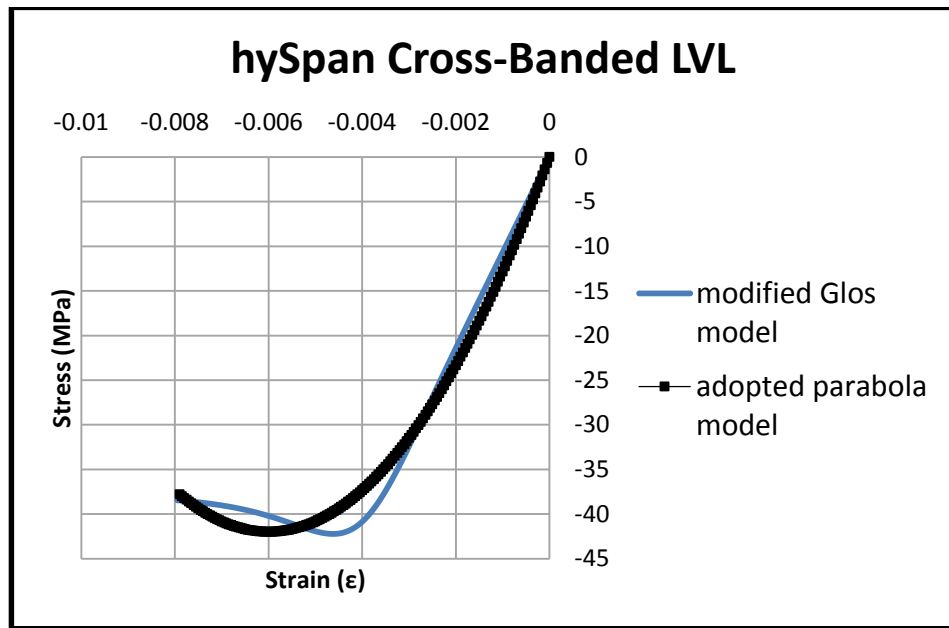
Figure 4.11 The adopted parabola model for hySpan Cross-Banded LVL
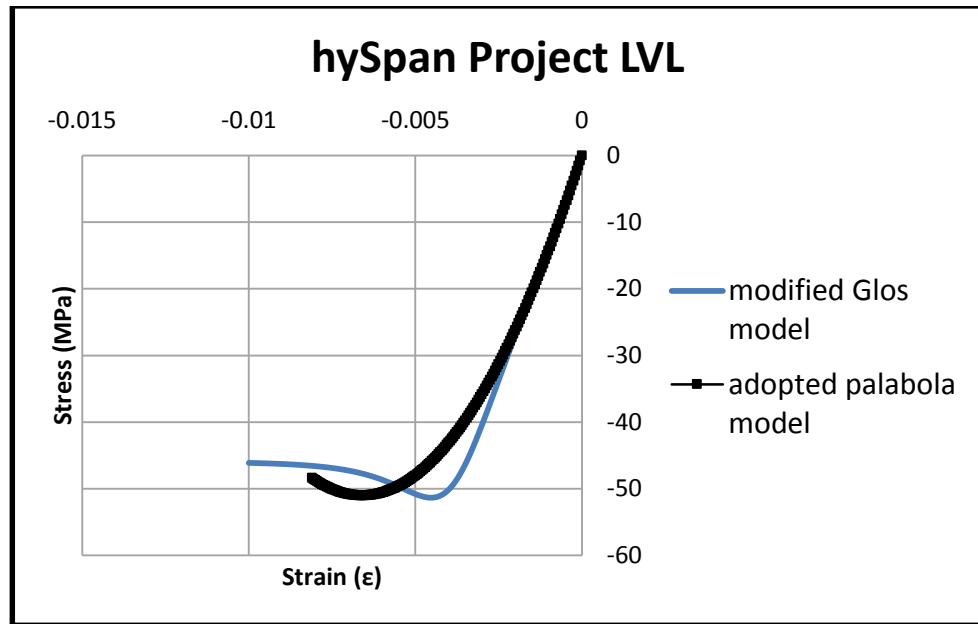
Figure 4.12 The adopted parabola model for hySpan Project LVL

4.2.3 Four Point Bending Tests

In this section the results of the full scale bending tests on LVL section is presented. The experimental results are used for calculating the flexural modulus of elasticity and the bending strength (f'_b) of the LVL sections. Moreover, a Finite Element model of the four point bending tests of LVL sections was developed, and the results of the FE model were verified against the experimental results, and were also used in the preliminarily FE model of the long span (6m to 8m) timber modules (chapter 7).

According to AS/AZS 4063.1 (AS/NZS 4063.1 2010), the bending strength (f'_b) and the apparent modulus of elasticity shall be determined from a simply supported four point bending test as shown in Figure 4.13. In this fashion a number of tests (15 tests for each test set-up) were conducted on two types of LVL sections, that is, hySPAN Cross-Banded and hySPAN Project. Figure 4.14 show the test set up for edge-wise four point bending tests, and Figure 4.15 and Figure 4.16 show the test set up for flat-wise tests.
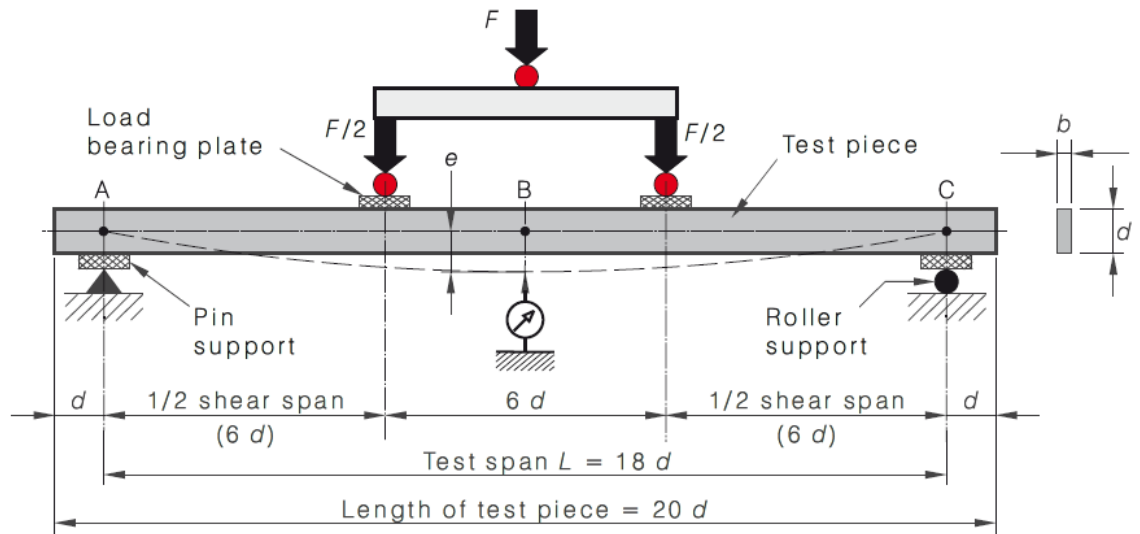
Figure 4.13 Test set-up for measuring the bending strength and apparent modulus of elasticity (4063.1:2010)
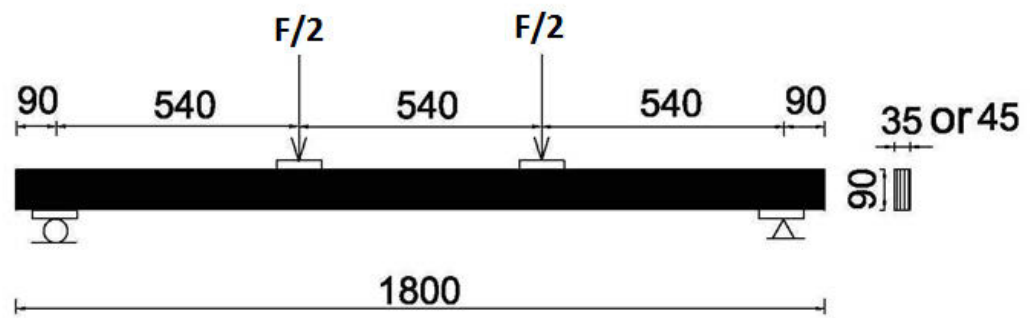
Figure 4.14 The test set up for edge-wise tests according to 4063.1:2010
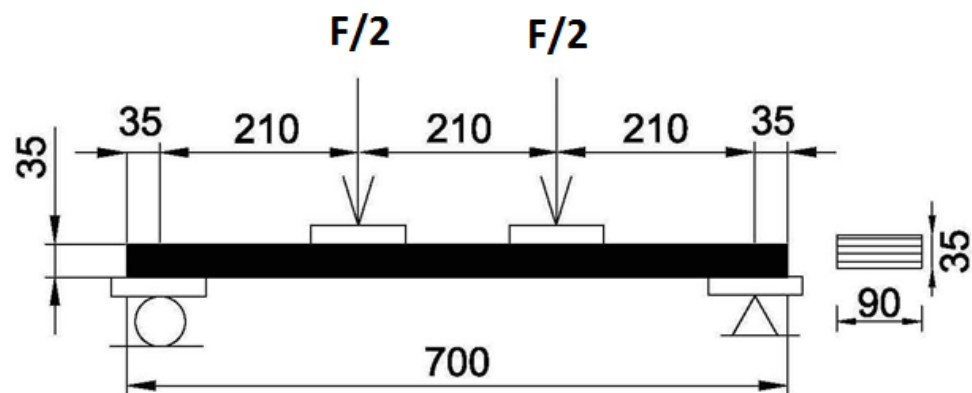
Figure 4.15 The test set up for flat-wise tests according to 4063.1:2010
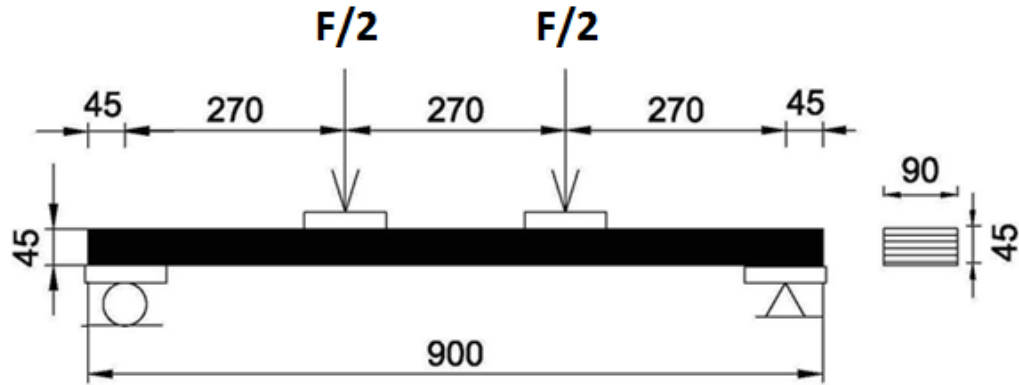
Figure 4.16 The test set up for flat-wise tests according to 4063.1:2010

According to AS/NZS 4063.1 (AS/NZS 4063.1 2010) load F was applied to the test specimens at a uniform rate of 0.18d mm/min (d is the depth of the section) until failure was occurred. Therefore, the load rate was set accordingly to initiate the failure within 3-5 minutes. The flexural modulus of elasticity in bending, E, was calculated from Equation 4.12:

$$E = \frac{23}{108} \left(\frac{L}{d}\right)^3 \left(\frac{\Delta F}{\Delta e}\right) \frac{1}{b}$$
Eq.4.12

$\Delta F/\Delta e$ is the linear elastic slope of the load-displacement graph where the load varies between 10% and 40% of the failure load (10%F_{max}-40%F_{max}).

When the failure occurs within the zone of the constant bending moment of a test piece, the bending strength, f'$_b$, shall be calculated from Equation 4.13, otherwise, (when the failure occurs out of the zone of the constant bending moment) f'$_b$, shall be calculated from Equation 4.14:

$$f'_b = \frac{F_{max}}{bd^2}$$
Eq.4.13

$$f'_b = \frac{3F_{max}(L - 2L_v)}{2bd^2}$$
Eq.4.14

Where F_{max} is the ultimate load, b and d are the width and depth of the section, respectively, L is the span of the beam and L_v is the horizontal distance from the center of the test span to the point of failure (Lv $\geq$ L/6). One LVDT was placed at mid span in all tests to capture the deflection up to the failure load (Figure 4.17) and 15 samples

were tested for each LVL section, where the results are presented in Table 4.4 and Table 4.5.

The purpose of evaluating the properties of single elements is to relate the final prototype tests results (the 6m and 8m modules) to the properties of the materials actually used to fabricate it. For this propose the average test results are appropriate as they relate to the most likely result in the prototype tests. Therefore, the average test results are used for analytical prediction of the ultimate loads and ultimate deflection, and to compare them with the actual experimental results. However for design purpose, 5th percentile characteristic values must be used which is calculated and presented in Appendix D.

 Figure 4.18 and Figure 4.19 show failure pictures of the beams subjected to Edge-Wise four-point bending tests. It can be observed from the pictures that excessing the bending strength of the extreme fibres of the sections (bottom fibres) triggered the failure and also shear within the beam contributed to propagation of the crack. Figure 4.20 shows load-deflection graphs for hySpan Project LVL in Edge-Wise tests. As shown in the figure (4.20), all graphs show a linear behaviour. As a result of non-linear behaviour of compressive fibres of the section at ultimate stage, a slight non-linear behaviour is observed at the ultimate stage of the load-bearing behaviour of LVL due to non-linear behaviour of compressive fibres of the section, but the actual failure is brittle. The test set up for flat-wise tests is shown in Figure 4.21 which was also shown schematically in Figure 4.14 and Figure 4.15. Photographs showing typical beam failure are presented in Figure 4.22 and it can be observed that the failure occurs within the zone of the constant bending moment of the test pieces and then it propagates along the tests pieces toward the supports. The behaviour and failure mode of the system is similar to edgewise tests, that is, a linear behaviour up to the failure point where a brittle failure occurs (Figure 4.23 and Figure 4.24). The slight non-linear behaviour at the ultimate stage is also as a result of non-linear behaviour of compressive fibres of the section.

Table 4.4 Edge-Wise four point bending test results (mean values)

	Cross-Banded 35mm*90mm	CoV	hySpan Project 35mm*90mm	CoV	hySpan Project 45mm*90mm	CoV
flexural MoE	11.5 (GPa)	4%	12.3 (GPa)	4%	13.3 (GPa)	5%
Bending Strength (f_b)	55.7 (MPa)	8%	60 (MPa)	8%	65.3 (MPa)	9%
P_{max}	10.1 (kN)	4%	10.5 (kN)	8%	14.7 (kN)	9%

Table 4.5 Flat-Wise four point bending test results (mean values)

	Cross-Banded 35mm*90mm	CoV	hySpan Project 35mm*90mm	CoV	hySpan Project 45mm*90mm	CoV
flexural MoE	9.6(GPa)	11%	13.1(GPa)	12%	15.2(GPa)	14%
Bending Strength (f_b)	52.4(MPa)	14%	72.6(MPa)	15%	80(MPa)	4%
P_{max}	9.2(kN)	14%	12.7(kN)	15%	18(kN)	14%

Figure 4.17 The test set up for Edge-Wise tests
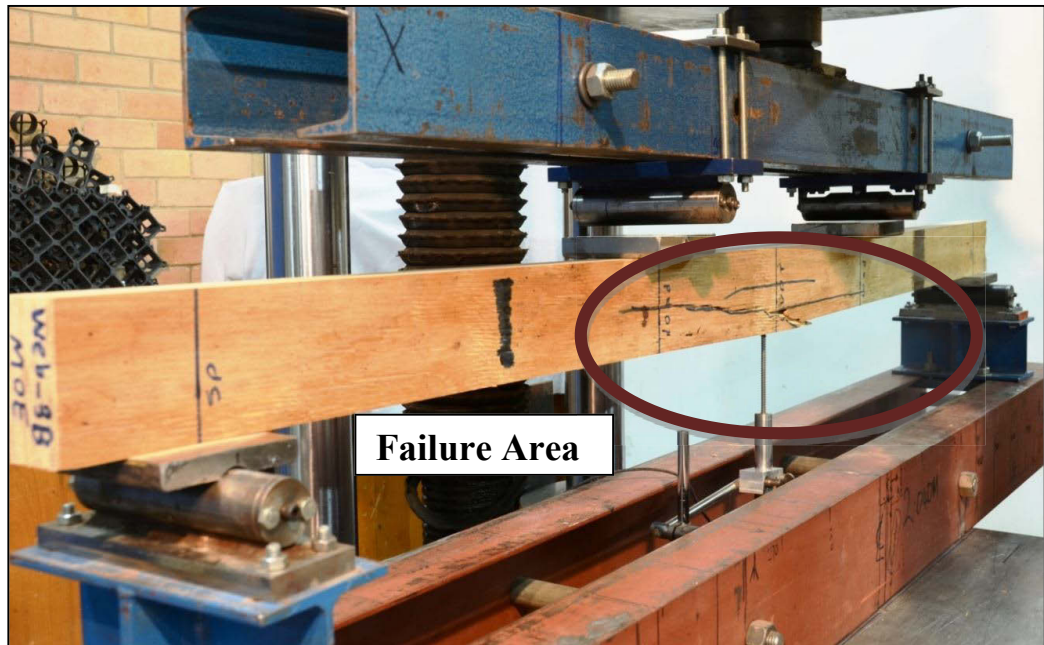
Figure 4.18 Failure pictures of a beam subjected to Edge-Wise four-point bending tests

Figure 4.19 Failure pictures of different beam subjected to Edge-Wise four-point bending
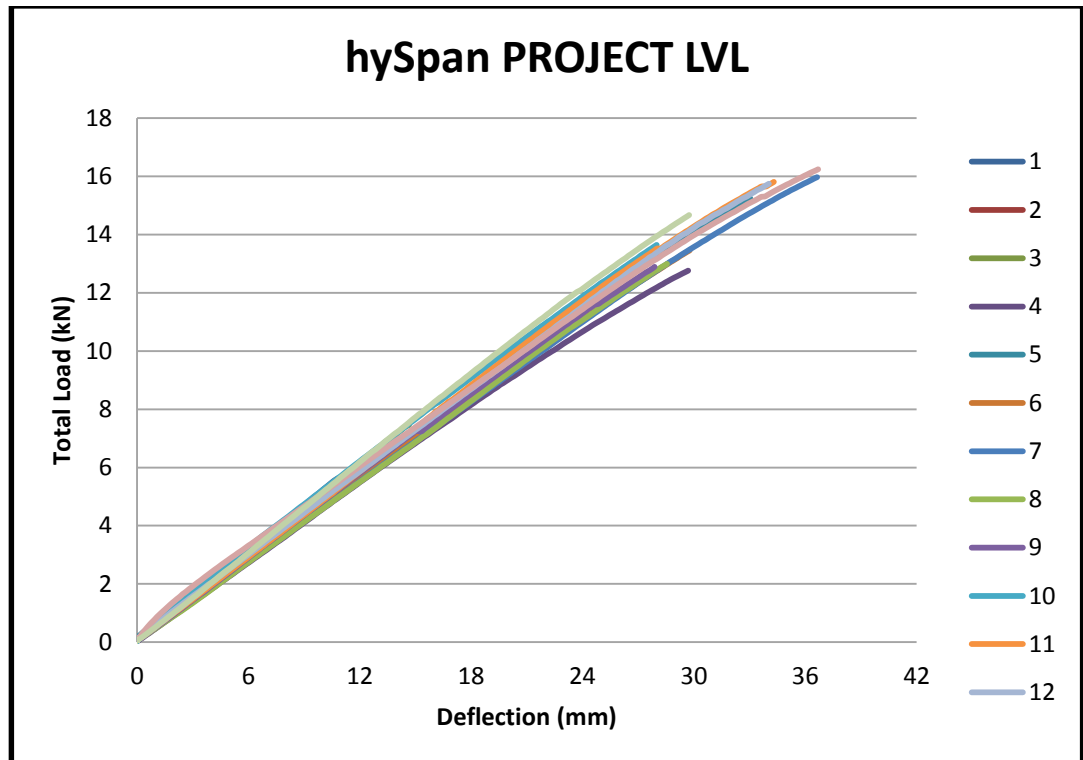
Figure 4.20 Load-deflection graphs for hySpan project LVL(45mm*90mm), Edge-Wise tests

Figure 4.21 Test set up for flat-wise four-point bending tests

Figure 4.22 Failure pictures in flat-wise four-point bending tests
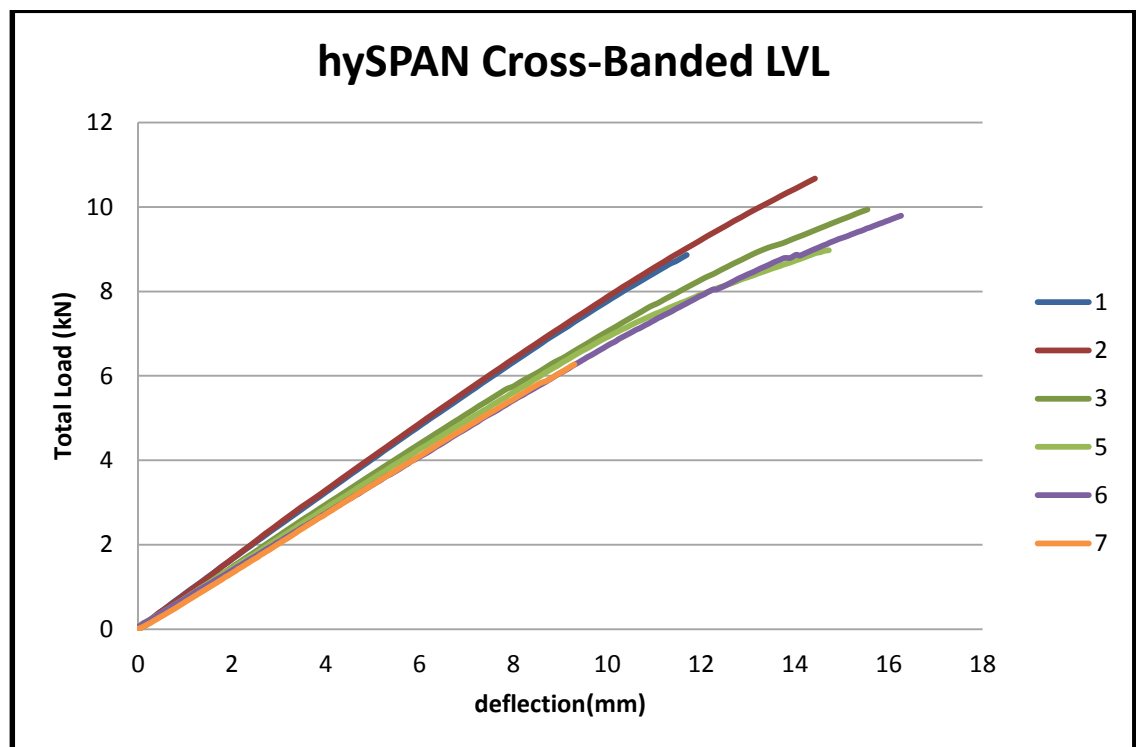
Figure 4.23 Load-deflection graphs for cross-banded LVL (35mm*90mm), flat-wise tests
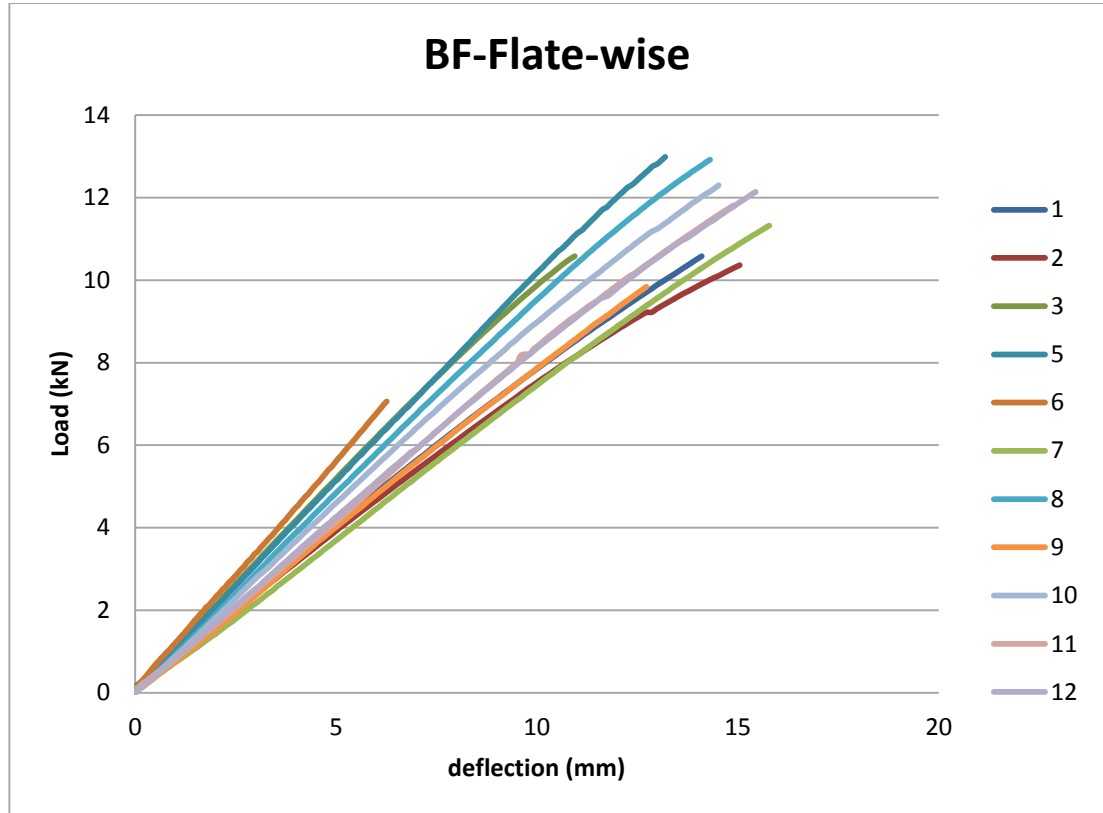
Figure 4.24 Load-deflection graphs for hySpan project LVL (35mm*90mm), flat-wise tests

4.2.4 Three Point Bending Tests (flexural shearing strength)

According to AS/NZS 4063.1:2010, the beam shear strength shall be determined using a three point bending test configuration as shown in Figure 4.25, where the steel bearing plate dimension is shown in Figure 4.26. Load F was applied at a uniform rate of loading to the test specimens until failure occurred.

Moreover, if the mode of failure is due to shear failure (evidenced by splitting along grain), the shear strength, f_v, shall be calculated from Equation 4.15. The shear failure is only likely happen where the beam shear strength is less than one-twelfth of the bending strength which is the case for test pieces with high bending strength and straight grained. Where there is doubt about the mode of failure, whether it is associated with bending or shear, it is conservative to assume a shear mode of failure.

$$f_v = \frac{0.75 F_{max}}{bd}$$
Eq.4.15

Where f_v is the shear strength of the beam, F$_{max}$ is the ultimate load, and b and d are the width and depth of the section, respectively.

Figure 4.25 Shear test configuration according to AS/NZS 4063.1:2010

Figure 4.26 Steel bearing plate
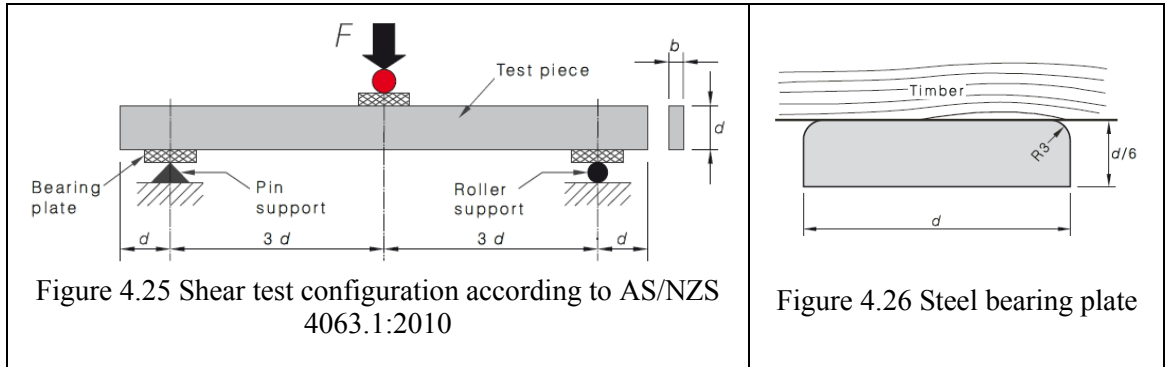
Eight test specimens were subjected to three-point bending test (see Figure 4.27) to calculate the flexural shear strength of hySPAN Project which used as the web of the timber modules. The test results are also summarised in Table 4.6. Also, Figure 4.28 shows the experimental test set up, Figure 4.29 and Figure 4.30 show the failure pictures of LVL under three-point bending test and Figure 4.30 and 4.31 show the load – displacement of LVL under three-point bending load for test 1 and test 2, respectively.
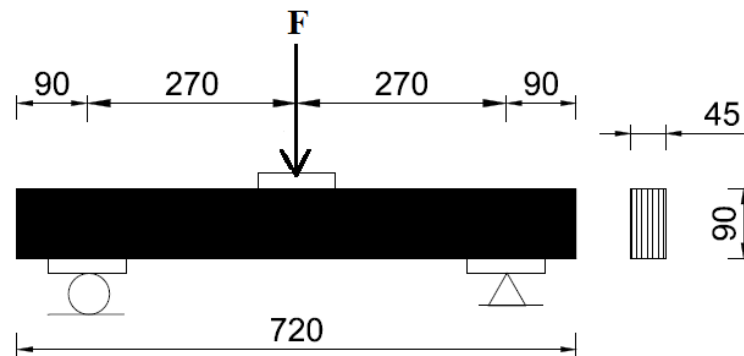
Figure 4.27 Shear test set up according to AS/NZS 4063.1:2010

Figure 4.28 The test set up for measuring the shearing strength

Table 4.6 Shear test results

Section name	F_{max}	f_v	CoV
hySPAN Project	(kN)	(MPa)	
45mm*90mm-1	36.8	6.8	
45mm*90mm-2	34.4	6.4	
45mm*90mm-3	38.5	7.0	
45mm*90mm-4	42.4	7.9	
45mm*90mm-5	37.1	6.9	
45mm*90mm-6	33.0	6.2	
45mm*90mm-7	35.7	6.6	
45mm*90mm-8	37.3	6.9	
Average	**36.9**	**6.83**	**7%**

Figure 4.29 Failure picture of LVL under three-point bending test

Figure 4.30 Failure picture of LVL under three-point bending test
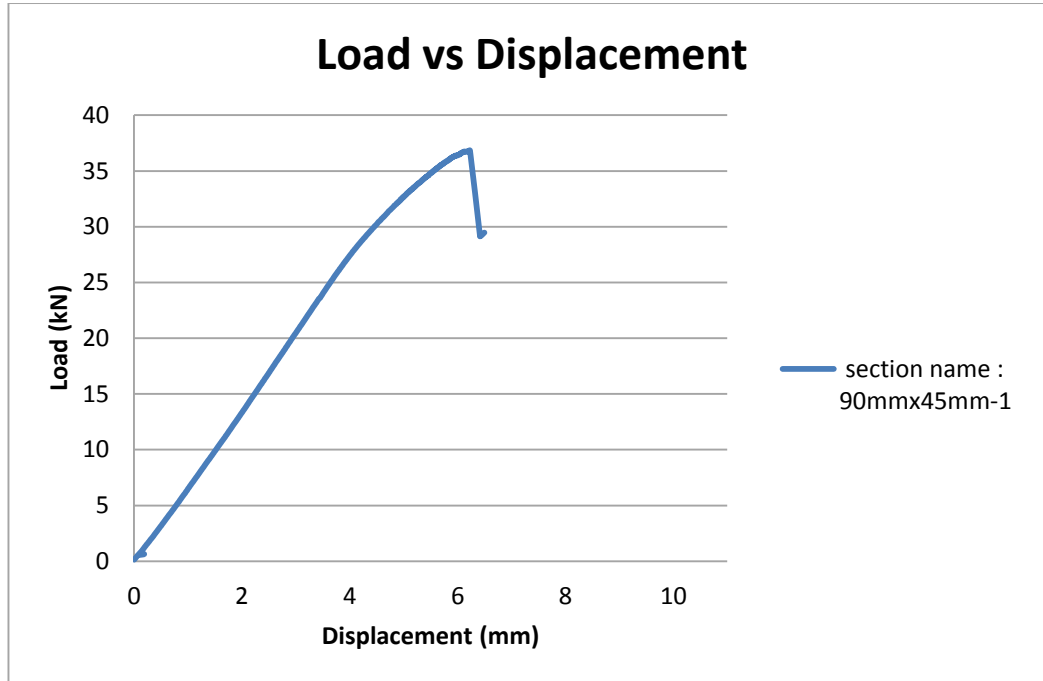
Figure 4.31 Load – Displacement of LVL under three-point bending load- test 1
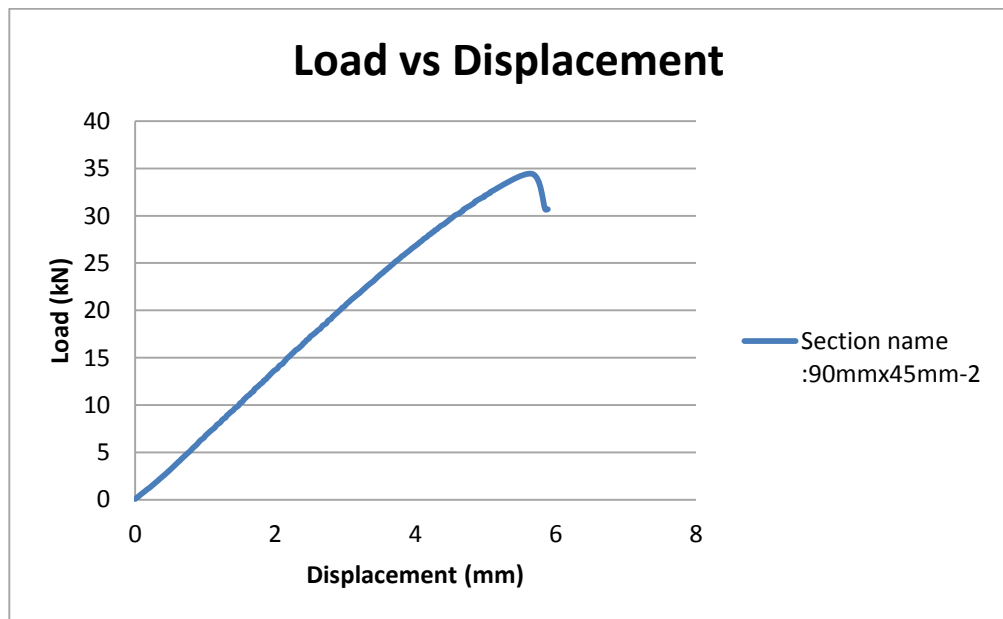
Figure 4.32 Load – Displacement of LVL under three-point bending load- test 2

4.3   Comparison between the Experimental Results and Analytically Predicted Results

According to European Standard EC 5.1 (EN 1995-1-1 2004+A1:2008) for a timber beam section under tensile stress, the ultimate load can be evaluated either when the tensile stress in the extreme fibres of the section exceeds the maximum bending stress, or when the tensile stress at half depth of the bottom flange exceeds the maximum tensile stress (Equations 9.2 and 9.4 of BS EN 1995-1-1:2004+A1:2008). Therefore, bending stress in extreme fibres of the section, or the tensile stress at half depth of the bottom flange will trigger the failure. It is important to note that the experimental results of the four-point bending tests conducted in this study, confirm the fact that when the extreme fibres of the LVL sections reach the maximum tensile stress, the bending capacity of the system did not stop, but continued until achieving the maximum bending stress. Equations 4.16 and 4.17 show the ultimate strength checks in the tension side of the section:

$$\sigma_{f,t,\max} \leq f_b \qquad\qquad\qquad\qquad \text{Eq.4.16}$$

$$\sigma_{f,t} \leq f_t \qquad\qquad\qquad\qquad\qquad \text{Eq.4.17}$$

Where $\sigma_{f,t,\max}$ the tensile design stress of the extreme fiber of flange, $\sigma_{f,t}$ is the mean design stress of flange and f_b and f_t are the bending strength and tensile strength capacity of the flange, respectively. Therefore, for the edgewise four-point bending tests the predicted ultimate load according to Eq.4.16 will be as given below:

$$\frac{M^* Y_c}{I} = 65.3 (MPa) \qquad\qquad\qquad \text{Eq.4.18}$$

$$\frac{\dfrac{(F_{\max}/2) \times 1620}{3} \times 45}{[\dfrac{45 \times 90^3}{12}]} = 65.3 MPa \qquad\qquad \text{Eq.4.19}$$

Where 65.3MPa is the bending strength capacity of hySPAN Project LVL (see Table 4.4), "I" is the second moment of area for 45mm*90mm LVL section, M* is the

maximum bending moment which is equal to $\dfrac{(F/2) \times L}{3}$ and L is the span of the LVL

beams (Figure 4.14, Figure 4.15, Figure 4.16). According to Equation 4.18 and 4.19 the

F_{max} will be equal to 14.62kN, and with considering the Modulus of Elasticity (MoE) of

hySPAN Project LVL equal to 13.3 GPa (taken from Table 4.4 , the flexural MoE), the

maximum deflection will be equal to 31mm (Eq. 4.20)

$$\delta_{max} = \frac{23(F_{max}/2)L^3}{648EI} = 31mm \qquad\qquad \text{Eq.4.20}$$

Similar trend can be taken to calculate the ultimate load as a result of Equation 4.17 in

which f_t is the tensile strength capacity of hySPAN Project (see Table 4.3).

$$\frac{\dfrac{\left(F_{max}/2\right) \times 1620}{3} \times 22.5}{[\dfrac{45 \times 90^3}{12}]} = 37.4MPa \qquad\qquad \text{Eq.4.21}$$

As a result of Equation 4.21, F_{max} will be equal to 16.8KN. However, if F_{max} is

calculated when the extreme fibers of the section reach maximum tensile stress, the

ultimate load will be 8.4kN which is below the average failure load as a result of the

experimental tests. Therefore Equation 4.16 governs the failure mode of system. A

comparison between the closed-form solutions and the average experimental results is

presented in Table 4.7.

Table 4.7 Comparison between the closed-form solution and the experimental result of Edge-
Wise four point bending for hySpan Project LVL

	Ultimate Load F_{max}
Predicted F_{max} when extreme fibers of section exceed max tensile stress	8.4 (kN)
Predicted F_{max} when half of tensile depth of section exceed max tensile stress	16.8(kN)
Predicted F_{max} when extreme fibers of section exceed max bending stress	14.7(kN)
Average experimental F_{max}	14.7(kN)

Ultimate loads of flat-wise four-point bending tests were also analytically predicted

with a similar approach and the predicted ultimate load and the maximum deflections

are summarised in Table 4.8 and Table 4.9. On the other hand, the failure loads and maximum deflections as a result of the conducted experimental tests (four-point bending tests) were also presented in Table 4.8 and Table 4.9. As it can be observed from the values of the tables, the experimental results are highly compatible with the analytically predicted responses.

Table 4.8 Comparison between the experimental results and analytically predicted results of the ultimate load of LVL beam

	Total Ultimate load (kN)	
	Analytically predicted	Average Experimental results
Cross-Banded 35mm*90mm, flat-wise tests	9.2	9.2
hySpan Project 35mm*90mm, flat-wise tests	12.7	12.7
hySpan Project 45mm*90mm, edge-wise tests	14.7	14.7

Table 4.9 Comparison between the experimental results and analytically predicted results of the maximum deflection of LVL beams

	Maximum deflection (mm)	
	Analytically predicted	Average Experimental results
Cross-Banded 35mm*90mm, flat-wise tests	13.1	13.3
hySpan Project 35mm*90mm, flat-wise tests	13.4	13.7
hySpan Project 45mm*90mm,edge-wise tests	31	32.6

As a result of the four-point bending tests, the behaviour of LVL was assessed, the actual peak loads and the failure modes of the sections were identified, and the values of the MOE of LVLs were evaluated. All these facts will be used in developing the Finite Element model of the LVL beams which will be presented in chapter 7.

4.4   Conclusion

In this chapter the results of tension and compression tests conducted on two types of LVL sections were reported. As a result of the tension and compression tests, a suitable constitutive law was proposed which can properly capture the stress-strain relationship, and the failure of LVL. It was observed that the behaviour of LVL is linear under tension, and the linear characteristics of LVL are preserved up to the failure where a brittle failure occurs. However, in compression, a ductile behaviour was observed followed by an initial linear response, and therefore, the failure was not brittle under compression loads. The proposed mathematical equation for stress-strain relationship of LVL can be incorporated into FE analyses of any LVL timber beams.

Moreover, a number of four-point bending tests were conducted on LVL beams in both edge-wise-and flat-wise directions. The results from bending tests were used for calculating the flexural modulus of elasticity and the bending strength (f'_b) of the LVL sections. All load-deflection graphs show a linear behaviour, and a slight non-linear behaviour is observed at the ultimate stage of the load-bearing behaviour of LVL which is caused by the ductile behaviour of compressive fibers of the section at ultimate stage, but the actual failure is a brittle one.

A linear variation over the depth of the section was assumed and Equations 4.16 and 4.17 were used to calculate the ultimate load capacity of the LVL beams prior to occurrence of failure. The experimental results show that the analytically calculated values for the ultimate loads was very close to the actual failure loads, and the plastic behaviour which was observed had negligible effect on the ultimate load and failure mode of the beams. Hence, the assumption of a linear variation over the depth of the section is considered to be appropriate to predict the ultimate load of the LVL beams where a brittle failure occurs (especially for LVL modules). This was also confirmed with the experimental results of the 8m floor modules reported in chapter 5.

The comparison between the closed-form prediction analysis and the experimental results indicates that when the extreme fibres of the LVL sections reach the maximum tensile stress, the load capacity of the system does not stop, but continues until the

maximum bending stress is reached, and this is compatible with the fact that the bending stress in extreme fibers of the section, or the tensile stress at half depth of the bottom flange (or half of the depth of tensile part of the section) will trigger the failure.

Finally, the compatibility between the closed-form solutions (the predicted ultimate load) and the experimental results confirm the fact that the ultimate load in LVL beams can be predicted by a proper closed-form solution and a brittle failure at the end. All of these observations and conclusion will be used in the following chapters to investigate and predict the behaviour of long span 6m and 8m LVL modules.

University of Technology, Sydney

CHAPTER 5

EXPERIMENTAL AND ANALYTICAL

INVESTIGATION OF PROPOSED LONG SPAN

LVL FLOOR MODULES

5 EXPERIMENTAL AND ANALYTICAL INVESTIGATION OF PROPOSED LONG SPAN LVL FLOOR MODULES

5.1 Introduction

In this chapter, the structural behaviour of the timber floor modules proposed for non-residential buildings is assessed through extensive experimental and analytical investigation. Laminated veneer lumber (LVL) is used as the only structural load bearing part of the system. The experimental investigation involved subjecting the LVL floor modules (6m and 8m span) to both destructive and non-destructive static loading to assess the strength and serviceability performance of the proposed system. The features that are investigated for serviceability tests include the assessment of linear characteristics of the modules through analysing the deflection as well as strain responses of the system versus service load. Stiffness of the system is also evaluated by assessing the load versus deflection of the modules. Moreover, the composite characteristic of the modules are investigated by evaluating the strain distribution over the depth of the section. Ultimate limit state tests are also conducted on 8m LVL modules (in which the loads are increased until failure occurs) to identify the termination of the linear-elastic characteristics and the failure modes of the system, and to thoroughly investigate the ultimate response of the system. Furthermore, a closed-form prediction analysis is conducted to calculate the ultimate load of the system and a comparison between the experimental results and the closed-from predicted results is undertaken and reported in this chapter.

5.2 Predicting the Response of the System

5.2.1 6m and 8m modules

In chapter 3 the proposed 6m and 8m long span LVL modules were introduced and in chapter 4 the material properties of LVL were thoroughly investigated 4. Figure 5.1 and Figure 5.2 show the dimensions of 6m and 8m modules, respectively.
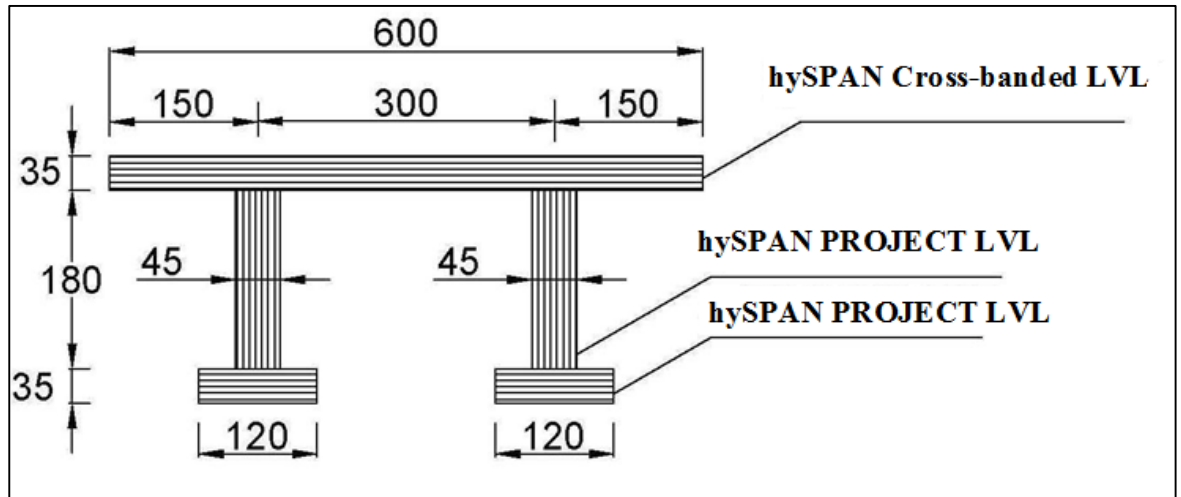
Figure 5.1 Dimensions of 6m modules
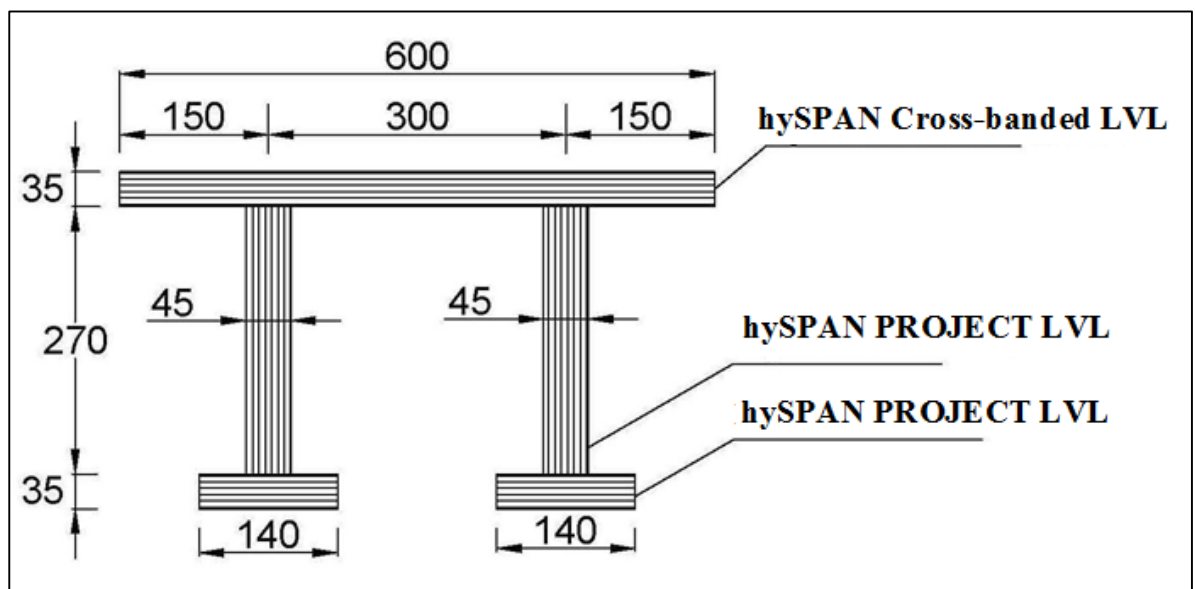
Figure 5.2 Dimensions of 8m modules

Table 5.1 summarises the material properties (mean values) of LVL according to the experimental investigation conducted in Chapter 4. The purpose of evaluating the properties of single elements was to relate the final prototype tests results (the 6m and 8m modules) to the properties of the materials actually used to fabricate it. For this purpose the average test results are appropriate as they relate to the most likely result in the prototype tests. Therefore, the average test results for the material properties (Table 5.1) are used for analytical prediction of the ultimate loads and ultimate deflection and to compare them with the actual experimental results. However for design purpose, 5th

percentile characteristic values must be used which is calculated and presented in Appendix D. Flat-wise properties for the top and bottom flanges as well as edge-wise properties for the webs are presented in Table 5.1 which replicates the orientation of the flanges and web in the tested modules. The values of Coefficient of Variation (CoV) indicate the variable nature of timber in general and LVL in particular.

Table 5.1 Material properties of LVL (mean values)

Component Name	Top flange cross-banded LVL (Flat-wise tests)	Webs hySpan-Project LVL (Edge-wise tests)	Bottom flanges, hySpan-Project LVL (Flat-wise tests)
Flexural MOE, E_x (GPa)	9.6	13.3	13.1
CoV (%)	11%	5%	12%
True MOE, $E_{x,true}$ (GPa)	10.7	13.7	13.7
CoV (%)	8%	5%	5%
Bending strength, f_b (MPa)	52.4	65.3	72.6
CoV (%)	14%	9%	15%
Tension strength, f_t (MPa)	34	37.4	37.4
CoV (%)	7%	9%	9%
Compression strength, f_c (MPa)	42	51.4	51.4
CoV (%)	8%	8%	8%
Shear strength, f_v (MPa)	5.1	6.83	5.9
CoV (%)	7%	7%	15%
Density, ρ (kg/m^3)	606.5	603.7	601.1
CoV (%)	1%	2%	2%

The prediction responses of the system is derived based on the assumption that the bond between the web and the flanges are fully composite and this assumption is thoroughly investigated during the experimental tests for both of seviceabilty and ultimate limit

state. Therefore, the procedure to calcute the neutral axis ($\bar{y}_c$) , second moment of area (I$_{eff}$) and the effective flexural stiffness (EI$_{eff}$) of the LVL modules are based on the "transformed section method" which were previously discribed in chaper 3 and here just the values are presented in Table 5.2 and Table 5.3 and Equations 5.1 , 5.2 and 5.3, using the same method described in chapter 3 and with tested properties of LVL .

Table 5.2 Calculation of the Neutral axis of 8m LVL modules

	MOE (MPa)	n (modular ratio)	A(mm^2)	y (mm)	Ay(mm^3)
Top Flange	9600	1	21000.0	322.5	6772500
Webs	13300	1.39	33665.6	170	5723156.3
Bottom Flanges	13100	1.34	13372.9	17.5	234026.0

$$\bar{y}_c = \frac{\Sigma Ay}{\Sigma A} = 187.1 mm$$

Eq.5.1

Table 5.3 Calculation of the flexural stiffness of 8m LVL modules

	I (mm^4)	A(mm^2)	d(mm)	I+Ad^2(mm^4)
Top Flange	2.1*10^6	21000.0	135.4	3.87E+08
Webs	2.04*10^8	33665.6	17.1	2.14E+08
Bottom Flanges	1.37*10^6	13372.9	169.6	3.86E+08

(I_{eff})=987528812.3mm^4=9.88E+08mm^4 Eq.5.2

$(EI)_{eff} = (E_{tf})(I_{eff})$=9.48E+12 Mpa.mm^4= 9.48E+06 Pa.m^4 Eq.5.3

The same approach was taken for the 6m LVL modules and Table 5.4 summarises the results. In the following sections, the values of Table 5.4 will be compared to the neutral axis and the flexural stiffnesses of the experimetal tests , and the assumption of a fully composite section will be assessed accordingly.

Table 5.4 Cross-sectional characteristic of the LVL modules based on the fully composite behaviour

	6m modules	8m modules
$\bar{y}_c$ (mm)	143.7	187.1
I_{eff} (mm^4)	4.2E+08	9.88E+08
EI_{eff} (Pa.m^4)	4.03E+06	9.48E+06

Based on the observations and conclusions made in chapter 4, the behaviour of LVL is linear elastic and the failure is a brittle one. Therefore, as long as the the 6m and 8m modules are assumed to behave fully composite like one solid section, they are expected to show a linear-elastic behaviour with brittle characteristics to failure. The ultimate load will be reached when the stress at any part of the system exceeds the ultimate properties of the LVL modules' components or interfaces. The extreme fibres at the top and bottom flanges experience compression and tension stresses as a result of the bending action. Moreover, the maximum shear of the section as well as the maximum shear at the interfaces must be checked. In order to simulate the uniform distributed loading, the specimens will be subjected to the four point bending loads as shown in Figure 5.3. in which the maximum bending moment is at FL/3 and the maximum shear force is equal to F, where F is the applied load at each third span. Equations 5.4 and 5.6 show the calculation of the ultimate loads of the system, which are based on the expressions given in section 9 of EC5 (2004).
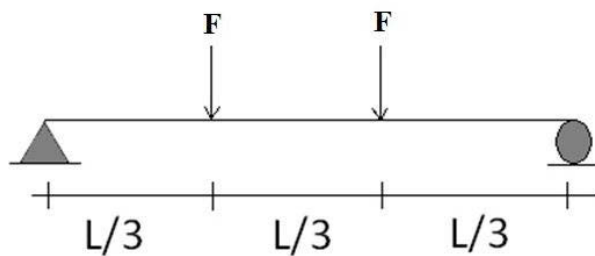
Figure 5.3 Four point bending loads

Equation 5.4 shows the ultimate load if exceeding the bending stress in extreme fibre of bottom flange cause the failure.

$$f_{b,bf} = n_{bf} \frac{My_{bf}}{I_{eff}} \quad \longrightarrow \quad F = \frac{3I_{eff}f_{b,bf}}{n_{bf}y_{bf}L} = 105kN \qquad \text{Eq.5.4}$$

Where y_{bf} is the distance between the extreme fibre of bottom flange and the neutral axis of the section and L is the span which is 8m. n_{bf} is the modular ratio of bottom flange, I_{eff} is the effective second moment of area of the section, and $f_{b,bf}$ is the bending design capacity of the materials used bottom flange (The values of n_{bf}, I_{eff} and $f_{b,bf}$ were presented in Table 5.2, Equation 5.2 and Table 5.1 , respectively). The corresponding maximum deflection is also presented in Equation 5.5.

$$\delta_b = \frac{23FL^3}{648(EI)_{eff}} = 201mm \qquad \text{Eq.5.5}$$

Where, EI_{eff} were calculated in Equation 5.3. Similarly, if exceeding the tension stress of bottom flanges cause failure, the ultimate load will be according to Equation 5.6.

$$F_{max} = \frac{3I_{eff}f_{t,bf}}{n_{bf}y_{(bf/2)}L} = 60kN \qquad \text{Eq.5.6}$$

Where $f_{t,bf}$ is the tension strength of bottom flange and $y_{bf/2}$ is the distance between the half of the depth of bottom flange and the neutral axis of the section, and $f_{t,bf}$ is the tension design capacity of the materials used bottom flange .The rest of the components were introduced as per Equation 5.4. The corresponding maximum deflection is also equal to 115mm which can be calculated according to Eq.5.7.

$$\delta_b = \frac{23FL^3}{648(EI)_{eff}} = 115mm \qquad \text{Eq.5.7}$$

Table 5.5 present the ultimate loads and the maximum deflection for 8m LVL modules, as a result of exceeding different design capacities. As it can be observed from the values of the table, exceeding the tension stress of bottom flanges is the weakest link of the system. This prediction, however, will be investigated with the experimental results in the following sections. Similar approach was taken for the 6m modules and Table

5.6 summarises the results. The ultimate load at each third span and the maximum deflection of 8m modules are predicted to be 60kN and 115mm, respectively, while the ultimate load (at each third span) and maximum deflection of 6m modules are predicted to be 46kN and 87mm, respectively.

Table 5.5 Ultimate loads and maximum deflections of 8m LVL modules

Failure Mode	Ultimate Load At each third span (kN)	Maximum Deflection At mid-Span (mm)
Exceeding Tension Stress in Bottom Flanges	60	115
Exceeding Bending Stress in Bottom Flanges	105	201
Exceeding Compression Stress in Top Flange	115	220
Exceeding Bending Stress in Top Flange	127	243
Exceeding Flexural Shear Stress in Web (at the centroid of section corresponding the maximum shear)	139	266
Exceeding Flexural Shear Stress in top flange (at the interface)	154	295
Exceeding Flexural Shear Stress in bottom flanges (at the interface)	169	324

Table 5.6 Ultimate loads and maximum deflections of 6m LVL modules

Failure Mode	Ultimate Load At each third span (kN)	Maximum Deflection At Mid-Span (mm)
Exceeding Tension Stress in Bottom Flanges	46	87
Exceeding Bending Stress in Bottom Flanges	78	148
Exceeding Compression Stress in Top Flange	99	189
Exceeding Bending Stress in Top Flange	103	197
Exceeding Flexural Shear Stress in Web (at the centroid of section corresponding the maximum shear)	94	179
Exceeding Flexural Shear Stress in top flange (at the interface)	99	190
Exceeding Flexural Shear Stress in bottom flanges (at the interface)	112	214

5.2.2   Floor System

The predicted neutral axis, flexural stiffness, the ultimate load and ultimate deflection of the 8m and 6m floor system are reported in Table 5.7 and Table 5.8. . If the three individual 8m modules are connected together side by side (Figure 5.4), the neutral axis location of the system will remain unchanged. The load and effective flexural stiffness of the system treble, and therefore the deflection remains unchanged (see Table 5.7 and 5.8). The procedure for calculating the $(y_c)_{floor}$ and the $(EI_{eff})_{floor}$ are exactly similar to that of presented in Table 5.2 and Table 5.3 and Equations 5.1 to 5.3. In Figure 5.4, the floor system is assumed to behave fully composite like one solid section where all beams are equally stiff. The values of Tables 5.7 and 5.8 will be compared with the finite element modelling (FEM) results in chapter 7. The possible methods of connecting the modules together and the finite element results of the floor system are also presented in detail in chapter 7.
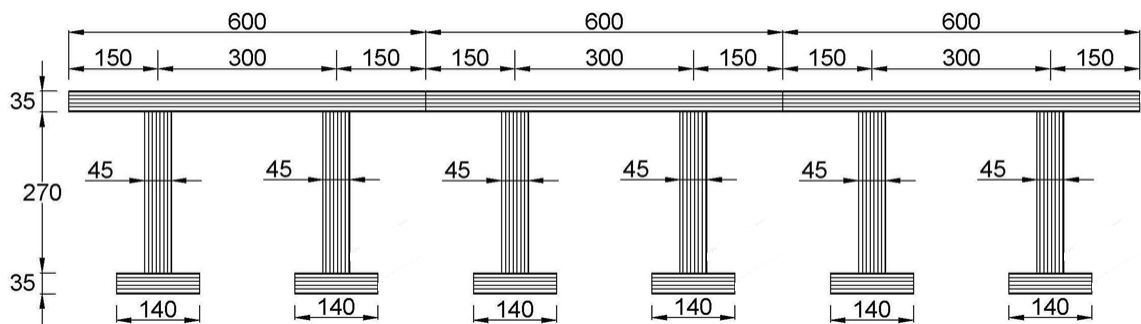
Figure 5.4 Floor System (by connecting three 8m modules side by side

Table 5.7 Analytically predicted response of 1.8*8m floor system

Neutral axis , $(y_c)_{floor}$	187.1mm
Flexural stiffness $(EI_{eff})_{floor}$	28.44E+06 Pa.m^4
Ultimate load (at each third span)	180 kN
Maximum Deflection	115 mm

Table 5.8 Analytically predicted response of 1.8*6m floor system

Neutral axis , $(y_c)_{floor}$	143.7mm
Flexural stiffness $(EI_{eff})_{floor}$	12.1E+06 Pa.m^4
Ultimate load (at each third span)	138kN
Maximum Deflection	87mm

5.3   Experimental Program

The name and number of the destructive and non-destructive tests conducted on LVL modules is presented in Table 5.9. All modules were tested under four point bending load with pin-roller boundary conditions. As shown in Table 5.9, a total number of six serviceability (SLS) and three destructive (ULS) tests were conducted on LVL timber modules.

Table 5.9 The experimental investigation plan

Name of the Modules	Overall Length (m)	Type of the Tests
L6-01	6.3	Subjected to serviceability load
L6-02	6.3	Subjected to serviceability load
L6-03	6.3	Subjected to serviceability load
U8-01	8.4	Subjected to serviceability load & ultimate load
U8-02	8.4	Subjected to serviceability load & ultimate load
U8-03	8.4	Subjected to serviceability load & ultimate load

As shown in Figure 1.1, the scope of this research project is limited to investigate the short term behaviour of the proposed floor system under static loading. The specimen's responses to long-term loading, in-plane loading, dynamic excitation, cyclic loading and loading history are outside the scope of this PhD research. Moreover, other aspects of performance such as assessment of acoustic performance, dynamic performance and the

possible interconnection systems alongside floor modules are not covered in the scope of this research project. The scope of this topic is limited to investigate the short term static behavior, but will address broader issues where relevant, by drawing from other research which is undertaken by other members of the UTS team (e.g. long term behavior and dynamic performance of the system (Rijal 2013 and Khorsandnia 2013)).

The features which were specifically investigated during the experimental program are summarised as follows:

- To evaluate the stiffness of the system by assessing deflection versus load and to interpret the serviceability and ultimate behaviour of the system.

- To evaluate the strength of the system by evaluating the stress versus strain characteristics at both serviceable and ultimate limit states.

- To assess the strain distribution over the depth of the section and to identify the composite behaviour and any non-linearity of the section.

- To clearly identify the failure modes of the system (whether that will be a material failure in the flanges and the webs, or a failure through web buckling, or a failure in the connections and interfaces).

5.3.1 The Test Setup

The 6m and 8m test specimens are thoroughly introduced in chapter 3 and the it was mentioned that Type 17 normal screws were used for the interfaces at 400mm spacing on each web (at an equal spacing of 37.5 cm and 38.5 cm for 6 m and 8 m span beams, respectively) and their role was to help the glue to set properly, while the actual bond between the flanges and the webs is provided by the glue (PURBOND). As shown in Figure 5.5a, the 8m modules are continued for 200mm off the support from each side; therefore, the overall lengths of the modules are 8.4m. The 6m modules however, have 150mm overhead from each side, with the overall span of 6.3m. All modules were tested under four point bending loads as shown in the figure (Figure 5.5b).
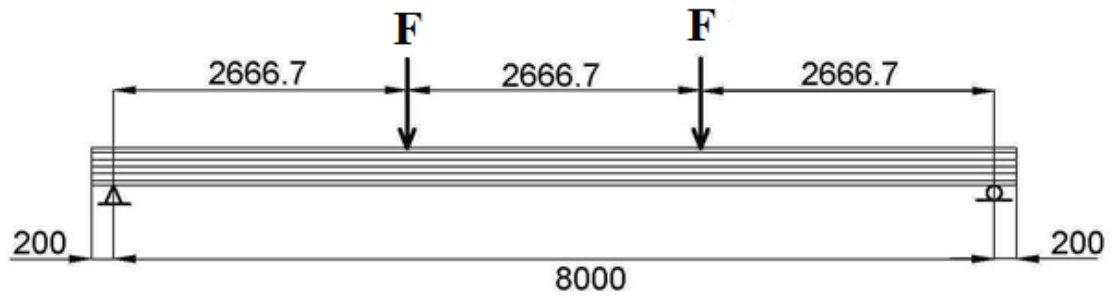
(a)
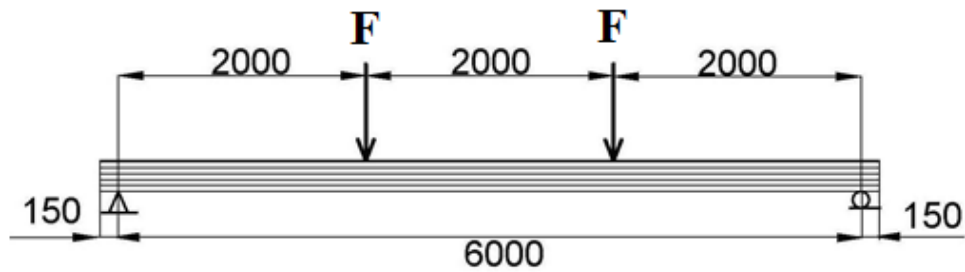
(b)

Figure 5.5 Schematic diagram of test setup (a) 8 m module (b) 6 m module

The pin-roller support boundary conditions were used for each test as shown in Figure 5.6. In order to replicate the pin support, a metal shaft was accommodated between the two steel plates with a groove in each plate so that the horizontal and vertical movement was constrained. However, for the roller support there was no groove on the plates so that the metal shaft could freely move in the horizontal direction in order to replicate the roller support. The pin and the roller supports sat on concrete blocks as shown in Figure 5.7.
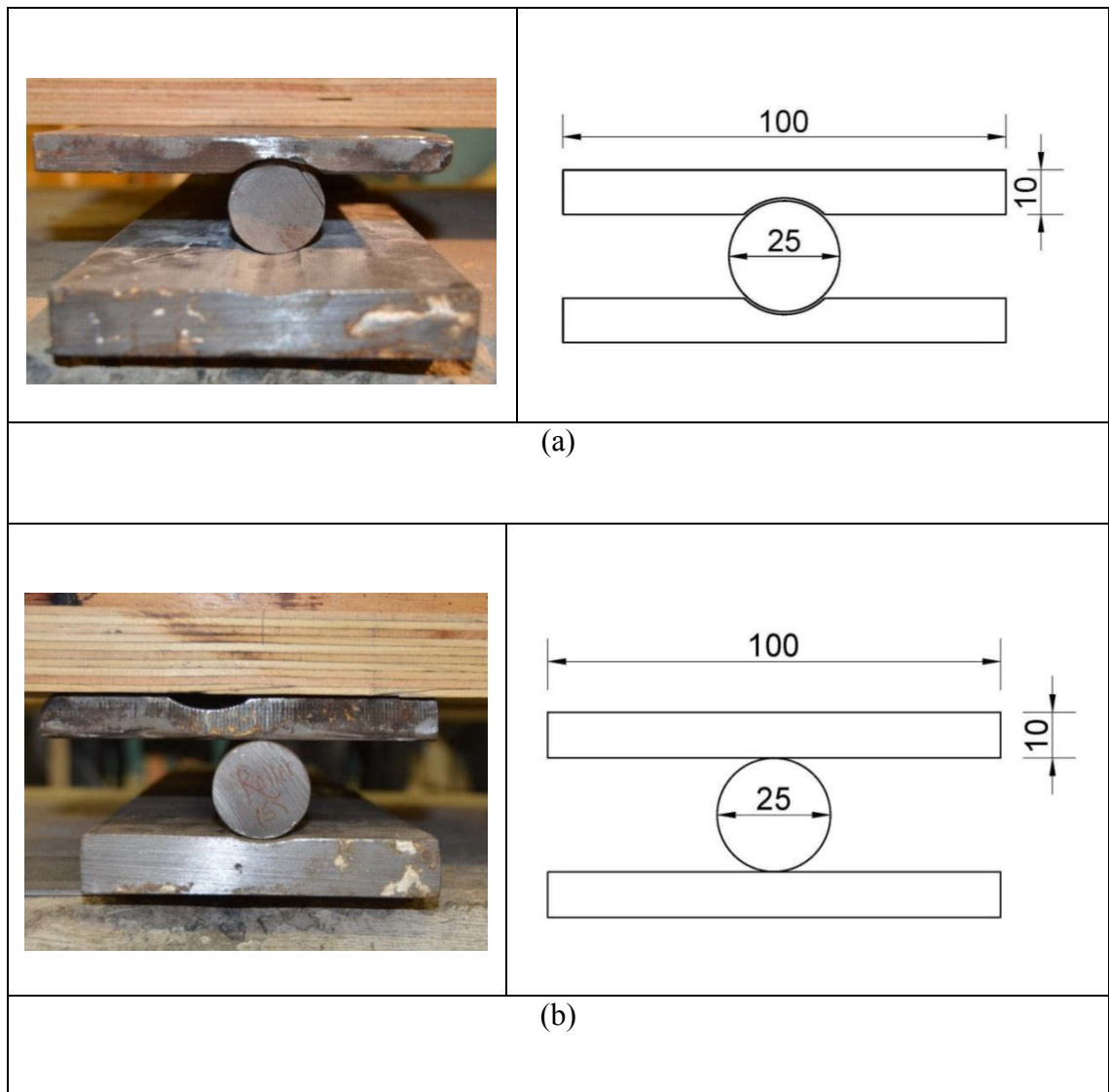
Figure 5.6 Boundary conditions (a) pinned support (b) roller support (dimensions in mm)

Figure 5.7 Layout of the 8m LVL Modules

The necessary equipment for conducting four point bending tests consists of four main parts: (1) the reaction frame, (2) the loading system consisting of the hydraulic jacks and the load cells, (3) the instrumentation and (4) the data processing system. The reaction frame consists of two main load frames and a connecting beam (Figure 5.8). The connecting beam is 3m long which carries the hydraulic jacks and the load cells (Figure 5.9). In order to conduct 4-point bending tests, the hydraulic jacks were placed at each third span of the timber modules. 130 kN (13 ton) hydraulic jacks were used for both the SLS and ULS tests, whereas 150 kN load cells were used for ULS tests and 45 kN load cells were used for SLS tests. The load was increased at a constant rate up to the service load and was returned to zero for the serviceability tests, whereas for the ultimate state tests the load was increased at a constant rate until the failure. The strain and deflection responses of the modules were measured thorough a number of instrumentations presented fully in the following section.
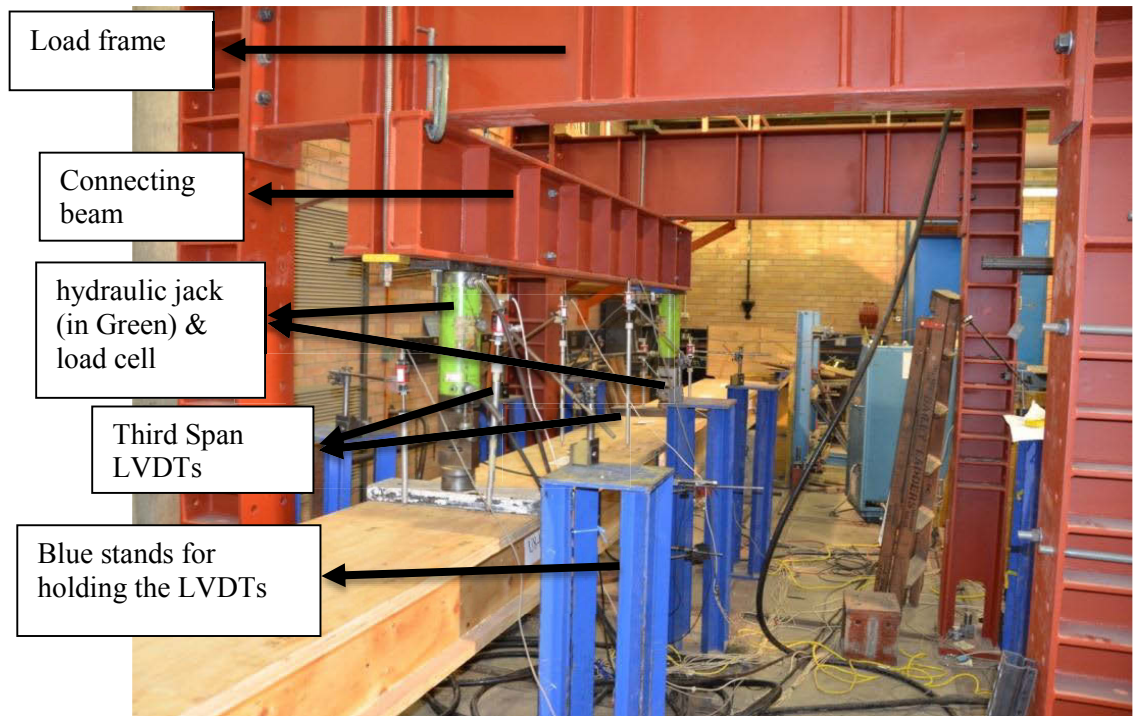
Figure 5.8 The Reaction frame
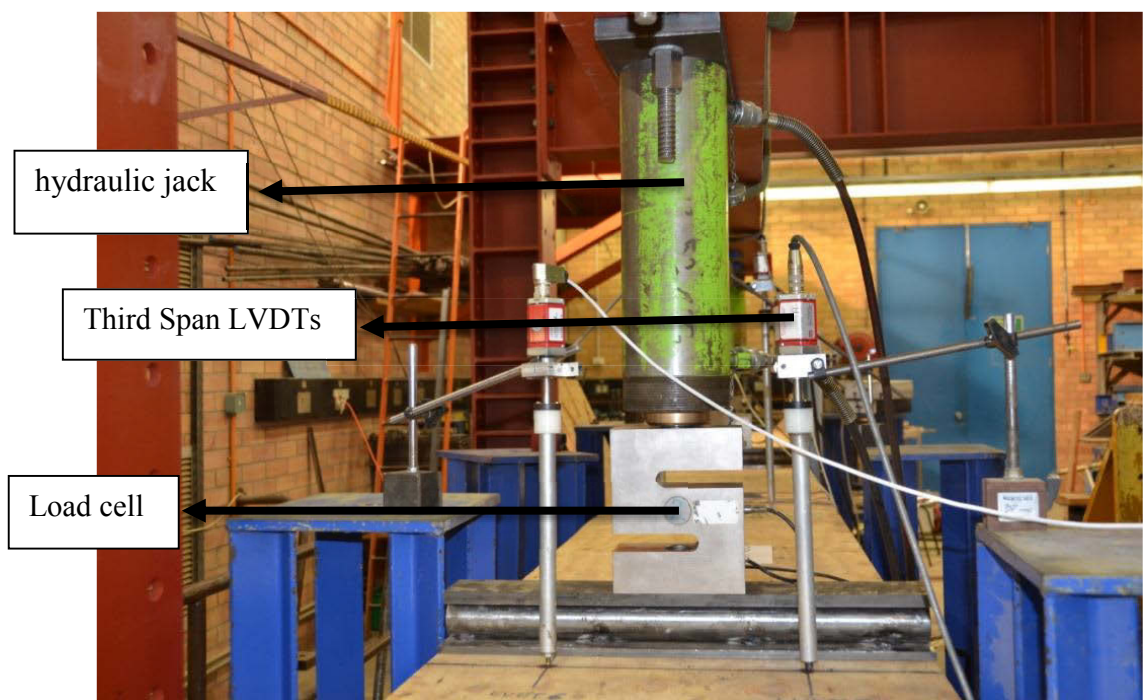
Figure 5.9 The hydraulic jacks and the load cells

The data processing system consisted of the terminal blocks, the data acquisition and a computer (Figure 5.10). All the instrumentations were connected to the terminal blocks through cables, which in turn were connected to the data acquisition system. The experimental data were transferred from the data acquisition system to a computer where they were recorded and saved.
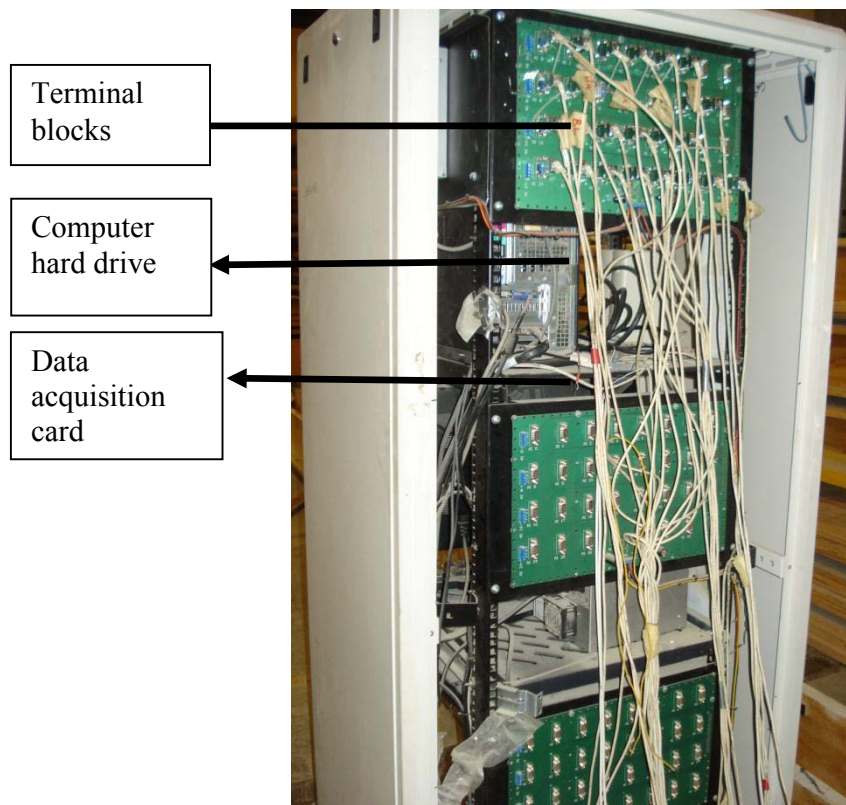
Figure 5.10 Data processing system

5.3.2   Instrumentation

Linear Variable Differential Transformers (LVDTs) were used to measure beam deflections at key locations alongside the modules. Figure 5.11 depicts the location and identification number of LVDTs. A total of six LVDTs were used to measure the vertical movement of the LVL modules, that is, two LVDTs at mid-span and two at each third span (Figure 5.12 and Figure 5.13).
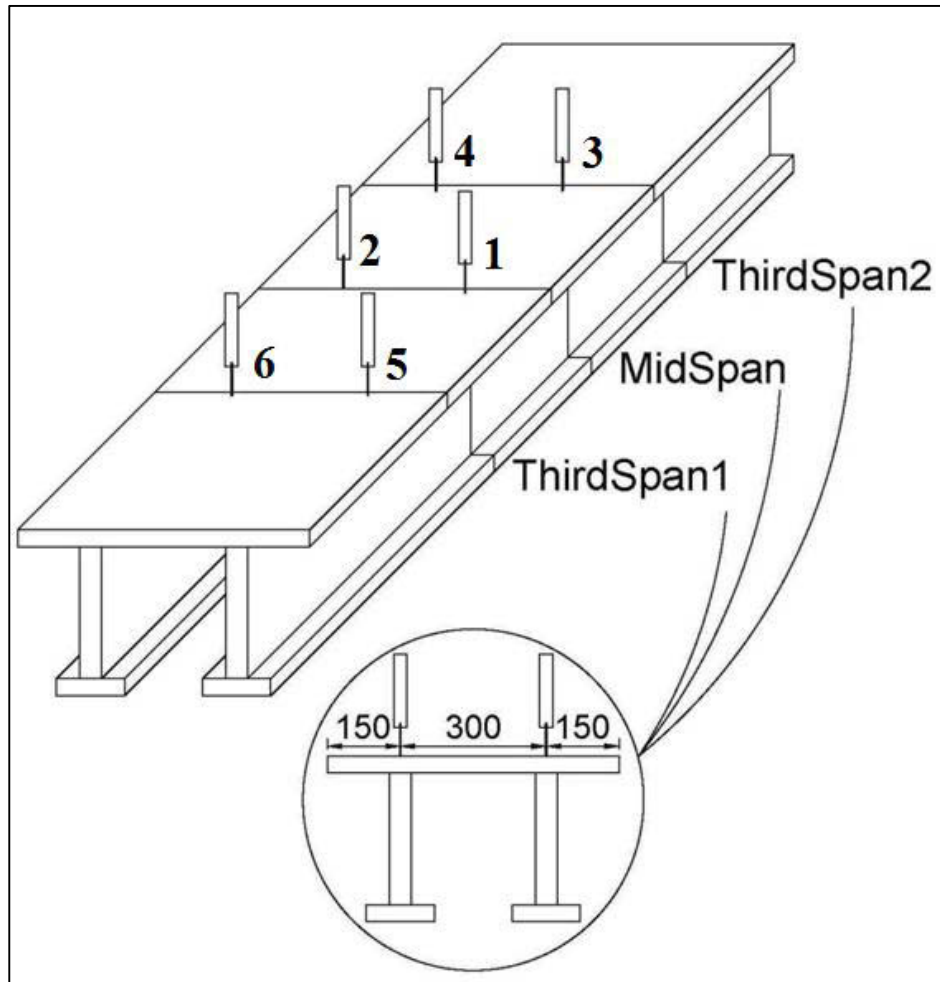
Figure 5.11 Locations and numbers of LVDTs (dimensions in mm)

Figure 5.12 Third-span LVDTs

Figure 5.13 Mid-span LVDTs

Futhermore, to capture any possible slip at interfaces, four LVDTs were installed horizontally on each end of the timber modules. As shown in Figure 5.14, the LVDTs were fixed horizontally on the webs with screws while the steel brackets were installed on the top and bottom flanges and thus, any relative movment between flages and webs could be measured during the tests.

Figure 5.14 Horizontal LVDTs for measuring any possible slip at interfaces

The travel range for the horizontal LVDTs was 25mm while the travel range of verical LVDTs (for measuring the defletion of the modules) was 150mm and 400mm for third span and mid-span LVDTs, respectively. As shown in Figure 5.15, type PL-60-11 strain gauges with the gauge length of 60mm were used for the experimental investigation, to assess the strain responses of the LVL modules versus load. The long strain gauges are suitable for timber because they negate the localised effects that occur in timber due to the grain structure.
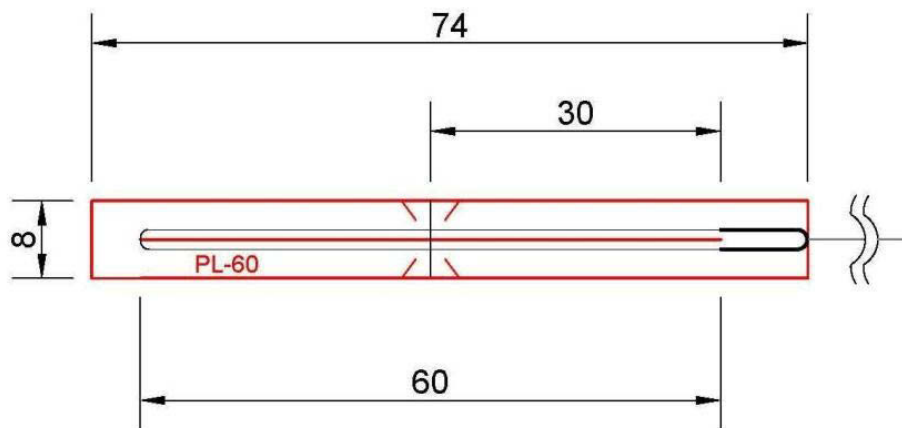
Figure 5.15 Type PL-60-11 Strain Gauges

Figure 5.16 depict the locations and the adopted names of the stain gauges used for the first test (U8-01). At mid-span, seven strain gauges were attached to the top flange (stain gauges a, b, c, d, aa, bb, cc) with 75mm spacing, in order to verify the linear characteristics of the specimens, and any possible shear lag in the system. A number of strain gauges were also attached overt the depth of the section to assess the composite behaviour of the system. Additionally, 10 stain gauges were attached at half a meter off the mid-span, to have a cross-check for the mid-span responses (Figure 5.16b). After conducting the first test (U8-01) and completing the data analysis, some of the strain gauges were eliminated due to their predicted behaviour. Hence, as shown in Figure 5.17, the number of strain gauges was reduced to 21 for the second and third destructive tests (U8-02 and U8-03) and finally 8 strain gauges were used at mid-span for the serviceability tests of the 6m modules which are shown in Figure 5.18. Figure 5.19a

and Figure 5.19b show the strain gauges at top flange and over the depth of the section for U8-03 at mid-span, respectively.
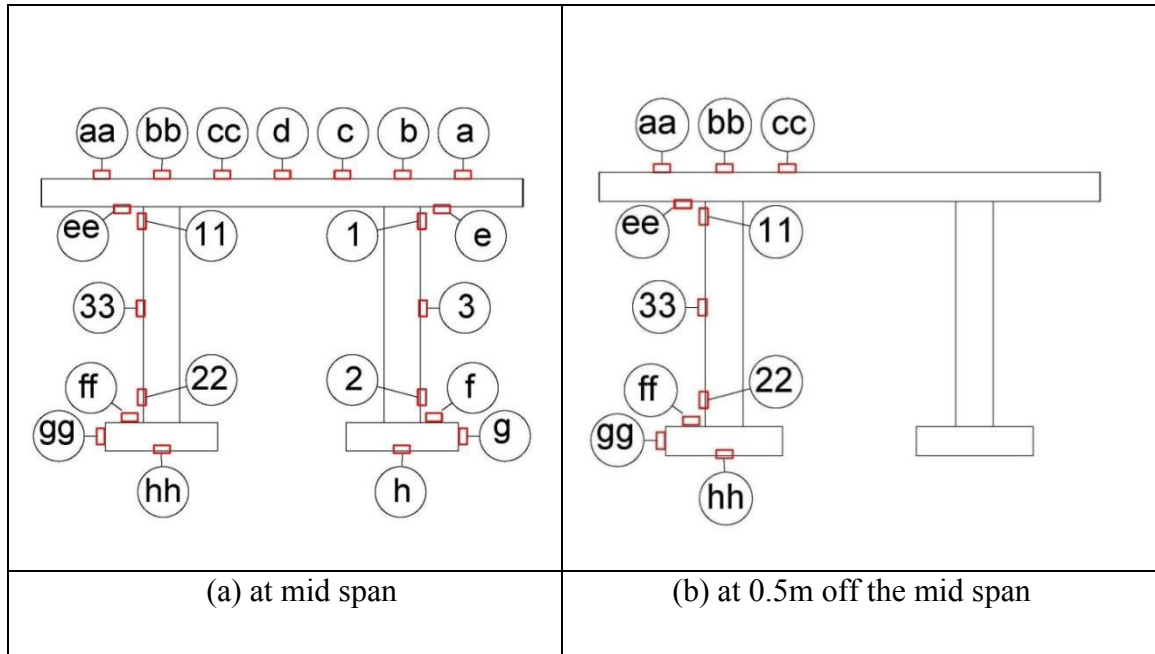
Figure 5.16 Adopted names and locations of the Strain Gauges U8-01

(a) at mid span, (b) at 0.5m off the mid span
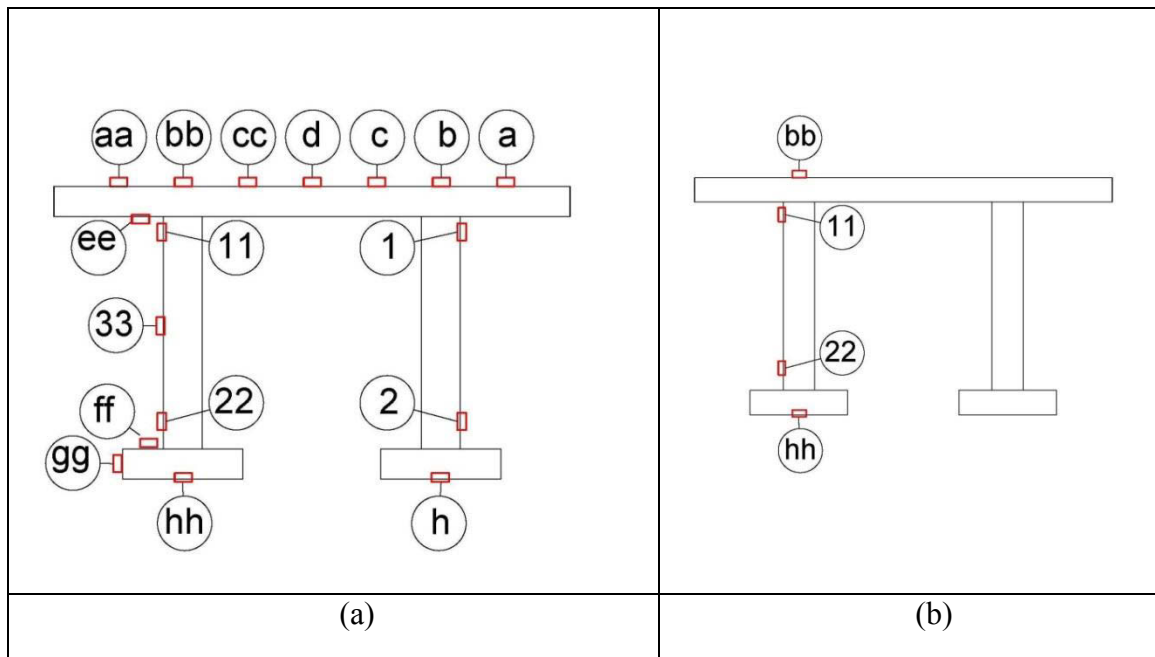
Figure 5.17 Adopted names and locations of the Strain Gauges for U8-02 and U8-03

(a) at mid span, (b) at 0.5m off the mid span
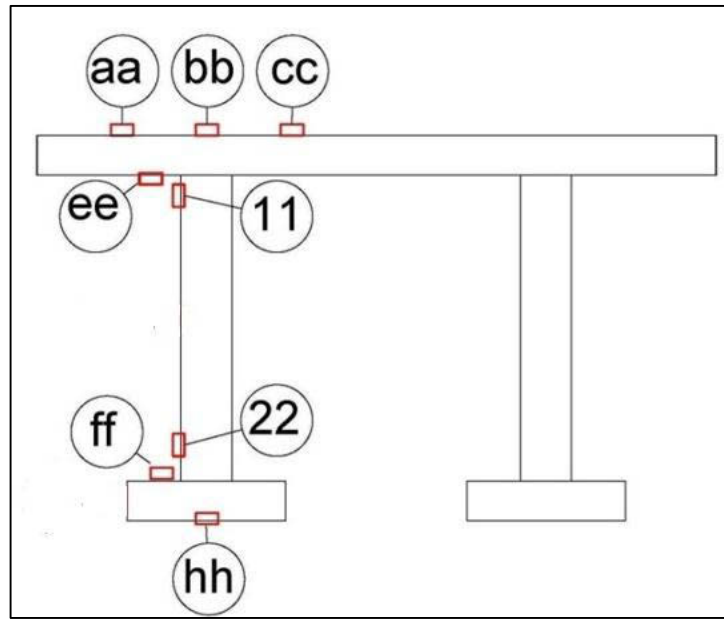
Figure 5.18 Adopted names and locations of the Strain Gauges for 6m modules
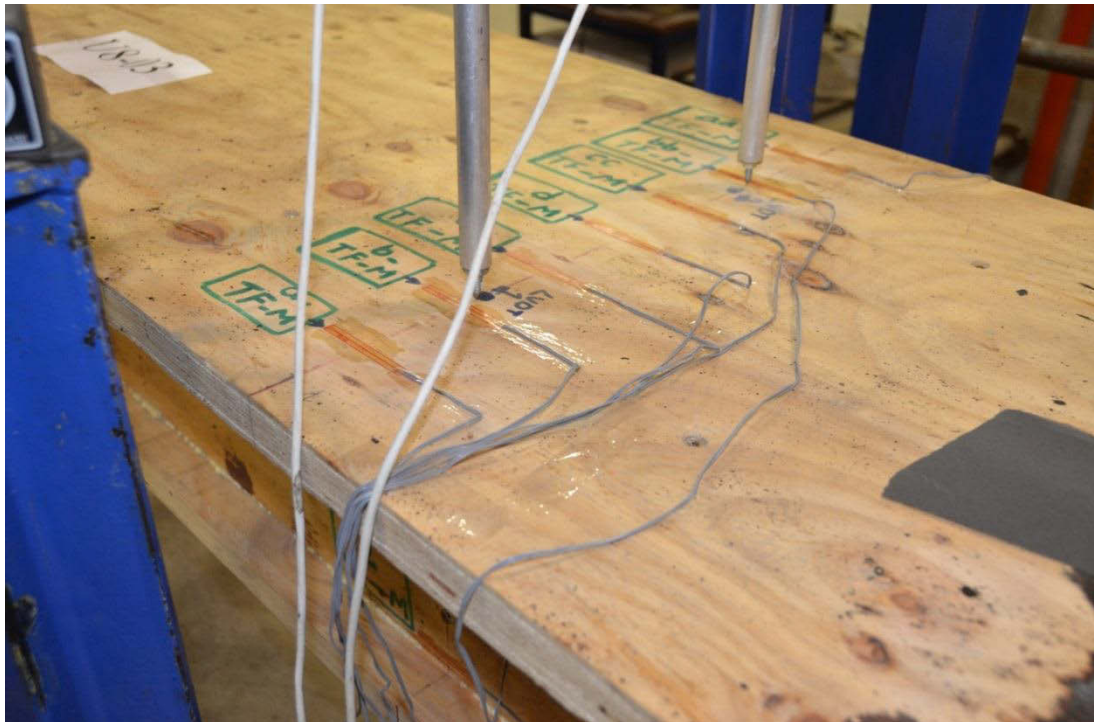
(a)
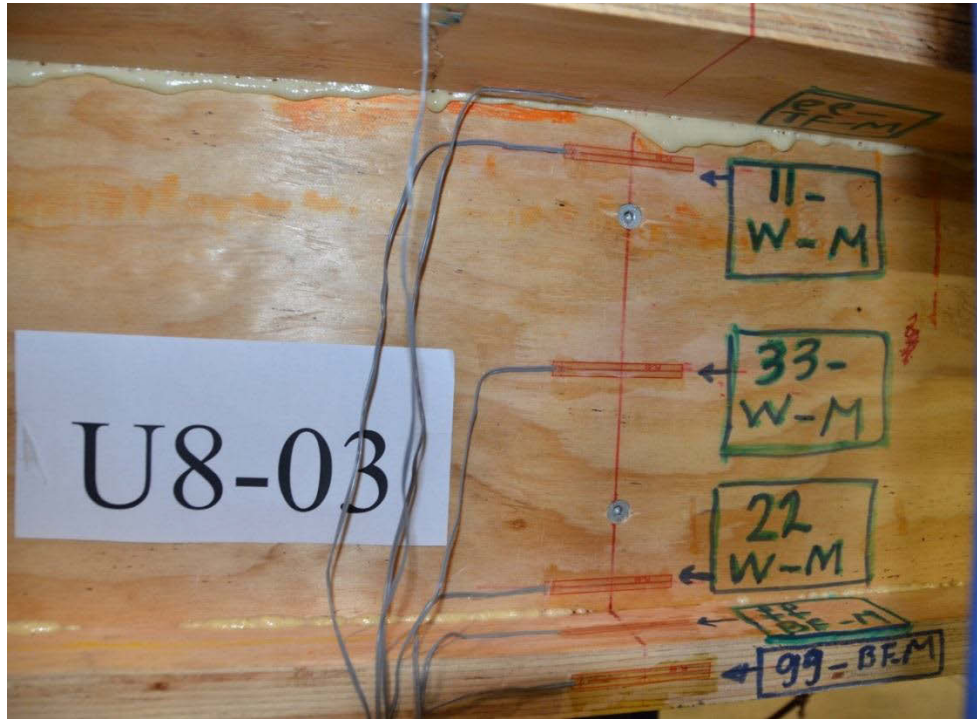
(b)

Figure 5.19 Strain gauges of U8-03 (a) at top flange, (b) over the depth of the section

5.4   Experimental Results

5.4.1   Failure Modes

The bond between the top and bottom flanges is assumed to be fully composite, and this assumption was to be investigated during the tests. In this regard, for the first and third destructive tests (U8-01 and U8-03), sufficient glue was used in fabrication of the modules in a way that excessive glue was visible along the interfaces alongside U8-01 and U8-03 (See Figure 5.19 for example, where excessive glue is visible at the interface). However, for the second destructive test, a lack of adequate glue was quite noticeable between the top flange and webs at about one third of the beam near the pin support so that the failure of the system can be assessed in case of lack of adequate glue. Figure 5.20 to Figure 5.22 show the failure of U8-01 and U8-03.

Figure 5.20 Failure of U8-01, east side of Module

Figure 5.21 Failure of U8-01, west side of Module
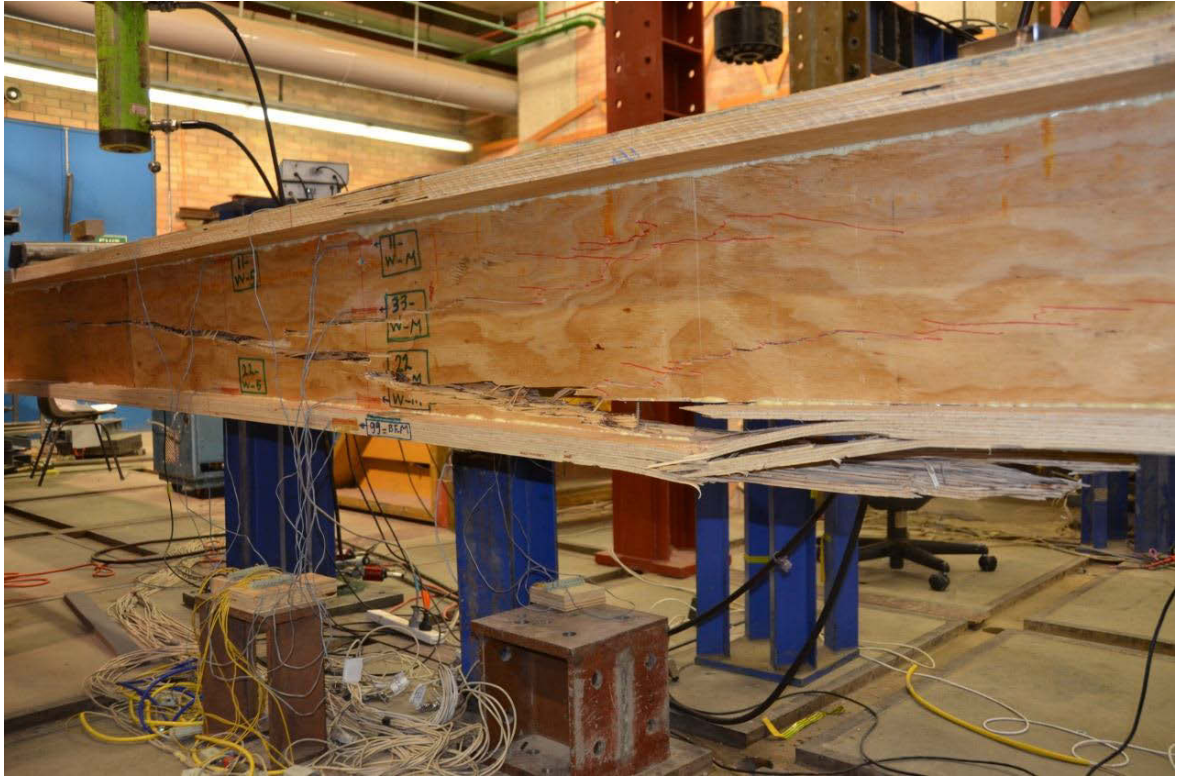
Figure 5.22 Failure of U8-03

As expected, in U8-01 and U8-03 the glue and the screws provided a fully composite structural bond as there was no slip or any failure at the interfaces. There was also no buckling in the top flange or webs, as the top flange was fully glued to the webs and so it operated like a stiffener. In both U8-01 and U8-03, the failure was a brittle one in which the load was increased at a constant rate until a sudden failure occurred in LVL. As can be observed in Figure 5.20 to Figure 5.22, the failure mode of the system was a combination of bending and shear failure in the LVL, that is, exceeding the tensile strength of the bottom flange triggered the failure, although the shear within the web also contributed to propagation of the crack.

However, due to less rigorous fabrication of U8-02, a lack of adequate glue was identified between the top flange and webs at about one third of the beam near the pin support. Consequently, the failure mode of the system was different to U8-01 and U8-03. A few reductions in load (premature load slip) were identified during the test and a notable slip was observed at the interfaces between the top flange and the webs, and the final failure was a premature failure of the LVL when compared to the other two

specimens (Figure 5.23). It was noted however, that the load was still well in excess of the design ultimate required to be resisted by the beam. After the U8-02 test was completed, the screws were removed from the top flange. It was interesting to note that all of the screws in the poorly glued side, up to the mid-span were clearly bent (Figure 5.24), and a few of them had failed (Figure 5.25) , and a notable slip of about 5mm was observed at the interfaces (Figure 5.26 and Figure 5.27).

Therefore, in U8-02 the glue failed first and the screws carried the load until some of the screws failed, and finally the failure of the beam happened at around mid-span. This test showed that the composite action of the modules is only provided if the glue acts perfectly.

Figure 5.23 Failure of U8-02

Figure 5.24 Deformation of one of the screws after failure of U8-02
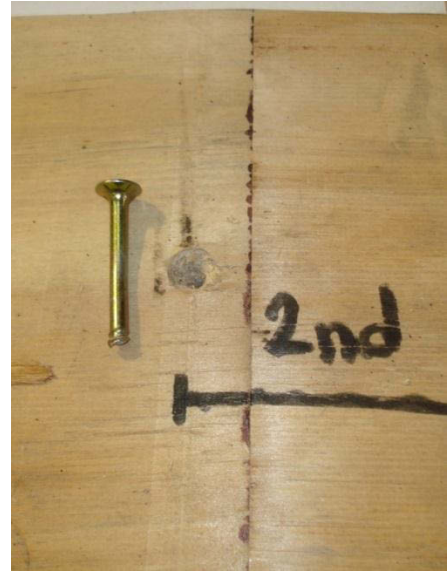
Figure 5.25 Failure of one of the screws after failure of U8-02

Figure 5.26 Notable slip at interfaces (East side web)

Figure 5.27 Notable slip at interfaces (west side web)

5.4.2   Stiffness and Strength of the Modules

The global stiffness (K) of the modules can be calculated from Equation 5.8 at mid-span, and Equation 5.9 at third-span where δ_{Mid} and δ_{Trd} are the measurements of LVDTs under mid-span and third-span, respectively, and F_{Ave} is the average reading of load cells 1 and 2 (Equation 5.10) located at each third span. Therefore, the slope of load-deflection graphs will represent the global stiffness (K) of the modules.

$$K_{Mid} = \frac{F_{Ave}}{\delta_{Mid}}$$

Eq.5.8

$$K_{Trd} = \frac{F_{Ave}}{\delta_{Trd}}$$

Eq.5.9

$$F_{Ave} = \frac{F_{LoadCell1} + F_{LoadCell2}}{2}$$

Eq.5.10

On the other hand, the general formula for calculating the deflection of a beam under Mid-Span and Third-Span are represented by Equations 5.11 and 5.12, respectively. Thus, the flexural stiffness (EI) of the system can be calculated by Equations 5.13 and 5.14, respectively.

$$\delta_{Mid} = \frac{23FL^3}{648EI}$$
Eq.5.11

$$\delta_{Trd} = \frac{5FL^3}{162EI}$$
Eq.5.12

$$(EI)_{Mid} = \frac{23L^3}{648} K_{Mid}$$
Eq.5.13

$$(EI)_{Trd} = \frac{5L^3}{162} K_{Trd}$$
Eq.5.14

Consequently, the flexural stiffness of the system can be obtained through experimental results, that is, by using the slope of the load-deflection curves or the global stiffness of the system (K) in Equations 5.13 and 5.14.

Figure 5.28 and Figure 5.29 shows the load –deflection graph for U8-01 at mid-span and third span, respectively. The deflections were plotted versus the average load readings of load cell 1 and load cell 2 (Ave Load as shown in the graphs). As can be observed from the graphs, U8-01 shows a complete linear behaviour up to the failure point where a sudden failure occurs (sudden drop in load indicating a brittle failure). Moreover, the results for SLS test are exactly overlapping the ULS test which also indicates the linear behaviour of the system. For the third destructive test (U8-03), the system showed similar behaviour to U8-01. As shown in Figure 5.30 and Figure 5.31, a complete linear behaviour was observed under serviceable and ultimate loads and the linear characteristics of the system were preserved up to the failure point, which was a brittle one.

Figure 5.32 presents the load-deflection graph for U8-02. Since the failure was a premature one due to lack of adequate glue at the interface (described in previous section), the load-deflection graph shows multiple drops in load, as well as a non-linear behaviour after the second failure. However, the behaviour of the module was fully linear up to 40kN (at each third span) or 16 kPa ($\frac{40*2}{8*0.6}$), which is still well above the service load (3 kPa). Furthermore, the serviceability test shows a linear behaviour as shown in Figure 5.32.
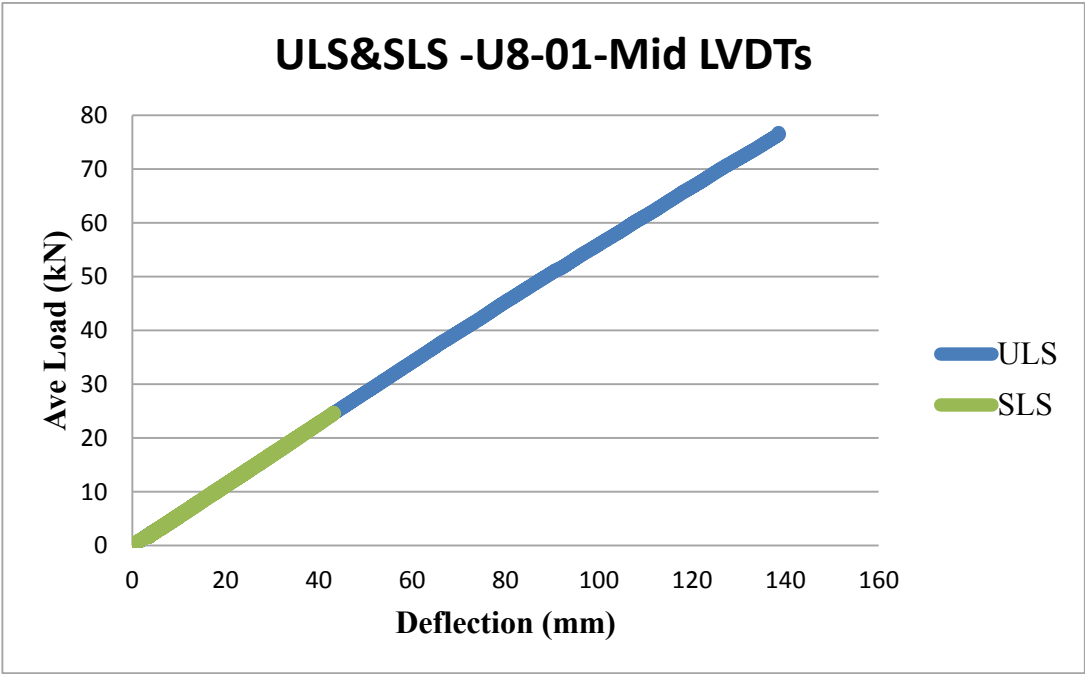
Figure 5.28 Load –deflection graph for U8-01 at mid-span
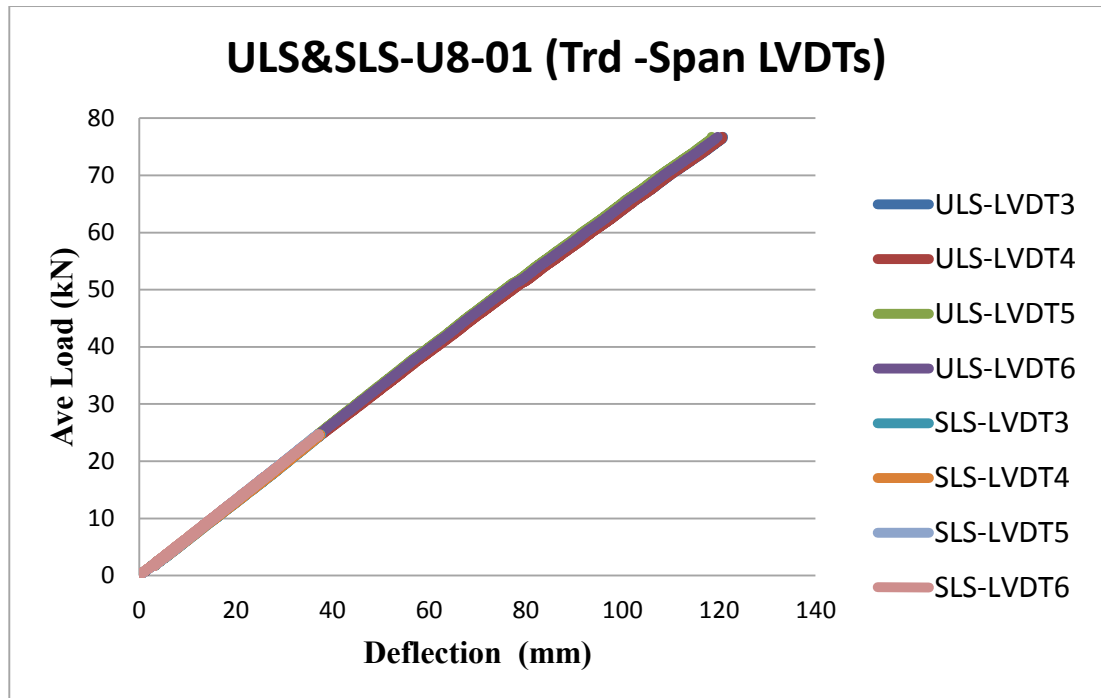
Figure 5.29 Load –deflection graph for U8-01 at third-span
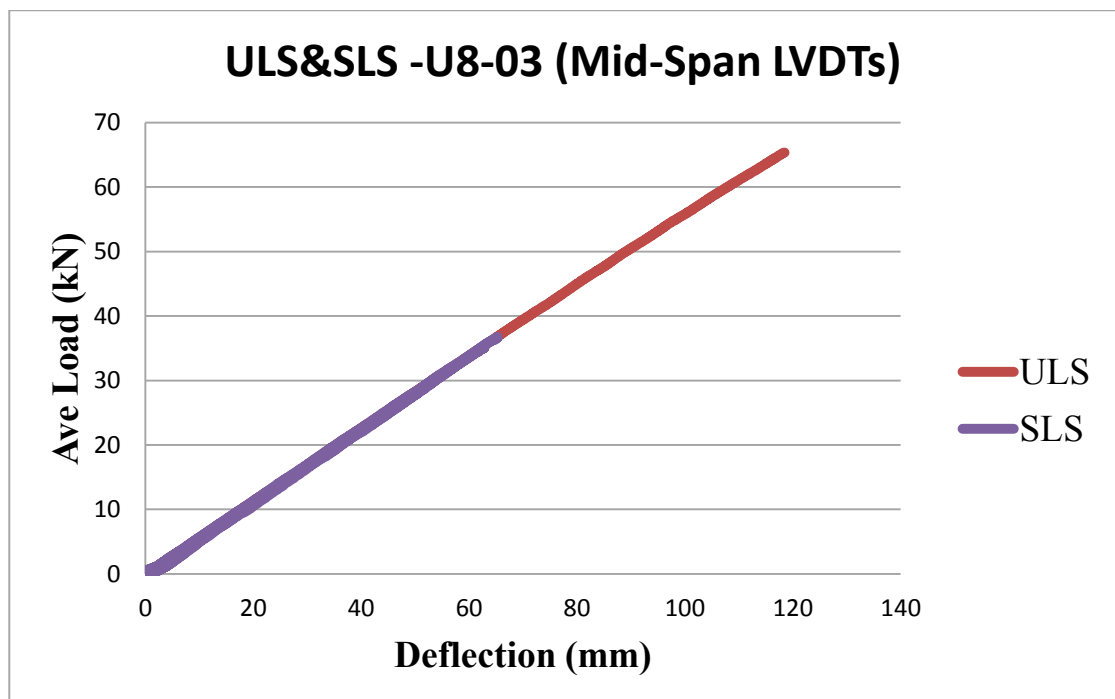
Figure 5.30 Load –deflection graph for U8-03 at mid-span
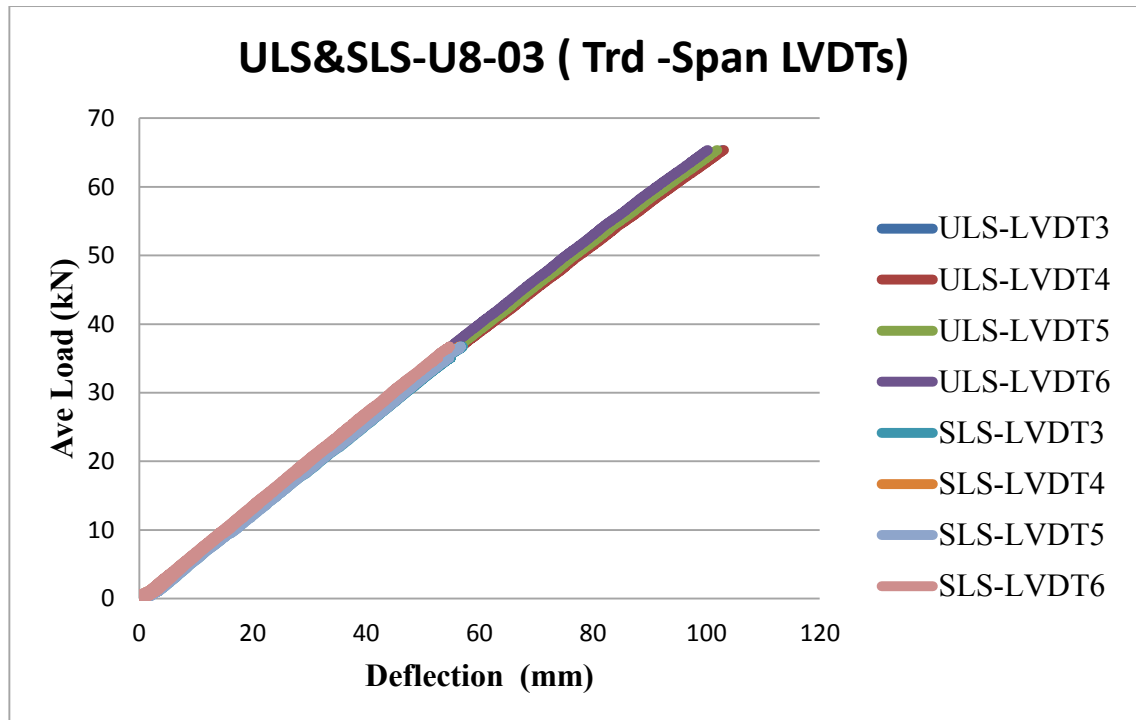
Figure 5.31 Load –deflection graph for U8-03 at third-span
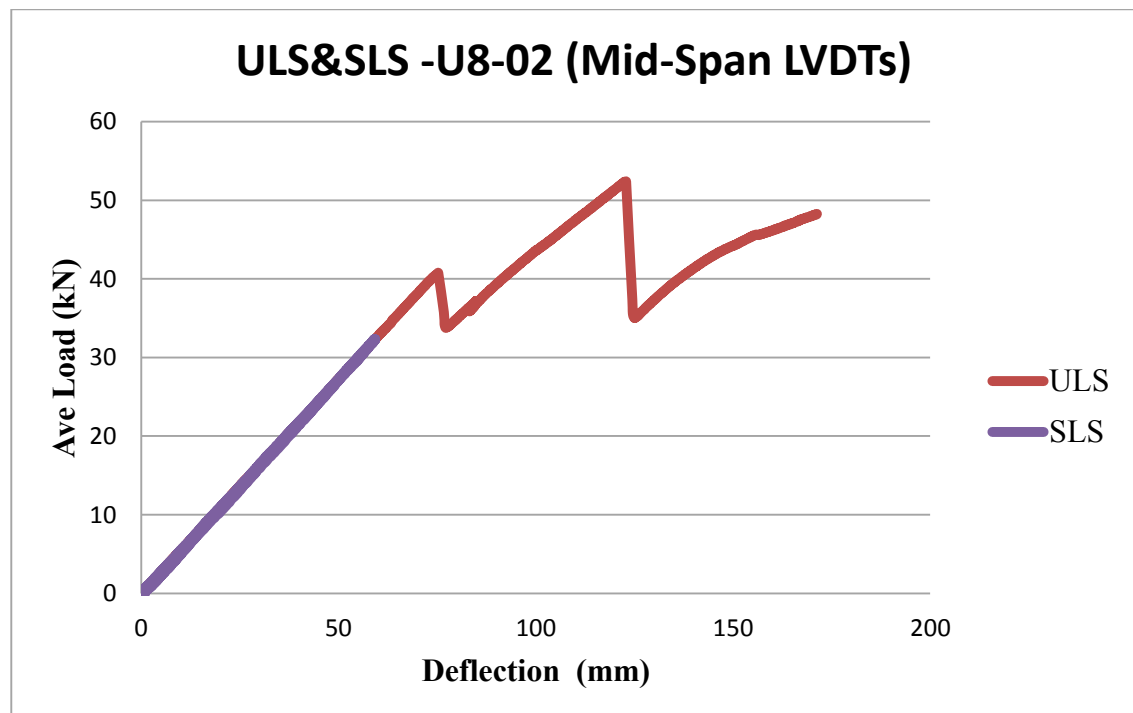
Figure 5.32 Load –deflection graph for U8-02 at mid-span
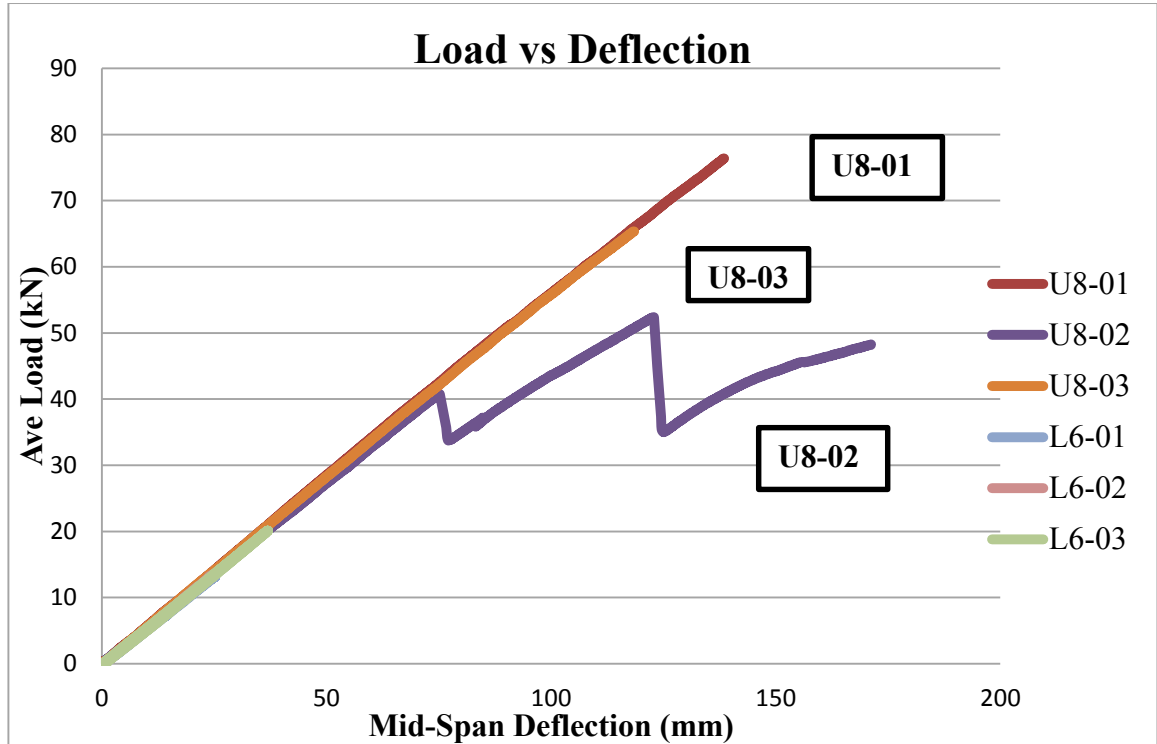
Figure 5.33 A comparison of Load-Displacement for all modules (mid-span)

Figure 5.33 shows a comparison of load-deflection graphs for all tests. It shows that all the modules (L6-01, L6-02, L6-03, U8-01, U8-02 and U8-03) show a similar global stiffness (K) under service and ultimate load. The linear behaviour of the system is also confirmed by plotting the load versus strain gauge readings for every single strain gauge, and all displayed a linear trend until the point of failure (see strain gauge graphs in Appendix B). Moreover, no shear lag was observed in top flange of LVL modules as the readings of all strain gauges were similar (see Appendix B).

Table 5.10 shows the values of the global stiffness (K) for all modules. For the destructive tests (U8-01, U8-02 and U8-03) the slope of the load displacement curve was measured between 10kN to 30 kN whereas, for L6-01 and L6-02 the slopes were measured between 5kN to 20kN, and between 5kN to 12kN for L6-01 (since L6-01 was loaded up to 13kN). As mentioned earlier, the flexural stiffness of the modules as a result of the experimental tests is obtained by using Equations 5.13 and 5.14. On the other hand, the predicted flexural stiffness with assuming fully composite behaviour was also presented in Table 5.4. A comparison between the predicted flexural stiffness

and the flexural stiffness of the modules as a result of the experimental tests is presented in Table 5.11.

Table 5.10 A comparison between the global stiffness of the modules

	LVDT1	LVDT2	LVDT3	LVDT4	LVDT5	LVDT6
	(KN/mm)	(KN/mm)	(KN/mm)	(KN/mm)	(KN/mm)	(KN/mm)
U8-01	0.57	0.57	0.65	0.65	0.67	0.67
U8-02	0.54	0.54	0.62	0.62	0.62	0.63
U8-03	0.56	0.56	0.65	0.65	0.65	0.67
L6-01	0.51	0.54	0.58	0.61	0.59	0.60
L6-02	0.54	0.55	0.62	0.62	0.61	0.63
L6-03	0.55	0.55	0.61	0.62	0.62	0.62

Table 5.11 A comparison between the experimental and predicted flexural stiffness of the modules at mid-span

	$EI_{(Experimental, average)}$	$EI_{(Prediction)}$	$EI_{(Pred)} /EI_{(Exp)}$
	$(N.mm^2)$	$(N.mm^2)$	
L6-01	4.07E+12	4.03E+12	0.99
L6-02	4.21E+12	4.03E+12	0.96
L6-03	4.23E+12	4.03E+12	0.95
U8-01	10.40E+12	9.48E+12	0.91
U8-02	9.86E+12	9.48E+12	0.96
U8-03	10.26E+12	9.48E+12	0.92

The values of Table 5.11 shows less than 10% difference between the experimental results and analytically predicted results, which is deemed acceptable because of the high variation in MoE (Table 5.1) as well as other material properties of the LVL which was observed during the material properties tests. Therefore, the fully composite behaviour of the modules was also investigated through calculating the stiffness of the system.

It is also noteworthy that after each serviceability and destructive test, the Moisture Content (MC) of the LVL samples were also measured according to AS/NZS 1080.1 (AS/NZS 1080.1 2012). Small blocks of LVL with the size of 100mmx100mmx50mm were weighed before and after placing in the oven for 24 hours, at the temperature of 102ºC to 105ºC. The percentage MC of the LVL blocks were calculated using Equation 5.15, in which M_0 and M_i are the oven dried mass and the initial mass of the LVL samples, respectively. The results show that the MC values of the timber modules were around 10% for all tests.

$$M.C. = \frac{M_i - M_0}{M_0} * 100$$
Eq.5.15

5.4.3 Composite Behaviour of the Modules

To investigate the composite characteristic of the modules, the strain distribution over the depth of the section at serviceability and ultimate limit states were assessed. As shown in Figure 5.34 to Figure 5.38 which are for the U8-03 module, the graphs depict the strain responses versus the location of gauges over the depth of the system at different load stages. As seen in the graphs, the locations of the strain gauges from the base of the system are specified along the vertical axis while the strain gauge responses are shown along the horizontal axis, and a linear regression was fit through the strain responses. All strain gauges above the neutral axis of the section have negative values (readings) as they are under compression and all the strain gauges below the neutral axis have positive readings as they are under tension. Therefore, the location of the neutral axis is identified by the point where the vertical axis intersects the diagonal regression line (the constant value of the regression line). The level of the composite action of the system is identified by the correlation of the strain gauge responses, i.e. coefficient R^2

of the regression line, where R^2 equals to 1 indicates a perfect correlation among the data. In summary, in the equations of the regression line, the constant value of the regression line represents the neutral axis of the module, and the value of coefficient R^2 represents the level of composite action of the system.

As shown in Figure 5.34 to Figure 5.38, the neutral axis of the U8-03 is located at 192.63 mm at 10kN, 191.71mm at 30kN, 191.01mm at 50kN and 190.31mm at 65kN (which is the failure load). However, from the prediction model with the assumption of a fully composite section, the neutral axis was calculated to be located at 187.1mm from the base (see Table 5.4), which is about 3% different from the location of the neutral axis obtained from experimental tests, and confirms the fully composite behaviour of the section. Table 5.12 summarises the results. This procedure was repeated for all the stain gauges on the east side web as well as the strain gauges which were located at 0.5m off the mid-span (for a cross-check) and Figure 5.39 shows the results.

It can be observed from the graphs (Figure 5.39) that the difference between the experimental results and the analytically predicted results remains below 3% for all strain gauges at all different load levels, which indicates a fully composite behaviour of the module.
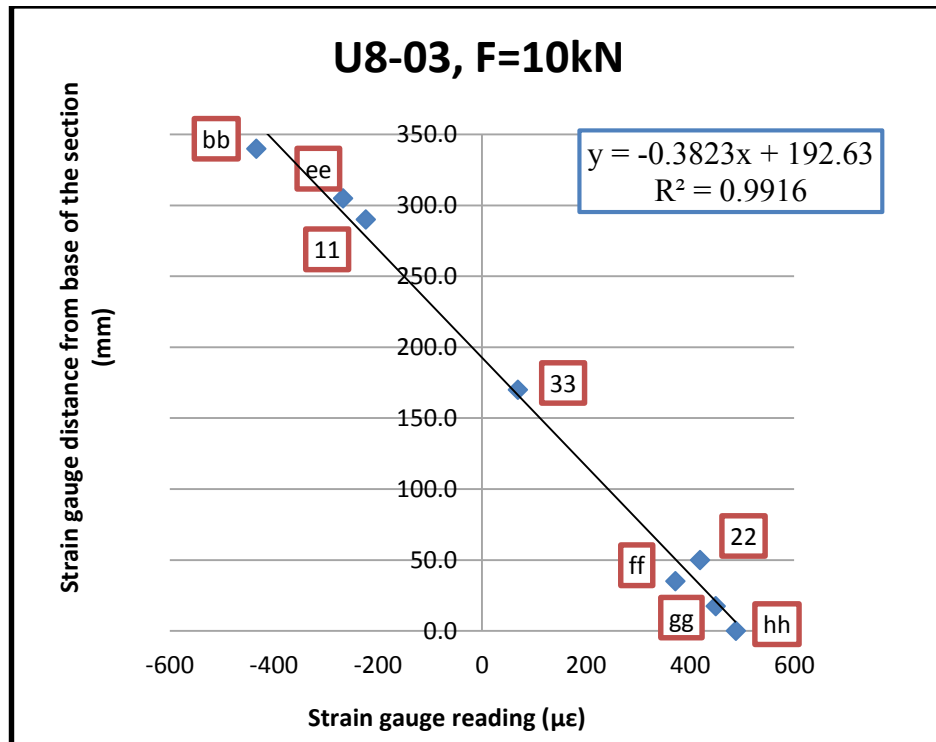
Figure 5.34 Strain gauges readings vs locations of the gauges for U8-03, west web (mid-span) at P=10kN
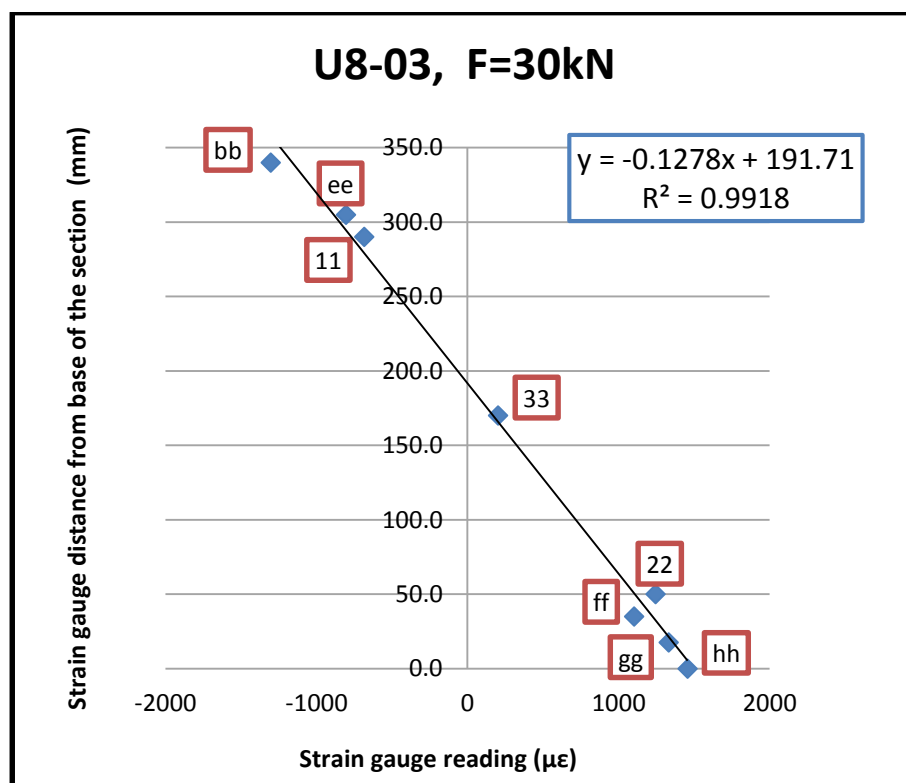
Figure 5.35 Strain gauges readings vs locations of the gauges for U8-03, west web (mid-span) at P=30kN
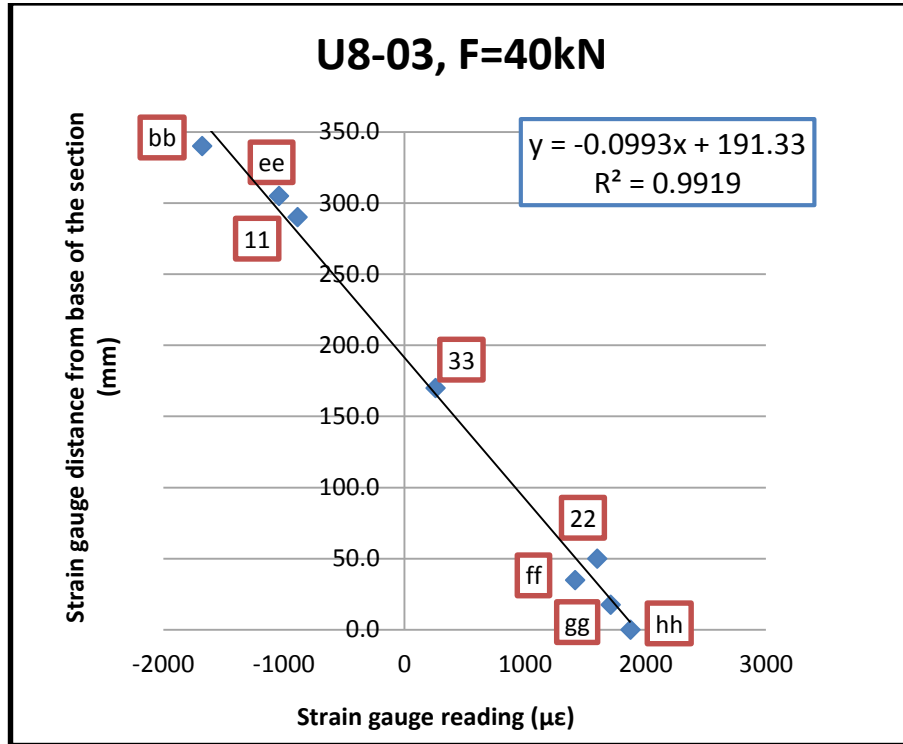
Figure 5.36 Strain gauges readings vs locations of the gauges for U8-03, west web (mid-span) at P=40kN
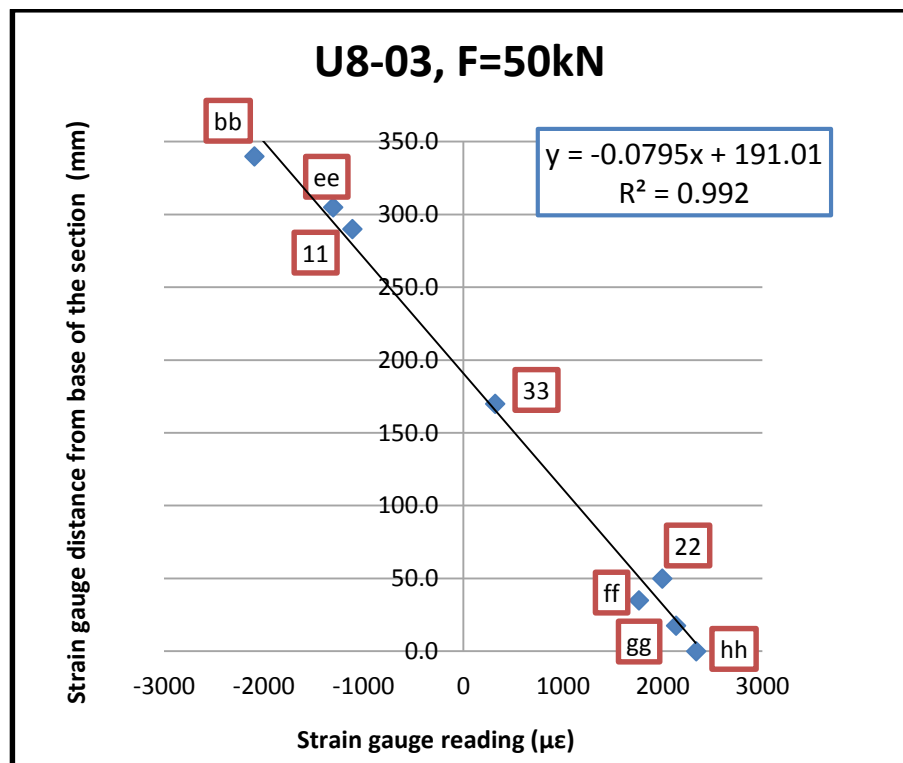
Figure 5.37 Strain gauges readings vs locations of the gauges for U8-03, west web (mid-span) at P=50kN
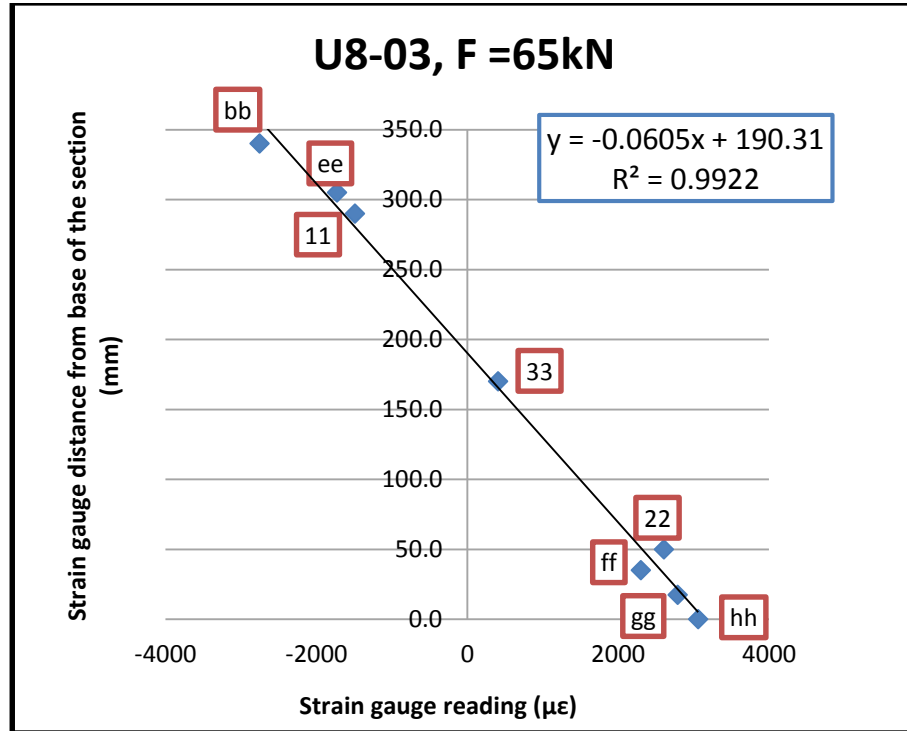
Figure 5.38 Strain gauges readings vs locations of the gauges for U8-03, west web (mid-span) at P=65kN
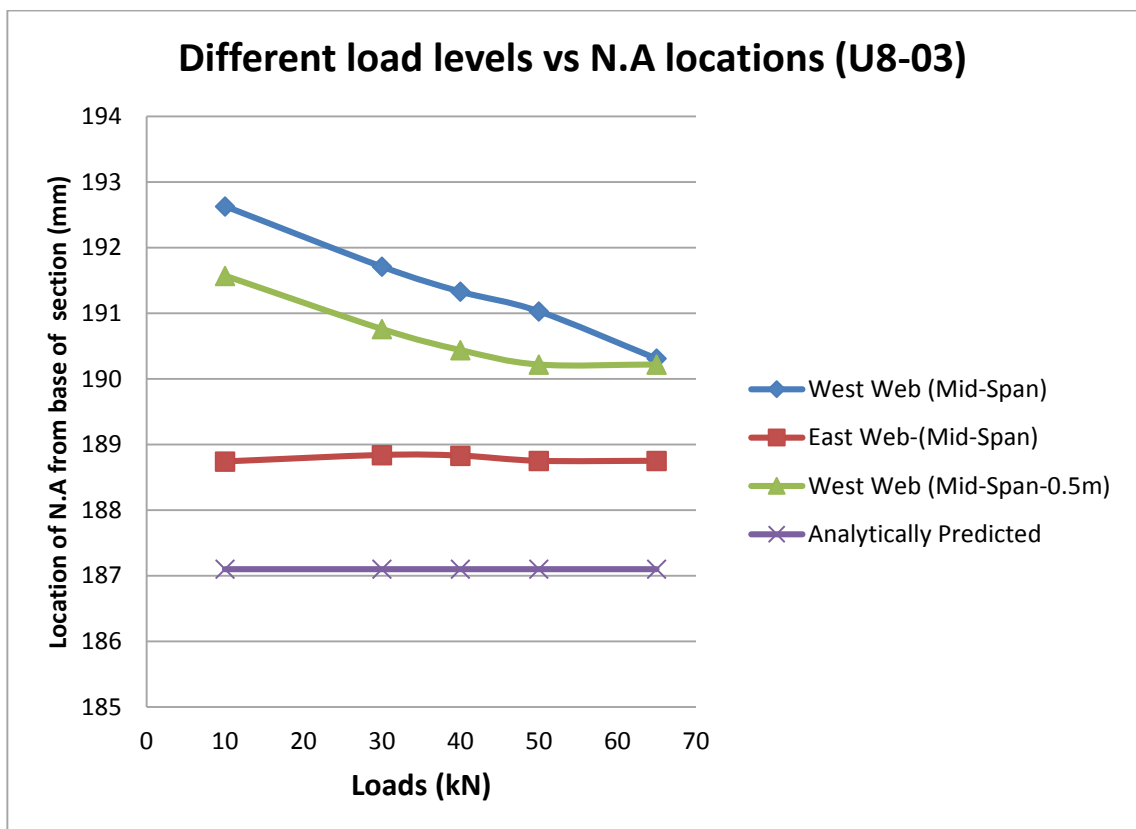
Figure 5.39 Location of N.A for at different load levels for U8-03

Table 5.12 Comparison between the experimental and analytical results for the location of N.A (U8-03, Mid-Span, West Web strain gauges)

Loads (U8-03)	Location of N.A at the west side Web (from base)	$(N.A)_{Pred}$=187.1mm $(N.A)_{Pred}/(N.A)_{Exp}$
F=10KN	192.63 (mm)	0.97
F=30KN	191.71 (mm)	0.98
F=40KN	191.33 (mm)	0.98
F=50KN	191.03 (mm)	0.98
F=65KN	190.31(mm)	0.98

The procedure which was presented for U8-03 was repeated for the rest of modules (U8-01, U8-02, L6-01, L6-02 and L6-03) and the same observations was made, that is, a fully composite behaviour for all modules under all load levels (see the graphs in Appendix C). Table 5.13 summarises the results of ultimate load, maximum mid-span deflection and the neutral axis as a result of the experimental tests and the analytically predicted response for all modules.

Table 5.13 Summary of the experimental and analytical results of the LVL modules

	Ultimate Load At each third span (kN)		Maximum Mid-Span Deflection (mm)		Neutral Axis from Base of section (mm)	
	Experimental	Analytical	Experimental	Analytical	Experimental	Analytical
U8-01	76	60	136	115	194	187.1
U8-02	52[1]	60	146[1]	115	185	187.1
U8-03	65	60	116	115	190	187.1
L6-01	-	46	-	87	152	143.7
L6-02	-	46	-	87	148	143.7
L6-03	-	46	-	87	146	143.7

[1] premature failure of U8-02 (see section 5.4.1)

5.5   Conclusions

In this chapter, the results of the experimental investigation conducted on 6m and 8m modules were reported. The experimental investigation involved subjecting the full-scale 8m and 6m modules to both serviceability and ultimate limit state tests. hySpan Cross-Banded LVL and hySpan Project LVL were made the only structural material of the system. Type 17 normal screws and PURBOND® glue were used at the interfaces in order to provide "infinite stiffness" which is used in practical design to meet serviceability requirements and the role of screws was to help the glue to set properly. If the glue bond fails due to any possible reason such as lack of adequate glue at the interfaces, the rapid loss of stiffness and strength occurs (which was observed in U8-02) and the role of screws becomes important as they are acting as the only load bearing part of the bond. In that case, the partially-composite behaviour of the modules should be considered for the ultimate limit state design requirements (chapter 6).

A perfect bond between the flanges and the webs provides a fully composite section (which was observed in U8-01 and U8-03). The fully composite behaviour of the system was also investigated and confirmed through assessing the strain responses over the depth of the section under both SLS and ULS loads. The load-deflection curves of the modules (at both mid-span and third-span span) show a linear behaviour and the linear characteristics of the modules was preserved up to the failure point where a brittle failure occurs. Moreover, the linear response of all strain gauges confirms the linear behaviour of the system up to the failure point. The ultimate design load of the system was also calculated according to the design standard EC5 (2004) and by using the transformed section method to predict the flexural stiffness of the system. The comparison between the analytically predicted values, and experimental results confirm that the analytically calculated flexural stiffness, failure load and maximum deflection of the system can accurately represent the characteristics of fully composite LVL modules with a flexurally dominated behaviour.

The results of the full scale experimental tests will be used to develop a FE model (in chapter 7). The experimental investigation results together with the conducted numerical investigation provide a robust model for predicting the performance of other

LVL beams with similar structural features (i.e. fully composite beams, when the behaviour of the beam is dominated by bending in longitudinal direction, and when there is no notch or hole in the beam) while the structural shape, dimensions, and spans can be varied according to the special requirements such as dynamic performance or fire resistance requirements.

University of Technology, Sydney

CHAPTER 6

EXPERIMENT AND ANALYTICAL

INVESTIGATION ON PARTIALLY-

COMPOSITE BEHAVIOUR OF LVL BEAMS

6 EXPERIMENT AND ANALYTICAL INVESTIGATION ON PARTIALLY-COMPOSITE BEHAVIOUR OF LVL BEAMS

6.1 Introduction

In chapter 5, the strength and serviceability performance of LVL modules were investigated under four-point bending loads, and the composite performance characteristics of the modules were assessed by evaluating the strain distribution over the depth of the section at both serviceable and ultimate limit states. Type 17 normal screws were used at 400mm spacing on each web and their primary role was to hold the web and the flanges in place while the glue sets properly. However, the actual bond between the flanges and the webs is provided by the glue (PURBOND®). However, if a lack of adequate glue was identified at interfaces due to any possible reason such as a less rigorous fabrication, then the role of screws are important when they are acting as the only load bearing part of the bond, and it should be clearly assessed. Moreover, the full scale LVL modules were glued and screwed and the glue provides "infinite stiffness" which is used in practical designs to meet SLS design, but not ULS design requirements. If the glue bond fails (particularly at a high load) the rapid loss of stiffness and strength occurs. Therefore, the partially composite behaviour of LVL modules is assessed in this chapter.

This chapter presents the results of a series of push-out tests which were conducted on the fabricated timber connections, using LVL as flanges and webs and type 17 normal screws as the shear connector, and the stiffness of the connections were evaluated at serviceability and ultimate limit state. A number of LVL beams (3.5m "T" shaped beams) were also fabricated using just screws as the load bearing shear connectors at interfaces, and were tested under serviceability and ultimate limit state loads with different screw spacing to evaluate the partially-composite strength and serviceable performance of full-scale LVL beams. Furthermore, a closed-form prediction analysis is conducted to calculate the partially-composite ultimate load of the system and a comparison between the experimental results and the closed-from predicted results is

undertaken and reported in this chapter. Finally, the partially-composite behaviour of long span 6m and 8m modules was analytically predicted, and screw spacing is specified so that the load bearing behaviour of the LVL modules is still in excess of the design ultimate required to be resisted by the modules (according to the Australian standards), even when there is no adequate glue used at the interfaces.

6.2   Experimental Program - Push out Tests

As the first phase of partially-composite experimental investigation of LVL beams, two different types of timber composite connections were fabricated and tested based on Eurocode 5 recommendations and the load-slip responses obtained from lab tests are used to determine the stiffness of the connections at serviceability, ultimate and near collapse levels. Moreover, an analytical model is derived for each type of connection based on the experimental results and using a non-linear regression, which can be implemented into non-linear FE analysis of timber beams with normal screws.

6.2.1   Test Specimens

As was presented in chapter 5, hySpan Cross-Banded LVL was used for top flange and hySpan Project LVL was used for webs and bottom flanges of 6m and 8m LVL modules. Therefore, to replicate the interfaces of 6m and 8m modules, two types of connections were built. In the first type, hySpan cross-banded LVL was used as the flanges and hySpan Project LVL was used for web to replicate the top flange-web interface of 6m and 8m modules. In the second type however, hySpan Project was used for the flanges and web to replicate the bottom flange-web interface of 6m and 8m modules. Figure 6.1 and Figure 6.2 show the dimensions and materials of connections. The connections were designed based on Figure 1.1 in Australian Standard AS1649 (2001). As illustrated in Figure 6.1 and Figure 6.2, the test specimens are 350 mm long and made of 90 mm wide and 35 mm deep flanges. The thickness of the web is 45 mm, with the length of 90mm. Figure 6.3 shows the dimensions of the normal screws, type 17 wood screws, used in fabricating the connections which were identical to the one used in 6m and 8m floor modules. 10 specimens were fabricated for each type of connections and tested under the load cycle described in section 6.2.2. Moreover, 3 connections of each type were fabricated and tested without load cycle to compare the

performance of connections with and without the load cycle (see section 6.3.2). The material properties of LVL were thoroughly investigated (chapter 4), and here just the values of MoE are presented in Table 6.1. The Moisture Content (MC) of the LVL samples were also measured according to AS/NZS 1080.1 (2012) .The results show that the MC values of the connections were around 10% for all tests with no significant difference among the MC values.
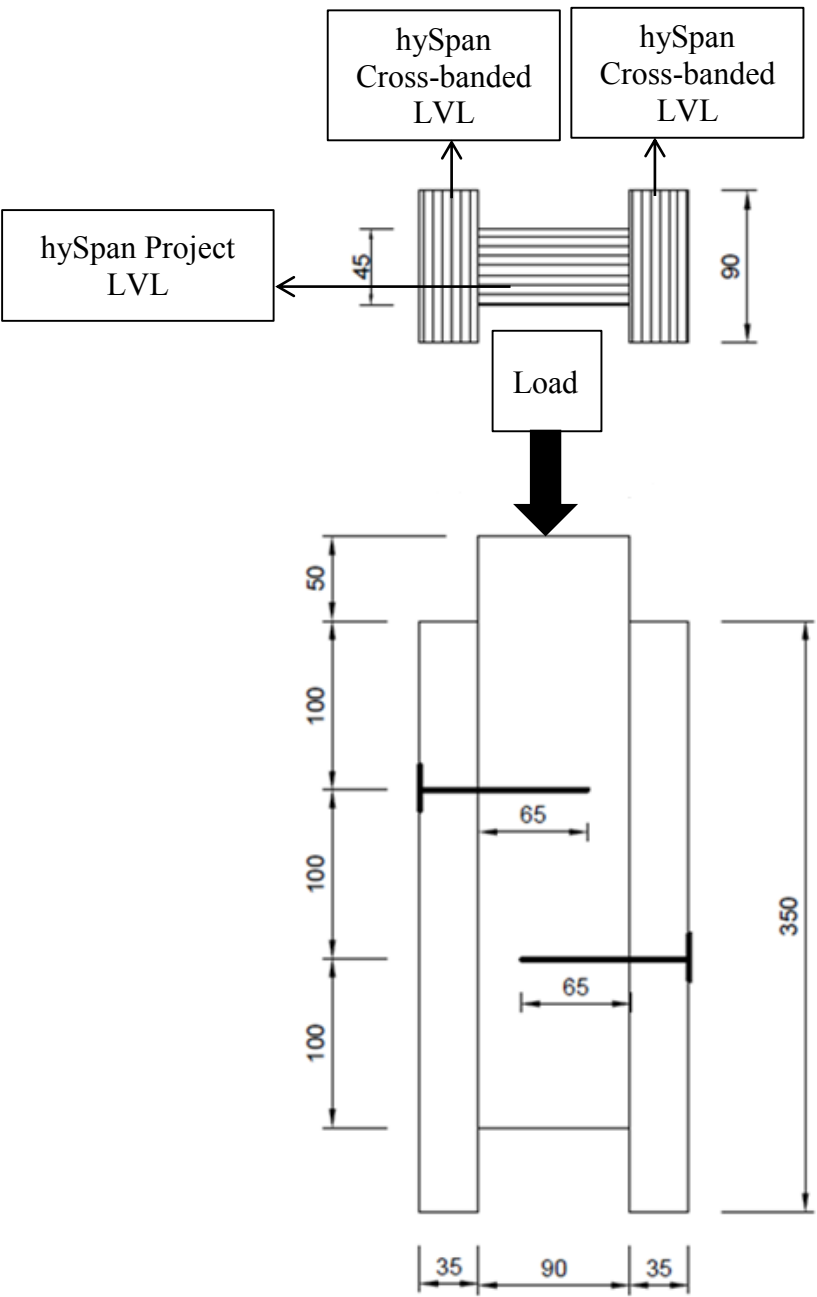
Figure 6.1 Dimensions and materials of the connection type 1 (mm)
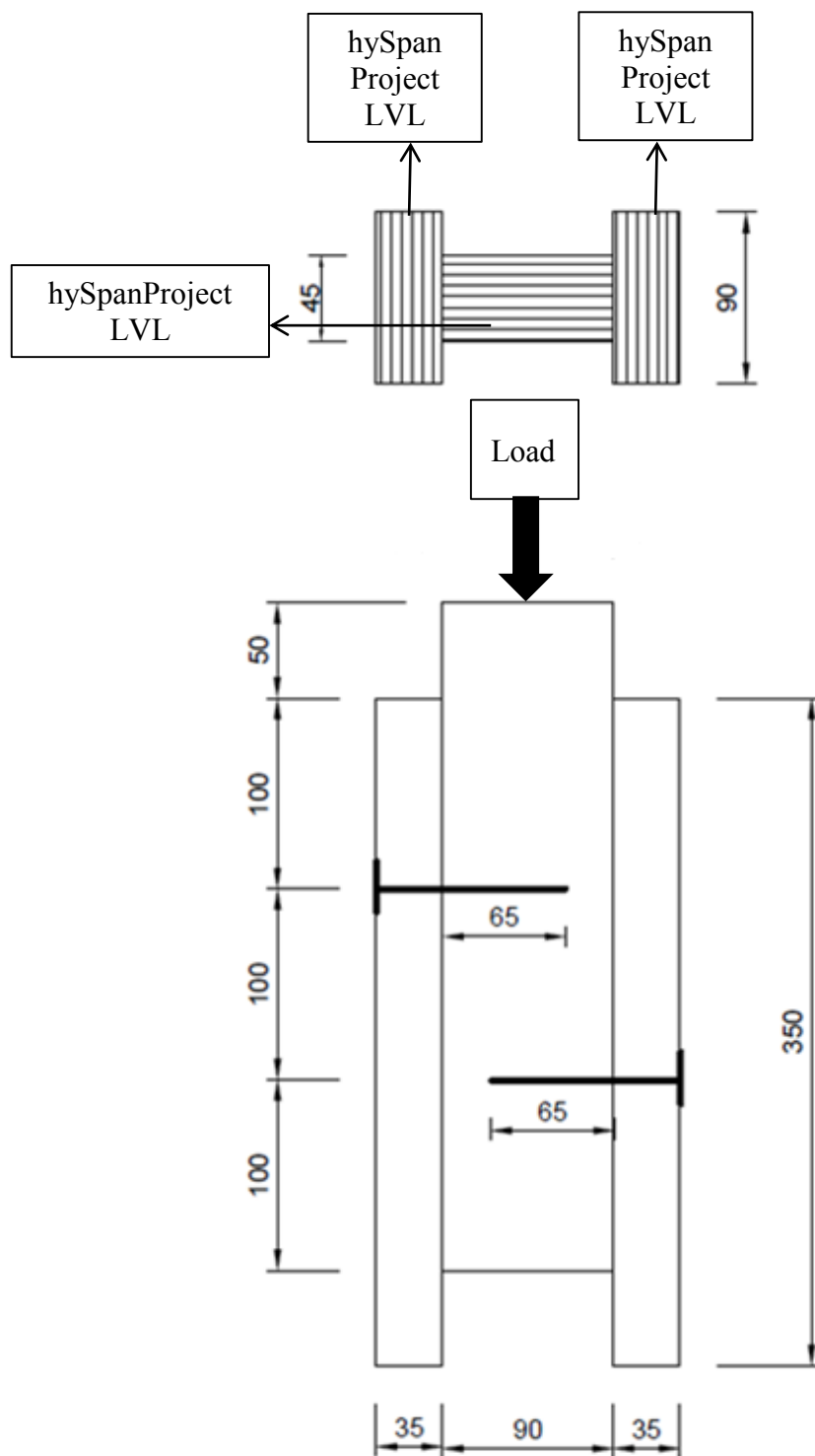
Figure 6.2 Dimensions and materials of connection type 2 (mm)
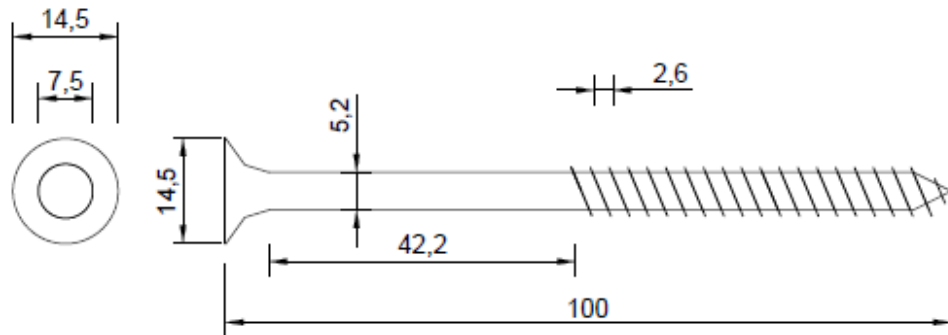
Figure 6.3 Dimensions of type 17 the normal screws (mm)

Table 6.1 MOE of LVL

Component Name	MOE (GPa)	CoV
hySPAN Cross-banded LVL, Flat-Wise tests	9.6	11%
hySPAN Project LVL, Edge-Wise tests	13.3	5%
hySPAN Project, Flat-Wise tests	13.1	12%

6.2.2 Test setup and loading procedure

Figure 6.5 shows the test set up for the push out tests. Two LVDTs with travelling range of 25 mm were installed in the front and back of the specimens (Figure 6.4) to capture the slip between flanges and the web. A steel bracket is installed at one of the flanges which hold the head of the front LVDT, and when the vertical load pushes the web down, the head movement of LVDT can measure the slip between that flange and the web. The slip between the other flange and web was measured with similar approach by the back LVDT (LVDT 2) as shown if Figure 6.5 and the slip of the connection was considered the average measurement of LVDT 1 and LVDT2.
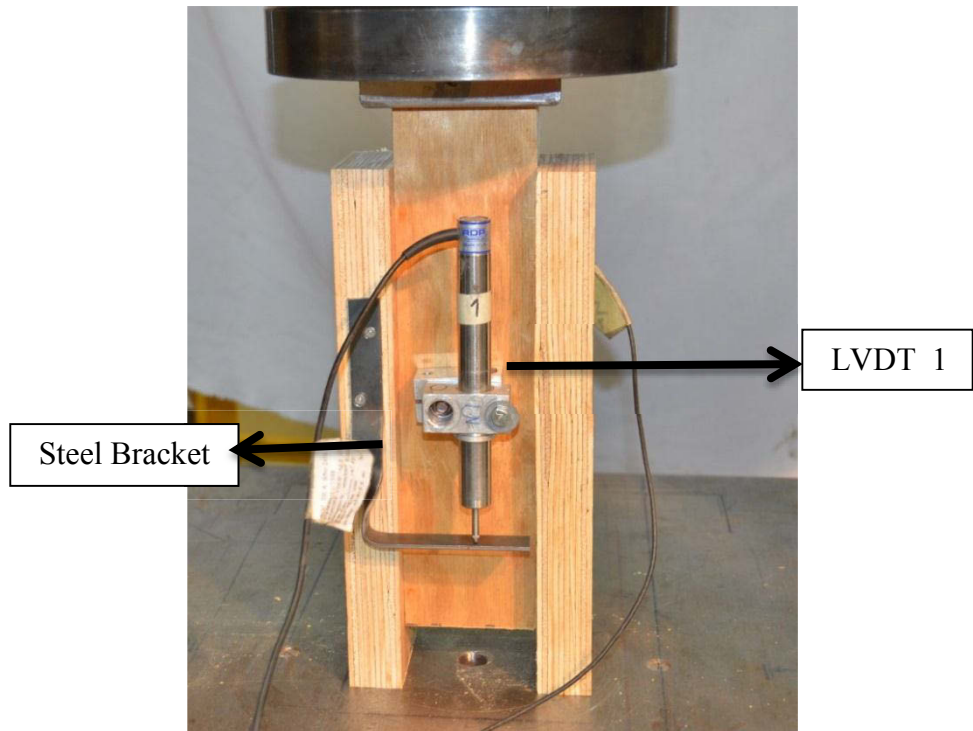
Figure 6.4 Push out test set up, front view
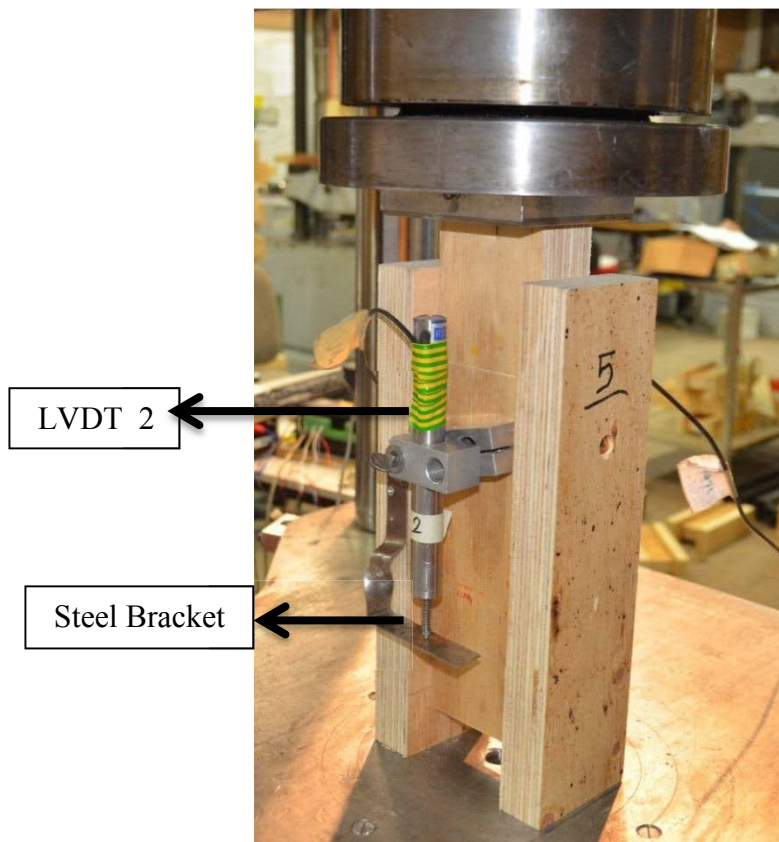
Figure 6.5 Push out test set up, back view

The adopted loading procedure is according to the European Standard BS EN 26891 (BS EN 26891-1991, ISO 6891:1983). The loading procedure is shown in Figure 6.6. As shown in Figure 6.6, a load was applied up to almost 40% of the estimated failure load (F_{est}) within about two minutes and maintained at this level for about 30 seconds, and then it reduced to 10% of the F_{est} and maintained at this level for about 30 seconds. Thereafter the load was increased up to failure point of the specimen with the same loading rate as the previous steps. The reason for the load cycle (unloading stage) is to eliminate the internal friction at the interfaces and let the specimen to settle. The final load-slip response of the push-out test can be idealized as shown in Figure 6.7.
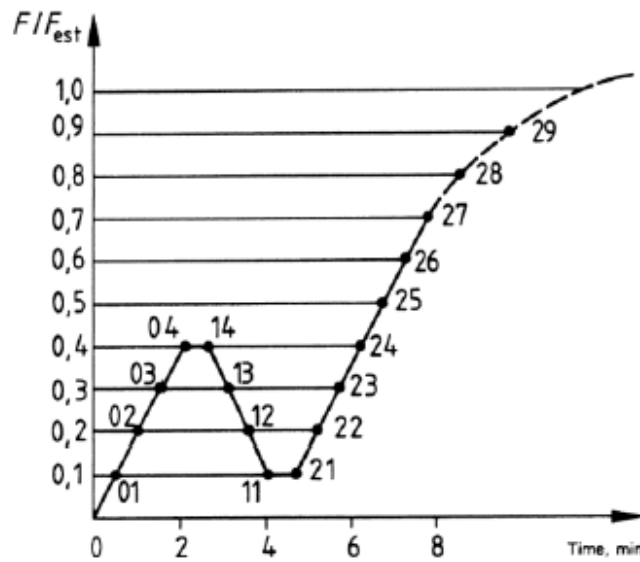
Figure 6.6 Loading procedure based on European Standard
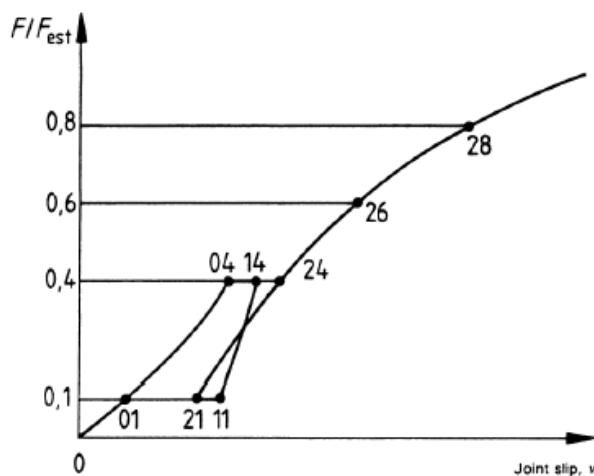
Figure 6.7 Idealized load-slip curves based on European Standard

6.2.3 Characteristic Behaviour of Connections

The performance of the connections can be assessed by various factors such as strength, stiffness and failure mode in serviceability- and ultimate limit states (SLS & ULS). The strength of the connection is defined as the maximum load captured during the push-out test before failure happens.

Moreover, the connection stiffness or slip modulus (Ks) is another feature of the connection that can be used to characterise the connection behaviour in SLS and ULS. The slip modulus represents the shear resistance of the connector to the relative displacement of the interfaces. According to BS EN 26891(1991), the slip modulus at different stages can be calculated as Equations 6.1 to 6.4. The initial stiffness of the connection (K_i) represents the first slope of the load-slip behaviour, however the slope of the load-slip curve between 10% and 40% of the failure load, or the slip modulus $K_{s,0.4}$, is usually used to identify the serviceability stiffness. Furthermore, the slope of the load-slip curve between 10-60% and 10-80% of the peak load correspond to the ultimate ($K_{s,0.6}$) and near collapse ($K_{s,0.8}$) stiffness of connection, respectively.

$$K_i = \frac{0.4F_{est}}{v_{04}}$$

Eq.6.1

$$K_{s,0.4} = \frac{0.4F_{est}}{\frac{4}{3}\left(v_{04} - v_{01}\right)}$$

Eq.6.2

$$K_{s,0.6} = \frac{0.6F_{est}}{v_{26} - v_{24} + \frac{4}{3}\left(v_{04} - v_{01}\right)}$$

Eq.6.3

$$K_{s,0.8} = \frac{0.8F_{est}}{v_{28} - v_{24} + \frac{4}{3}\left(v_{04} - v_{01}\right)}$$

Eq.6.4

Where F_{est} represents the peak-load, v is the relative slip and the subscripts comply with the milestones in of the diagram shown in Figure 6.7.

6.3   Push out Test Results

6.3.1   Strength and Stiffness of the Connections

The load-slip results for connection type 1 (with hySPAN Cross-banded as the material of the flanges) and connection type 2 (with hySPAN Project as the material of the flanges) are shown in Figure 6.8 and Figure 6.9, respectively. All the graphs are derived for a single screw by halving the values of the captured load during the push-out test and plotting it versus the average slip measured by LVDT 1 and 2.

As shown in the figures, all specimens showed similar bi-linear behaviour, that is, a linear response at the beginning which represents the initial stiffness and then a non-linear behaviour after $0.4F_{max}$. Experimental observation for all the specimens indicates the failure of the screws at the interfaces between the flanges and the web, as well as crushing of the LVL which was caused by bending of the screw in the timber. The ductility of the connection is provided by crushing of LVL around the screws and also, the plastic deformation of screws which can give some softening behaviour. There is a sudden drop in the load at the failure point which caused by the shear failure of the screws.

Table 6.2 presents the values of peak load and the stiffness of the connections. As shown in the table, the average peak-load for connection type 1 and 2 is around 8.5kN, and also there is not much difference between stiffness of connections type 1 and 2. However, the values of stiffness of both connection types show variation. For example, the average value of initial stiffness for connection type one is 2.12 kN/mm, and it has 32% of variation, which indicates the variable behaviour of timber (i.e. 12% variation in MoE of LVL) and variable behaviour of screws, as well as other possible variable factors during the experimental tests such as slight differences in fabricating the connections, screw installation, loading rate and localized failure of LVL.
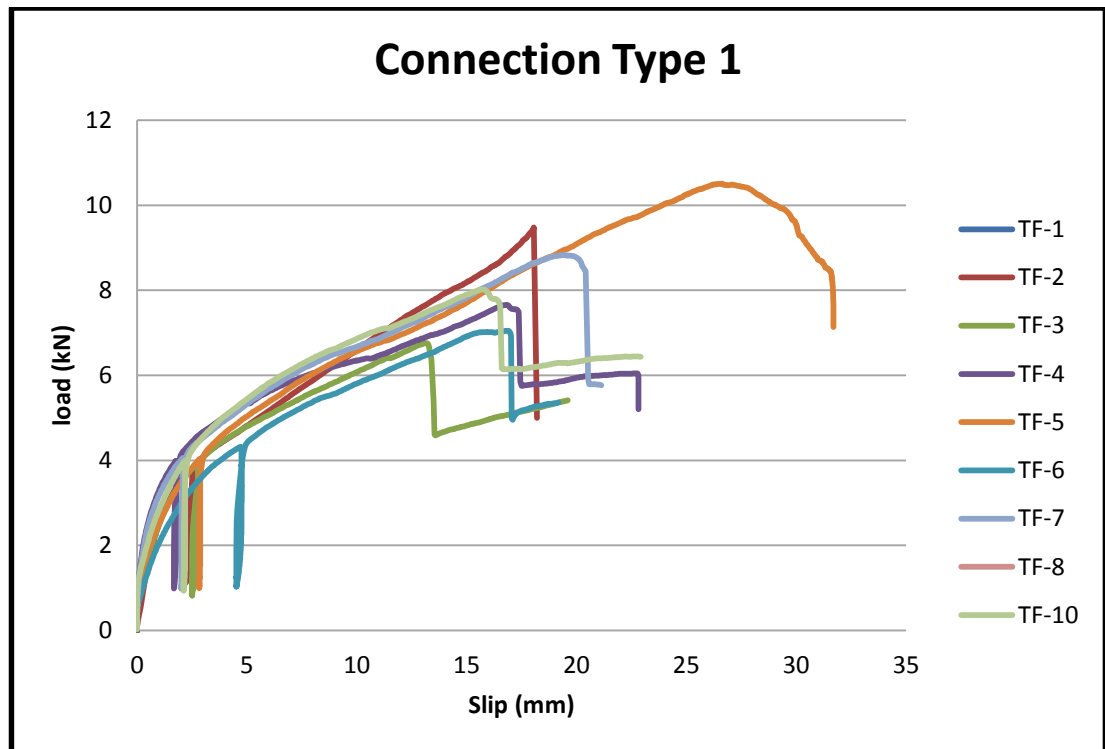
Figure 6.8 Load-slip Response of connection type 1 for a single screw
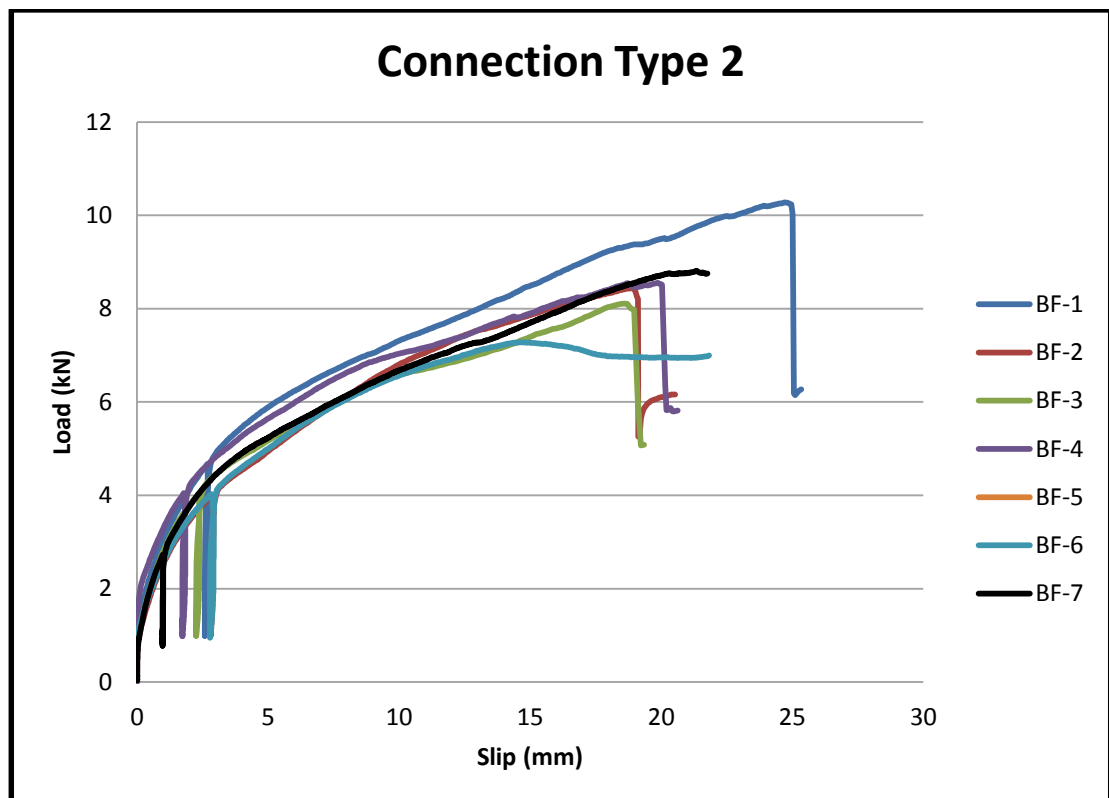
Figure 6.9 Load-slip Response of connection type 2 for a single screw

Table 6.2 Strength and Stiffness of Connections

	P_{max} (kN)	K_i (kN/mm)	$K_{s,0.4}$ (kN/mm)	$K_{s,0.6}$ (kN/mm)	$K_{s,0.8}$ (kN/mm)
Connection Type 1					
AVE	8.45	2.12	1.64	1.25	0.68
CoV	14%	32%	32%	30%	17%
Connection Type 2					
AVE	8.46	2.32	1.78	1.24	0.71
Cov	11%	17%	17%	21%	17%

6.3.2 Analytical Model for Shear-Slip Behaviour of the Connections

An analytical model for each type of connection (i.e. type 1 and 2) can be developed using the load-slip response of the connections. In this regards, a nonlinear regression is applied to all the curves obtained from the push-out tests, and the best mathematical expressions of the load-slip behaviour of connections was derived.

 Figure 6.10 and Figure 6.11 show the load-slip responses obtained from push-out tests where the load cycle and post-failure behaviour are eliminated from all the curves. Moreover, three additional sample of each connection type (1 and 2) were tested without the load cycle (i.e. the load was constantly increased until the failure happens) which are also presented in Figure 6.9 and Figure 6.10 (TF-11, 12 and 14 and BF-8, 9 and 10). The graphs show that there is no significant difference in load-slip response of the connections as a result of two different loading procedures (with and without load cycle). According to Figure 6.10 and Figure 6.11, the load-slip response of connections can be divided into two stages. The first stage of the response starts with a sharp increase in the load level which represents the initial stiffness, K_0, of the connection. The second stage of behaviour is followed by strain-hardening part with the stiffness, K_p, which is associated with a gradual increase in the load level and a large slip. After

that, the failure occurs in the connection with a sudden drop in the load which occurs immediately after the fracture of the screws.
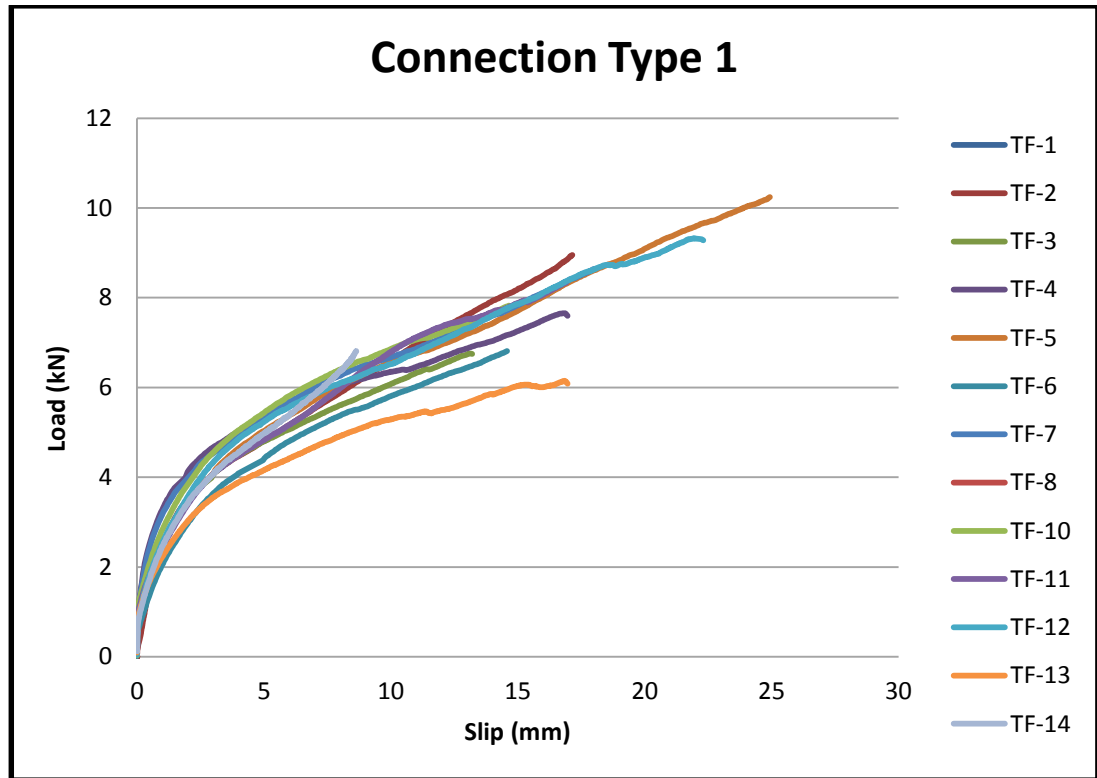
Figure 6.10 Response of connection type 1 without the load cycle (the unloading stage eliminated)
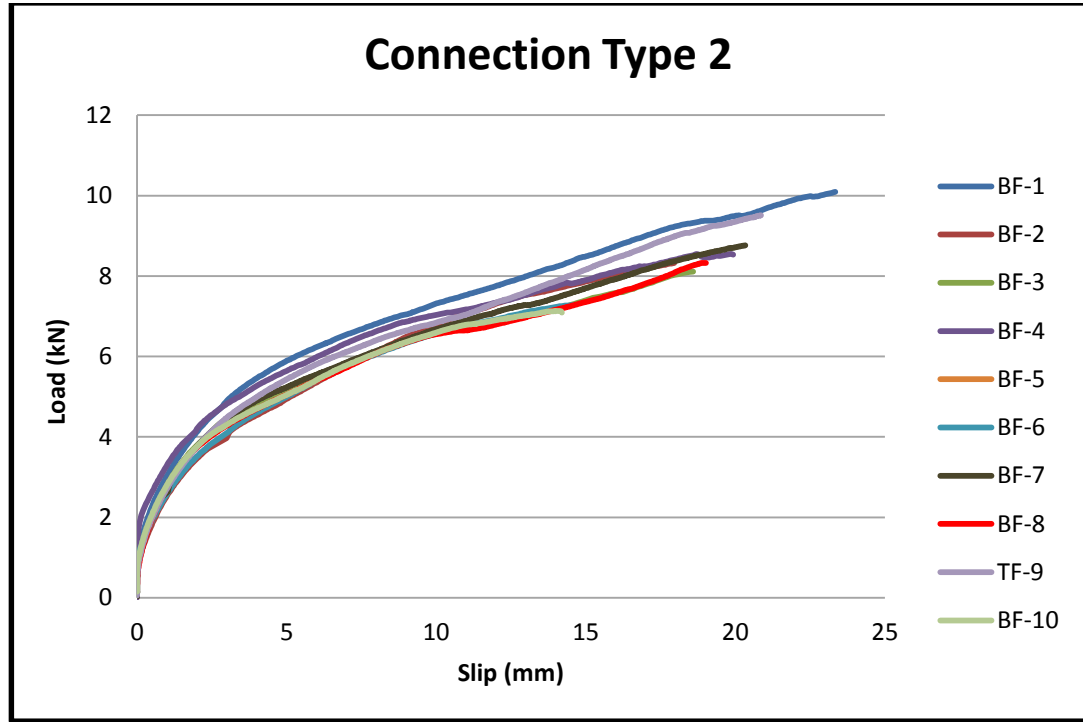
Figure 6.11 Response of connection type 2 without the load cycle (the unloading stage eliminated)

The Richard-Abbott model (Chan and Chui 2000) with four unknown parameters can be employed to represent the behaviour of connections. The Richard-Abbott model was originally proposed for semi-rigid steel connections, and for timber connections with normal screws it can be expressed as Equation 6.5:

$$P = \frac{(K_0 - K_p)v}{\left[1 + \left(\frac{(K_0 - K_p)v}{P_0}\right)^n\right]^{1/n}} + K_p v \qquad \text{Eq.6.5}$$

Where K_0 is the initial stiffness, K_p is the strain-hardening stiffness, P_0 is a reference shear force and n is a parameter associated with the sharpness of the curve. Table 6.3 presents the values for K_0, K_P, P_0 and n for connection type 1 and 2 . Values of R^2 represent the accuracy of the regression curve. If R^2 is equal to 1, all data are 100% correlated. Moreover, since the behaviour of connection type 1 and 2 are similar (See Figure 6.10, 6.11 and 6.12) the constant values were calculated considering all

specimens, and Figure 6.12 shows the load-slip response including all specimens as well as the regression curve (the bold black curve).

Table 6.3 Constant values of the analytical model

	K_0	K_P	P_0	n	R^2
Connection Type 1	6.029	0.2418	4.367	1	0.98
Connection Type 2	5.482	0.1859	5.27	1	0.97
All Specimens	**5.647**	**0.2125**	**4.822**	**1**	**0.97**

Therefore, with substituting the values of K_0 , K_P, P_0 and n in Equation 6.5, the mathematical expression of the behaviour of the timber connection with normal screws will be as follows:

$$P = \frac{(5.4345)v}{[1+(1.127v)]} + 0.2125v$$

Eq.6.6

Where P and v represent the shear force and the slip, respectively. Equation 6.6 can adequately express the first and second stages of the behaviour of timber connections with normal screws which can be easily incorporated into nonlinear FE analyses of timber beams with normal screws.
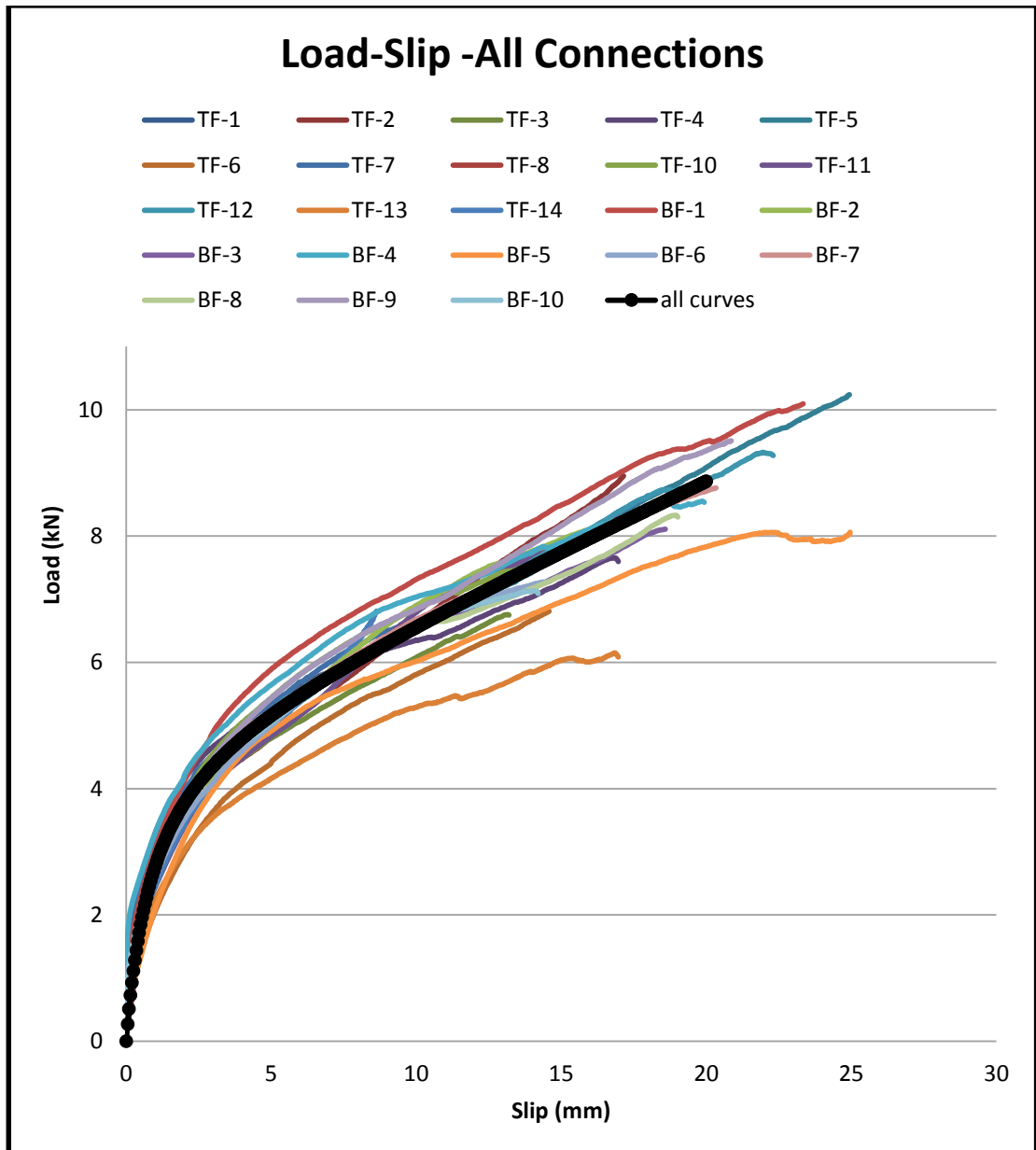
Figure 6.12 Response of connections without the load cycle (the unloading stage eliminated)

6.4 Experimental Investigation on Partially-Composite Behaviour of LVL Beams

6.4.1 Test Specimens and Experimental Program

In order to investigate the partially-composite performance of LVL beams at serviceability and ultimate limit state, three beams were fabricated and tested under

four-point bending loads. Figure 6.13 shows the cross-sectional dimensions of LVL beams and Figure 6.14 shows the type of LVL used for the fabrication of the beams. As shown in Figure 6.13 and Figure 6.14, the top flange was 90 mm wide and 35mm deep, while the web has a width of 45 mm and a depth of 90 mm. Cross-Banded LVL was used for the top flange and hySpan Project LVL was used for web. The bond between top flange and web was provided by Type 17 normal screws (Figure 6.3) and there was no glue used at the interface. The LVL beams were fabricated and tested with different screw spacing as shown in Figure 6.15.
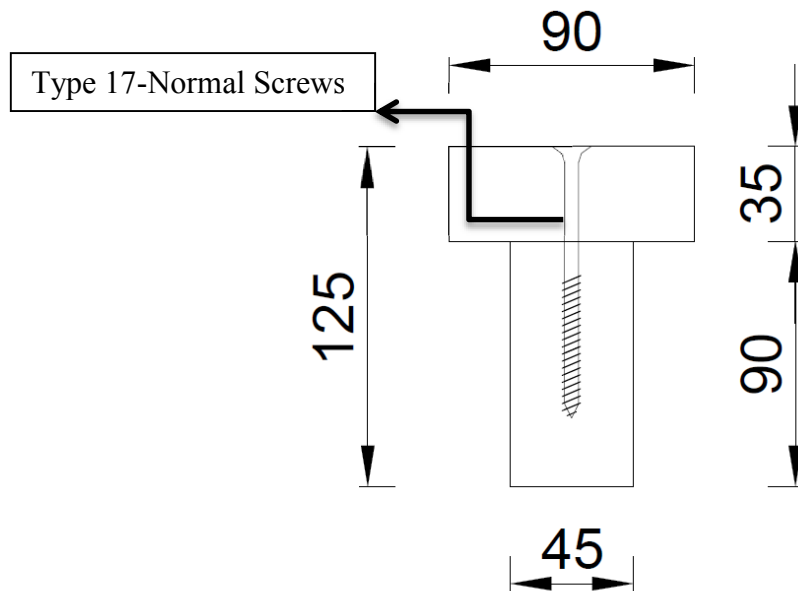
Figure 6.13 Cross-sectional dimensions of LVL beams
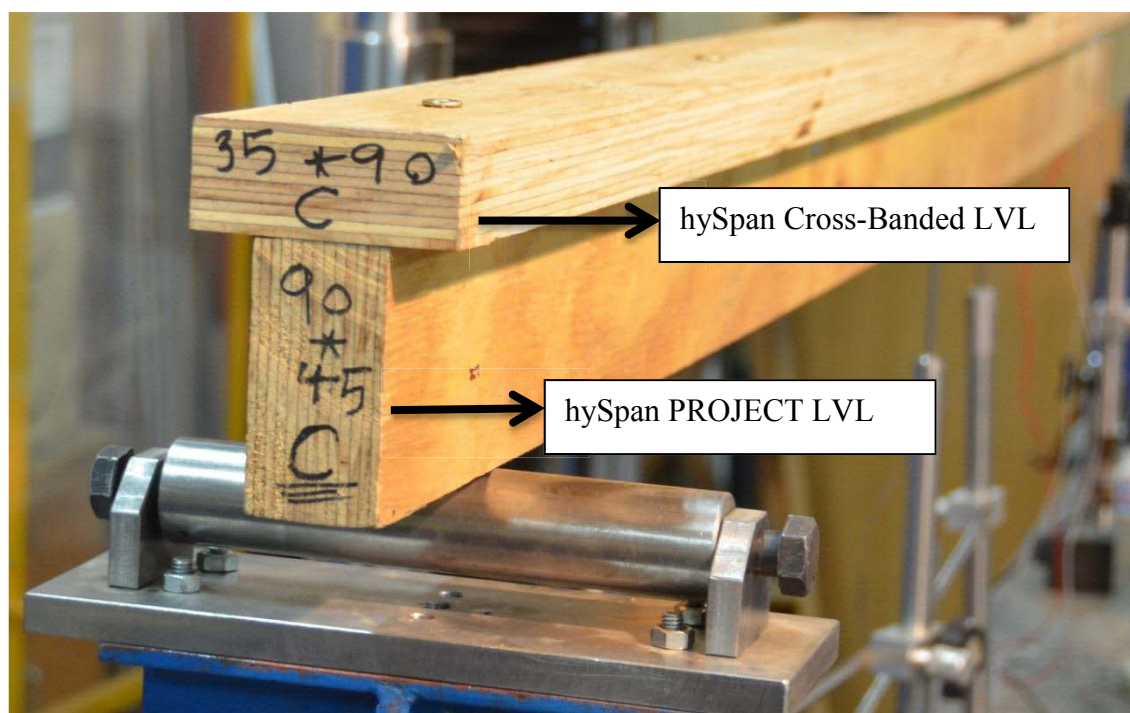
Figure 6.14 Cross section of LVL beams

Three beams (Beam a, b and c) were fabricated and tested under four-point bending loads with different screw spacing as shown in Figure 6.15, that is, the serviceability tests were conducted at 1600mm screw spacing and after completing the serviceability test, the number of screws were increased to 5 (800mm spacing). This approach was repeated until all the serviceability tests were conducted at all specified screw spacing (Figure 6.15). After serviceability tests were completed, three ultimate limit state were conducted on beams a, b, c, at 100mm, 200mm and 400mm screw spacing respectively, that is, the load was increased at a constant rate until failure occurred in each beam. Table 6.4 summarises the plan for destructive tests.

Table 6.4 Plan for destructive tests

	Screw Spacing
Beam a subjected to ultimate load	100mm
Beam b subjected to ultimate load	200mm
Beam c subjected to ultimate load	400mm
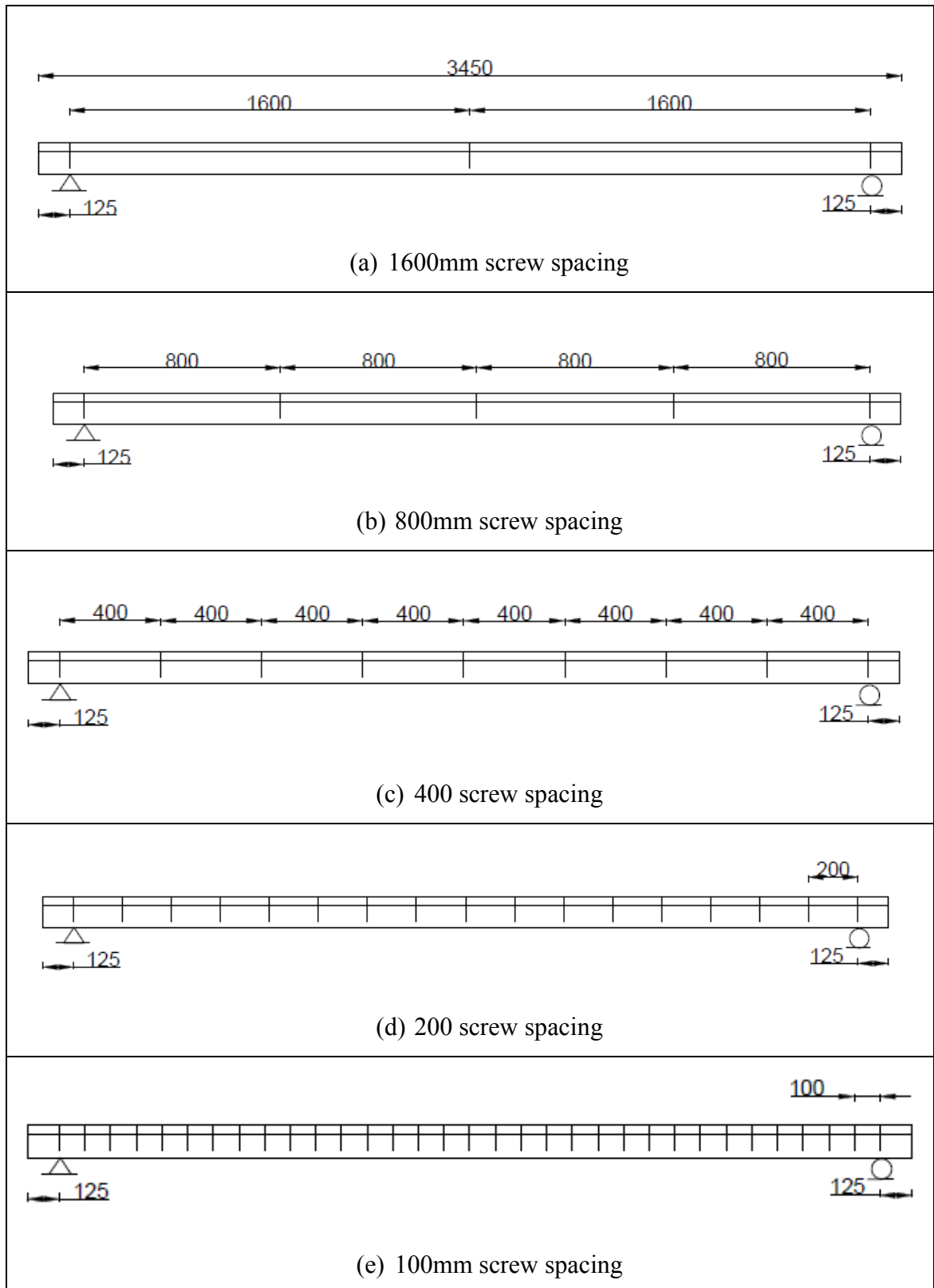
Figure 6.15 The fabricated LVL beams with Different screw spacing

a)1600mm, b)800mm, c)400mm, d)200mm and e)100mm

6.4.2   Instrumentations and Test Set up

Figure 6.16 shows the four-point bending test set up for LVL beams. As shown in Figure 6.16 and Figure 6.17, the LVL beams were supported with a pin and a roller. Three linear variable differential transformers (LVDTs) were places at mid-span and each third span of the LVL beams in order to measure the vertical deflection of the beams during tests at these key locations (Figure 6.17).
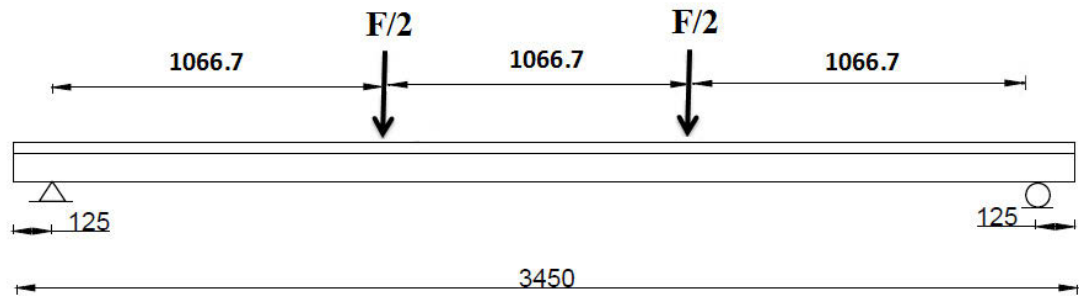
Figure 6.16 Test set up for LVL beams
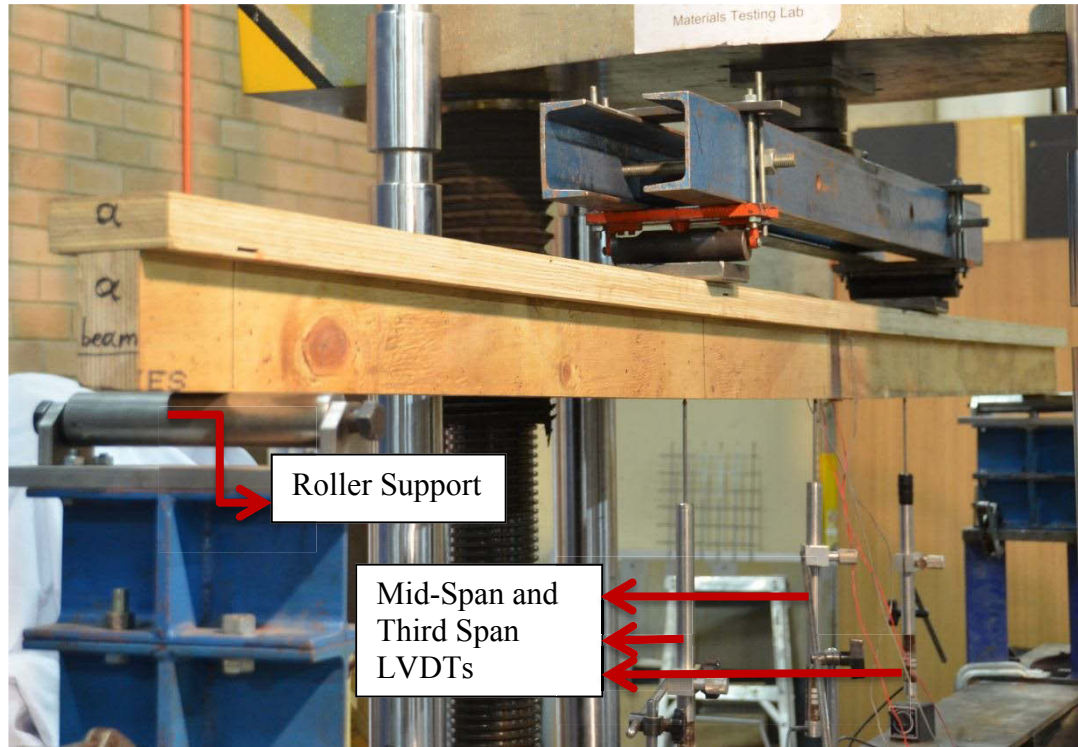
Figure 6.17 LVDTs and Pin-Roller supports for LVL beams

6.4.3   Analytically Predicted Responses

The effective (apparent) stiffness of the composite section can be calculated according to EC5 (2004) and Equations 6.7 to 6.11 show the calculation procedure.

$$(EI)_{eff} = E_{web}I_{web} + E_{tf}I_{tf} + \gamma_{web}E_{web}A_{web}\alpha_{web}^2 + \gamma_{tf}E_{tf}A_{tf}\alpha_{tf}^2 \qquad \text{Eq.6.7}$$

Where the section properties in Equation 6.7 are given by Equations 6.8 to 6.11.

$$I_{web} = \frac{b_{web}d^3_{web}}{12} \qquad \text{Eq.6.8a}$$

$$I_{tf} = \frac{b_{tf}d^3_{tf}}{12} \qquad \text{Eq.6.8b}$$

$$A_{tf} = b_{tf}d_{tf} \qquad \text{Eq.6.9a}$$

$$A_{web} = b_{web}d_{web} \qquad \text{Eq.6.9b}$$

Where b_{tf} and b_{web} are the width of top flange and web, respectively, and d_{tf} and d_{web} are the depth of top flange and web, respectively.

$$\gamma_{TF} = \frac{1}{1 + \dfrac{\pi^2 E_{tf} A_{tf} S_s}{K_i L^2}}$$

Eq.6.10a

In which S_s is the screw spacing, K_i is the stiffness of the screws and L is the span of beam

$$\gamma_{web} = 1$$
Eq.6.10b

$$\alpha_{web} = \frac{\gamma_{tf}E_{tf}A_{tf}(d_{tf} + d_{web})}{2*(\gamma_{tf}E_{tf}A_{tf} + \gamma_{web}E_{web}A_{web})} \qquad \text{Eq.6.11a}$$

$$\alpha_{TF} = 0.5*(d_{web} + d_{tf}) - a_{web} \qquad \text{Eq.6.11b}$$

And finally, the neutral axis y_c from the base of the composite section can be calculated from Equation 6.12.

$$y_c = 0.5 * d_{web} + a_{web}$$

Eq.6.12

Accordingly, the (EI)$_{eff}$ of the composite "T" section was calculated for different screw spacing and Table 6.5 summarises the values of flexural stiffness of the composite section. The serviceability stiffness of screws (K$_i$) was presented in Table 6.2 and was used for calculating the γ_{TF} in Equation 6.10.a.

Table 6.5 (EI)$_{eff}$ and the Neutral Axis of the partially composite section

Screw Spacing	(EI)$_{eff}$ (N.m^2)	Neutral Axis (mm)
100mm	80458.2	57.2
200mm	67577.1	53.4
400mm	56723.9	50.1
800mm	49198.6	47.9
1600mm	44658.2	46.6

The ultimate predicted load of the system can be derived from Equations 9.2, B.7 and B.8 of EC5 (2004). Therefore, the ultimate design loads can be calculated from Equation 6.13a , as a result of exceeding the bending strength of web for the LVL beam with 100mm screw spacing.

$$\frac{\gamma_{web}E_{web}a_{web}M_{max}}{(EI)_{eff}} + \frac{0.5E_{web}h_{web}M_{max}}{(EI)_{eff}} = 65.3(MPa)$$

Eq. 6.13a

Where M$_{max}$ is the maximum bending moment of the LVL beam which is equal to $\frac{(F_{max})/2 \times L}{3}$, and L is the span of the beam, and 65.3MPa is the bending strength capacity of hySPAN Project (see Table 5.1) By substituting M$_{max}$ into Equation 6.13a, the ultimate load of LVL beam with 100mm screw spacing is equal to 12.95kN . Moreover, the maximum deflection of the beam (Mid-Span deflection) can be

calculated with Equation 6.14a and Table 6.6 summarises the analytically predicted maximum deflection of the LVL beams as well as the ultimate load.

$$\delta_{max} = \frac{23(\frac{F_{max}}{2})L^3}{648(EI)_{eff}}$$ Eq.6.14a

Table 6.6 Analytically predicted maximum deflection and ultimate design load of the LVL beams

Screw Spacing	Analytically Predicted Failure load (kN)	Analytically Predicted Mid-Span deflection (mm)
100mm	12.95	93.62
200mm	11.66	100.33
400mm	10.42	106.79

6.5   Experimental Results of LVL Beams

6.5.1   Failure Mode of the System

Figure 6.18, Figure 6.19 and Figure 6.20 show the failure of LVL beams with 400mm, 200mm and 100mm screw spacing, respectively. As shown in the figures, exceeding the bending and tensile stress in the web (hySpan PROJECT LVL) triggered the failure of the LVL beams. The final failure of the beams was brittle with a sudden drop in the load bearing behaviour of the system. After completing each test, screws were removed from the beams and it was observed that they were not noticeably bent and none of them had failed, which indicates that they did not exceed their ultimate shear strength (Figure 6.21). However, for U8-02 (Chapter 5), when screws were removed after completing the test, it was observed that they were significantly bent and some of them had failed after the serviceability limit state was passed, although the load bearing behaviour of the system was not affected at the serviceability limit state. Therefore, in section 6.6, screw spacing was designed and specified to be applied for 6m and 8m long

span LVL modules, for a safe serviceability and ultimate design, considering the partially-composite behaviour of modules (when the glue is not used at the interfaces).
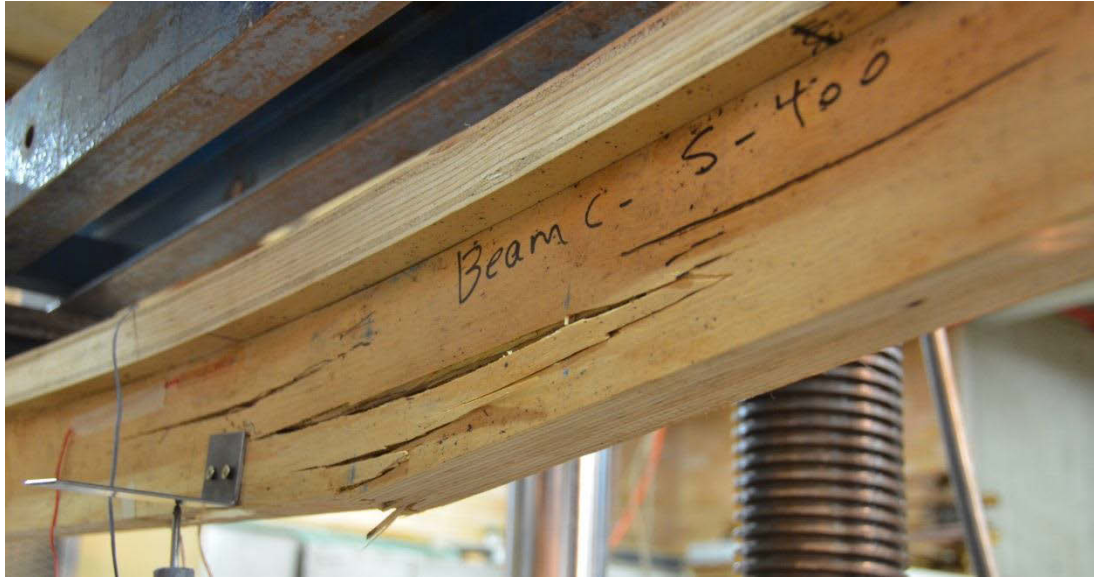
(a)

(b)

Figure 6.18 Failure of LVL beam with 400mm screw spacing, (a) right side of beam, (b) left side of beam

(a)

(b)

Figure 6.19 Failure of LVL beam with 200mm screw spacing (a) right side of beam, (b) left side of beam

(a)

(b)

Figure 6.20 Failure of LVL beams with 100mm screw spacing (a) right side of beam, (b) left side of beam
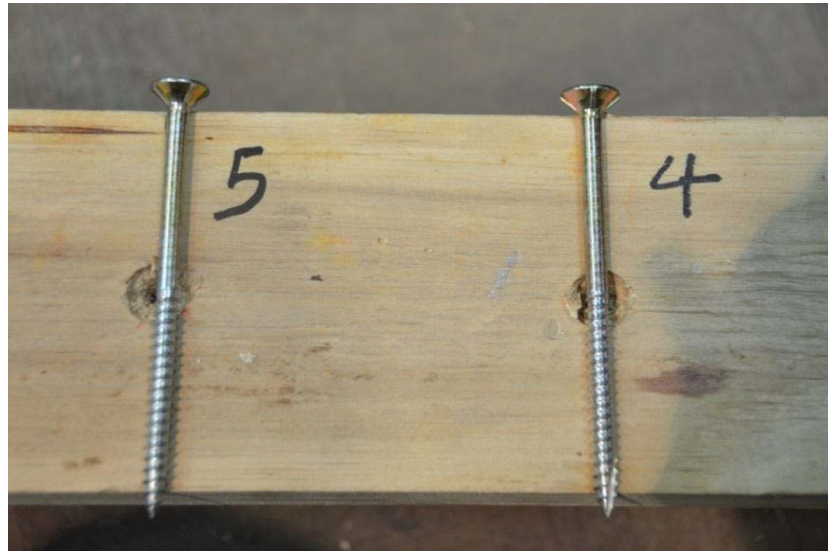
Figure 6.21 Deformation of the screws after completing the test of LVL beam (with 100mm screw spacing)

6.5.2   Flexural Stiffness of the LVL Beams

The procedure of calculating the flexural stiffness of the LVL beams was described in Equations 5.8 to 5.14 of chapter 5. The same method was used in this chapter to calculate the stiffness of LVL beams. Figure 6.22 shows the load-deflection graphs for the serviceability tests of the beams. It can be observed that the stiffness of the LVL beams increases with decreasing screw spacing in the beams. Figure 6.23 shows the results of the three ultimate limit tests and the load-deflection graphs for LVL beams with 100mm, 200mm, and 400mm screw spacing. As shown in the graphs, the behaviour of beams is non-linear as a result of the partially-composite behaviour of the beam, and the failure is a brittle one. The softening behaviour of the beams is provided by crushing of LVL around the screws. The plastic deformation of screws may give some softening behaviour as well. After completing each test, screws were removed from the beams and it was observed that they were not noticeably bent and none of them had failed, which indicates that they did not exceed their ultimate shear strength (Figure 6.21). The sudden drop in the load-deflection graphs confirms the brittle failure of LVL beams. Figure 6.24 shows that the behaviour of LVL beams can be represented by a bi-linear model (bi-linear graphs) in which the stiffness of beams drops from serviceability stiffness to ultimate stiffness at the yield point. Load and deflection of

beams at yield point can be analytically predicted by Equation 6.13b and 6.14b, respectively.

$$\frac{\gamma_{web}E_{web}a_{web}\left[\dfrac{(F_{yield})/2}{3}L\right]}{(EI)_{eff}} + \frac{0.5E_{web}h_{web}\left[\dfrac{(F_{yield})/2}{3}L\right]}{(EI)_{eff}} = 26.12(MPa) \qquad \text{Eq.6.13b}$$

$$\delta_{yield} = \frac{23(\dfrac{F_{yield}}{2})L^3}{648(EI)_{eff}} \qquad \text{Eq.6.14b}$$

The procedure was described in section 6.4.3, however the strength capacity of beams should be considered up to the serviceability limit (40% of the ultimate strength capacity or 65.3*0.4=26.12). K_i is the stiffness of screws up to serviceability limit (presented in Table 6.2), and $(EI)_{eff}$ is the effective flexural stiffness of beams at serviceability limit state (presented in Table 6.5). Table 6.7 and Table 6.8 present the analytically predicted loads and deflections of LVL beams at yield point. The yielding loads and deflections of LVL beams with different screw spacing are also summarised in Table 6.7 and Table 6.8 as a result of the experimental tests (see Figure 6.24), and a comparison between the experimental results and analytically predicted results are presented in the tables. The difference between the experimental results and the analytical results is due to variation in properties of LVL and screws (stiffness of screws for example) as well as other possible variable factors during the experimental tests such as slight difference in fabrication of the beams, screw installation, localized failure of LVL and slight difference in loading rate.

Table 6.7 A Comparison between the analytically predicted yield point load and the experimental results

Screw Spacing	Yield Point - Load (kN)		
	Analytically Predicted	Experimental Results	(Exp)/(Pred)
100	5.2	4.9	**0.94**
200	4.7	4.5	**0.96**
400	4.2	3.9	**0.93**

Table 6.8 A Comparison between the analytically predicted yield-point deflection and the experimental results

Screw Spacing	Yield Point - Deflection (mm)		
	Analytically Predicted	Experimental Results	(Exp)/(Pred)
100	37.4	25.7	**0.70**
200	40.1	30.1	**0.75**
400	42.7	34.1	**0.80**

Figure 6.25 shows a comparison between all the graphs. It shows that the stiffness of the beams which were tested under both serviceability and ultimate limit tests are compatible which indicates the linear behaviour of the system up to serviceability limit.
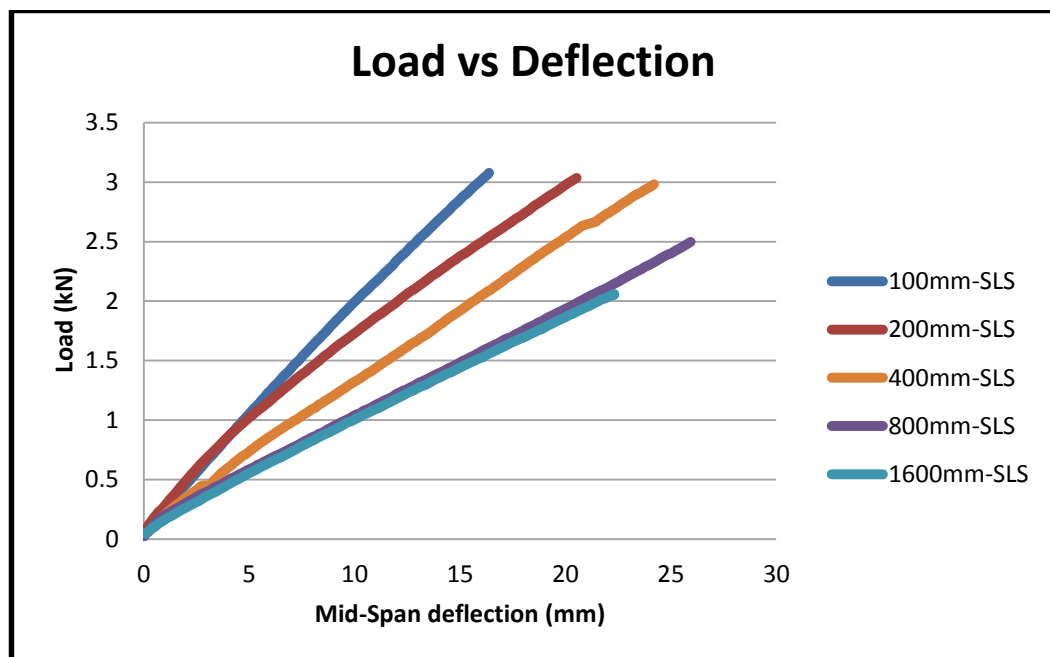
Figure 6.22 Load-deflection graphs for LVL beams with different screw spacing (serviceability tests)
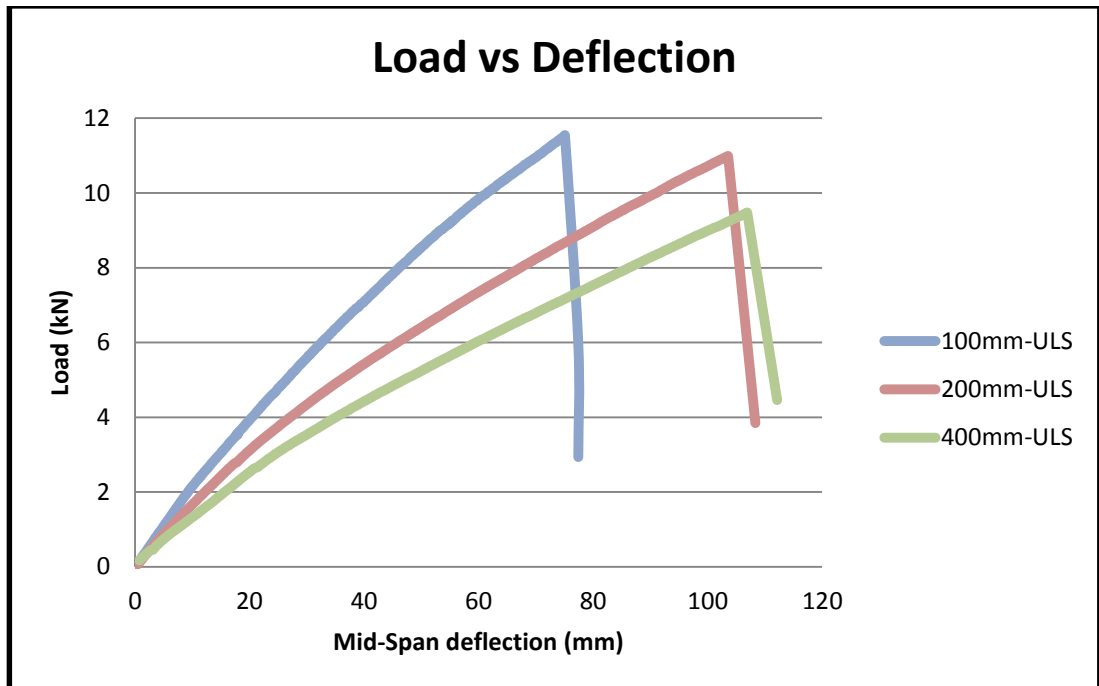
Figure 6.23 Load-deflection graphs for LVL beams with different screw spacing (ultimate limit tests)
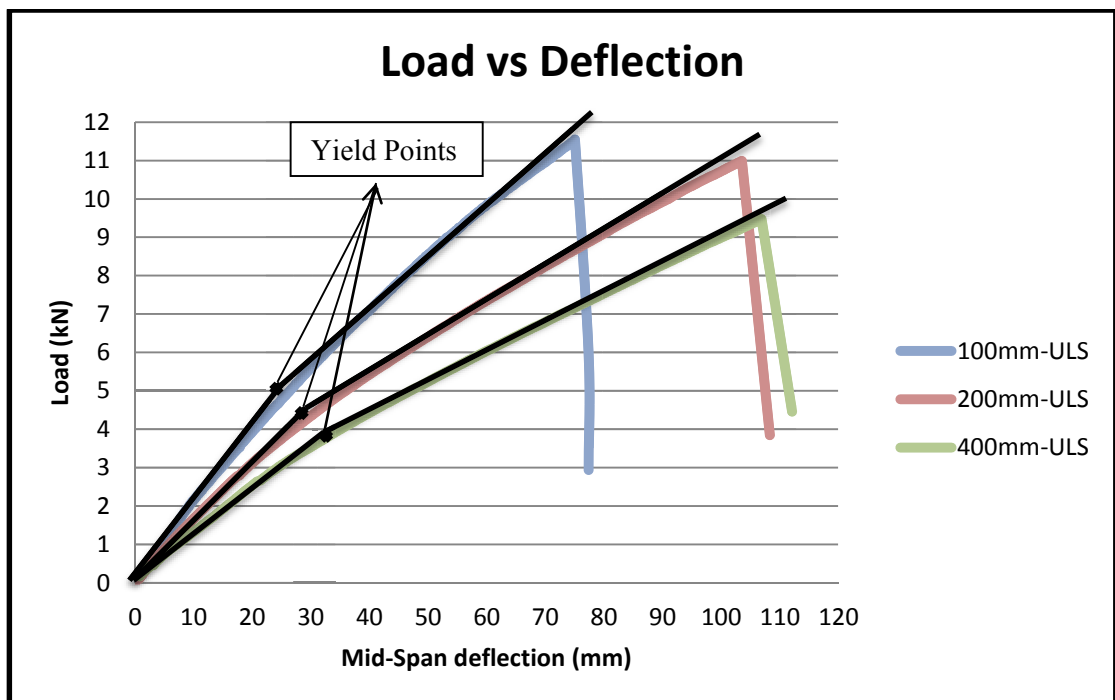
Figure 6.24 The bi-linear behaviour of LVL beams with different screw spacing
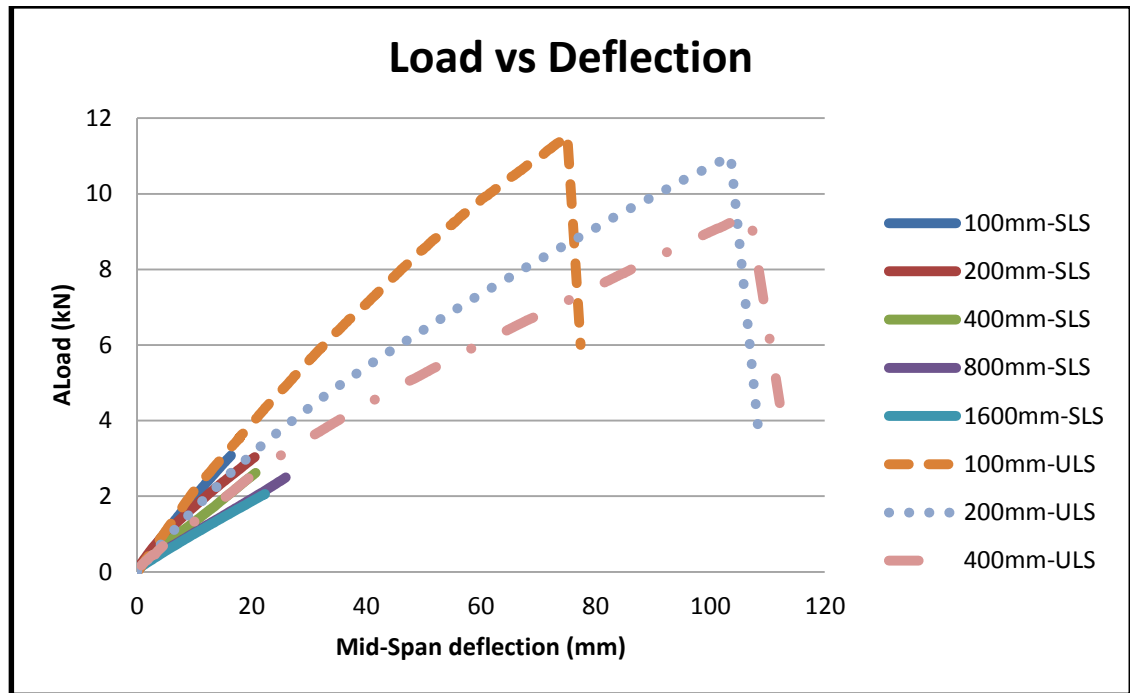
Figure 6.25 A comparison between all Load-deflection graphs for serviceability and destructive tests

Table 6.9 summarises the flexural stiffness of the LVL beams obtained from the experimental tests. A comparison between the analytically predicted flexural stiffness and the experimental investigation results is also presented in Table 6.9. The flexural stiffness of the beams was calculated at the serviceability limit. The experimental results show up to 30% difference with the analytical results which is due to variation in properties of LVL and screws (strength and stiffness of screws) as well as other possible variable factors during the experimental tests such as slight difference in fabrication of the beams, screw installation, localized failure of LVL and slight difference in loading rate.

Table 6.10 shows the comparison between the analytically predicted ultimate load and the ultimate loads obtained from the destructive tests, and Table 6.11 summarises a comparison between experimental and analytically predicted results of the maximum deflection (mid-span deflection) of the LVL beams. The comparison shows good correlation between the experimental and analytical results which indicates that the prediction model can adequately capture the ultimate load and the maximum deflection

of the LVL beams. This procedure was also used to predict the partially-composite behaviour of long span 6m and 8m modules in the following section.

Table 6.9 Comparison between the analytically predicted flexural stiffness and the experimental results

Screw Spacing	$(EI)_{eff}$ $(N.mm^2)$		$EI_{(Pred)}/EI_{(Exp)}$
	Analytically predicted	Experimental Results	
100mm	8.04E+10	10.87+10	**0.74**
200mm	6.76E+10	8.85+10	**0.76**
400mm	5.67E+10	7.42+10	**0.76**
800mm	4.92E+10	6.68+10	**0.74**
1600mm	4.47+10	6.34+10	**0.70**

Table 6.10 Comparison between the analytically predicted flexural stiffness and the experimental results

Screw Spacing	Ultimate Load (kN)		**(Exp)/(Pred)**
	Analytically Predicted	Experimental Results	
100mm	12.95	11.6	**0.90**
200mm	11.66	11.0	**0.94**
400mm	10.42	9.5	**0.92**

Table 6.11 Comparison between the analytically predicted maximum deflection and the experimental results

Screw Spacing	Maximum deflection (mm)		**(Exp)/(Pred)**
	Analytically Predicted	Experimental Results	
100mm	93.6	77.0	**0.82**
200mm	100.3	103.6	**1.03**
400mm	106.8	106.9	**1**

6.6 Partially-Composite Behaviour of 6m and 8m LVL Modules

In this section the effective flexural stiffness of 6m and 8m modules are analytically predicted, and the partially-composite behaviour of modules is assessed. Moreover, the required screw spacing is specified so that the load bearing behaviour of the LVL modules is still in excess of the design ultimate required to be resisted according Australian design standards, even when there is no glue used at the interfaces.

6.6.1 Cross-section Characteristics

The effective (apparent) stiffness of the section can be calculated according to EC5 (2004). Figure 6.26 shows the dimensions of the components of the section and Equations 6.15 to 6.19 show the calculation procedure.
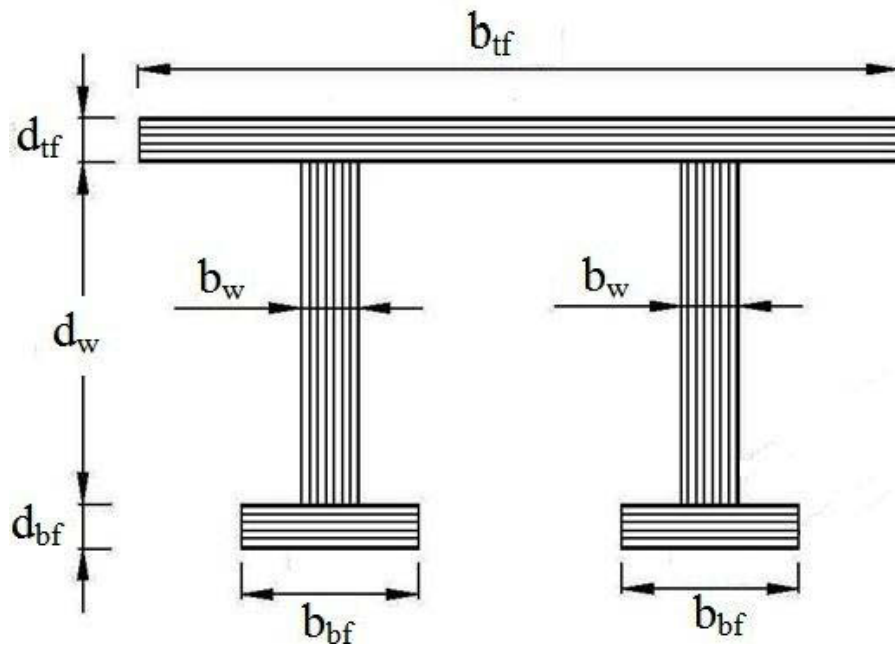
Figure 6.26 Dimensions of the Components

$$(EI)_{eff} = E_{tf}I_{tf} + E_wI_w + E_{bf}I_{bf} + \gamma_{tf}E_{tf}A_{tf}\alpha_{tf}^2 + \gamma_w E_w A_w \alpha_w^2 + \gamma_{bf}E_{bf}A_{bf}\alpha_{bf}^2$$

Eq.6.15

Where the values of E are presented in Table 6.1 and the section properties in Equation 6.15 are given by Equations 6.16 to 6.20.

$$I_{tf} = \frac{b_{tf}d_{bf}^3}{12}$$ Eq.6.16a

$$I_w = \frac{2*b_w d_w^3}{12}$$

Eq.6.16b

$$I_{bf} = \frac{2*b_{bf}d_{bf}^3}{12}$$

Eq.6.16c

$$A_{tf} = b_{tfF}d_{tf}$$ Eq.6.17a

$$A_w = 2*b_w d_w$$

Eq.6.17b

$$A_{bf} = 2*b_{bf}d_{bf}$$ Eq.6.17c

Where b_{tf} and b_w and b_{bf} are the width of top flange, web and bottom flange, respectively, and d_{tf} , d_{web} and d_{bf} are the depth of top flange, web and bottom flange, respectively.

$$\gamma_{tf} = \frac{1}{1 + \dfrac{\pi^2 E_{tf}A_{tf}S_{tf}}{K_i L^2}}$$ Eq.6.18a

$$\gamma_{web} = 1$$ Eq.6.18b

$$\gamma_{bf} = \frac{1}{1 + \dfrac{\pi^2 E_{bf}A_{bf}S_{bf}}{K_i L^2}}$$ Eq.6.18a

In which S_{tf} and S_{bf} are the screw spacing in top flange interface and bottom flange interface, respectively. K is the stiffness of the screws and L is the span of beam

$$\alpha_w = \frac{\gamma_{tf} E_{tf} A_{tf} (d_{tf} + d_w) - \gamma_{bf} E_{bf} A_{bf} (d_w + d_{bf})}{2 * (\gamma_{tf} E_{tf} A_{tf} + \gamma_w E_w A_w + \gamma_{bf} E_{bf} A_{bf})} \qquad \text{Eq.6.19a}$$

$$\alpha_{tf} = 0.5 * (d_w + d_{tf}) - a_w \qquad \text{Eq.6.19b}$$

$$\alpha_{bf} = 0.5 * (d_w + d_{bf}) + a_w \qquad \text{Eq.6.19b}$$

And finally, the neutral axis y_c from the base of the section can be calculated from Equation 6.20.

$$y_c = d_{bf} + 0.5 * d_w + a_w \qquad \text{Eq.6.20}$$

Accordingly, the $(EI)_{eff}$ of 8m LVL modules was calculated for different screw spacing and Table 6.12 summarises the values of flexural stiffness of the partially composite section, where K_i is the stiffness of the screws up to serviceability limit (Table 6.2), and used for calculating the γ_{tf} and γ_{bf} in Equation 6.18.

Table 6.12 The analytically predicted flexural stiffness and the neutral axis of 8m LVL modules

Screw Spacing	Effective Flexural stiffness (N.mm^2)	Neutral axis (mm)
400mm	3.36E+12	170.1
200mm	4.29E+12	172.5
100mm	5.51E+12	175.2
50mm	6.77E+12	178.5
Fully composite (see chapter 5)	9.48E+12	187.1

As Table 6.9 showed that the predicted EI is about 75% of the experimental EI, it is likely that the calculated values of Table 6.12 give a lower bound of flexural stiffness.

However, a lower bound of flexural stiffness (values of Table 6.12) will result in higher bound for the deflection which provides a conservative design.

6.6.2   Serviceability Check

According to AS/NZS 1170 (2002) and AS 1720.1 (2010), Equation 6.21 and 6.22 must be satisfied to check the serviceability performance of LVL modules (see chapter 3, section 3.3.2):

$$\Delta_b = \frac{5(G+0.7Q)L^4}{384(EI)_{eff}} \leq Span/300 \qquad\qquad \text{Eq.6.21}$$

$$\Delta_b = \frac{5(G+0.4Q)L^4}{384(EI)_{eff}} \leq Span/400 \qquad\qquad \text{Eq.6.22}$$

Where G+0.7Q is the short term serviceability load combination and G+0.4Q is the long term serviceability load combination. G is the self-weight plus the permanent loading, and Q is the imposed loading. L is the span of the modules and $(EI)_{eff}$ is the flexural stiffness of the modules. Therefore the minimum required flexural stiffness of the modules can be calculated from Equations 6.23 and 6.24.

$$(EI)_{eff} = \frac{300*5*(G+0.7Q)L^3}{384} \qquad\qquad \text{Eq.6.23a}$$

$$(EI)_{eff} = \frac{400*5*(G+0.4Q)L^3}{384} \qquad\qquad \text{Eq.6.23b}$$

With 1kPa permanent load plus the self-weight and 3kPa imposed load, and substituting the values in Equations 6.23a and 6.23b, the minimum required flexural stiffness of the 8m modules is 4.38E+12 N.mm^2 and 4.4E+12 N.mm^2 for short term and long term serviceability deflection limit, respectively. From the values presented in Table 6.12, it can be observed that the flexural stiffness of the modules with 100mm screw spacing can provide the required stiffness for the 8m LVL modules.

However, in order to consider the effect of creep in timber, the $(EI)_{eff}$ of LVL modules needs to be calculated based on Equation 6.24 in which the modification factor for creep is considered :

$$(EI)_{eff} = \frac{300 * 5 * (j_2 G + 0.7Q)L^3}{384}$$ Eq.6.24a

$$(EI)_{eff} = \frac{300 * 5 * j_2 * (G + 0.4Q)L^3}{384}$$ Eq.6.24b

Where the values of j_2 were presented in Table 3.6 in chapter 3. With j_2 equal to 2 (the long-term creep factor for initial moisture content less than 15%), the required flexural stiffness to satisfy the long term deflection limit for span/300 are 6.24E+12 N.mm^2 (for Equation 24a) and 6.6E+12 (for Equation 24b). From the values presented in Table 6.12, it can be observed that the flexural stiffness of the modules with 50mm screw spacing can provide the required stiffness for the 8m LVL modules (for the deflection limit of span/300), even when there is no adequate glue used at the interfaces. The required flexural stiffness to satisfy the long term deflection limit of span/400 (Equation 24b with considering span/400 as the deflection limit) can only be provided with the use of glue, which provides infinite stiffness.

Moreover, the short term deflection check as a result of impact loading (point load) must satisfy Equation 6.25, where P is 1kN impact load.

$$\Delta_{vib} = \frac{P^* L^3}{48(EI)_{eff}} \leq 1mm - 2mm$$ Eq.6.25

By considering 6.24E+12 N.mm^2 for the required flexural stiffness (provided by 50mm screw spacing), the Δ_{vib} is equal to 1.7mm and hence, Equation 6.25 is satisfied as well.

6.6.3   Strength of the LVL floor modules

The design capacity of the system needs to be checked under the flexural and axial action. Equation 6.26, which inferred from Equation 3.2 (3) of AS 1720.1 (2010), must be satisfied when the system is subjected to a combine bending and axial actions.

$$\frac{\sigma^*_{axial}}{\phi\sigma_{axial}} + \frac{\sigma^*_{bending}}{\phi\sigma_{bending}} \leq 1$$

Eq.6.26

Where σ^*_{axial} and $\sigma^*_{bending}$ are the axial and bending stress due to design action, respectively. $\phi\sigma_{axial}$ and $\phi\sigma_{bending}$ are the axial and bending stress capacity of the timber cross-section, respectively. The extreme fibres at the top and bottom flanges experience the most compression and tension stresses as a result of bending and axial actions and need to be checked. Therefore, Equations 6.27 and 6.28 must be satisfied, in which the σ^*_{axial} and $\sigma^*_{bending}$ are derived from EC.5, appendix B (BS EN 1995-1-1:2004+A1:2008) and $\phi\sigma_{axial}$ and $\phi\sigma_{bending}$ are according to AS1720.1 (2010) (inferred from Equation 3.2 (3) of AS 1720.1 (2010)), and were defined in chapter 3, section 3.3.4.1.

$$\frac{\left[\dfrac{\gamma_{bf}E_{bf}a_{bf}M^*}{(EI)_{eff}}\right]}{[\phi k_1 k_4 k_6 k_{12} f'_{t,bf}]} + \frac{\left[\dfrac{0.5E_{bf}d_{bf}M^*}{(EI)_{eff}}\right]}{[\phi k_1 k_4 k_6 k_9 k_{12} f'_{b.bf}]} \leq 1 \qquad \text{Eq.6.27}$$

$$\frac{\left[\dfrac{\gamma_{tf}E_{tf}a_{tf}M^*}{(EI)_{eff}}\right]}{[\phi k_1 k_4 k_6 k_{12} f'_{c,tf}]} + \frac{\left[\dfrac{0.5E_{tf}d_{tf}M^*}{(EI)_{eff}}\right]}{[\phi k_1 k_4 k_6 k_9 k_{12} f'_{b,tf}]} \leq 1 \qquad \text{Eq.6.28}$$

M* is the bending moment due to the design action and can be calculated with 3kPa imposed loading and 1kPa permanent loading, and the load combination of 1.2G+1.5Q. The ϕ factor and other k factors are presented in Table 3.7. The values of $f'_{t,bf}$ (the tension design capacity of bottom flange), $f'_{b,bf}$ (the bending design capacity of bottom flange), $f'_{c,tf}$ (the compression design capacity of top flange) and $f'_{b,tf}$ (the bending design capacity of top flange) are presented in Table D.2. The other parameters of Equation 6.27 and 6.28 (γ_{tf} and γ_{bf}) have been previously defined in section 6.6.1 (see

Eq 6.16 to 6.20), and (EI)$_{eff}$ is the flexural stiffness of the system with considering 50mm screw spacing.

When the values of the parameters are applied in Equations 6.27 and 6.28, the strength check of the 8m modules are equal to 0.22 and 0.12, respectively which are well below 1 and ensure a safe ultimate limit state design for the combined bending and axial actions. It is also confirmed that the design of the section is governed by the stiffness of the system (long term deflection limit) and the strength of the system is much higher than the required design capacity specified by the standards.

Equation 6.29 must also be satisfied to check the flexural shear strength of the 8m LVL modules.

$$\phi f_s \geq f^*{}_s \qquad \text{Eq.6.29}$$

Equation 6.30 shows the calculation of ϕf_s in which $f'_{s,w}$ is the shear design capacity of the webs and needs to be modified by the modification factors given in Equation 6.30.

$f^*{}_s$ on the other hand, is the shear stress due to loading which can be calculated using Equation 6.31 (derived from EC.5, appendix B).

$$\phi f_s = \phi k_1 k_4 k_6 [f'_{s,w}] \qquad \text{Eq.6.30}$$

$$f^*{}_s = \frac{V^*(\gamma_{bf} E_{bf} A_{bf} a_{bf} + 0.5 E_w b_w d_w{}^2)}{b_w (EI)_{eff}} \qquad \text{Eq.6.31}$$

V^* is the maximum acting shear force at the supports (with 3kPa imposed load and 1kPa permanent load). Other parameters of Equation 6.31 have been previously defined in section 6.6.1 and (EI)$_{eff}$ is the flexural stiffness of the 8m modules with considering 50mm screw spacing. When the values of ϕf_s and $f^*{}_s$ are applied into Equation 6.29, the result will be 6.1Mpa $\geq$ 1.45Mpa, and hence, a safe shear flexural design of the system is also ensured.

Finally, the load on a single screw should be taken according to Equation 6.32 and 6.33, which calculates the shear force on a single screw of the bottom flange interface and top the flange interface, respectively.

$$F_{bf} = \frac{\gamma_{bf} E_{bf} A_{bf} a_{bf} S}{(EI)_{eff}} V^*$$

Eq.6.32

$$F_{tf} = \frac{\gamma_{tf} E_{tf} A_{tf} a_{tf} S}{(EI)_{eff}} V^*$$

Eq.6.33

Where F_{bf} and F_{tf} are the shear load on a single screw in bottom flange and top flange, respectively, and the rest of parameters of Equations 6.32 and 6.33 have been previously defined. When the values of the parameters are applied in Equations 6.32 and 6.33, F_{bf} and F_{tf} are equal to 1.6kN and 1.9kN, respectively which are below the maximum characteristic shear force that can be taken by a single screw.

Therefore, all the required serviceability and ultimate design checks ensured a safe design of the 8m LVL modules with 50mm screw spacing, when the screws are considered as the only bond (shear connecter) at the interfaces.

The same approach can be taken for 6m modules. Table 6.13 summarises the values of flexural stiffness for the partially composite section for 6m LVL modules.

Table 6.13 The analytically predicted flexural stiffness and the neutral axis of 6m LVL modules

Screw Spacing	Effective Flexural stiffness (N.mm^2)	Neutral axis (mm)
400mm	1.02E+12	125.6
200mm	1.34E+12	126.6
100mm	1.81E+12	128.7
40mm	2.60E+12	133.2
Fully composite (see chapter 5)	4.19E+12	146.6

With 1kPa permanent load plus the self-weight and 3kPa imposed load, and substituting the values in Equations 6.23a and 6.23b, the minimum required flexural stiffness of the 6m modules is 1.80E+12 N.mm^2 and 1.79E+12 N.mm^2 for short term and long term serviceability deflection limit, respectively. From the values presented in Table 6.13, it can be observed that the flexural stiffness of the modules with 100mm screw spacing can provide the required stiffness for the 6m LVL modules.

However, in order to consider the effect of creep in timber, the $(EI)_{eff}$ of LVL modules needs to be calculated based on Equation 6.24a and 6.24b in which the modification factor for creep is considered. With j_2 equal to 2 (the long-term creep factor for initial moisture content less than 15%), the required flexural stiffness to satisfy the long term deflection limit for span/300 are 2.5E+12 N.mm² (for Equation 24a) and 2.6E+12 (for Equation 24b). From the values presented in Table 6.13, it can be observed that the flexural stiffness of the modules with 40mm screw spacing can provide the required stiffness for the 6m LVL modules (for the deflection limit of span/300), even when there is no adequate glue used at the interfaces. The required flexural stiffness to satisfy the long term deflection limit of span/400 (Equation 24b with considering span/400 as the deflection limit) can only be provided with the use of glue, which provides infinite stiffness.

Moreover, the short term deflection check as a result of impact loading (point load) must satisfy Equation 6.25, where P is 1kN impact load. By considering 2.6E+12 N.mm² for the required flexural stiffness (provided by 40mm screw spacing), the Δ_{vib} is equal to 1.90mm and hence, Equation 6.25 is satisfied as well.

For strength check of 6m modules, Equations 6.27 to 6.33 were checked and they ensure a safe design (0.2 and 0.1 for Equations 6.27 and 6.28, respectively and 1.5kN, 1.7kN and 2.1 kN for Equations 6.31, 6.32 and 6.33, respectively). Therefore, all the required serviceability and ultimate design checks confirmed a safe design of the 6m LVL modules with 40mm screw spacing, when the screws are considered as the only bond (shear connecter) at the interfaces.

6.7   Conclusions

In this chapter the partially-composite behaviour of LVL beams were assessed through an extensive experimental and analytical investigation. As the first phase of partially-composite experimental investigation of LVL beams, two types of timber composite connections were fabricated and tested based on Eurocode 5 recommendations, and the load-slip responses obtained from lab tests are used to determine the strength and stiffness of the connections at serviceability, ultimate and near collapse levels. The connections were fabricated to replicate the interfaces of 6m and 8m LVL modules.

Type 17 normal screws were used as the only shear connecter of the connections. As a result of the push-out tests, a mathematical expression of the behaviour of the timber connection with normal screws was proposed which can capture the first and second stages of the behaviour of timber connections with normal screws and can be easily incorporated into nonlinear FE analyses of timber beams with normal screws.

In order to investigate the partially-composite performance of LVL beams at serviceability and ultimate limit state, three "T" shaped beams with 100mm, 200mm, and 400mm screw spacing were fabricated and tested under four-point bending loads. It was observed that exceeding the bending and tensile stress in the web (hySpan Project LVL) triggered the failure of the LVL beams. The final failure of the beams was brittle with a sudden drop in the load bearing behaviour of the system. The screws did not exceed their ultimate shear strength as they were not significantly bent or there was no failure observed in the screws. Moreover, it was observed that the behaviour of LVL beams can be represented by a bi-linear model in which the stiffness of beams drops from serviceability stiffness to ultimate stiffness at the yield point. An analytical model was also developed to capture the load and deflection of the beams at yield –point as well as the ultimate failure load. The comparison between the experimental results and the analytically predicted results showed good correlation for ultimate load and ultimate deflection of the beams, which indicates the adequacy of the prediction model in capturing the ultimate behaviour of the beams.

Finally, the effective flexural stiffness of 8m and 6m modules is analytically predicted using different screw spacing, and the required screw spacing is specified so that the load bearing behaviour of the LVL modules is still in excess of the design ultimate required to be resisted according Australian design standards, even when there is no glue used at the interfaces. All the serviceability and ultimate design checks ensured a safe design of the 8m and 6m LVL modules.

University of Technology, Sydney

CHAPTER 7

NUMERICAL INVESTIGATION OF TIMBER

FLOOR MODULES

7 NUMERICAL INVESTIGATION OF TIMBER FLOOR MODULES

7.1 Introduction

Finite Element modelling and numerical investigation of engineering structures is one of the main computing tools for engineers as it can reduce or eliminate the costly experiential investigation and save a lot time and money. Finite element (FE) method is a numerical modelling technique to determine the behaviour of a real structure to external and internal loads by dividing it into several elements. Then, the response of the system will be determined by describing the response of each single element. The accuracy of the FE results depends upon the choice of element type, boundary conditions, and mesh size, accuracy of input data such as material properties, method of connecting elements and other factors. Extensive numerical research works have been conducted on timber beams to investigate their behaviour and performance, and as mentioned in chapter 2 there is a need for a simplified material model and a constitutive law, which can adequately capture the behaviour and the failure of timber.

There are many commercially FE software's available such as ANSYS, ABAQUS, SAP, LS-DYNA, ATENA, MICTROSTRAN, SPACEGASS, DIANA, ALGOR, and MFEAP. However, in this study, ANSYS (ANSYS 2013) was used for numerical investigation of LVL modules. ANSYS (2014) is a strong general-purpose finite element computer programme which can be used for linear and non-linear static and dynamic structural analysis, acoustic, heat transfer, fluid flow and electromagnetic problems. After modelling a structure (a beam for example) with a FE program, the FE model needs to be verified against a few full-scale experiments case to confirm whether or not the results are accurate and acceptable. Once it was confirmed that the FE results are accurate, the calibrated FE model can be used for the parametric study, and to simulate the behaviour and performance of other dimensions and spans of the structure under various types of loads.

In this study, a technique of modelling timber beams is proposed and investigated. The results of the FE model are verified against the experimental results. The results of the

full scale experimental tests together with the numerical investigation provide a robust model of predicting the performance of any timber beams with similar structural features to long span LVL modules, while the structural shape, dimensions, and spans can be varied according to the special requirements such as dynamic performance or fire resistance requirements.

7.2   Numerical Investigation

The reason of using ANSYS (2014) in this study was due to its ready availability at UTS and the high performance cluster nodes at UTS computing resources, where multiple ANSYS models could be run simultaneously. Moreover, ANSYS is a strong FE program with many material models and structural features, which make it possible to simulate a wide range of structural systems. Any other FE package can also be used provided that material models and boundary conditions can be properly simulated.

In the following sections the proposed constitutive law which was obtained from the tension-compression tests (see chapter 4) is incorporated into the FE analysis of LVL beams. A Finite Element model to capture the behaviour and failure of the four point bending tests of LVL sections (chapter 4) is developed, and the results of the FE model are verified against the experimental results. The FE analysis of LVL sections was also used as the preliminary FE analysis of the 6m and 8m long span LVL modules, as well as the actual floor system (1.8m*8m). All the FE results are verified against the experimental results and are reported in this chapter. Moreover, the details of the proposed finite element model, the type of elements and material model used for the FE analysis of the LVL beams are reported in the following sections.

7.2.1   Geometric Properties of Model

As mentioned in chapter 4, a number of edge-wise and flat-wise four-point bending tests were conducted on LVL beams and the dimensions are shown in Figure 7.1a, Figure 7.1b and Figure 7.1c. The results of the full scale four point bending tests are used to identify the behaviour of LVL up to the failure point. The bending strength, Modulus of Elasticity, failure loads and failure mode of LVL beams were assessed during the conducted tests and the results were used for the FE analysis of LVL beams.

The dimensions of the FE model were based on the measurements of the tested timber beams (Figure 7.1a to Figure 7.1c).
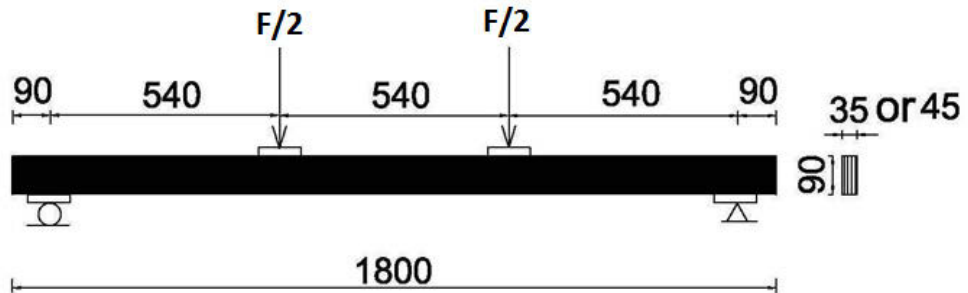
(a)
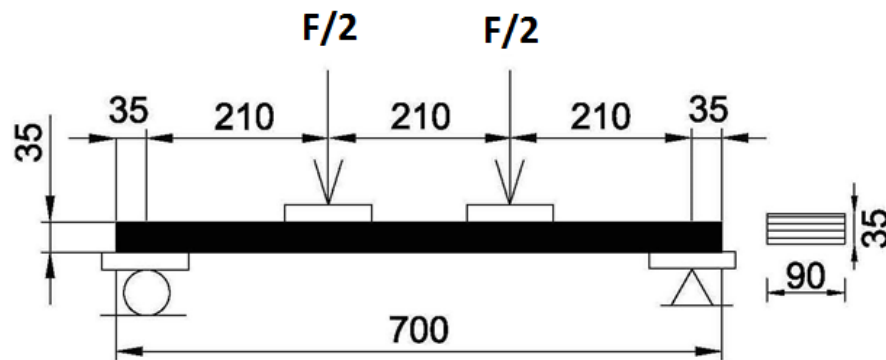
(b)
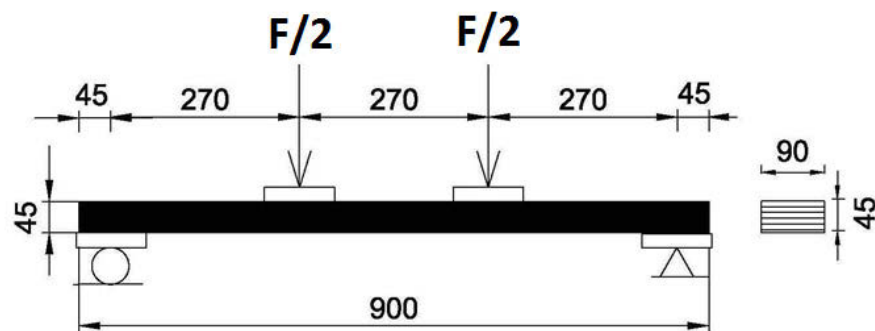
(c)

Figure 7.1 Test setups for flat-wise and edge-wise tests according to 4063.1:2010, (a). The test set up for edge-wise tests, (b) The test set up for flat-wise tests, (c) The test set up for flat-wise tests

7.2.2   Element Type

All LVL beams were modelled using SOLID185 element, which is an eight-node solid element with three degrees of freedom (x, y and z) for each node, and it can be used for the 3-D modelling of solid structures.   SOLID185 is capable of simulating plastic deformation, creep, large deflection and strain. The geometric properties of the element are shown in Figure 7.2 (ANSYS 2014).
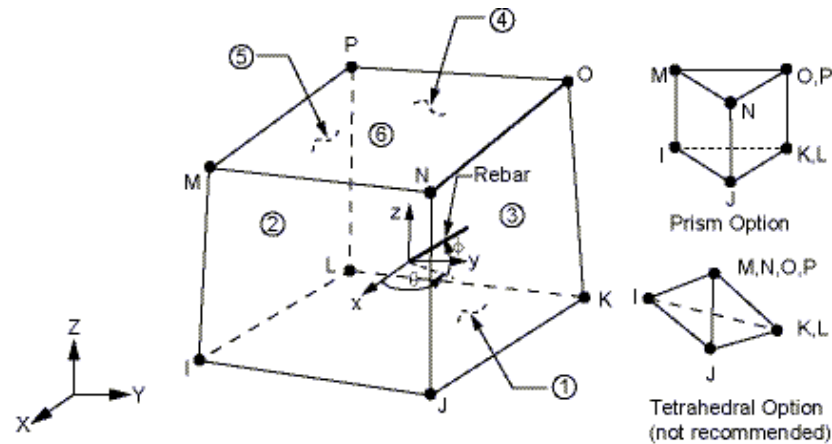
Figure 7.2 Geometric properties of SOLID185 (ANSYS 2011)

7.2.3   Material Properties

A summary of the material properties of LVL is presented in Table 7.1 which are based on the experimental investigations conducted on LVL (see chapter 4, chapter 5 and Table 5.1). Properties of LVL were assessed in edgewise and flatwise directions which replicate the orientation of LVL in tested beams. The value of Poisson's ratio of the LVL timber components (pine timber) was approximated using Wood Handbook, which is equal to 0.3 (General Technical Report FPF-GTR-113 1999). The density of LVL was also calculated according to standard (AS/NZS 4063.1.2010) and was considered 601 kg/m^3 for all LVL beams.

Table 7.1 A summary of the material properties of LVL

Component Name	cross-banded LVL (Flat-wise tests)	hySpan-Project LVL (Edge-wise tests)	hySpan-Project LVL (Flat-wise tests)
True MOE, $E_{x,true}$ (GPa)	10.7	13.7	13.7
Tension strength, f_t (MPa)	34	37.4	37.4
Compression strength f_c (MPa)	42	51.4	51.4

7.2.4 Material Model and Constitutive Law

A suitable constitutive law and an appropriate material model are critically needed for the FE model in order to determine the state of stress under any given load and to determine whether or not the failure has occurred. Although several criteria and material models have been developed which can be applicable to orthotropic materials such as wood (see chapter 2), but they are used for research purposes only and are very difficult to be used in practical design, simply because of too many input parameters and limitations. Therefore, there is a need for a simplified material model and a constitutive law, which can adequately capture the behaviour and the failure of wood in general, and Engineered Wood Products (EWPs) such as LVL in particular. As a result of the tension and compression tests conducted on LVL sections, a suitable constitutive law was developed and proposed in chapter 4, which can accurately capture the stress-strain relationship and the failure behaviour of LVL, and it can also be incorporated into FE analysis of any LVL beam. Equations 7.1 and 7.2 show the mathematical model which represent the behaviour of hySpan Cross-Banded LVL and hySpan project LVL, respectively.

$$\sigma(\varepsilon) = \begin{cases} -\dfrac{|\varepsilon| + (1.24 * 10^{14})|\varepsilon^7|}{(9.35 * 10^{-5}) + (8.42 * 10^{-5})|\varepsilon| + (3.29 * 10^{12})|\varepsilon^7|} \quad, \quad -\varepsilon_u \leq \varepsilon \leq 0 \quad (R^2 = 0.97) \\ \\ (10.7 * 10^3)\varepsilon \quad, \quad 0 \leq \varepsilon \leq \varepsilon_t \quad (R^2 = 0.92) \end{cases}$$

Eq.7.1

$$\sigma(\varepsilon) = \begin{cases} -\dfrac{|\varepsilon| + (1.35 * 10^{14})|\varepsilon^7|}{(7.32 * 10^{-5}) + (6.28 * 10^{-4})|\varepsilon| + (2.94 * 10^{12})|\varepsilon^7|} \quad, \quad -\varepsilon_u \leq \varepsilon \leq 0 \quad (R^2 = 0.91) \\ \\ (13.7 * 10^3)\varepsilon \quad, \quad 0 \leq \varepsilon \leq \varepsilon_t \quad (R^2 = 0.97) \end{cases}$$

Eq.7.2

The proposed constitutive law given Equations 7.1 and 7.2 was used in FE model of LVL beams to introduce a bi-linear stress-strain curve for the normal stress in an isotropic plastic model.

As mentioned earlier, besides a suitable constitutive law for capturing the state of stress under any given load, a suitable failure model is also required to determine whether the failure happened or not. Since the behaviour of the LVL beams is dominated by bending in longitudinal direction and there is no defect (such as hole or notch) along the length of the beams, the effect of perpendicular directions is negligible and a uniaxial model can represent the global response of the LVL beams. Therefore, in this study, the behaviour of LVL beams was assumed to be uniaxial. For this purpose, the available material model UNIAXIAL in the FE program ANSYS (2014) was used which permits different (defined) stress-strain behaviours as well as different strength values in tension and compression. The tension and compression side of the stress-strain curve can be easily defined under UNIAXIAL TENSION and UNIAXIAL COMPRESSON,

respectively, with as many data as required. Therefore, Equations 7.1 and 7.2 or any other constitutive law can be defined under these commands.

A composite yield surface is used to model different yield behaviour in tension and compression for uniaxial material model. In tension the Rankine maximum stress criterion is used and in compression, the von Mises yield criterion is used (see section 2.6) . Figure 7.3 shows the yield surfaces for uniaxial model in compression and tension for plastic behaviour:
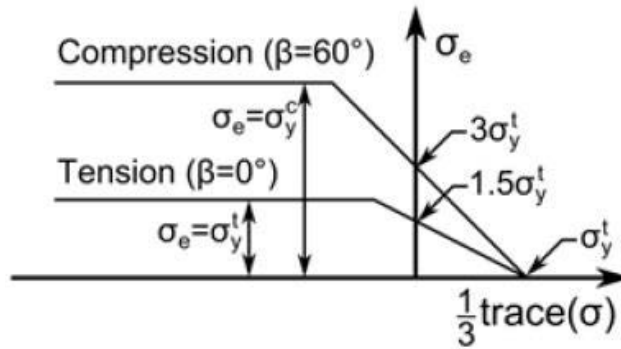
Figure 7.3 Yield Surfaces for Compression and Tension

The yield surfaces are plotted in the meridian plane in which the horizontal and vertical axis are von Mises equivalent stress and pressure, respectively. The development of the yield stress in tension and compression follows the user input piecewise linear stress-strain curves for compression and tension (ANSYS 2014). The compression and tension yield stress develop as a function of the equivalent uniaxial plastic strain (ε_t^{-Pl}).

The plastic flow potential is defined by the von Mises yield criterion in compression. The flow potential in compression is:

$$Q(\sigma, \sigma_y^c) = \sigma_e - \sigma_y^c \qquad \text{for trace } (\sigma) < -\sigma_y^c \qquad \text{Eq.7.1}$$

In tension, the Rankine cap yield surface is replaced by an ellipsoidal surface defined by:

$$\frac{\left(\frac{1}{3}trace(\sigma) - Q\right)^2}{c^2} + \sigma_e^2 = 9Q \qquad \text{for trace } (\sigma) < -\sigma_y^c \qquad \text{Eq.7.2}$$

Where c is a constant function of the user-defined plastic Poisson's ratio, v^{pl} :

$$c = \sqrt{\frac{9(1-2v^{pl})}{5+2v^{pl}}}$$ Eq.7.3

The v^{pl} is the plastic Poisson's ratio.

Moreover, The failure criteria to model the strain softening or to model the orthotropic behaviour of LVL was not aimed to be evaluated in this study because there was no defect (such as hole or notch) along the length of the beams and the effect of perpendicular directions was negligible and therefore, a uniaxial material model could sufficiently represent the global response of the LVL beams. The UNIAXIAL material model permits to terminate the stress-strain curve at the maximum stress value (or the corresponding strain), and in that way the brittle failure of LVL can be captured.

7.2.5 Boundary Conditions

The boundary conditions for the model were set as pin-roller, which is close to the real boundary condition of the timber beams as shown in Figure 7.4a and Figure 7.4b. Movements in global X, Y and Z axis were restrained to simulate the pin support while movements in global Y and Z axis was restrained for to replicate the roller support.

a. Pin support   b. Roller support
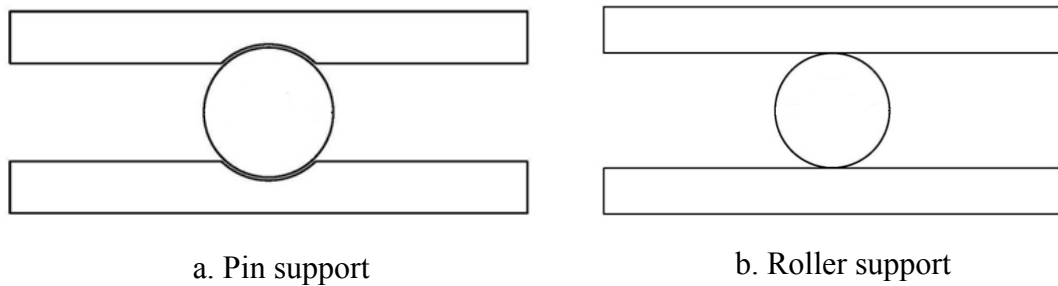
Figure 7.4 Pin and Roller supports

7.2.6 Mesh Size

Mesh sensitivity analysis was also conducted for the FE model, with squared shape mesh (or very close to square) and with different mesh size including 45mm, 22.5mm, 9mm, 5mm and 3.5mm. The analysis showed that a mesh size around 1/10 of the depth of section is an appropriate size for LVL which gives adequately accurate results, that

is, 9mm mesh size for the edge-wise tests (with 90mm section depth) and 3.5mm mesh size for flat-wise tests (with 35mm section depth). Figure 7.5a shows the cross sectional view of the continuum-based ANSYS model for hySpan Project LVL (Edge-Wise tests) with 9mm mesh size and Figure 7.5b shows the overall view of the model. Figure 7.6 shows the mesh sensitivity analysis for edge-wise tests of hySpan Project LVL. As shown in the figure, a mesh density above 10000 elements which corresponds to 9mm mesh size (or 1/10 of the depth of section) gives accurate results.
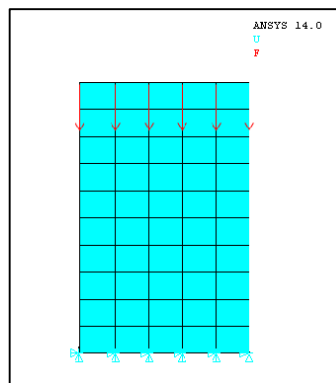
a . Cross sectional view
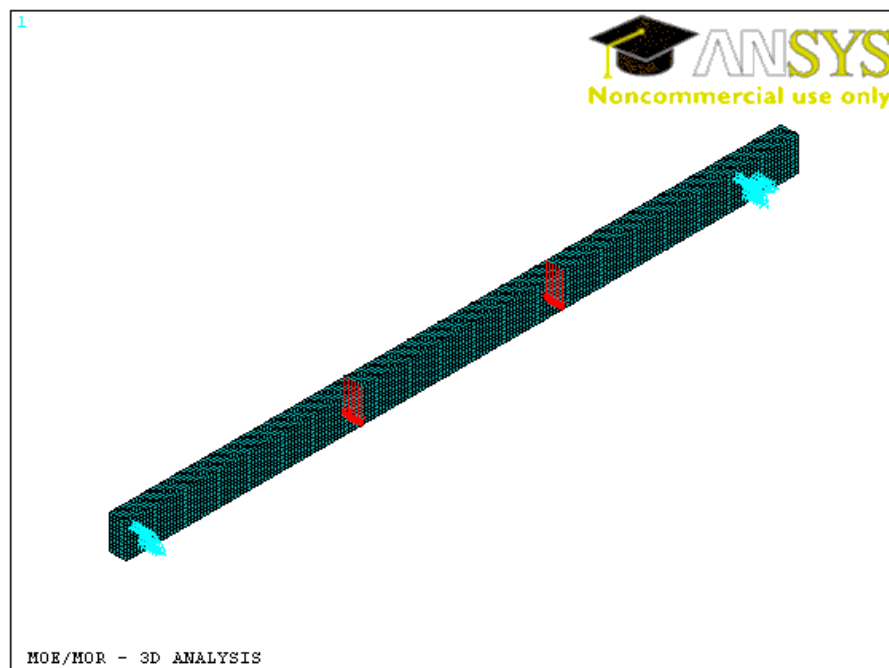
b.3D view

Figure 7.5 Continuum-Based ANSYS model for hySpan Project LVL, Edge-Wise tests with 9mm mesh size
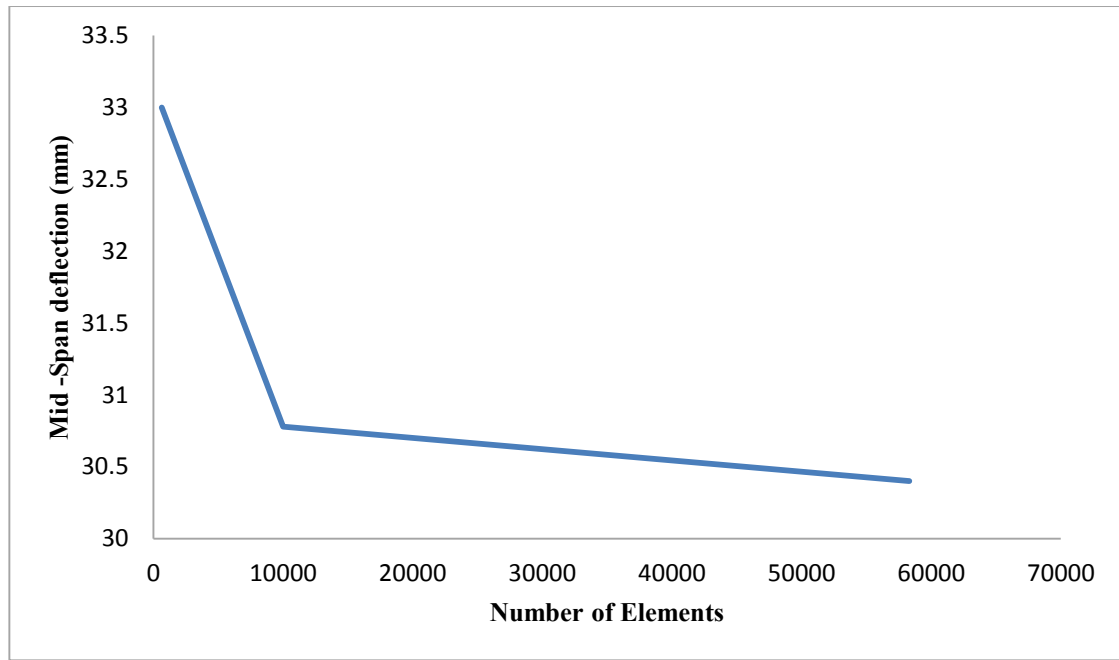
Figure 7.6 Mesh sensitivity analysis for edge-wise tests of hySpan Project LVL

7.2.7 FE Results and the Comparison between Analytically Predicted Results and the Experimental Results

Figure 7.7 to 7.9 present the FE results for the load-deflection curves as well as a comparison with the experimental test results. It is observed from the FE results that the constitutive law and the FE modelling strategy proposed in this study can adequately capture the behaviour of LVL. The failure mode (a brittle failure) and the actual failure load of LVL beams can also be accurately captured by the FE modelling. For example, for the hySPAN Project edgewise tests (Figure 7.7) the average failure load is 14.7 kN which is compatible with the predicted F_{max} when the extreme fibers of the section exceed max bending stress (see chapter 4) and it is also compatible with the FE modelling result proposed in this study. Table 7.2 summarises a comparison between the failure load values of FE model, analytical prediction model and experimental investigation for the edgewise and flat-wise experimental tests. As shown in Table 7.2, the values of the predicted F_{max} are very close to the experimental tests results as well as FE model results. Figure 7.8 and Figure 7.9 are also present the FE results and experimental results of flat-wise four point bending tests. The stiffness, ultimate load and ultimate deflection of the beams captured by the FEM are highly compatible with

the experimental results. The UNIAXIAL material model permits to terminate the stress-strain curve at the maximum stress value (or the corresponding stain), and in that way the brittle failure of LVL is captured. Because the ultimate tensile strength of LVL is lower than the maximum elastic compressive strength (before occurring the softening), as shown in Figures 4.9 and 4.10, the brittle failure occurs in FEM before the compressive fibres exceed their linear elastic behaviour. Hence, a slight non-linear behaviour observed in some of the experimental results at the ultimate strength was not observed in FEM results. However, as it can be observed in experimental and numerical results of U8-03 and U8-01(see Figure 7.12 and 7.13), the effect of non-linear behaviour of the compressive fibres are negligible when the depth of section increases.

A comparison between the values of mid-span deflections (maximum deflections) of LVL beams are also summarised in Table 7.3 and it can be observed that the experimental results are highly compatible with numerical results (the analytically predicted and the FE). To sum up, all the FE results of LVL beams show a linear behaviour (load- deflection response), while the linear characteristics of LVL is almost preserved up to the failure load where a brittle failure occurs. The stiffness, ultimate load and ultimate deflection of the beams captured by the FEM are highly compatible with the experimental results. This FE model was used as the preliminary FE model for 8m and 6m LVL modules and the results are presented in the following section.
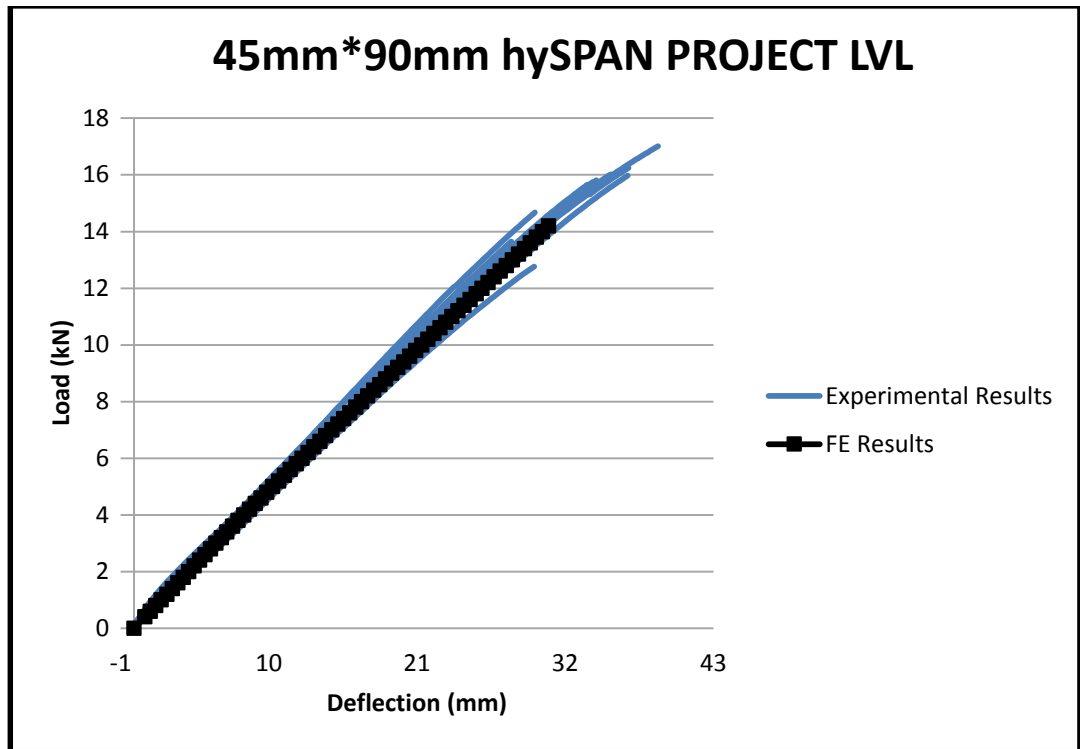
Figure 7.7 Compression between FE and experimental results, Edge-Wise tests
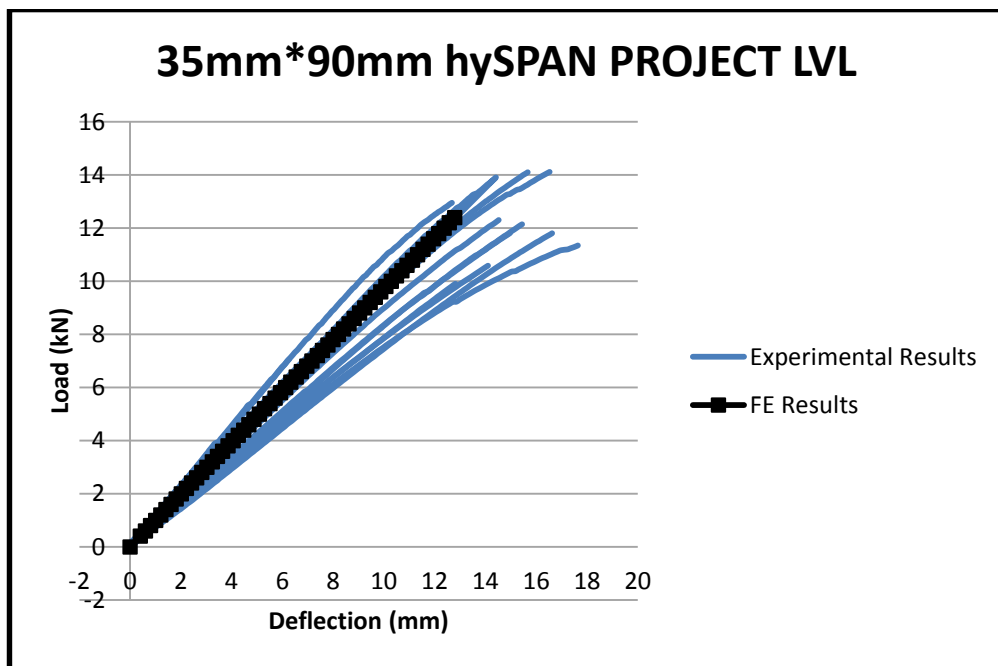
Figure 7.8 Compression between FE and experimental results, Flat-Wise tests
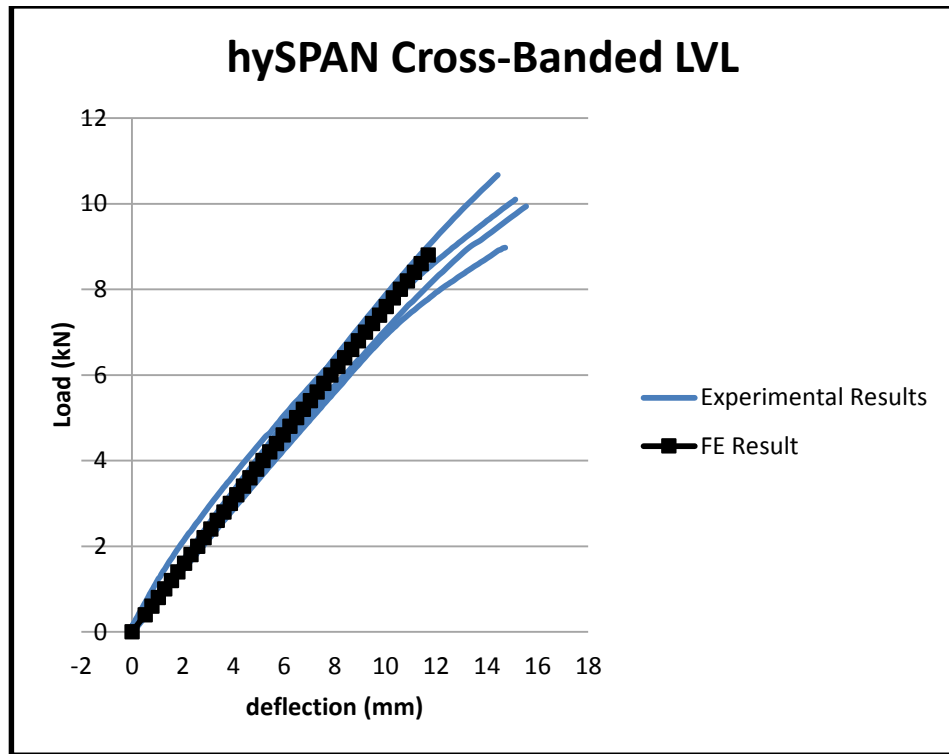
Figure 7.9 Compression between FE and experimental results, Flat-Wise tests

Table 7.2 Comparison between the experimental results, FE results and analytically predicted results of the ultimate load of LVL beam

	Ultimate load (kN)				
	FE results	Difference with experimental results	Analytically predicted	Difference with experimental results	Average Experimental results
Cross-Banded 35mm*90mm, flat-wise tests	8.8	4.3%	9.2	0%	9.2
hySpan Project 35mm*90mm, flat-wise tests	12.4	2.4%	12.7	0%	12.7
hySpan Project 45mm*90mm, edge-wise tests	14.2	3.4%	14.7	0%	14.7

Table 7.3 Comparison between the experimental results, FE results and analytically predicted results of the maximum deflection of LVL beams

	Maximum deflection (mm)				
	FE results	Difference with experimental results	Analytically predicted	Difference with experimental results	Average Experimental results
Cross-Banded 35mm*90mm, flat-wise tests	11.7	12%	13.1	1.5%	13.3
hySpan Project 35mm*90mm, flat-wise tests	12.8	6.6%	13.4	2.2%	13.7
hySpan Project 45mm*90mm, edge-wise tests	30.8	5.5%	31	4.9%	32.6

7.2.8 FE Results of 6m and 8m modules, and the Comparison between Analytically Predicted Results and the Experimental Results

As mentioned earlier, the same strategy which was used for modelling of LVL beams was also used for FE modelling of 6m and 8m floor modules. Therefore, SOLID185 was chosen as the element type and the UNIAXIAL material model, which is available in ANSYS (2014), was used to define the LVL constitutive law and to determine the maximum stress (and corresponding strain) values where the compression and tension curves terminate.

The interface between flanges and webs was investigated to be fully composite (see chapter 5) as no slip was observed during the four point bending tests of 6m and 8m modules. To model a fully composite section, nodes at the interface between the all components were coupled. Moreover, as it was investigated in section 7.2.6 that a mesh size of about 1/10 of the depth of section is an appropriate size for LVL beams, which gives adequately accurate results, therefore a mesh size of about 4cm to 5cm was adopted to model the 6m and 8m modules. Figure 7.10 and Figure 7.11 show the cross-sectional view and the 3D view of the FE model of 8m LVL modules, respectively.
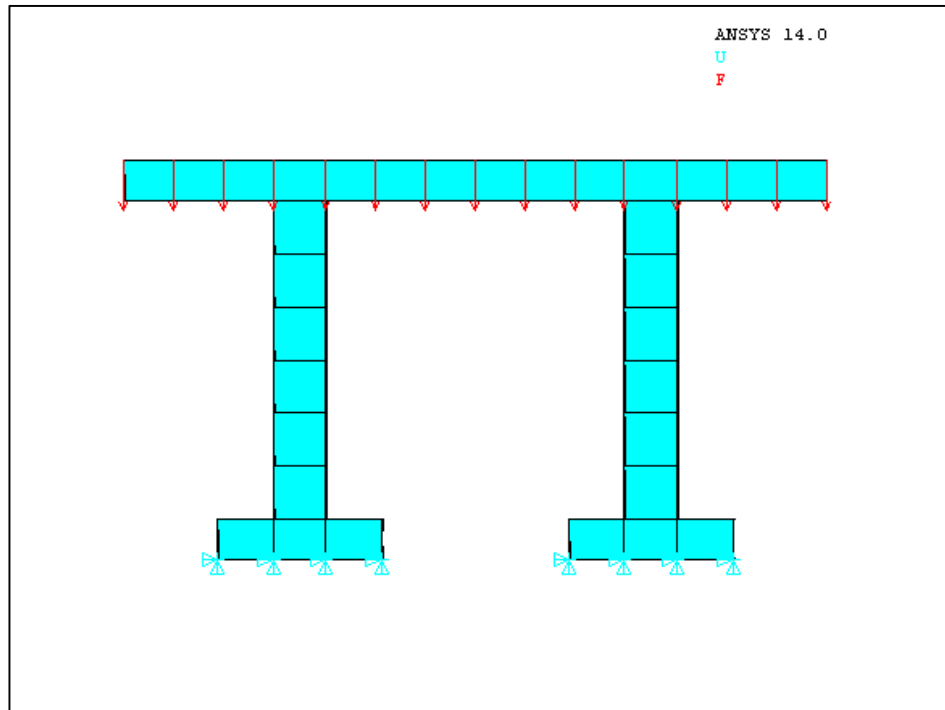
Figure 7.10 Cross sectional view of ANSYS model of 8m LVL modules
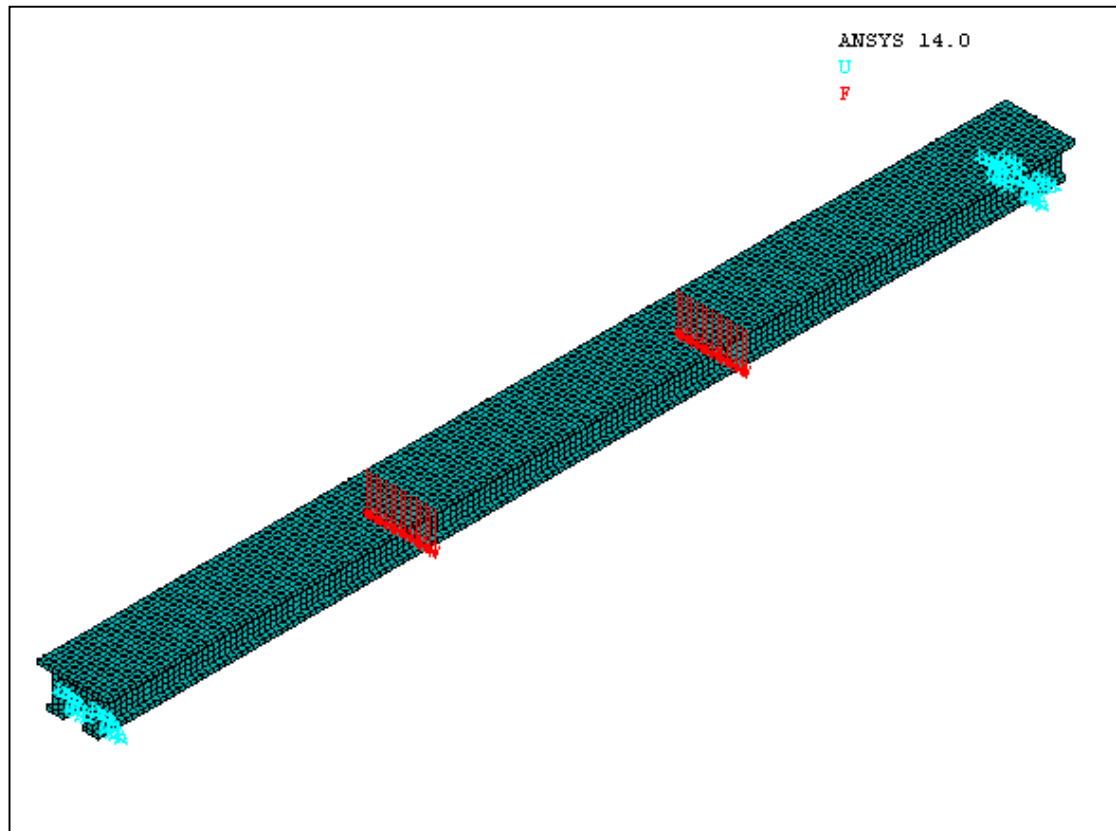
Figure 7.11 3D view of ANSYS model of 8m LVL modules

The experimental investigation of 8m and 6m modules were presented in chapter 5, and the predicted responses of the system was also calculated and reported in Table 5.5 to 5.8. Figure 7.12 summarises the load-deflection graphs of 6m and 8m tests, and a comparison between the FE results and the experimental counterparts is shown in Figure 7.13. As can be observed from Figure 7.13, the FE analysis adequately captures the flexural stiffness, the linear behaviour, the brittle failure and the failure load of 8m and 6m modules. Table 7.4 summarises a comparison between the failure load values of FE model, analytical predicted results and experimental results of the long span floor modules. As shown in the table, the results are highly compatible which shows the adequacy of the proposed FE method in using the proposed constitutive law for LVL, the UNIAXIAL material model and the suitable failure criteria.
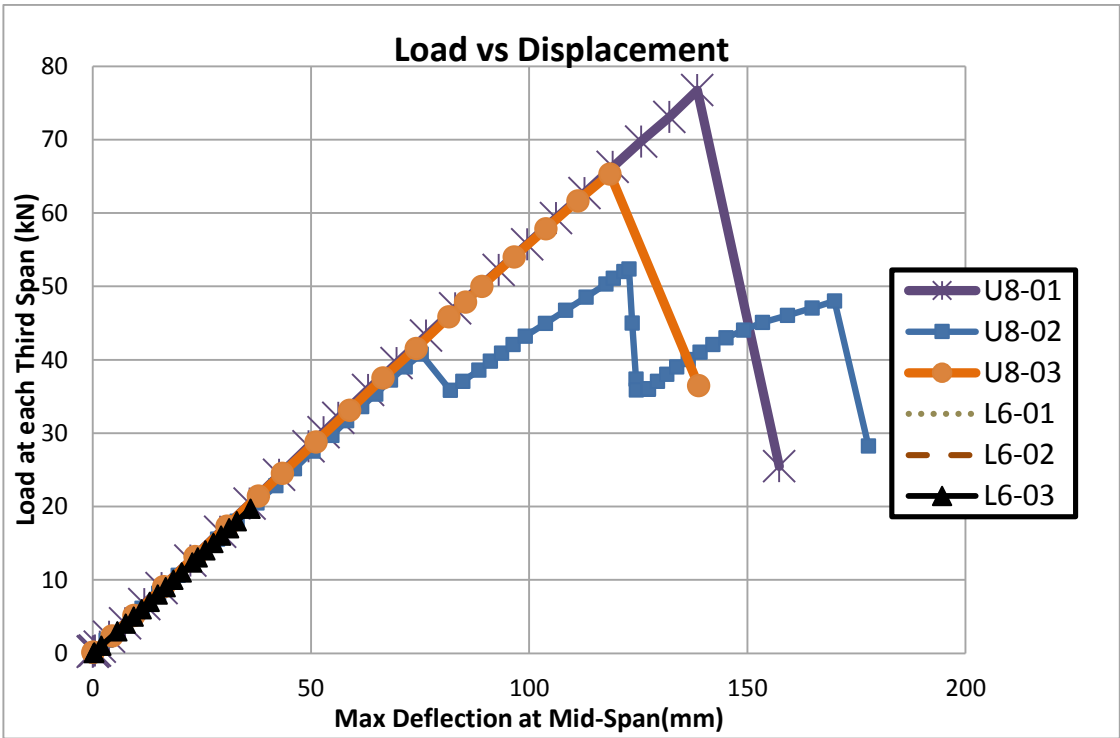
Figure 7.12 Load vs max deflection of modules for the SLS and ULS tests
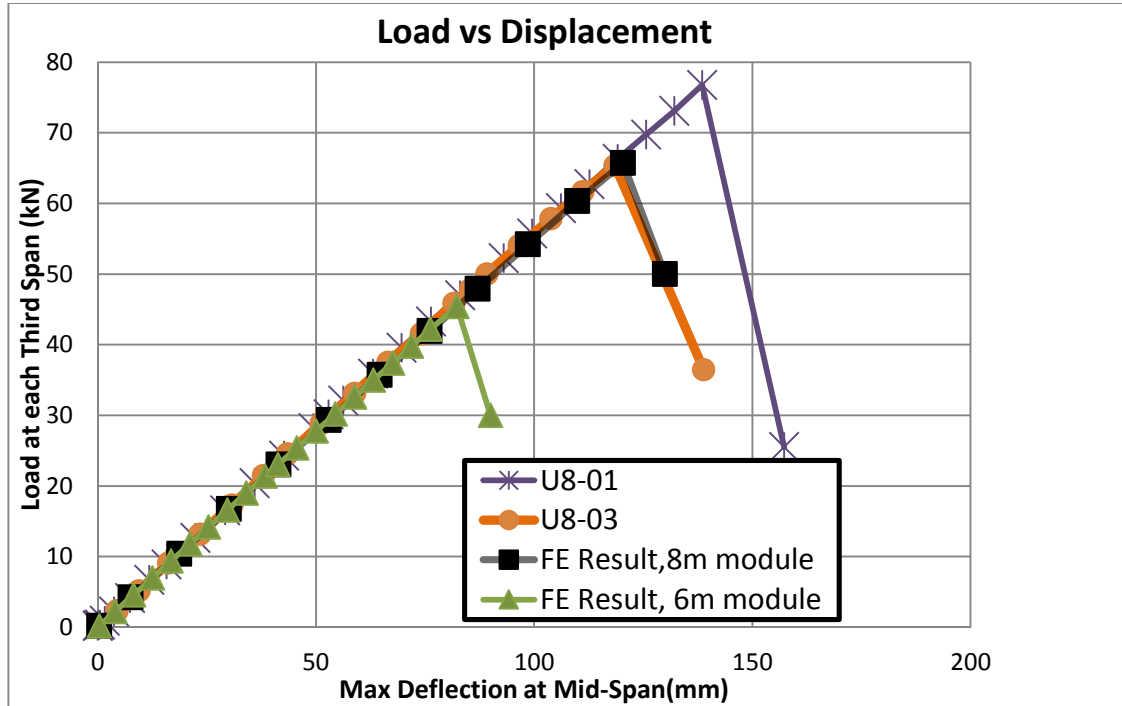
Figure 7.13 Comparison between FE and experimental results for 6mm and 8m LVL modules

Figure 7.14 shows the actual floor model (1.8m wide) by putting 3 of the 8m modules side by side, and connecting them by pin supports alongside the modules. Figure 7.15 presents the FE results of the floor system and shows that the failure load and EI for the floor are about three times higher than a single module, and the ultimate deflation remains unchanged. The predicted response of the system was also calculated according to the European standard (BS EN 1995-1-1:2004 +A1:2008) and a comparison between the experimental results, FE results and analytically predicted results are presented in Table 7.4 and 7.5. As shown in tables (7.4 and 7.5), all the results are highly compatible.
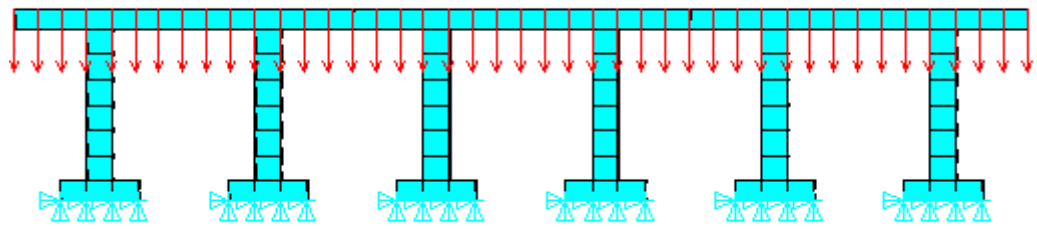
(a)
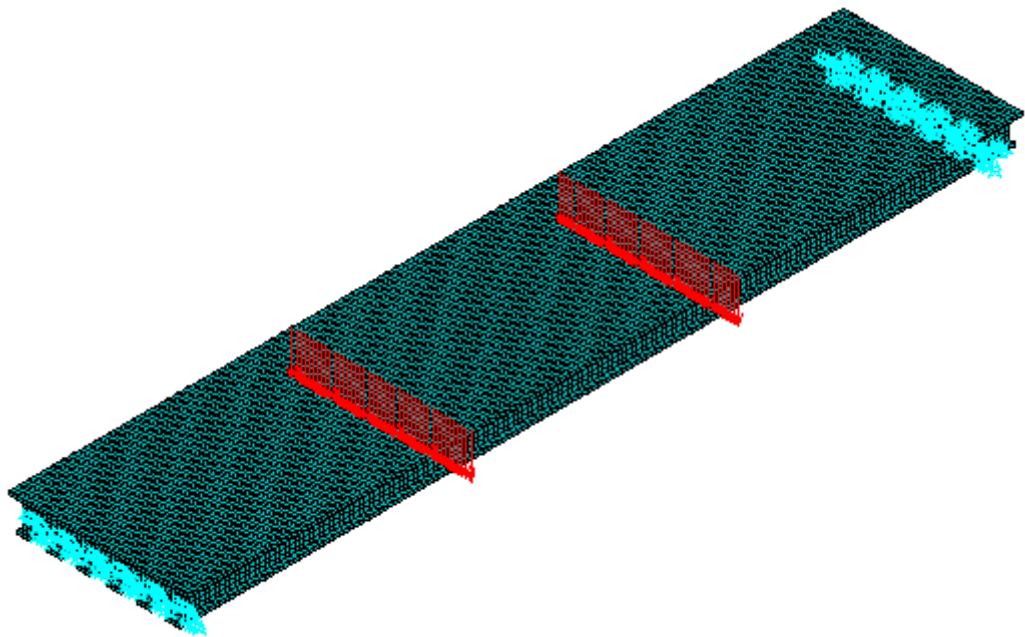
(b)

Figure 7.14 Ansys Model of the floor system (1.8m wise)

(a) front view, (b) 3D side view
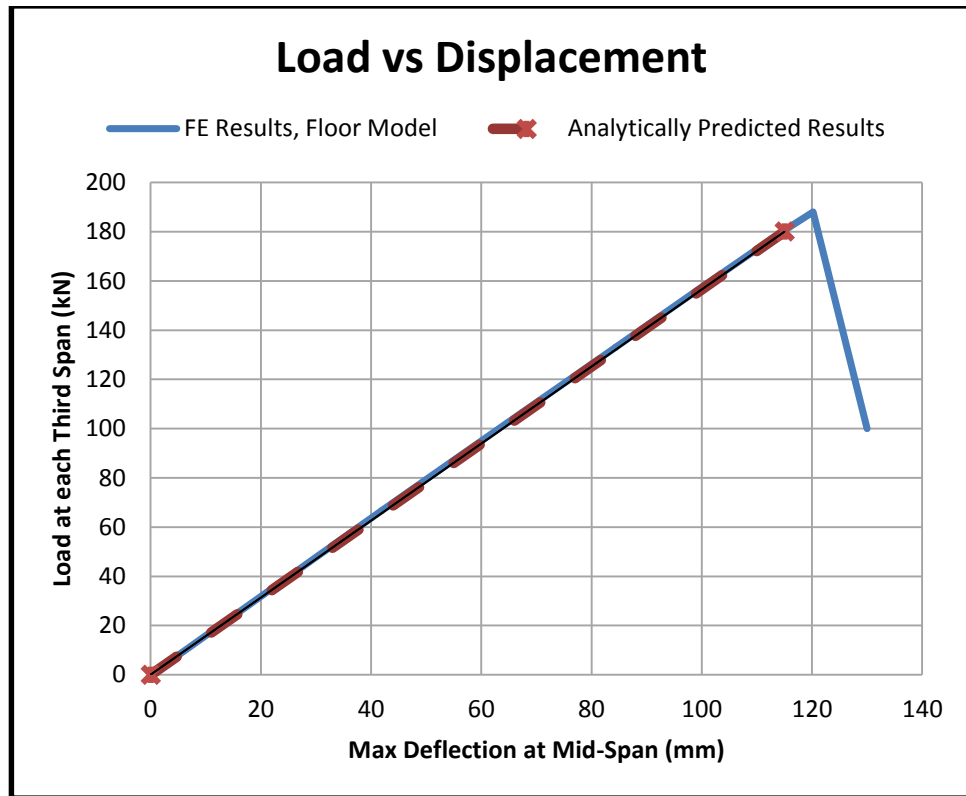
Figure 7.15 The Comparison between the FE results and analytically predicted results of the Floor system (1.8m wide)

Table 7.4 Comparison between the experimental, analytically predicted and FE results of the ultimate load of LVL beams

	Ultimate load (at each third span) (kN)		
	FE Results	Analytically predicted	Experimental results
U8-01	65.7	60	76
U8-03	65.7	60	65
6m clear span modules	45.5	46	-
1.8m*8m Floor system	188	180	-

Table 7.5 Comparison between the experimental, analytically predicted and FE results of the ultimate load of LVL beams

	Max deflection at Mid-Span (mm)		
	FE Results	Analytically Predicted	Experimental results
U8-01	120.4	115	136
U8-03	120.4	115	116
6m clear span modules	82.3	87	-
1.8m*8m Floor system	120.2	115	-

There are several ways of connecting the floor modules side by side. Figure 7.16 schematically shows a possible system to provide pin support alongside the modules. Another way is to use a double steel plate (on top and bottom of top flange) which cause more resistance in the connection. Furthermore, the tongue and groove connections are also a popular type of connecting the timber modules side by side, to make the floor system (see for example Lignatur® system (Figure 2.25) in chapter 2).
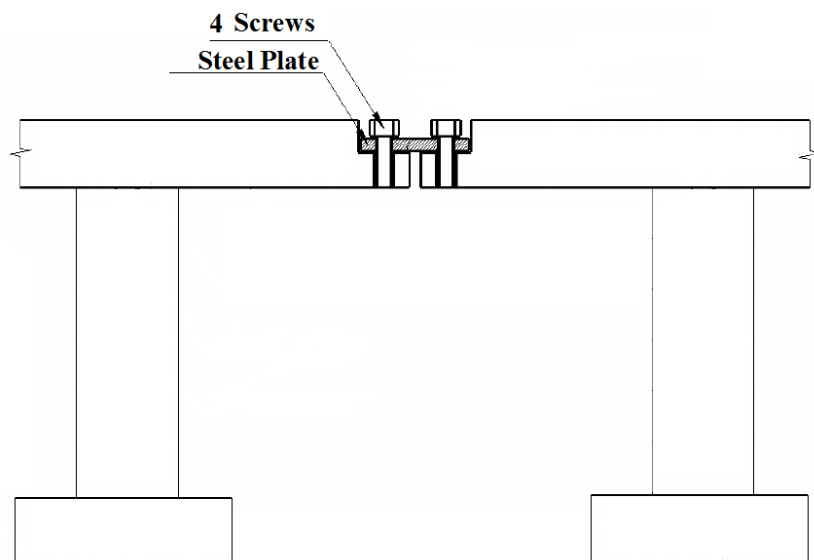
Figure 7.16 Possible interconnection system between LVL floor modules (this figure is schematic)

7.2.9 Comparison of the FE results with the FE results of 2D/3D ABAQUS model and Hashin damage model

Finally, the results of the FE model of this study are compared with 2D/3D FE model developed in ABAQUS by Khorsandnia (Khorsandnia and Crews 2014) and Hashin damage model (Khorsandnia, Valipour and Crews 2013).

Timber exhibits behaviour similar to quasi-brittle materials such as concrete (although timber is generally more ductile in compression). The intention of the 2D/3D ABAQUS model was to find out whether quasi-brittle constitutive law of material can be used as a simple alternative for predicting load-deflection and failure mode of flexure dominated timber element. In this regard, 'Concrete Damaged Plasticity' model in ABAQUS was used, which is one of the most well-known damage models in the existing commercial software (ABAQUS). This damage model has two main failure mechanisms, i.e. tensile cracking and compressive crushing of the material. The model is employed to model timber beams adopting Glos stress-strain relationship (Glos 1981). Two different continuum-based models in 2D and 3D were developed for U8-03. The Poisson ratio for timber was taken as 0.3 in the developed continuum-based FE models and modulus of elasticity in the direction parallel to the grain was adopted as the elastic modulus of timber. A mesh size of about H/10 was adopted for the analysis of timber beams with the developed 2D and 3D FE models (Khorsandnia and Crews 2014). The FE results of the two different 2D and 3D continuum-based ABAQUS model, and the results of the FE model which is developed by the author (the uniaxial material model developed in this study) are presented in Table 7.6 and Figure 7.17.

The FE results of this study are also compared with a simple orthotropic model using Hashin damage criteria (Khorsandnia and Crews 2013). Hashin damage model (Hashin 1980) can be calibrated using seven input parameters, namely, tensile strength of timber along the grains and perpendicular to grains, compressive strength of timber along the grains and perpendicular to grains, shear strength along the grain and perpendicular to grains, and a coefficient that determines the contribution of the shear stress to the fibre tensile initiation criterion (see section 2.6). A mesh size of about H/10 was adopted for the analysis of timber beams in Hashin damage model (Khorsandnia and Crews 2014).

The FE results of U8-03 developed by Hashin model are presented in Figure 7.17and Table 7.6.

Table 7.6 The FE results of ultimate loading capacity and corresponding deflection for U8-03

U8-03	FE Results of ABAQUS 2D	FE Results of ABAQUS 3D	FE Results of ABAQUS Hashin model	FE Results of Uniaxial Material Model (developed in this study)	Experimental results
Ultimate load capacity (kN)	118.5	118.2	118.7	131.4	129.8
Comparison with Experimental Results	-8.7%	-8.7%	-8.6%	+1.2%	
Max deflection at Mid-Span (mm)	108.5	107.9	108.4	120.4	116
Comparison with Experimental Results	-6.5%	-6.9%	-6.7%	+3.8%	
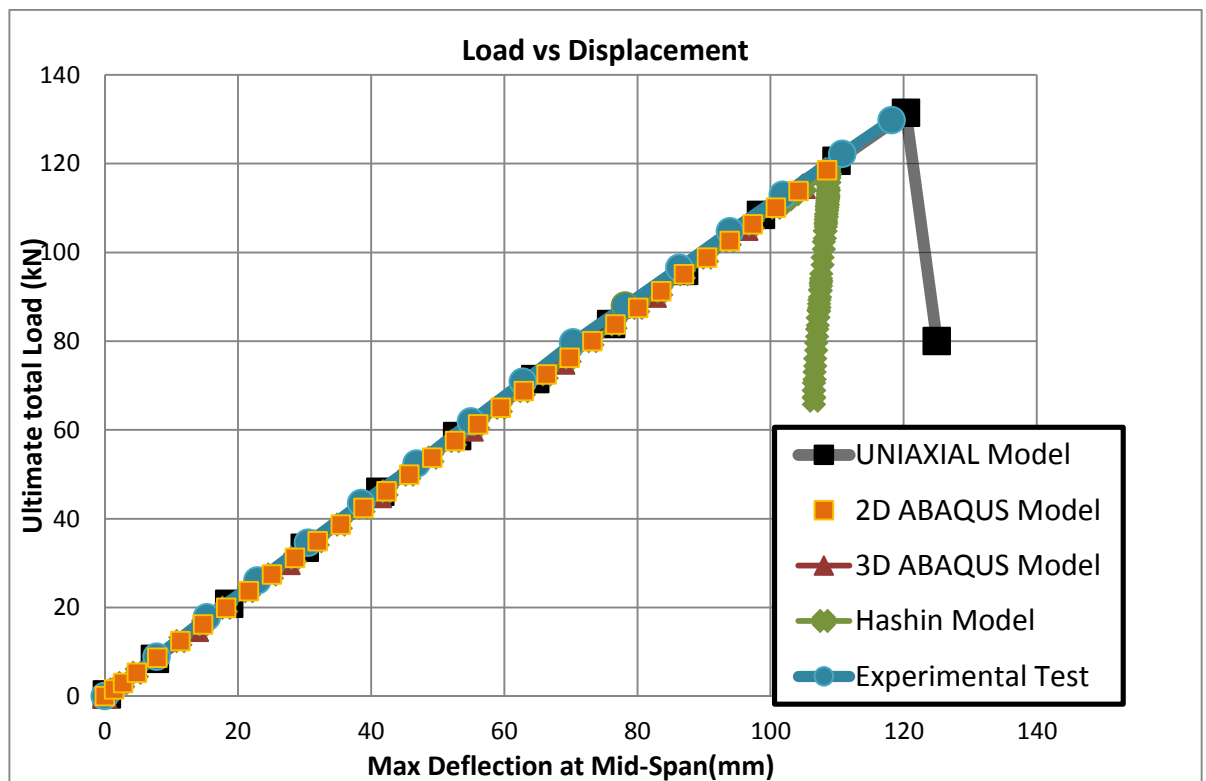
Figure 7.17 A comparison between the FE modelling results and experimental results of U8-03

As shown in Table 7.6 and Figure 7.16, all FEM results show a linear behaviour while the linear characteristics of LVL modules are almost preserved up to the failure load where a brittle failure occurs. The values of the initial and ultimate stiffness, and ultimate loads and the corresponding deflection captured by FE models of this study are also adequately compatible and accurate.

7.3   Conclusions

In this chapter, a continuum-based Finite Element model to capture the behaviour and failure of LVL beams and 8m and 6m LVL modules was developed and verified against the experimental results. Since the behaviour of LVL beams is dominated by bending in longitudinal direction, a uniaxial material model was implemented in FE model, while the state of stress under any given load was precisely defined by a suitable proposed constitutive law. The developed FE model and constitutive law was verified against the experimental results of the proposed 8m and 6m modules as well as a series of destructive and non-destructive tests conducted on LVL beams under 4-point bending loads (including the 35mm*90mm and 45mm*90mm beams in both flat wise and edgewise directions). The results of the FE model and experimental tests showed accurate compatibility in determining the initial and ultimate stiffness of LVL beams as well as the failure load, and confirmed the adequacy of the developed FE model for capturing the behaviour and failure load of any LVL beams with similar structural features to the tested beams (i.e. fully composite beams with no hole or notch alongside the beam, with a flexurally dominated behaviour in the longitudinal direction).

The ultimate load of the system was also calculated according to the design standards. The comparison between the analytically predicted values, FE results and experimental results confirm that the analytically calculated failure load and flexural stiffness of the system can represent the characteristics of fully composite LVL modules with a flexurally dominated behaviour.

The results of the FE model of this study are compared with Hashin damage model and 2D/3D FE model developed in ABAQUS by Khorsandnia (Khorsandnia and Crews 2014; Khorsandnia, Valipour and Crews 2013). The Hashin damage model and two

different continuum-based models in 2D and 3D were developed for U8-03. The FE results of the ABAQUS models, and the results of the FEM which is developed by the author (the uniaxial material model developed in this study) are compared and the results show compatibility which confirms the adequacy of the developed uniaxial FE model.

Finally, the results of the full scale experimental tests together with the conducted numerical investigation provide a model for predicting the performance of any timber beams with similar structural features to the LVL modules (i.e. fully composite beams with no hole or notch alongside the beam, and when the behaviour of the beams are dominated by bending in the longitudinal direction) while the structural shape, dimensions, and spans can be varied according to the special requirements such as dynamic performance or fire resistance requirements. Partially composite behaviour of LVL was predicted by analytical method which was presented in chapter 6.

University of Technology, Sydney

CHAPTER 8

CONCLUSIONS

8   CONCLUSIONS

8.1   The Proposed Floor System

The main objective of this research project was to propose a long span timber floor system for non-residential applications in Australia and New Zealand which meets both strength and serviceability design criteria, and to investigate the short term behaviour and the structural performance of the proposed system (which has not been previously researched and developed using radiata pine LVL). The prediction response of the proposed system (8m and 6m modules) showed that the maximum deflection of the system (stiffness of the system) governs the design of the section. The first fundamental frequency of the system was also predicted to be around 13Hz which indicates a safe serviceability design. All prediction responses of the system including the serviceability and ultimate performance and dynamic behaviour of the system ensured a safe design of the proposed LVL modules. . Optimising the proposed section by changing the spacing between webs or changing the width of the top and bottom flanges can be done through the verified FE model (please chapter 7 of the thesis), whilst minimising the need for additional costly experiments. Some of the advantages of the system are as follows:

- Significant low structural depth while being structurally very sound.

- Can provide a void between flanges in order to fit the insulations and other services.

- Can be prefabricated so they can be under high quality controlled processes.

- Can provide good vibration performance (Rijal 2013).

- Has high stiffness to weight ratio

- Non-structural layers (such as concrete topping) may be applied on top or bottom of system, in case of special dynamic performance or fire resistance requirements

8.2   LVL Properties, Test Results

The behaviour of two types of LVL, that is, hySPAN cross-banded LVL and hySPAN Project LVL, are investigated through a number of experimental and analytical tests. A summary of the mean characteristic values for hySPAN cross-banded LVL and hySPAN Project LVL were presented in chapter 5 Table 5.1. As a result of the tension and compression tests, a suitable constitutive law was proposed which can properly capture the stress-strain relationship, and the failure of LVL. A modification factor, α=200, is needed to be introduced to the Glos model (1981), so that it can represent the behaviour of LVL, which is linear under tension with a brittle failure and a ductile behaviour under compression following an initial linear response. The following mathematical model represents the behaviour of hySpan Cross-Banded LVL (Equation 8.1) and hySpan project LVL (Equation 8.2), respectively, which can be incorporated in the available material model UNIAXIAL in the FE program ANSYS (2013) and can be used to predict the behavior and failure of LVL beams (see chapter 7).

$$\sigma(\varepsilon) = \begin{cases} -\dfrac{|\varepsilon| + (1.24*10^{14})|\varepsilon^7|}{(9.35*10^{-5}) + (8.42*10^{-5})|\varepsilon| + (3.29*10^{12})|\varepsilon^7|} & , \quad -\varepsilon_u \leq \varepsilon \leq 0 \\[4em] (10.7*10^3)\varepsilon & , \quad 0 \leq \varepsilon \leq \varepsilon_t \end{cases}$$

Eq.8.1

$$\sigma(\varepsilon) = \begin{cases} -\dfrac{|\varepsilon| + (1.35*10^{14})|\varepsilon^7|}{(7.32*10^{-5}) + (6.28*10^{-4})|\varepsilon| + (2.94*10^{12})|\varepsilon^7|} & , \quad -\varepsilon_u \leq \varepsilon \leq 0 \\[4em] (13.7*10^3)\varepsilon & , \quad 0 \leq \varepsilon \leq \varepsilon_t \end{cases}$$

Eq.8.2

The proposed mathematical equation for the stress-strain relationship of LVL was used for the FE modelling of LVL beams in this study and the FE results showed good correlation with experimental results.

The load-deflection graphs of the 4-point bending tests on LVL beams showed a linear behavior. When the depth of section was small (i.e. 35mm and 45mm deep), slight non-linear behaviour was observed at the ultimate stage of the load-bearing behaviour of LVL which is caused by the ductile behaviour of the compressive fibres of the section at ultimate stage, but the actual failure was a brittle one (Figure 4.20, 4.23 and 4.24). The comparison between the closed-form prediction analysis and the experimental results indicates that when the extreme fibres of the LVL sections reach the maximum tensile stress, the load bearing capacity of the system does not stop, but continues until the maximum bending stress is reached. This is compatible with the fact that the bending stress in the extreme fibres of the section, or the tensile stress at half depth of the bottom flange (or half of the depth of the tensile zone of the section) will trigger the failure (details are presented in section 4.3).

8.3   Experimental Investigation of the Proposed System

The experimental investigation involved subjecting the full-scale 8m and 6m modules to both serviceability and ultimate limit state tests. hySpan Cross-Banded LVL and hySpan Project LVL were made the only structural material of the system. Type 17 normal screws and PURBOND® glue were used at the interfaces in order to provide "infinite stiffness" which is used in practical design to meet serviceability requirements and the role of screws was to help the glue to set properly. If the glue bond fails due to any possible reason such as lack of adequate glue at the interfaces, the rapid loss of stiffness and strength occurs (which was observed in U8-02) and the role of screws becomes important as they are acting as the only load bearing part of the bond. In that case, the partially-composite behaviour of the modules should be considered for the ultimate limit state design requirements (chapter 6).

A perfect bond between the flanges and the webs (which was observed in U8-01 and U8-03) provides a linear load-deflection response up to the failure point where a brittle failure occurs (Figure 8.1and Figure 8.2). Also, the linear response of all strain gauges

confirms the linear behaviour of the system up to the failure point (see Figures in Appendix B).

Moreover, a perfect bond between the flanges and the webs provides a fully composite section. The fully composite behaviour of the system was also investigated and confirmed by assessing the strain responses over the depth of the section under both SLS and ULS loads. As an example, Figure 8.3 shows the location of neutral axis at different load levels (up to the failure load) as a result of strain gauges readings over the depth of the section, and the analytically predicted location of neutral axis with the assumption of a fully composite section, for U8-03. As shown in the Figure (8.3) the experimental and analytical results show a good correlation, which confirmed the fully composite performance of the section.
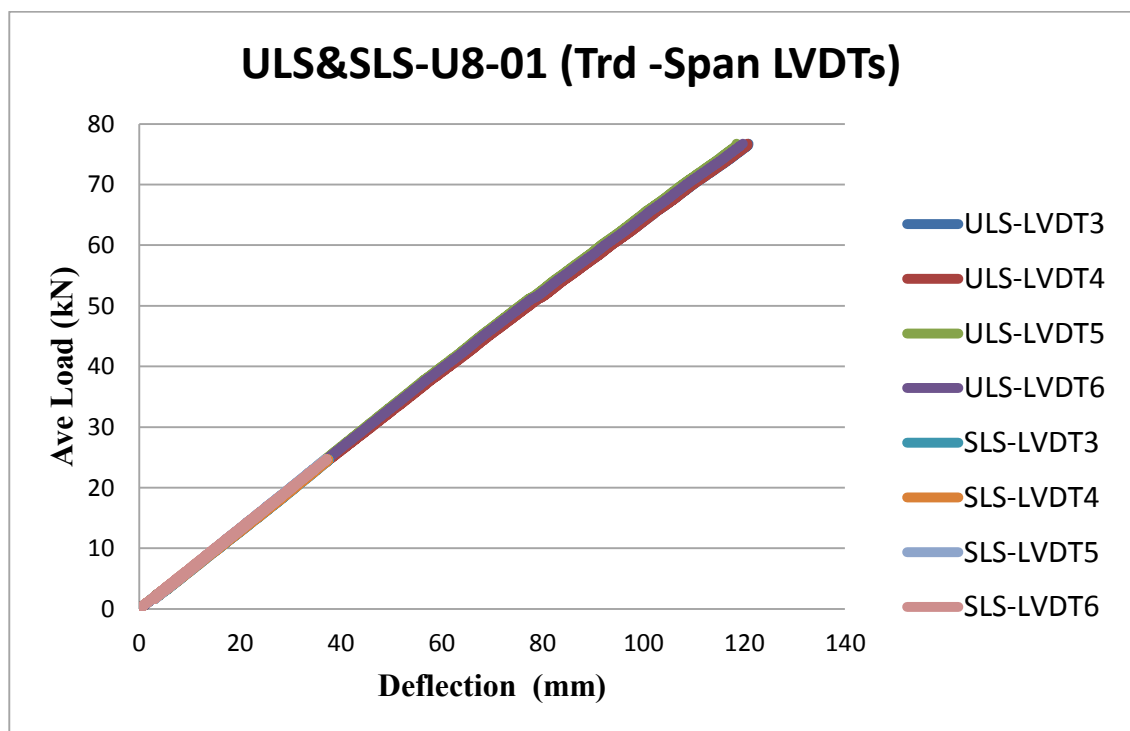
Figure 8.1 Load –deflection graph for U8-01 at third-span
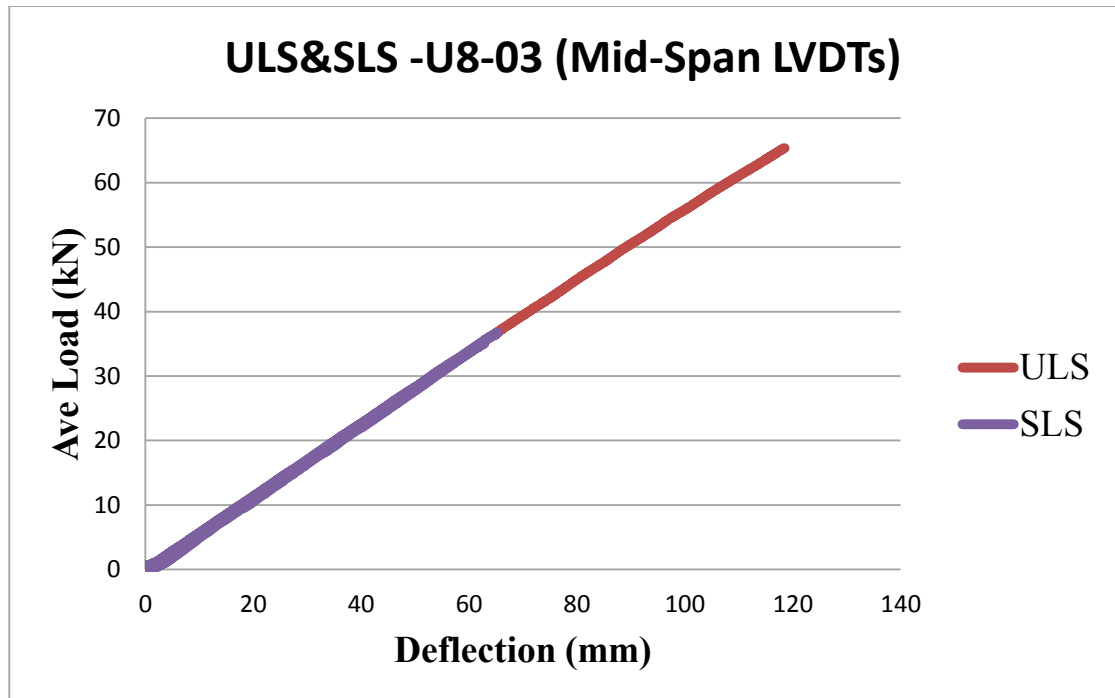
Figure 8.2 Load –deflection graph for U8-03 at third-span
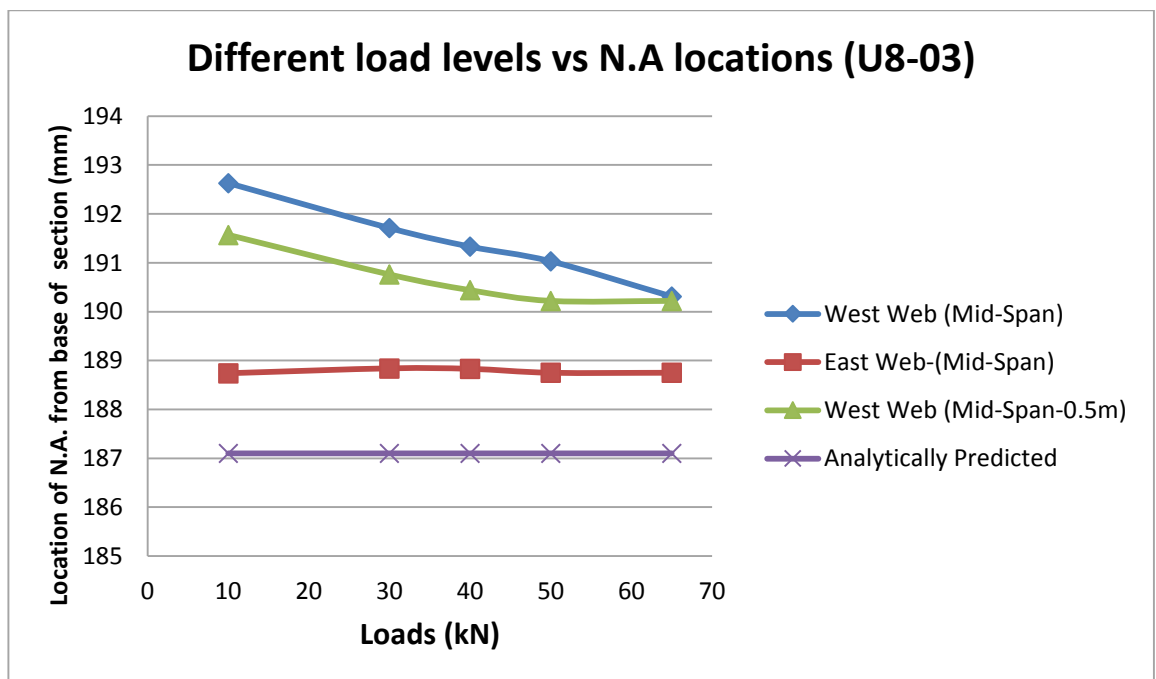
Figure 8.3 Location of N.A for at different load levels for U8-03

The comparison between the analytically predicted results, and experimental results confirm that the analytically calculated flexural stiffness (using the transformed section

method with the assumption of a fully composite section), the ultimate design load (calculated according to BS EN 1995-1-1 2004+A1:2008) and maximum deflection of the system can accurately represent the characteristics of fully composite LVL modules.

If the glue does not provide a perfect bond at the interfaces due to any possible reason such as lack of adequate glue the interfaces or a less rigorous fabrication, then screws used at the interfaces act as the only load bearing part of the bond, and hence, the partially composite behaviour of the modules should be clearly assessed to meet the ULS requirements.

As the first phase experimental tests to assess the partially -composite behavior of the modules, push-out tests were conducted on timber connections fabricated with only normal screws. All connections showed similar bi-linear behaviour under push-out tests, that is, a linear response at the beginning which represents the initial stiffness and then a non-linear behaviour after $0.4F_{max}$. Experimental observation for all the specimens indicates the failure of the screw at the interfaces between the flanges and the web, as well as crushing of the LVL which was caused by bending of the screw in the timber. The ductility of the connection is provided by crushing of LVL around the screw and also, the plastic deformation of screws which can give some softening behaviour. There is a sudden drop in the load at the failure point which caused by the shear failure of the screws.

As a result of the push-out tests, a mathematical expression of the behaviour of the timber connection with normal screws was proposed (Equation 8.3) which can capture the first and second stages of the behaviour of timber connections with normal screws and can be incorporated into nonlinear FE analyses of timber beams with normal screws.

$$P = \frac{(5.4345)v}{[1 + (1.127v)]} + 0.2125v \qquad\qquad \text{Eq.8.3}$$

Where P and v represent the shear force and the slip, respectively. Moreover, three "T" shaped beams with 100mm, 200mm, and 400mm screw spacing were fabricated and tested under four-point bending loads. It was observed that exceeding the bending and

tensile stress in the web (hySpan PROJECT LVL) triggered the failure of the LVL beams. The final failure of the beams was brittle with a sudden drop in the load bearing behaviour of the system. The screws did not exceed their ultimate shear strength as they were not significantly bent and there was no failure observed in the screws. It was also observed that the behaviour of LVL beams can be represented by a bi-linear model in which the stiffness of beams drops from serviceability stiffness to ultimate stiffness at the yield point. The load and deflection of the beams at yield point, and the ultimate load and deflection can be analytically predicted according to EN 1995-1-1 (2004+A1:2008) and showed compatinility with experimental results (see chapter 6).

Further, it was analytically calculated that the flexural stiffness of the modules with 50mm screw spacing can provide the required stiffness and strength to meet the SLS and ULS design requirement, for the 8m LVL modules. Therefore, 50mm screw spacing is required so that the load bearing behaviour of the LVL modules is still in excess of the design ultimate required to be resisted according Australian design standards, even when there is no glue used at the interfaces. All the serviceability and ultimate design checks ensured a safe design of the 8m LVL modules with only normal screws at 50mmmm screw spacing (see chapter 6). The same approach was taken for 6m modules.

8.4   Finite Element Results

Since the behaviour of LVL beams is dominated by bending in longitudinal direction, a uniaxial material model was implemented in FE model, while the state of stress under any given load was precisely defined by a suitable proposed constitutive law (Equations 8.1 and 8.2). For this purpose, the available material model UNIAXIAL in the FE program ANSYS (2013) was used which permits different (defined) stress-strain behaviours as well as different strength values in tension and compression. The tension and compression side of the stress-strain curve can be easily defined under UNIAXIAL TENSION and UNIAXIAL COMPRESSION, respectively, with as many data as required. A comparison of the results of the FE model and experimental tests showed adequate compatibility in determining the stiffness of LVL beams and the ultimate load and deflection. This confirms the robustness of the developed FE model for capturing

the behaviour and failure load of LVL beams. As an example, Table 8.1 presents a comparison between the experimental, analytically predicted and FE results of the failure load of LVL beams. The mesh sensitivity analysis showed that a mesh size around 1/10 of the depth of section is an appropriate size for LVL and gives adequately accurate results (see chapter 7). Only the performance of fully composite modules was predicted by the FE modelling. Partially composite behaviour of LVL was predicted by analytical method (chapter 6). The results of the full scale experimental tests (including the composite and partially composite investigations) together with the conducted numerical investigation provide a model for predicting the performance of any timber beams with similar structural features to the LVL modules (i.e. composite beams with no hole or notch alongside the beam, and when the behaviour of the beams are dominated by bending in the longitudinal direction) while the structural shape, dimensions, and spans can be varied according to the special requirements such as dynamic performance or fire resistance requirements.

Table 8.1 Comparison between the experimental, analytically predicted and FE results of the ultimate load of LVL beams

	Ultimate load (kN)				
	FE Results	Difference with experimental results	Analytically predicted	Difference with experimental results	Experimental results
U8-01	131.4	13.5%	120	21%	152
U8-03	131.4	1%	120	7.7%	130
Cross-Banded LVL 35mm*90mm, flat-wise tests	8.8	4.3%	9.2	0%	9.2
hySpan Project LVL 35mm*90mm, flat-wise tests	12.4	2.4%	12.7	0%	12.7
hySpan Project LVL 45mm*90mm, edge-wise tests	14.2	3.4%	14.7	0%	14.7

8.5   Future Work and Recommendation

The finite element modelling of LVL modules in this study was according to a uniaxial material model, and this is due to the fact that the behaviour of LVL modules is

dominated by bending in longitudinal direction. However, future work on the numerical analysis of the floor system can consider the two-way action of the system. This can be supplied by an experimental study on the floor system by connecting three or four of the 8m modules side by side with a pin support alongside the modules, and the stiffness of the floor and the failure load of the system can be investigated considering the effect of longitudinal and horizontal direction. Further experimental and analytical investigation can be conducted on different options for connecting the modules, to study their performance and to incorporate them in the FE modelling of the system when considering the two-way action of the system. The specimen's responses to long-term loading, in-plane loading, dynamic excitation, cyclic loading were outside the scope of this PhD research and can be further investigated.

REFERENCES

ANSYS 2013® "ANSYS Inc 2013", ANSYS release 14.

ABAQUS 2011, Ver. 6.11. Documentation edn, © Dassault Systèmes.

Aicher, S., Klock, W., Dill-Langer, G., and Radovic, B. (2003), "Nails and nailplates as shear connectors for timber-concrete composite constructions", Otto Graf Journal, Vol. 14, pp.189-209.

Amadio, C., Ceccotti, A., Di Marco, R., and Fragiacomo, M. (2000), "Numerical evaluation of long-term behaviour of timber-concrete composite beams", 6th World Conference on Timber Engineering , Whistler Resort, British Columbia, Canada.

Amana, E. J. (1967), "Application of the Orthotropic Plate Theory to Stiffened Plywood Plates", Ph.D. Thesis, Imperial College, London, UK.

Amana, E.J., and Booth, L.G. (1967), "Theoretical and Experimental Studies on Nailed and Glued Plywood Stressed Skin Components: Part 1", Theoretical study. Journal of Institute of Wood Science, Vol.4, No.1, pp. 43-69.

APA– The Engineered Wood Association. (1982), "Design and fabrication of plywood lumber beams". American Plywood Association, Tacoma, WA. 22 pp.

APA – The Engineered Wood Association. (1990), "Design and Fabrication of Plywood Stressed-Skin Panels", Technical Data Sheet, APA – The Engineered Wood Association, Tacoma (WA), USA.

APA (2013), "Cross Laminated Timber",
 from <http://www.apawood.org/level_b.cfm?content=prd_clt_main> .

AS 1649 (2001), "Australian Standard ^{TM} , Timber - Methods of tests for mechanical fasteners and connectors - Basic working loads and charactresitc strenhths".

AS 1720.1 (2010) ,"Australian Standard®, AS 1720.1—2010, Timber structures, Part 1: Design methods".

AS/NZS 4357.1 (2005), "Australian/New Zealand Standard [TM], structural Laminated Veneed Lumber (LVL) Part1: Method of test for measurement of dimensions and shape".

AS/NZS 4357.3 (2006), "Australian/New Zealand Standard [TM], structural Laminated Veneed Lumber (LVL) Part3: Determination of structural properties - Evaluation methods".

AS/NZS 4063.1 (2010), "Australian/New Zealand Standard [TM], Characterization of Structural Timber, part 1: Test Method".

AS/NZS 1080.1 (2012), "Australian/New Zealand Standard [TM], Timber-Method of test-Moisture content".

AS/NZS 1170.0 (2002), "Australian /New Zealand Standard [TM], Structural Design Action,Part 0: General principles".

AS/NZS 1170.1 (2002), "Australian /New Zealand Standard [TM], Structural Design Action,Part 1: Permanent, imposed and other actions".

AS/NZS 2269 (1994), "Australian/New Zealand Standard [TM], Plywood- Structural".
ATSM (1986) "Standard specification for evaluating performance of prefabricated wood I-joists", Draft (7/88), American Society for Testing and Materials, Philadelphia, PA 60pp.

Bach, L., Cheng, R.J.J. (1996), "Development of a Stressed Skin Panel System Using Corrugated Waferboard", International Wood Engineering Conference Proceedings, Vol. 4, pp. 175-181.

Baird, J.A., and Ozelton, E.C. (1984), "Timber Designers Manual", Granada, London, 518p.

Bayne, K., and Taylor, S. (2006), "Attitudes to the use of Woods as a Structural Material in Non-residential Building Applications: Opportunities for Growth", Project No.PN05.1020 Forest & Wood products Australia.

Bazan, I. M. M. (1980), "Ultimate bending strength of timber beams", PhD. in Civil Engineering, Halifax, Nova Scotia Technical College, Canada.

Boughton, G., and Crews, K. (1998), "Timber design handbook , in accordiance with the Australian Limit State Timber Design Code AS 1720.1-1997", Standard No. Hb108-1998.

Bou Saïd, E., Jullien, J.F. and Ceccotti, A. (2004), "Long term modelling of timber-concrete composite structures in variable climates", 8th World Conference on Timber Engoneering, Lahti, Finland.

BS EN 26891:1991, ISO 6891:1983 (1991),"Timber structures - Joints made with mechanical fasteners - General principles for the determination of strength and deformation characteristics".

Beer, F. P. and Johnston, E. R.(1992), "Mechanics of Materials", 2nd edn, The McGraw-Hill Companies Inc., New York (NY), USA.

Buchanan A.H. (2000), "Fire performance of timber construction Progress", Structural Engineering and Materials, Vol. 2, pp. 278-289.

Buchanan, A.H. (2001),"Structural design for fire safety", John Wiley and Sons, New York, NY, USA.

Buchanan, A.H. (2007),"Timber Design Guide", New Zealand Timber Industry Federation Inc, Third edition 2007.

Brunner, M., Romer, M., and Schnüriger, M. (2007), "Timber-concrete- composite with an adhesive connector (wet on wet process)", Materials and Structures, Vol. 40, No. 1, pp. 119–126.

CaterHoltHarvey (2010),"Wood product Australia",
 from <http://www.chhwoodproducts.com.au/> .

Ceccotti, A. (2002), "Composite concrete-timber structures", Progress in Structural Engineering and Materials, Vol. 4, No. 3, pp. 264–275.

Ceccotti, A., Follesa, M., Lauriola, M.P., and Sandhaas, C. (2006), "Which seismic behaviour factor for multi-storey buildings made of cross-laminated wooden panels?", Proceedings, CIB Working Commission W18-Timber Structures, Florence (Italy), Paper No. CIB-W18/39-15-4, 8 pp.

Ceccotti, A., Fragiacomo, M., and Giordano, S. (2006), "Long-term and collapse tests on a timber-concrete composite beam with glued-in con- nection", Materials and Structures, Vol. 40, No. 1, pp. 15–25.

Corder, E. S. and Jordan, D. E. (1975), "Some Performance Characteristics Of Wood Joist Floor Panels", Forest Products Journal, vol. 25, no. 2.

Carpinteri, A. (1997), "Structural Mechanics: A General Approach", 1st edn, E & EF Spon,an Imprint of Chapman & Hall, London, UK.

Chan, S.L., and Chui, P.P.T. (2000), "Non-linear static and cyclic analysis of steel frames with semi rigid connection", First ed2000, Killington, Oxford: Elsevier.336.

Chung, H., Dodd, G., Emms,G., McGunnigle, K., and Schmid, G. (2005), "Maximising Impact Sound Resistance of Timber Framed Floor/Ceiling System", Peport PN04.2005 Forest and wood Products Research and Development Corporation, Australia.

Conners, T.E., and Appleton,W.I. (1989), "Segmented models for stress-strain diagrams", Wood science and Technology, Vol. 23, pp. 65-73.

Crews, K., Brown, B., and Gerber, C. (2005), "Investigation Of Composite Action Behaviour In A Light Weight Autoclave Areated Concrete-Timber Composite Floor System", University of Technology Sydney, UTS Report No: C05-43-006 for CSR and Hyne & Son Timber.

Crews, K., Gerber, C., Choi, F., Buchanan, A., and Fragiacomo, M. (2007), "Innovative Engineered Timber Building Systems for Non Residential Applications", Milestone 2, Report Version 1-3, University of Technology Sydney.

Desler, H. F. (2002), "Wood Structural Panels in Structural Components", in T.G.Williamson (ed.), APA Engineered Wood Handbook, The McGraw-Hill Companies Inc., New York (NY), USA.

Deam, B., Fragiacomo, M., and Buchanan, A. (2007), "Connections for composite concrete slab and LVL flooring systems", Materials and Structure, Vol. 41, No. 3, pp. 495–507.

Dias, A. M. P. G., Van De Kuilen, J. W., Lopez, S., amd Cruz, H. (2007), "A non-linear 3D FEM model to simulate timber-concrete joints". Advances in Engineering Software, Vol. 38, No. 8-9, pp. 522-530.

DIN 1052:2008-12 (2008), "Design of Timber Structures-General Rules and Rules for Buildings", December 2008.

DIN 1055-100:2003-03 (2003), "Action on Structures - Part 100 : Basis of Design, Saftey Concept and Design Rules", May 2003.

Dolan, J. D., Murray, T. M., Johnson, J. R., Runte, D., and Shue, B. C. (1999), "Preventing Annoying Wood Floor Vibrations", Journal of Structural Engineering , Vol. 125, No. 1, pp. 19-24.

Eberhardsteiner, J., and Gingerl, M., et al. (1999), "Experimental investigation of the strength of solid wood under biaxial loading oblique to the grain direction", COST Action E8 Workshop Damage in Wood, Bordeaux, France.

EC5 (2004), BS EN 1995-1-1:2004+A1 2008, "Eurocode 5: Design of Timber Structures-Part 1-1 General Common Rules for Buildings".

EN 1995-1-2 (2004), "Design of timber structures, Part 1-2: General – Structural fire design", CEN, 2004.

EN 13501-2 (2003), "Fire classification of construction products and building elements - Part 2: Classification using data from fire resistance tests, excluding ventilation services", CEN, 2003.

EN 1995-1-1 (2004+A1:2008), "Eurocode 5: Design of the Timber Structure, Part 1-1: General- Common rules and rules for buildings" , section 9: components and assemblies.

Erchinger, C., Frangi, A., and Fontana, M. (2010), "Fire design of steel to-timber dowelled connections", Engineering Structures, Vol.32, pp. 580-589.

EWPA (2008), "Plywood Box Beam Span Tables for Detached Housing Construction", Project number: PN08.1065.

Foschi, R. O. (1982), "Structural Analysis of Wood Floor Systems", Journal of the Structural Division, vol. 108, no. ST7, pp. 1557–1574.

Foschi, R. O. (1969a), "Buckling of the Compressed Skin of a Plywood Stressed-Skin Panel with Longitudinal Stiffeners", Research Report, Department of Fisheries and Forestry, Ottawa (ON), Canada.

Foschi, R. O. (1969b), "Stress Distribution in Plywood Stressed-Skin Panels with Longitudinal Stiffeners", Research Report, Department of Fisheries and Forestry,Canadian

Finnforest Kerto. (2010a), "Stronger Support for Wooden Structures", from <http://www.finnforest.com/products/kerto/Documents/Kerto_eng.pdf>.

Finnforest (2010b), "I Finnforest floor systems (Fully engineered for better performance)", from <http://www.finnforest.co.uk/> .

Finnforest .(2010c), "Kerto-Ripa, Ribs and Box culverts", from <http://www.ffebrochure.eu/UK/finnforest/KertoRipa/>.

Finnforest. (2010d), "Leno®-Brettsperrholz ", from <http://www.finnforest.de/ >.

Fleischmann, M. (2005), "Numerische Berechnung von Holzkonstruktionen unter Verwendung eines realitätsnahen orthotropen elasto-plastischen Werkstoffmodells", Doctoral Thesis, Vienna University of Technology, Austria.

Fortino, S., and Toratti, T. (2010), "A three-dimensional moisture-stress FEM analysis for timber structures", 11th World Conference on Timber Engineering 2010, Riva del Garda, Trentino, Italy.

Fragiacomo, .M. (2005), "A finite element model for long-term analysis of timber-concrete composite beams", Structural Engineering and Mechanics , Vol. 20, No. 2, pp. 173-190.

Fragiacomo, M. (2006), "Long-term behaviour of timber-concrete composite beams. II: Numerical analysis and simplified evaluation", Journal of Structural Engineering, Vol. 132, No. 1, pp. 23–33.

Fragiacomo, M., and Ceccotti , A. (2006), "Long-Term Behavior of Timber-Concrete Composite Beams. I: Finite Element Modeling and Validation", ASCE, Journal of structural engineering, Vol. 132, No. 1, pp. 13-22.

Frangi, A., and Fontana, M. (2003), "Elasto-plastic model for timber–concrete composite beams with ductile connection", Structural Engineering International, Vol. 13, No. 1, pp. 47–57.

Frangi A., Erchinger C., and Fontana M. (2008), "Charring model for timber frame floor assemblies with void cavities", Fire Safety Journal, Vol. 43, pp. 551-564.

Frangi F., Fontana M., Hugi E., and Wiederkehr, R. (2010), "Fire Safety of Multi Storey Timber Buildings", 11th World Conference on Timber Engineering, Riva, Italy.

Frangi A., Erchinger C., and Fontana M. (2010), "Experimental analysis on the fire behaviour of steel-to-timber connections with slotted-in steel plates and nail connections", Fire and Materials, Vol.34, pp. 1-19.

Franke, B., and Franke, S., and Quennville, P. (2012) "Numerical Modelling and Analysis of the Failure Behaviour of Dowel-Type Connections in Wood", European Congress Computational Methods in Applied Sciences Enginering (ECCOMAS 2012). Eberhardstenier.J. Vienna, Austria.

General Tecchnical Report FPL-GTR-113 (1999), "wood handbook-wood as an engineer material", Forest Products laboratory, United States Department of Agriculture, Madison MI US.

Goodman, J. R., Vanderbilt, M. D., Criswell, M. E. and Bodig, J. (1974), "Composite and Two-Way Action in Wood Joist Floor Systems", Wood Science, vol. 7, no. 1, pp.25–33.

Gere, J. M. (2004), "Mechanics of Materials", 6th edn, Brooks/Cole, a Division of Thomson Learning Inc, Belmont (MA), USA.

Gere, J. M. & Timoshenko, S. P. (1999), "Mechanics of Materials", 5th edn, Stanley Thornes (Publisher) Ltd, Cheltenham, UK.

Ghali, A. and Neville, A. M. (1989), "Structural Analysis – A Unified Approach", 3rd edn, E& FN Spon, an imprint of Chapman & Hall, London, UK.

Girkmann, K. (1954), "Flächentragwerke, Einführung in die Elastostatik der Scheiben", Platten, Schalen und Faltwerke, Springer Wien New York, Wien, Austria.

Gerber, C. (2006), "Wood Stressed-Skin Panels: An Investigation Into Their Behaviour, Load Distribution and Composite Properties", Faculty of Engineering, University of Technology Sydney PhD.

Gere, J. M., and Timoshenko, S. P. (1999), "Mechanics of Materials", 5th edn, Stanley Thornes (Publisher) Ltd, Cheltenham, UK.

Germer, J. (1986), "Designer joists", Progress Building, Vol. 11, No. 9, pp. 21-23.

Glos,P. (1981),"Zur Modellierung des Festigkeitsverhaltens von Bauholz bei Druck-, Zug- und Biegebeanspruchung", Laboratorium für den konstruktiven Ingenieurbau (LKI), TU München, 1981 – Forschungsbericht.

Grant, G. (2010), "Evaluation of Timber Floor Systems for Fire resistance and other performance", Depatment of Civil Engineering Christchurch, New Zealand, University of Canterbury. Master of Engineering in Fire Engineering.

Grantham, R., Enjily, V., Fragiacomo, M., Nogarol, C., Zidaric, I., and Amadio, C. (2004), "Potential upgrade of timber frame buildings in the UK using timber-concrete composites", Proceeding of 8th World Conference on Timber Engineering ,Vol. 2, Lathi, Finland, pp 59–64.

Grosse, M. (2005), "Zur numerischen Simulation des physikalischen nichtlinearen Kurzzeittragverhalten von Nadelholz am Beispiel von Holz-Beton-Verbundkonstrukionen", Doctoral thesis, Bauhaus-University Weimar, Germany.

Gutkowski, R., Brown, K., Shigidi, A., and Natterer, J. (2008), "Laboratory tests of composite wood-concrete beams", Construction Building and Materials, Vol. 22, No.6, PP. 1059–1066.

Guan, Z. W., and E. C., Zhu. (2009), "Finite element modelling of anisotropic elasto-plastic timber composite beams with openings", Engineering Structures, Vol. 31, No. 2, : pp. 394-403.

Gitterbjelker (2013), "Gitterbjelker Letteetasjeskillere Av Gitterbjelker" from: <http://bredesenopset.no/takstoler/content_1/filelist_8c69b11b-ff69-4ca0-850b-71e8b095d09f/1358413821609/gitterbrosjyre.pdf>

Hashin, Z. (1980), "Failure Criteria for Unidirectional Fiber Composites", Journal of Applied Mechanics, vol. 47, no. 2, pp. 329-34.

Hashin, Z. and Rotem, A. (1973), "A Fatigue Failure Criterion for Fiber Reinforced Materials', Journal of Composite Materials", vol. 7, no. 4, pp. 448-64.

Hanes, R.M. (1970),"Human Sensitivity to Whole-Body Vibration in Urban Transportation Systems: A Literature Review", Applied Physics Laboratory, the John Hopkins University, Silver Springs, MD.

Hamm, P., Richter, A., and Winter, S. (2010), "Floor Vibrations – New Results", World Conference on Timber Enginering , Italy.

Heyer, O.C., and Blomquist, R.F. (1964), "Stressed Skin Panel Performance After Twenty-Five Years of Service", USDA Forest Service, Research Paper, FPL-18, Madison, Wisconsin.

Henry, D.K. (1971), "A Procedural Analysis for Examining Structural Efficiency and Comparing Relative material Costs of Stressed Skin Panel", M Sc. Thesis, The Pennsylvania State University, Pittsburgh, Pennsylvania.

Hoyle, R. J. (1973a), "Wood technology in the design of structures", 4th edition, Mountain Press Publishing Co., Missoula, MT. 390 pp.

Hoyle, R. J. (1986), "Design of composite beams". Pages 227-289 in A.D. Freas, R. C. Moody, and L. A. Soltis, eds. Wood: Engineering design concepts, Pennsylvania State University, University Park, PA.

Hoyle, R.J. and Woeste, F.E. (1989), "Wood Technology in the Design of Structures (5th Ed.)", Iowa State University Press, Ames, Iowa, 370p.

Hu, L. J., Chui, Y.H., and Onsyko, D. (2001), "Vibration serviceability of timber floors in residential construction", Progress in Structural Engneering and Materials, Vol. 3, pp. 228-237.

Hu, L. J., Desjardins, R., Chui, Y. H. (2006), "Nature of Vibrations Induced by Footsteps in Lightweight and Heavyweight Floors", 9th World Conference on Timber Engineering USA.

HySPAN ®CaterHoltHarvey (2010), "Engineered wood Products hySPAN® , span guide for residebtioal framing", from <http://www.chhwoodproducts.com.au/ >.

HyJoist ® (2013), "HyJoist ® CaterHoltHarvey",
 From: < http://www.chhwoodproducts.com.au/hyjoist/>.

Harper Timber (2013), Plywood "Strength, Durability & Workability", from <http://harpertimber.com.au/timber-and-building-products/plywood.php>

Jorissen, A .(2006), "The design of timber floors", Eindhoven (TU/e) and SHR Timber Research, Wageningen, The Netherlands, 9th World Conference on Timber Engineering ,USA.

Jöbstl, R. A., Moosbrugger, T., Bogensperger, T., and Schickhofer, G.A .(2006), "Contribution to the design and system effect of cross laminated timber", Proceedings, CIB Working Commission W18-Timber Structures, Florence (Italy), Paper CIB-W18/39-12-5, 17 pp.

Kuenzi, E. W. (1955), "Theoretical Design of a Nailed or Bolted Joint Under Lateral Load", Research Report, Report No. D1951, U.S. Department of Agriculture,Forest Service Research, Forest Products Laboratory, Madison (WI), USA.

Koop, L. (2005), "Design of an Industrial, Flexible, Dismountable and Integrated timber floor system for residential and office buildings", Graduate report (in Dutch), University of Technology Eindhoven, The Netherlands.

KAUFMANN (2010), "Mayr-Melnhof Kaufmann- Europe's Leading Partner for Timber Solutions". from <http://www.mm-holz.com/158>.

Källsner, B., and König, J. (2000), "Thermal and mechanical properties of timber and some other materials used in light timber frame construction", In Proceedings of CIB W18, 33th Meeting, Delft.

Keil, B. (1977) , "Plywood lumber are joined for wood, energy savings at Wood I". Plywood Panel Mag. 18(2):pp14-15.

Kliger, I.R., and Pellicane, P.J. (1996), "Shear Properties of Components Used in Stressed Skin Panels. Journal of Materials in Civil Engineering", Vol.8, No. 2, pp. 77-82.

Kliger, I.R. (1996), "Flexural Behavior of Roof Units for Industrial Buildings", Proceedings of International Wood Engineering Conference, Vol. 4, pp. 161-68.

Kliger, I.R., and Pellicane, P.J. (1997),"Stiffness Evaluation of Stressed Skin Panels of Mixed Construction". Journal of Structural Engineering", Vol. 133, No. 8, pp. 1046-1053.

Kliger, I. R. and Pellicane, P. J. (1998), "Stiffness Modelling of Stressed-Skin Panels of Mixed Wood Construction", in Proceedings of 'The 5th World Conference onTimber Engineering', Lausanne, Switzerland, pp. 84–89.

Kolb, J. (2008), "Systems in Timber Engineering Loadbearing Structures and Component Layers". Uttwil, Switzerland.

Koehl, S. (1976), "Plywood joists make Canadian debut", British Colombia Lumberman Vol. 61(6), pp. 53.

König, J., and Walleij, L. (2001), "Timber frame assemblies exposed to standard and parametric fires, Part 2: A design model for standard fire exposure", SP Trätek, Report I 0001001, Stockholm.

Khorsandnia, N. (2013), "Finite Element Analysis For Predicting the Short-Term and Long-Term Behaviour of Timber-Concrete Cpmposite Structures", Thesis submitted for fulfilment of requirements for the degree of Doctor of Philosophy to FEIT University of Technology Sydney

Khorsandnia, N. and Crews, K. (2014), "Application of Quasi-brittle Material Model for Analysis of Timber Members", Submitted to Australian Journal of Structural Engineering

Kuhlmann, U., and Schänzlin, J. (2001), "Grooves as shear connectors for timber-concrete composite decks". Proceeding of RILEM Conference on Joints in Timber Structures, RILEM, Bagneux, France, pp 283–290.

Kuhlmann, U., and Aldi, P. (2008), "Fatigue of timber-concrete-composite beams: Characterization of the connection behaviour through push-out tests", Proceeding of 10th World Conference on Timber Engineering, Miyazaki, Japan.

KURT, R. (2005), "An Alternative Building Component, Stressed Skin Panel (SSP)". KSU Journal of Science and Engineering, Vol. 8, No.1, pp. 60-64.

Liu, W.F and Bulleit, W. M. (1995), "Overload Behavior of Sheathed Lumber Systems",Journal of Structural Engineering, vol. 121, no. 7, pp. 1110–1118.

Lewis, W. C., Dawley, E. R. (1943), "Design of plywood webs in box beams: Stiffeners in box beams and details of design". USDA Forest Sev. No. 1318-A. Forest Prod. Lab., Madison, WI. 12 pp., reaffirm. 1958.

Lignatur. (2010), "Lignatur Workbook". The Swiss Original. Science 1984, from <http://www.lignatur.ch/planung_workbook.html>.

Lumberworx ® (2013), "Lumberworx I beams"
 from <http://www.branz.co.nz/Appraisal/545

Leichti, R. J., Falk, R.H., and Laufenberg, T.L. (1990), "Prefabricated Wood Composite I Beams: A literature Review". Wood and Fiber Science 2(1): pp 62-79.

Lukaszewska, E., Johnsson, H., and Fragiacomo, M. (2008), "Performance of connections for prefabricated timber-concrete composite floor", Materials and Structures , Vol. 41, No. 9, pp. 1533–1550.

Lukaszewska, E., Fragiacomo, M., and Johnsson, H. (2010), "Laboratory tests and numerical analyses of prefabricated timber-concrete composite floors", Journal of Structural Engineering , Vol. 136, No. 1, pp. 46–55.

Mackenzie-Helnwein, P., Müllner, H. W., Eberhardsteiner, J. and Mang, H. A. (2005), "Analysis of layered wooden shells using an orthotropic elasto-plastic model for multi-

axial loading of clear spruce wood", Computer Methods in Applied Mechanics and Engineering 194 (21-24 SPEC. ISS): pp. 2661-2685.

Massiveholz KLH .(2010), from <http://www.klh.at/produkt-brettsperrholz-klh.html?L=3>.

Mackenzie-Helnwein, P., Müllner, H. W., Eberhardsteiner, J. and Mang, H. A. (2005), "Analysis of layered wooden shells using an orthotropic elasto-plastic model for multi-axial loading of clear spruce wood". Computer Methods in Applied Mechanics and Engineering 194 (21-24 SPEC. ISS): pp 2661-2685.

McCullough, B. (1943), "Oregon tests on composite (timber-concrete) beams", Journal of American Concrete Institute, Vol. 14, No. 5, pp. 429–440.

Mcdowall, M. (2007), "Structural Plywood & LVL Design Manual", Engineering Wood Product Acociation of Australia.

McKeever, D., and Adair C. (1995), "Wood products used in new non-residential building constructions", Wood Product Promotion Council.

McNatt, J. D. (1980), "Hardboard-webbed beams: Research and application". Forest Products Journal, Vol. 30, No. 10, pp. 57-64.

Meierhofer, U. (1993), "A timber/concrete composite system", Structural Engineering International, Vol. 3, No. 2, pp. 104–107.

Mestek, P., Kreuzinger, H., and Winter, S. (2008), "Design of Cross Laminated Timber CLT", World Conference on Timber Engineering 2008, Japan, pp. 156-163.

Merz, K., (1996), "Large Size Composite Wood Panels Utilized for Load Bearing Modules in Timber Structures", Proceedings of International Wood Engineering Conference, Vol. 4, PP. 169.

MHM. (2010), "MHM Massive-Holz-Mauer", from <http://www.massivholzmauer.de/>

Miotto, J., and Dias, A. (2008), "Glulam-concrete composite structures: Experimental investigations into the connection system", Proceeding of 10th World Conference on Timber Engineering, Miyazaki, Japan.

Moelven. (2010), "Moelven MassiveTre elements",
 from <http://www.moelvenmassivtre.no/>.

Mohr, B. (1999), "Floor Vibrations", Proceedings of the 32th CIB - W18 conference, Graz, Austria, August 1999, pages CIB-W-18/32-20-1 - 11.

Moses, D. M., and Prion, H. G. L. (2004), "Stress and Failure Analysis of Wood Composites: a new model ". Composites Part B 35, pp. 251-261.

Moss P.J., Buchanan A.H., Fragiacomo M., and Lau P.H, Chuo T. (2009), "Fire performance of bolted connections in laminated veneer lumber", Fire and Materials, Vol. 33, pp. 223-243.

Möhler, K. (1956), "On the load carrying behavior of beams and columns of compound sections with flexible connections", Habilitation, Technical University of Karlsruhe, Germany (in German).

Mungwa, M., and Kenmou, D. (1993), "Instantaneous and time-dependant analysis of composite wood-concrete cross-sections using Dischinger's equations of state: Part 1-Instantaneous analysis", Materials and Structures, Vol. 26, No. 2, pp. 98-102.

Murray, T.M., Allen, D.E., and Ungar, E. (2003) "Floor vibrations due to human activity", Steel design guide series 11, American Institute of Steel Construction. Chicago, Illinois. Oct. 2003.

McLain, T. E. (1999), "Structural Wood Panels", in K.F. Faherty & T.G. Williamson (eds),Wood Engineering and Construction Handbook, 3rd edn, The McGraw-Hill Companies Inc., New York (NY), USA.

McCutcheon, W. J. (1986), "Stiffness of Framing Members with Partial Composite Action", Journal of Structural Engineering, vol. 112, no. 7, pp. 1623–1637.

Möhler, K., Abdel-Sayed, G. and Ehlbeck, J. (1963), "Zur Berechnung Doppelschaliger,Geleimter Tafelelemente", Holz als Roh- und Werkstoff, vol. 21, no. 8, pp. 328–333.

Mansour, A. E. (1976), "Charts for Buckling and Postbuckling Analysis of Stiffened Plates under Combined Loading", SNAME T & R Bulletin, vol. 2–22, no. July.

Moody, R. C. and McCutcheon, W. J. (1984), "Sheathing Properties and Component Performance on Light-Frame Structures", in Proceedings of Structural Wood Composite: Meeting Today's Needs and Tomorrow's Challenges, Forest Products Research Society (Publisher), Minneapolis (MN), USA, pp. 93–99.

Nagaraj, M. (2005), "Experimental and Computational Investigation of FRP Reinforrced Glulam columns Associated Software Development", Dalhousie University, Master of Applied Science.

Nahas, N. N. (1986), "Survey of failure and post-failure theories of laminated fibrereinforced composites", Journal of Composite Technoly and Resreach, Vol. 8, No. 4, pp. 38–53.

Natterer, J., Hamm, J., and Favre, P. (1996), "Composite wood-concrete floors for multi-story buildings", Proceeding of the International Wood Engineering Conference, New Orleans, Vol. 3, pp. 431–435.

Nelson, S.A. (1975), "Wood Structures: a design guide and commentary", Prefabricated wood joist, section 8.6.2: pp. 213-215, ASCE Struct, New York.

NZS 3603 (1993), "New Zealand Standard®, Timber structures Standard".

Onsysko, D. M. (1988), "Performance and acceptability of wood floors - Forinteckstudies". Nat. Res. Council of Canada Publ.28822, Forintek Canada Corp, Ottawa.

Östman B., and Rydholm, D. (2002), "National fire regulations in relation to the use of wood in European and some other countries", SP Trätek, Report P0212044, Stockholm, 2002.

Ozelton, E. C. and Baird, J. A. (2002), "Timber Designers' Manual", 3rd edn, Blackwell Publishing, London, UK.

Patterson, D. W. (1973), "Nailed Wood Joints Under Lateral Loads", M.S. Thesis, Colorado State University, Fort Collins (CO), USA.

Paevere, P., and Mackenzie, C. (2006), "Emerging Technologies and Timber Products in Construction-Compendium of Products and technologies", Project No.PN05.1020, Foerst and Wood Products Research and Development Corporation.

Parrod, P., Landis, E. N., Davis, W., Vasic, S. (2002), "Morphology-based models for wood and wood composites", 15th ASCE Engineering mechanics conference, New York.

Pillai, U., and Ramakrishnan, P. (1977), "Nail shear connectors in timber- concrete composites", Journal of the Institution of Engineers (India), Civil Engineering Division, Vol. 58(CI1), pp. 34–39.

Pincus, P. (1970), "Behaviour of wood concrete composite beams", Journal of the Structural Division, Vol.96, No.7, pp. 2009–2019.

Porteous, J., and Kermani, A. (2007), "Structural Timber Design to Eurocode 5", First published 2007 by Blackwell Publishing Ltd.

Pryda truss systems (2013), "Guide to Specification Pryda Floor Truss & Rafter Truss Systems" from : <http://www.pryda.com.au>

Potius™ (2010), "Floor & Roof Panels, Building Systems LTD." from <http://www.potius.co.nz/> .

Qudjene, M., and Khelifa, M. (2009), "Elasto-Plastic Constitutive Law for Wood Behaviour Under Compression Loading", Construction and Building Materials, Vol. 23, No.11, pp. 3359-3366.

Raadschelders, J. G. M. and Blass, H. J. (1995), "Stressed Skin Panels" , in H.J. Blass, P.Aune, B.S. Choo, R. Görlacher, D.R. Griffiths, B.O. Hilson, P. Racher & G.Steck (eds), Timber Engineering – STEP 1, Centrum Hout, Almere, The Netherlands.

Richart, F. E., and Williams, C. B. (1943) "Tests of composite timber- concrete beams", Journal American Concrete Institute, Vol. 14, No. 4, pp. 253–276.

Rijal,R. (2013) "Dynamic performance of timber and timber-concrete composite systems", Thesis submitted for fulfilment of requirements for the degree of Doctor of Philosophy to FEIT University of Technology Sydney

Robins, J.G. (1987), "The wooden wonder: a short history of wooden aeroplane", Bartholomew & Sons Ldt., Edinburgh .

Rowlands, R. E. (1985), "Strength (failure) theories and their experimental correlation", Failure mechanics of composites vol. 3. Amsterdam (North-Holland), pp. 71–125.

Smith, G. R. (1966a), "Photoelastic Examination of Longitudinally Framed Stressed-Skin Panels", Technical Report, Report No. TDD/55, Plywood Manufacturers of British Colombia, Vancouver (B.C.), Canada.

Smith, G. R. (1966b), "The Stress Distribution of a Longitudinally Framed Stressed-Skin Panel", Technical Report, Report No. TDD/62, Plywood Manufacturers of British Colombia, Vancouver (B.C.), Canada.

SIA 164. (1992), "SIA 164 :1992 Civil Engineering ,Timber Structures", Swiss Society of Engineers and Architects.

SIA 265. (2003), "SIA 265 :2003 Civil Engineering ,Timber Structures", Swiss Society of Engineers and Architects.

Sun, C.T., Quinn, B.J., Tao, J., Oplinger, D.W. & Hughes, W.J. (1996), "Comparative Evaluation of Failure Analysis Methods for Composite Laminates", Office of Aviation Research, Washington, D.C., USA.

Schänzlin, J. (2003), "Time dependent behavior of composite structures of board stacks and concrete". Ph.D. thesis, Univ. of Stuttgart, Germany (in German).

Schänzlin, J., and Fragiacomo, M. (2007), "Extension of EC5 Annex B formulas for the design of timber-concrete composite structures." Proceeding of 40th Meeting of Working Commission W18—Timber Structures, International Council for Research and Innovation in Building and Construction (CIB), Rotterdam, Netherlands, 10.

Schmidt, J., and Kaliske, M. (2009), "Models for numerical failure analysis of wooden structures", Engineering Structures, Vol. 31, No. 2, pp. 571-579.

Serrano, E., and Gustafsson, P. J. (2007), "Fracture mechanics in timber engineering - Strength analyses of components and joints", Materials and Structures/Materiaux et Constructions, Vol. 40, No. 1, pp. 87-96.

Sigrist , C. and Gerber, C. (2002), "Evaluation of floor systems for multi-storey buildings", 7th Word Conference on Timber Engineering Shah Alam, Malaysia.

Sigrist, C. (2002), "COST E5, Investigation on optimisation on materials and systems in light timber floors".

Smith A. L., Hicks S.J., and Devine P.J. (2007), "SCI Guide P354: Design of Floors for Vibration: A new Approach", SCI Publication 354, The Steel Construction Institute .

Snow, M., Asiz, A., and Smith, I. (2006), "Modelling Fracture in Bolted Engineered Wood Joints", World Conference on Timber Engineering **,** Portland, Oregon, USA, paper 139.

Stalnaker, J.J., and Harris, C.E. (1989), "Structural Design in Wood", Van Nostrand Reinhold, New York, 448p.

Steiger, R., Gülzow, A. and Gsell, D. (2008), "Non destructive evaluation of elastic material properties of crosslaminated timber (CLT)", Conference COST E53, Delft, The Netherlands, pp 171-182.

Stluka, R. T. (1960), "Theoretical of Design of Nailed or Bolted Joint Under Load", M.S.Thesis, University of Wisconsin, Madison (WI), USA.

Steinberg, E., Selle, R., and Faust, T. (2003), "Connectors for timber- lightweight concrete composite structures", Journal of Structural Engineering, Vol. 129, No. 11, pp. 1538–1545.

SmartJoist (2013), "SmartJoist desing Guide", from:
<http://www.tilling.com.au/sites/default/files/SmartJoist%20Design%20Guide%202011_RGB.pdf>

Timoshenko, S. P. & Gere, J. M. (1961), "Theory of Elastic Elasticity", 2nd edn, The McGraw-Hill Companies Inc., New York (NY), USA.

Timoshenko, S. P. and Goodier, J. N. (1987), "Theory of Elasticity", 3_{rd} edn, The McGraw-Hill Companies Inc., New York (NY), USA.

Timoshenko, S. P. & Young, D. H. (1968), "Elements of Strength of Materials", 5th edn, D.Van Nostrand Company Inc., Princeton, USA.

Timoshenko, S. P. and Woinowsky-Krieger, S. (1959), "Theory of Plates and Shells", 2nd edn, McGraw-Hill Kogakusha Ltd., Tokyo, Japan.

Tang, R.C., and Leichti, R.J. (1984), "Manufacturing composite wood I beam by using small diameter trees and its engineering performance", Symposium of utilization of medium and small diameter trees, Taichung, Taiwan.

Tsai, S. W. and Wu, E. M. (1971), "A general theory of strength for anisotropic materials", Journal of Composites, Vol 5, No. 1, pp. 58-80.

Turrini, G., and Piazza, M. (1983a), "A technique for stiffness and strength upgrading of wooden floors", Recuperare, Vol. 5, pp. 224–237 (in Italian).

Turrini, G., and Piazza, M. (1983b), "Static behavior of timber-concrete composite structures", Recuperare, Vol. 6, pp. 214–225 (in Italian).

TECBEAM ® (2010), from <http://www.tecbeam.com.au/>

TECSLAB ® (2013), from <http://www.tecslab.com.au/>

USDA. (1987) ,"Wood handbook: Wood as an engineering material". Agric. Handb. 72. USDA Forest Serv., Forest Prod. Lab., Washington, DC, 466 pp.

Van der Linden, M. (1999), "Timber-concrete composite floor systems", Ph.D thesis, Delft University, Netherlands.

Vanderbilt, M. D., Goodman, J. R. and Criswell, M. E. (1974), "Service and Overload Behavior of Wood Joist Floor Systems", Journal of the Structural Division, vol.100, no. ST1, pp. 11–29.

Vick, C.B., and Wittenberg, D.C. (1971), "Wind Resistance of Stressed Skin Curtain Wall Panels Bonded with Elastomeric Adhesives", USDA Forest Service, Research Paper SE-81. Asheville, North Carolina.

Von Karman, T. (1924), "Die Mittragende Breite', Festschrift, vol. August Foppls,Springer Verlag, Berlin, Germany.

Von Halász, R. and Cziesielski, E. (1966), "Berechnung und Konstruktion Geleimter Traeger mit Stegen aus Furnierplatten", vol. Heft 47, W. Ernst und Sohn, Berlin,Germany.

Wolfe, R. W. (1990), "Performance of Light-Frame Redundant Assemblies", in Proceedings of The 1990 International Timber Engineering Conference, vol. 1, Steering Committee of the International Timber Engineering, Tokyo, Japan, pp.124–131.

Wilkinson, T. L. (1971), "Theoretical Lateral resistance of Nailed Joints", Journal of the Structural Division, vol. 101, no. ST5, pp. 1381–1398.

Wilkinson, T. L. (1972), "Analysis of Nailed Joints with Dissimilar Members', Journal of the Structural Division", vol. 98, no. ST9, pp. 2005–2013.

Wardle, T.M., and Peek, J.D. (1970), "Plywood Stressed Skin Panels: Geometric Properties and Selected Designs", Timber Research and Development Association, High Wycombe.

Weckendorf, J., Zhang, B., Kermani ,A., and Reid, D. (2006), "Assessment of Vibrational Performance of Timber Floors", WCTE 2006 - 9th World Conference on Timber Engineering - Portland, OR; August 06-10, 2006.

Wyatt, T. A. (1989), "SCI design guide: Design Guide on the Vibration of Floors", SCI Publication 076. The Steel Construction Insitute. 1989.

Yasumura, M., and Daudeville, L. (2000), "Fracture of multiply-bolted joints under lateral force perpendicular to wood grain", Journal of Wood Science, Vol. 46, No. 3, pp. 187-192.

Yeoh, D., Fragiacomo, M., Buchanan, A., and Deam, B. (2009a), "Experimental behaviour at ultimate limit state of a semi-prefabricated timber-concrete composite floor system", Proceeding of International Symposium on Timber Structures from Antiquity to the Present, Istanbul, Turkey, June 25-27, pp. 287–298.

Yeoh, D., Fragiacomo, M., Buchanan, A., and Gerber, C. (2009b), "Preliminary research towards a semi-prefabricated LVL-concrete composite floor system for the

Australasian market". Austalian Jouirnal of Structural Engineering , Vol. 9, No. 3, pp. 225–240.

Yeoh, D. (2010) ,"Behaviour and design of timber-concrete composite floor system", Ph.D. thesis, University of Canterbury, New Zealand.

Yeoh, D., Fragiacomo, M., De Franceschi, M., and Buchanan, A. (2011), "Experimental tests of notched and plate connectors for LVL-concrete composite beams", Journal of Structural Engineering, Vol. 137, No. 2, pp. 261–269.

Yeoh, D., Fragiacomo, M., and Deam, B.. (2011), "Experimental Behaviour of LVL-Concrete Composite Floor Beams at Strength Limit State", Engineering Structures, Vol. 33, No. 9, pp. 2697-2707.

Appendix A. Structural Performance Check of the Selected Section

Calculation of the capacity of LVL Timber Floor Modulus, in accordance with "Design Procedures for Timber Floor systems in Australia and New Zealand"

Introduction

The most common types of sections which have low structural depth while being structurally very sound, are the composite I and composite box beams. They have a high stiffness and can carry a high load for a minimum self-weight. Moreover, they can provide a void between flanges so that the insulations as well as some other services (plumbing and wiring) can be fit into it. Based on these facts, as well as a thorough investigation of the best possible options for long span floors, two sections were designed using Laminated Veneer Lumber (LVL) as the only structural material of 8m timber modules. Figure A.1 shows the dimensions for 8m span timber module.
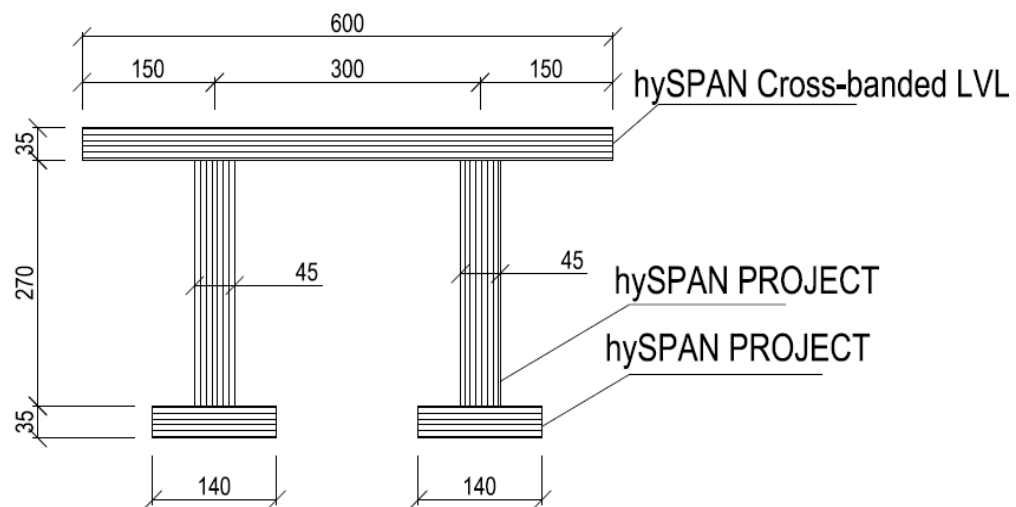
Figure A.1 Dimensions for 8m span timber modules (mm)

Material Properties Input	
Timber Density:	$\rho = 601$ kg/m3
Top Flange Modulus of Elasticity :	$E_{tf} = 10.5$ GPa
Web Modulus of Elasticity :	$E_w = 13.2$ GPa
Bottom Flange Modulus of Elasticity :	$E_{bf} = 13.2$ GPa
Top Flange Bending Strength :	$f'_{b,tf} = 40$ MPa
Web Bending Strength :	$f'_{b,w} = 50$ MPa
Bottom Flange Bending Strength :	$f'_{b,bf} = 50$ MPa
Top Flange Tension Strength (parallel to grain):	$f'_{t,tf} = 20$ MPa
Web Tension Strength(parallel to grain):	$f'_{t,w} = 25$ MPa
Bottom Flange Tension Strength(parallel to grain):	$f'_{t,bf} = 25$ MPa
Top Flange Compression Strength (parallel to grain):	$f'_{c,tf} = 34$ MPa
Web Compression Strength(parallel to grain):	$f'_{c,w} = 42$ MPa
Bottom Flange Compression Strength(parallel to grain):	$f'_{c,bf} = 42$ MPa
Top Flange Shear Strength :	$f'_{c,tf} = 4$ MPa
Web Shear Strength :	$f'_{c,w} = 4.6$ MPa
Bottom Flange Shear Strength :	$f'_{c,bf} = 4.6$ MPa
Note: The material properties are provided in Chh website For Cross-banded LVL, 80% of the values of hySPAN PROJECT were considered	

Geometry Input	
Beam Span (Overall):	8.4m
Beam Span (support to support):	8m
Top Flange width:	b_{tf}= 600mm
Web Width :	b_w= 45mm
Bottom Flange width:	b_{bf}= 140mm
Joist Spacings	S=300mm
Top Flange depth:	d_{tf}= 35mm
Web depth :	d_w= 270mm
Bottom Flange depth:	d_{bf}= 35mm
Beam total depth	h=340mm
Loading Input	
Superimposed Permanent Load	SDL = 1.0 kPa
Live Load (office)	LL = 3 kPa
Self Weight with g = 9.81 m/s2	

a) Floor Modulus design, Serviceability Check

Section Properties

Checking the maximum effective flange width due to shear lag and plate buckling (BS-EN-1-1-2004, section 9):

Bottom Flange: MIN [(b_w+0.1L), (b_w+20d_{bf})] =745mm≥ 300mm Ok

Top Flange: (b_w+0.1L) =845mm ≥ 300mm OK

Therefore the whole section is structurally effective

Calculating of Neutral Axis Location					
	MOE (Mpa)	n	$A(mm^2)$	Y (mm)	$A*Y$
Top Flange	10500	$n_{tf}=1$	$(n_{tf})(b_{tf})(d_{tf})$	$d_{bf} + d_w + (d_{tf}/2)$	6772500
Web	13200	$n_w = E_w / E_{tf} = 1.26$	$(n_w)(b_w)(d_w)$	$d_{bf} + (d_w/2)$	5193257.1
Bottom Flange	13200	$n_{bf} = E_{bf} / E_{tf} = 1.26$	$(n_{bf})(b_{bf})(d_{bf})$	$d_{bf}/2$	215600
			$\sum A = 63868.5$		$\sum AY = 12181357.1$

Neutral Axis $= \bar{y} = (\sum AY)/(\sum A) = 190.7$ mm

Calculating the I and EI				
	I	$A(mm^2)$	d	$I + Ad^2$
Top Flange	$(n)(b_{tf})(d_{tf}^3)/12$	$(n_{tf})(b_{tf})(d_{tf})$	$d_{bf} + d_w + (d_{tf}/2) - \bar{y}$	3.67E+08
Web	$(n)(b_w)(d_w^3)/12$	$(n_w)(b_w)(d_w)$	$\bar{y} - d_{bf} + (d_w/2)$	1.99E+08
Bottom Flange	$(n)(b_{bf})(d_{bf}^3)/12$	$(n_{bf})(b_{bf})(d_{bf})$	$\bar{y} - (d_{bf}/2)$	3.71E+08

$I_{eff} = \sum (I + Ad^2) = 9.36E+08$ mm^4

$(EI)_{eff} = E_{tf} * I_{eff} = 9.8e+12$ Mpa.mm^4 = 9832704.64 Pa.m^4

SLS load combinations

- Permanent Load : $1(kPa)(b_{tf}) = 0.6$ kN/m

- Self –Weight: $[(b_{tf})(d_{tf}) + 2(b_w)(d_w) + 2(b_{bf})(d_{bf})]$ (601 kg/m3)= 0.331 kN/m

- Q: Live Load: $3(kPa)(b_{tf}) = 1.8$ kN/m

AS/NZS 1170.0-2002 (Serviceability Limit State)			
SLS Load Combinations:			Criteria
1. G	0.931 kN/m	selfweight & permanent loading	Span/400
2. G+Q	2.73 kN/m	imposed loading (instantaneous)	Span/300
3. G+ 0.7Q	2.19 kN/m	imposed loading (short-term)	Span/300
4. G+0.4Q	1.65 kN/m	imposed loading (long-term)	Span/400
5.	1.00kN	imposed *impact* loading (vibration)	1mm-2mm

j_2: the direction factor for deflection check

AS 1720.1 (2010)	
Duration factor for M.C. <=15%	j_2
Short term	1
Long Term	2

Instantaneous deflection check:

$$\Delta_b = \frac{5j_2(G+Q)L^4}{384(EI)} = \frac{5*1*2.73*8^4}{384(EI)} = 14.8mm \leq Span/300 = 26.7mm \longrightarrow ok$$

Short Term deflection check:

$$\Delta_b = \frac{5(G+0.7Q)L^4}{384(EI)} = \frac{5*2.19*8^4}{384(EI)} = 11.9mm \leq Span/300 = 26.7mm \longrightarrow ok$$

Long Term deflection check:

$$\Delta_b = \frac{5(j_2G+0.7Q)L^4}{384(EI)} = \frac{5*3.12*8^4}{384(EI)} = 17mm \leq Span/300 = 20mm \longrightarrow ok$$

$$\Delta_b = \frac{5j_2(G+0.4Q)L^4}{384(EI)} = \frac{5*2*1.65*8^4}{384(EI)} = 18mm \leq Span/400 = 20mm \longrightarrow ok$$

Deflection check for 1kN point load:

$$\Delta_{vib} = \frac{P^*L^3}{48(EI)} \quad = 1mm \leq 2mm \longrightarrow ok$$

b) Ultimate Limit Strength Check

Load combinations in ULS:

Combination (a): Permanent: 1.35G=1.26 kN/m

Combination (b): Long Term: 1.2G + (1.5*0.4) Q=2.20 kN/m

Combination (c): Short Term: 1.2G + 1.5Q=3.82 kN/m

Ultimate bending moment, $M_{\text{mid-Span}}$: $\dfrac{wL^2}{8}$

Combination (a): $M_{\text{mid-Span}} = (1.35G)L^2/8 = 10.06 \text{kN.m}$

Combination (b): $M_{\text{mid-Span}} = (1.2G + 0.6Q)\, L^2/8 = 17.58 \text{kN.m}$

Combination (c): $M_{\text{mid-Span}} = (1.2G + 1.5Q)\, L^2/8 = 30.54 \text{ kN.m}$

Required k Factors *(AS 1720.1-2010)*:

	φ	K_4	K_6	K_9	K_{12}	K_{19}
Tension	0.9	1	1	--	--	1
Compression	0.9	1	1	1	1	1
Shear	0.9	--	--	--	1	1

	K_1
permanent	0.57
Long Term	0.8
Short term	0.97

Bending Stress Check:

Design Capacity: $\Phi k_1 k_4 k_6 k_{12}[f_b]$

Stress due to loading: $n\dfrac{MY}{I}$

y = distance between the extreme fibers to the neutral axis

Ratio= Stress due to loading / Design Capacity= $n\dfrac{MY}{I}$ / $\Phi k_1 k_4 k_6 k_9 k_{12}[f_b]$ ≤ 1

Tope Flange, Bending check	Design Capacity (MPa)	Stress due to loading (MPa)	Ratio
1.35 G (permanent)	0.9*0.57*40=20.52	10.06*(340-$\bar{y}$)/I=1.6	0.08≤1
1.2G + 0.6Q (long Term)	0.9*0.8*40=28.8	17.58*(340-$\bar{y}$)/I=2.8	0.10≤1
1.2G + 1.5Q (short Term)	0.9*0.97*40=34.92	30.54 *(340-$\bar{y}$)/I=4.9	0.14≤1

Bottom Flange, Bending check	Design Capacity (MPa)	Stress due to loading (MPa)	Ratio
1.35 G (permanent)	0.9*0.57*50=25.65	n_{bf}*10.06*($\bar{y}$)/I=2.6	0.11≤1
1.2G + 0.6Q (long Term)	0.9*0.8*50=36	n_{bf}*17.58*($\bar{y}$)/I=4.5	0.12≤1
1.2G + 1.5Q (short Term)	0.9*0.97*50=43.65	n_{bf}*30.54*($\bar{y}$)/I=7.8	0.18≤1

Axial Stress Check:

Design Capacity in compression: $\Phi k_1 k_4 k_6 k_9 k_{11} k_{12}[f'_c]$

Design Capacity intension: $\Phi k_1 k_4 k_6 k_{12}[f'_t]$

Stress due to loading: $n\dfrac{MY}{I}$

y = distance between the centre of the flanges to the neutral axis

Ratio= Stress due to loading / Design Capacity= $n\dfrac{MY}{I}$ / $\Phi k_1 k_4 k_6 k_9 k_{12}[f'_c]$ ≤1

Or

Ratio= Stress due to loading / Design Capacity= $n\dfrac{MY}{I}$ / $\Phi k_1 k_4 k_6 k_{12}[f'_t]$ ≤1

Tope Flange, Axial check	Design Capacity (MPa)	Stress due to loading (MPa)	Ratio
1.35 G (permanent)	0.9*0.57*34=17.44	10.06*(340-$\bar{y}$ -(d_{tf}/2))//I=1.4	0.08≤1
1.2G + 0.6Q (long Term)	0.9*0.8*34=24.48	17.58*(340-$\bar{y}$ -(d_{tf}/2))//I=2.4	0.10≤1
1.2G + 1.5Q (short Term)	0.9*0.97*34=29.68	30.54*(340-$\bar{y}$ -(d_{tf}/2))//I=4.3	0.14≤1

Bottom Flange, Axial check	Design Capacity (MPa)	Stress due to loading (MPa)	Ratio
1.35 G (permanent)	0.9*0.57*25=12.82	n_{bf}*10.06*($\bar{y}$ -(d_{bf}/2))/I=2.3	0.18≤1
1.2G + 0.6Q (long Term)	0.9*0.8*25=18.00	n_{bf}*17.58*($\bar{y}$ -(d_{bf}/2))/I=4.1	0.23≤1
1.2G + 1.5Q (short Term)	0.9*0.97*25=21.83	n_{bf}*30.54*($\bar{y}$ -(d_{bf}/2))/I=7.1	0.33≤1

Combination of axial and bending stress:

Tope Flange	bending stress ratios	axial stress ratios	Combined Ratio
1.35 G (permanent)	0.08	0.08	0.16
1.2G + 0.6Q (long Term)	0.10	0.10	0.20
1.2G + 1.5Q (short Term)	0.14	0.14	0.28

Bottom Flange	bending stress ratios	axial stress ratios	Combined Ratio
1.35 G (permanent)	0.11	0.18	0.29
1.2G + 0.6Q (long Term)	0.12	0.23	0.35
1.2G + 1.5Q (short Term)	0.18	0.33	0.51

Shear Stress Check:

Design Capacity: $\Phi k_1 k_4 k_6 k_{11}[f'_v]$

Stress due to loading: $\dfrac{VQ}{Ib_w}$

Q_{max}= maximum first moment of inertia (up to NA) =

$Q_{max} = (n_{tf})(b_{tf})(d_{tf})(h- \bar{y} - (d_{tf}/2))) + (n_w)(dw)(h-d_{tf}-\bar{y})^2/2)= 3136641.537$ mm^3

Ratio= Stress due to loading / Design Capacity= $\dfrac{VQ}{Ib_w}$ / $\Phi k_1 k_4 k_6[f'_v] \leq 1$

Maximum Shear load:

Maximum shear Load: $\dfrac{wL}{2}$

Combination (a): V_{max}= (1.35G)L/2=5.03kN

Combination (b): V_{max} = (1.2G + 0.6Q) L/2=8.79kN

Combination (c): V_{max} = (1.2G + 1.5Q) L/2=15.27 kN

	Design Capacity (MPa)	Stress due to loading (MPa)	Ratio
1.35 G (permanent)	0.9*0.57*4.6=2.35	(5.03Q/(45I))=0.37	0.16≤1
1.2G + 0.6Q (long Term)	0.9*0.8*4.6=3.31	(8.79Q/(45I))=0.65	0.20≤1
1.2G + 1.5Q (short Term)	0.9*0.97*4.6=4.01	(15.27Q/(45I))=1.13	0.28≤1

Shear Stress Check in the Glue Lines:

Shear Design Capacity of the Glue: [f'_s]
Note: the shear strength of the glue is more than LVL, but here it was conservatively assumed to be equal to the shear strength of LVL, which is 4.6MPa

Stress due to loading: $\dfrac{VQ}{Ib_w}$

$Q_{tf}= (n_{tf})(b_{tf})(d_{tf})(d_{bf}+d_w+ (d_{tf}/2) - \bar{y}) = 2767267.2$ mm^3

$Q_{bf} = (n_{bf})(b_{bf})(d_{bf})(2)(\bar{y}-(d_{bf}/2)) = 2134136.6$ mm^3

Ratio= Stress due to loading / Design Capacity= $\dfrac{VQ}{Ib_w}$ / [f'_s] ≤ 1

Maximum Shear load:

Maximum shear Load: $\dfrac{wL}{2}$

Combination (a): $V_{max}= (1.35G)L/2=5.03$kN

Combination (b): $V_{max} = (1.2G + 0.6Q) L/2=8.79$kN

Combination (c): $V_{max} = (1.2G + 1.5Q) L/2=15.27$ kN

Top Flange Glue Line	Design Capacity (MPa)	Stress due to loading (MPa)	Ratio
1.35 G (permanent)	4.6	$(5.03Q_{tf}/(45I))=0.33$	$0.07\leq1$
1.2G + 0.6Q (long Term)	4.6	$(8.79Q_{tf}/(45I))=0.58$	$0.13\leq1$
1.2G + 1.5Q (short Term)	4.6	$(15.27Q_{tf}/(45I))=1.00$	$0.22\leq1$

Bottom Flange Glue Line	Design Capacity (MPa)	Stress due to loading (MPa)	Ratio
1.35 G (permanent)	4.6	$(5.03Q_{bf}/(45I))=0.25$	$0.06\leq1$
1.2G + 0.6Q (long Term)	4.6	$(8.79Q_{bf}/(45I))=0.44$	$0.10\leq1$
1.2G + 1.5Q (short Term)	4.6	$(15.27Q_{bf}/(45I))=0.77$	$0.17\leq1$

Appendix B : Linear Behaviour of the LVL Floor Modules

The linear behaviour of the LVL modules is also confirmed by plotting the load versus strain gauge readings for every single strain gauge for U8-01 (Figures B.1 to B.5), and all displayed a linear trend until the point of failure. No shear lag was observed on top flange (Figure B.6. and B.7). Adopted names and locations of the strain gauges for U8-01 are shown in Figure 5.16. Similar linear trend to U8-01 was also observed for the rest of the modules (L6-01, L6-02, L6-03, U8-02 and U8-03)
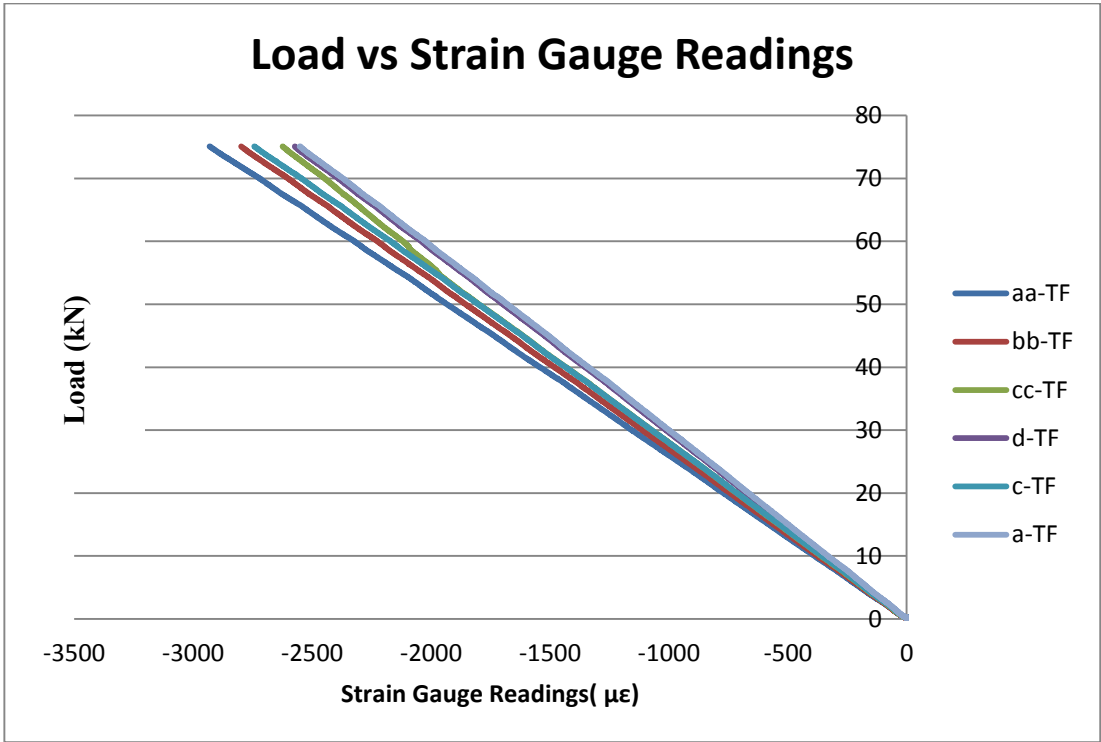
Figure B.1 Load vs. strain gauge readings at mid-span, top flange, for U8-01
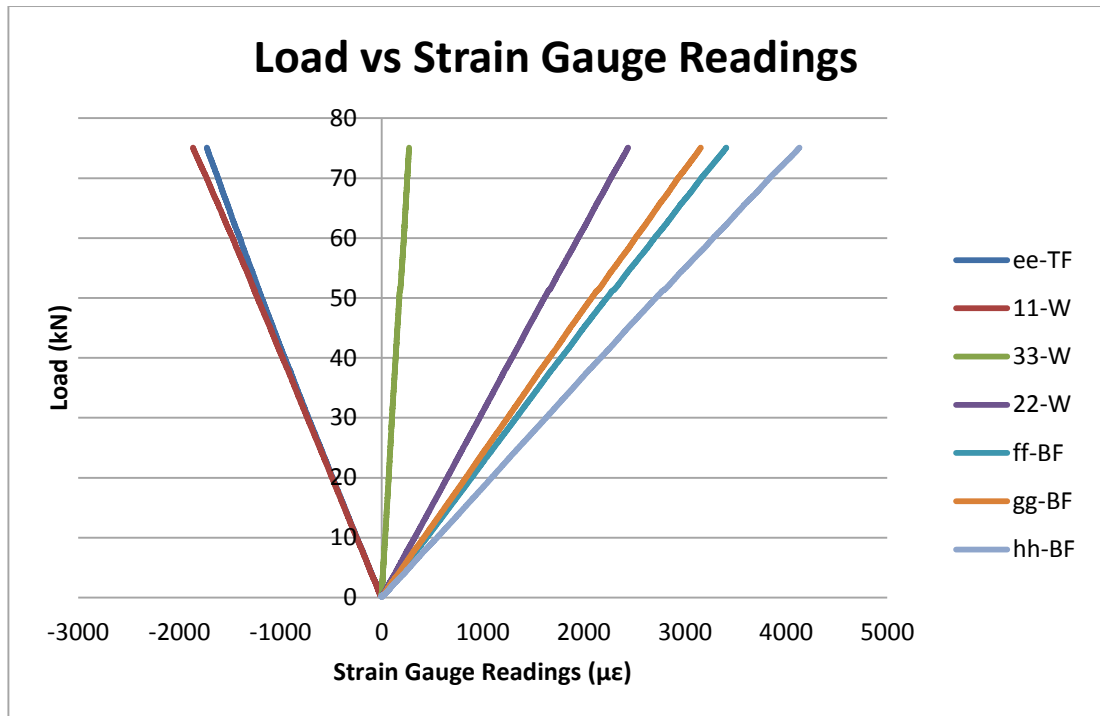
Figure B.2. Load vs. strain gauges reading at mid-span, west web, for U8-01
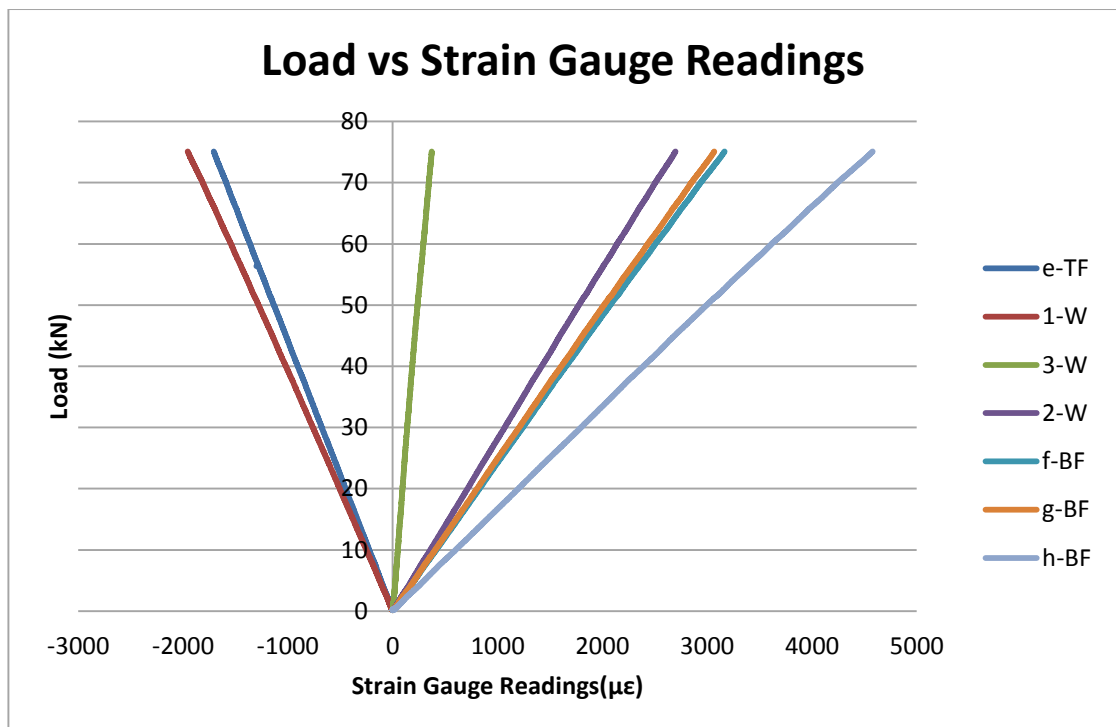
Figure B.3. Load vs. strain gauges reading at mid-span, east web, for U8-01
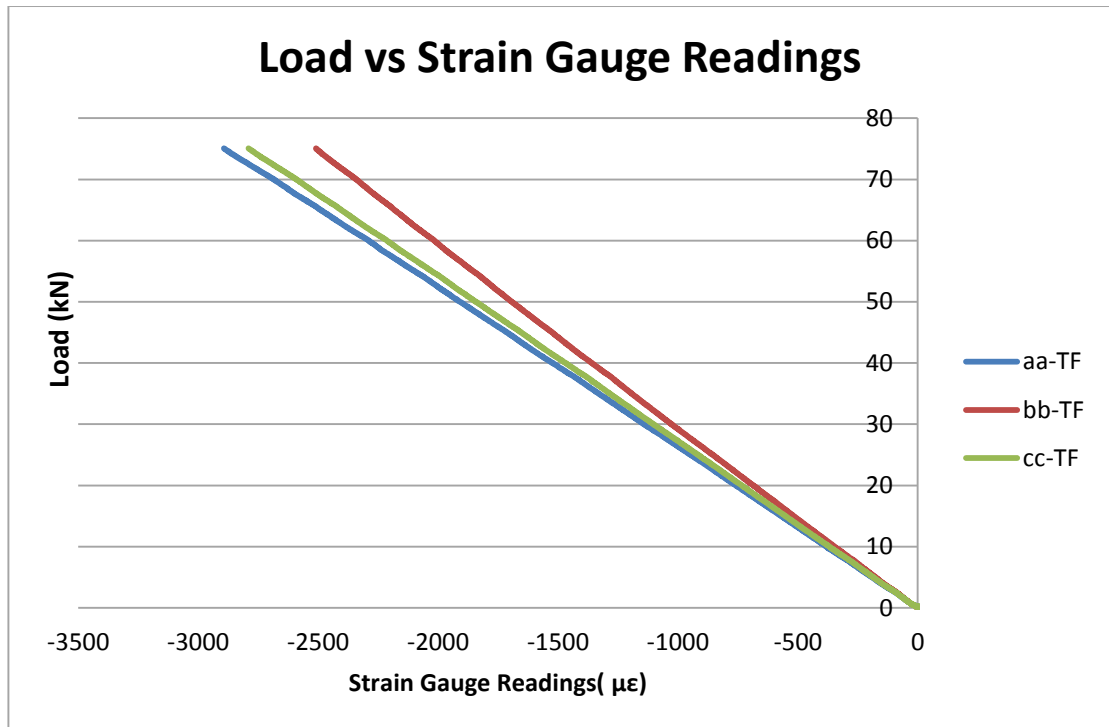
Figure B.4. Load vs. strain gauges reading at 0.5m off mid-span, top flange, for U8-01
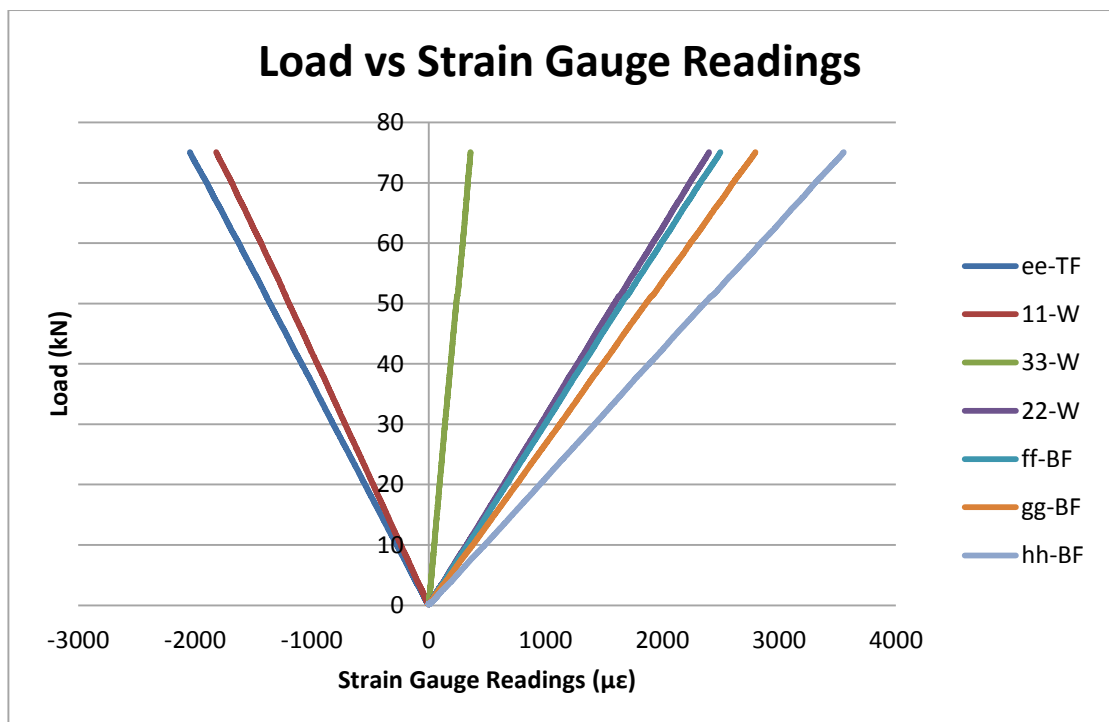
Figure B.5. Load vs. strain gauges reading at 0.5m off mid-span, west web, for U8-01
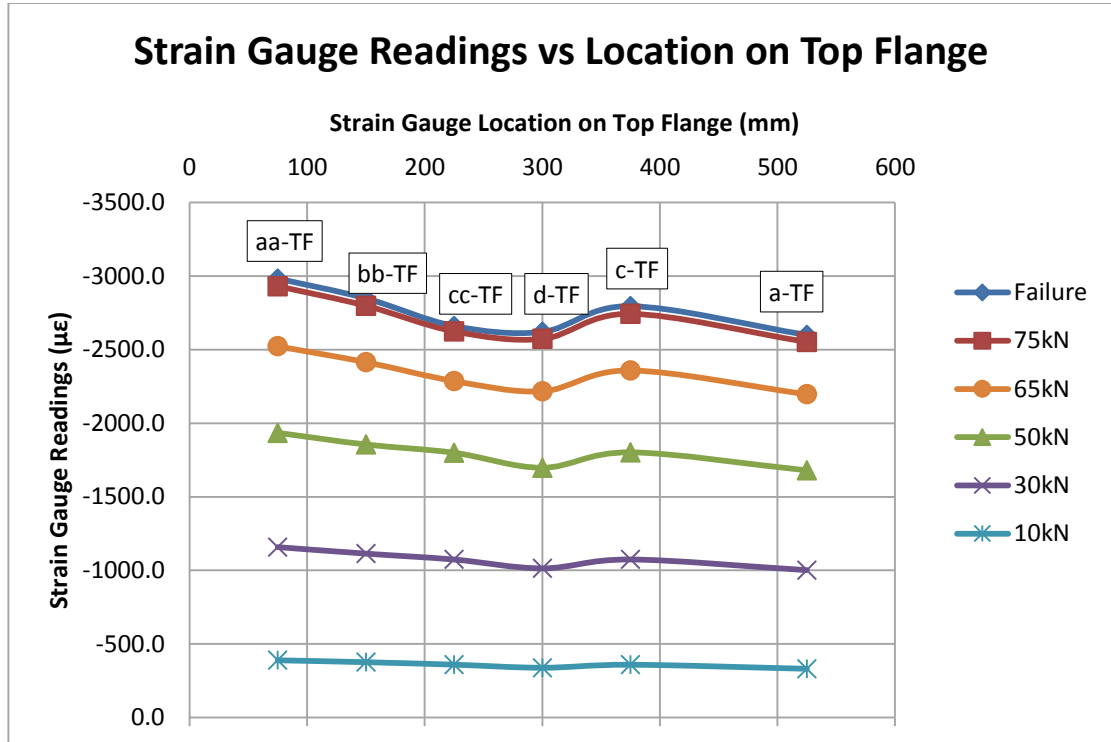
Figure B.6. Strain gauge readings vs location of gauges on top flange at mid-span, for U8-01
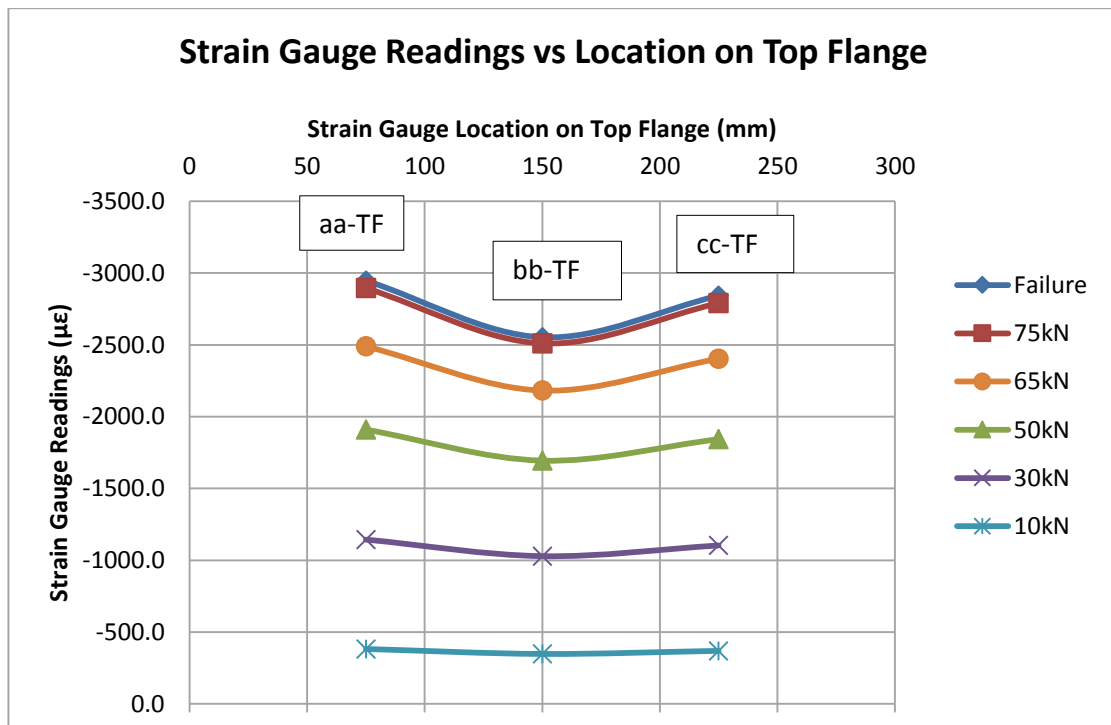
Figure B.7. Strain gauge readings vs location of gauges on top flange at 0.5m off mid-span, for U8-01

Appendix C: Composite Performance of LVL Modules

The adopted names and locations of the Strain Gauges were shown in Figures 5.16, 5.17 and 5.18 in Chapter 5.
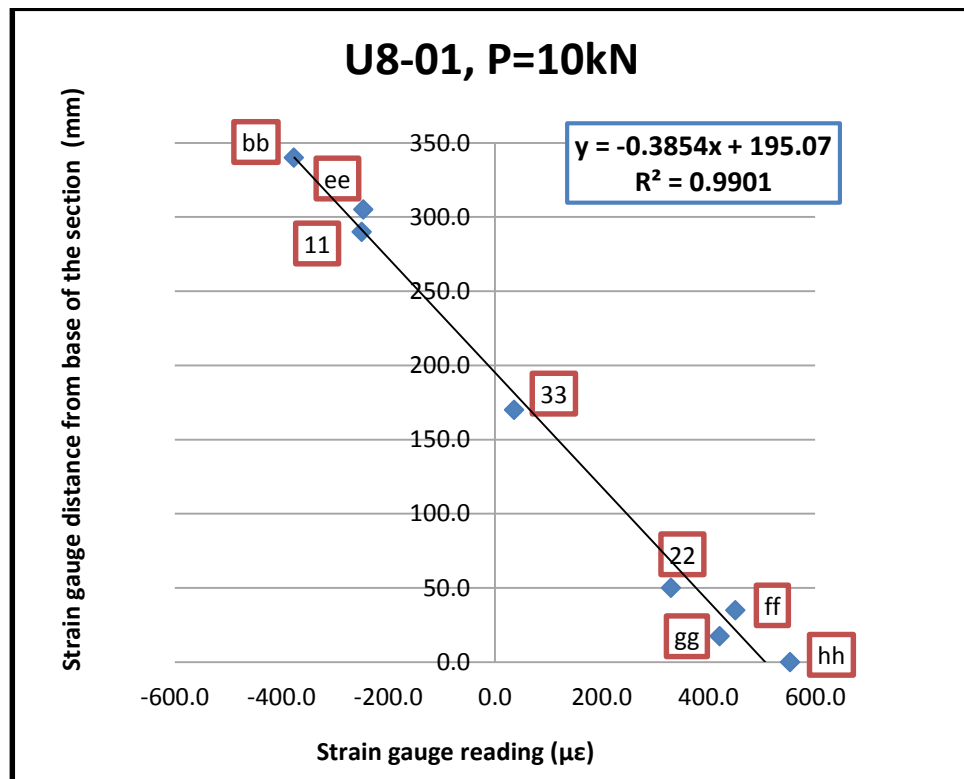
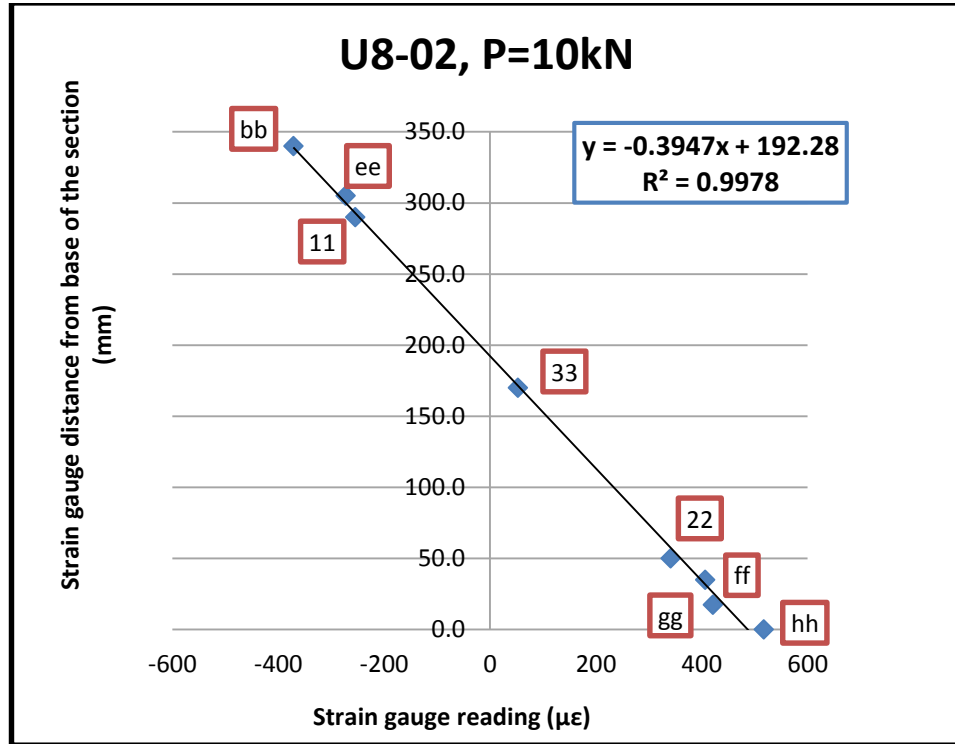Figure C.1. Strain gauges readings vs locations of the gauges for U8-01, west web (mid-span) at P=10kN
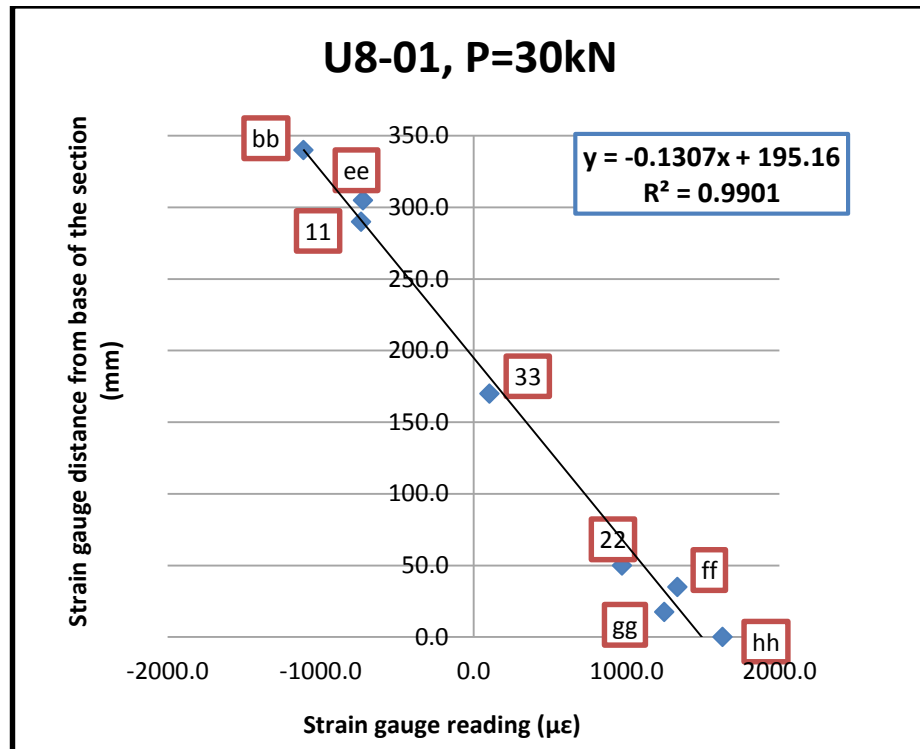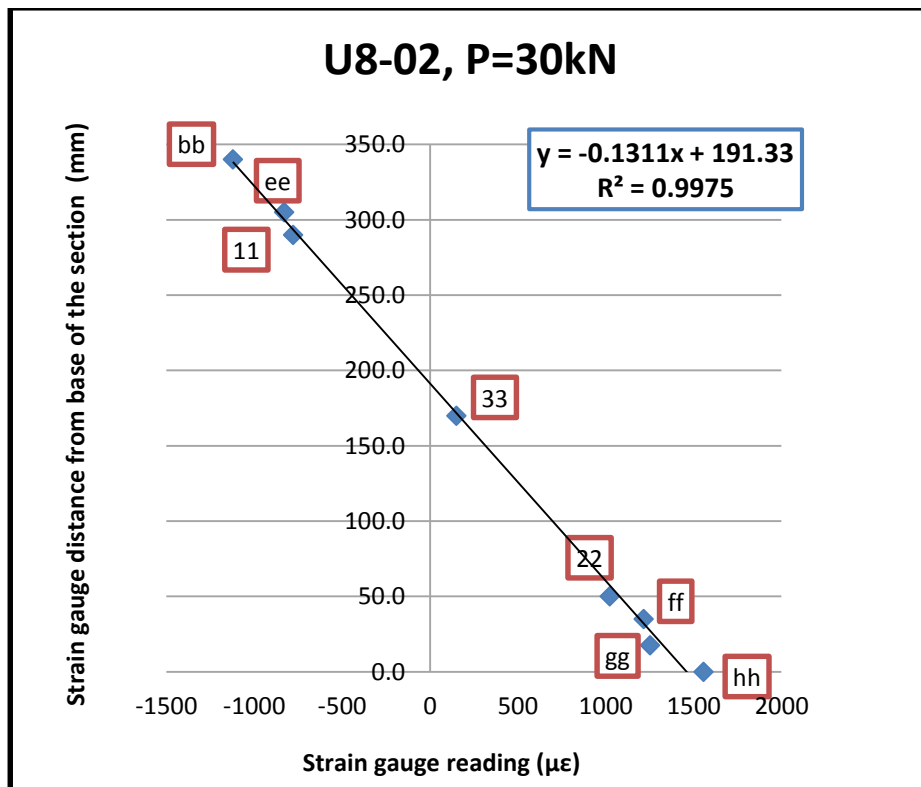
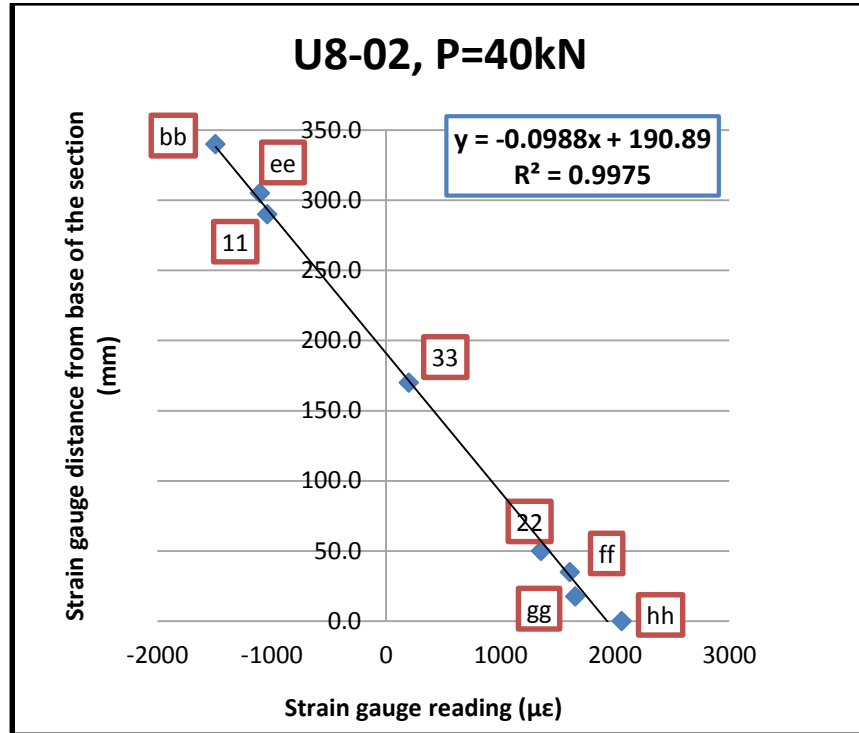Figure C.2. Strain gauges readings vs locations of the gauges for U8-01, west web (mid-span) at P=30kN
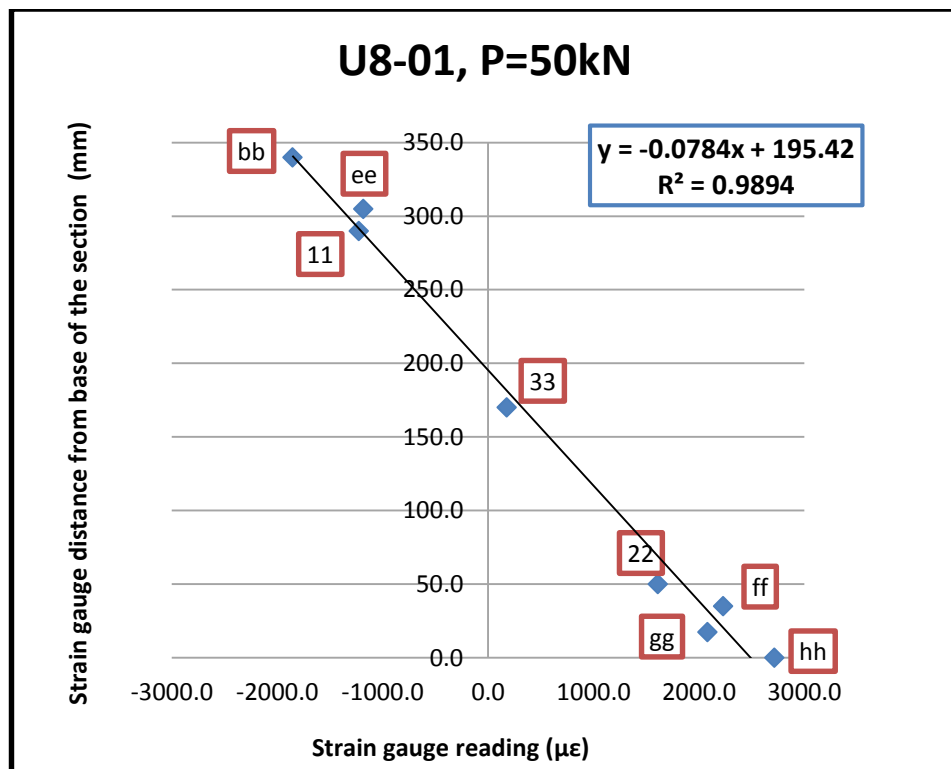
Figure C.3. Strain gauges readings vs locations of the gauges for U8-01, west web (mid-span) at P=50kN
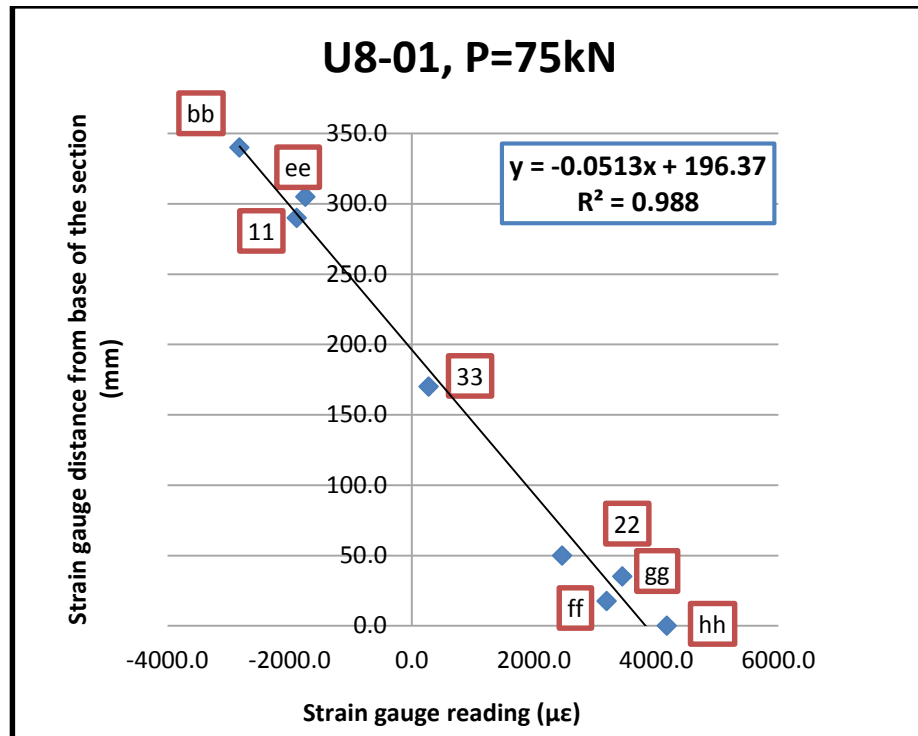
Figure C.4. Strain gauges readings vs locations of the gauges for U8-01, west web (mid-span) at P=75kN
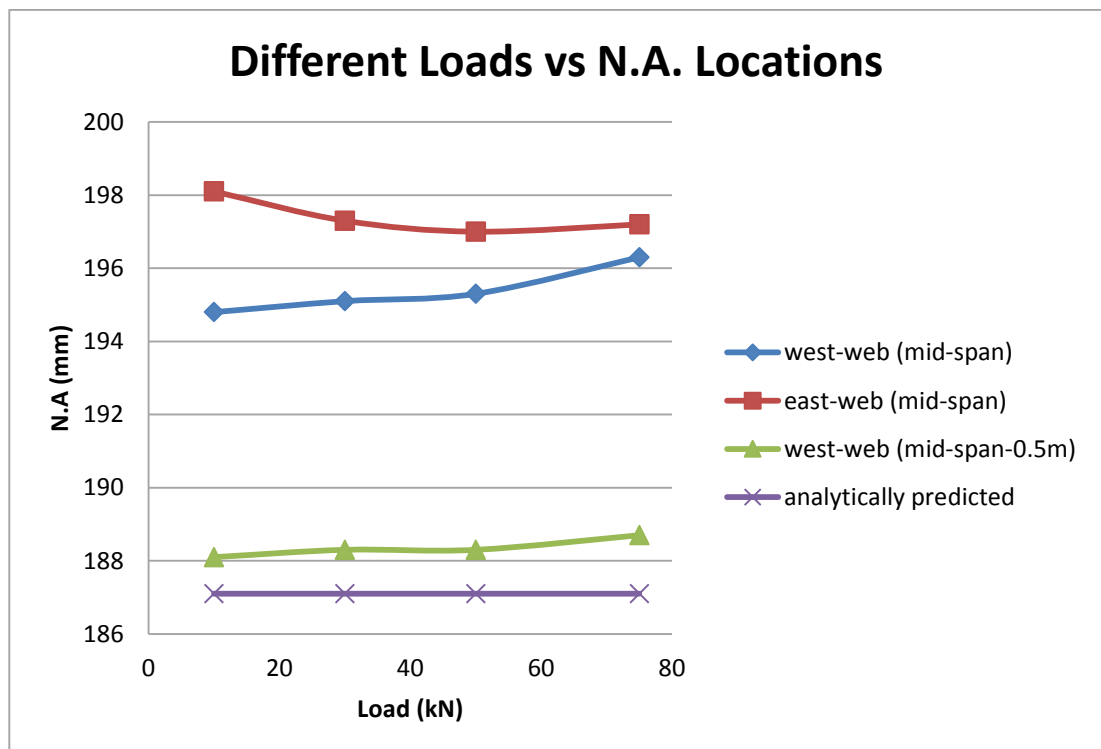
Figure C.5. Location of N.A for at different load levels for U8-01

Figure C.6. Strain gauges readings vs locations of the gauges for U8-02, west web (mid-span) at P=10kN

Figure C.7. Strain gauges readings vs locations of the gauges for U8-02, west web (mid-span) at P=30kN

Figure C.8. Strain gauges readings vs locations of the gauges for U8-02, west web (mid-span) at P=40kN
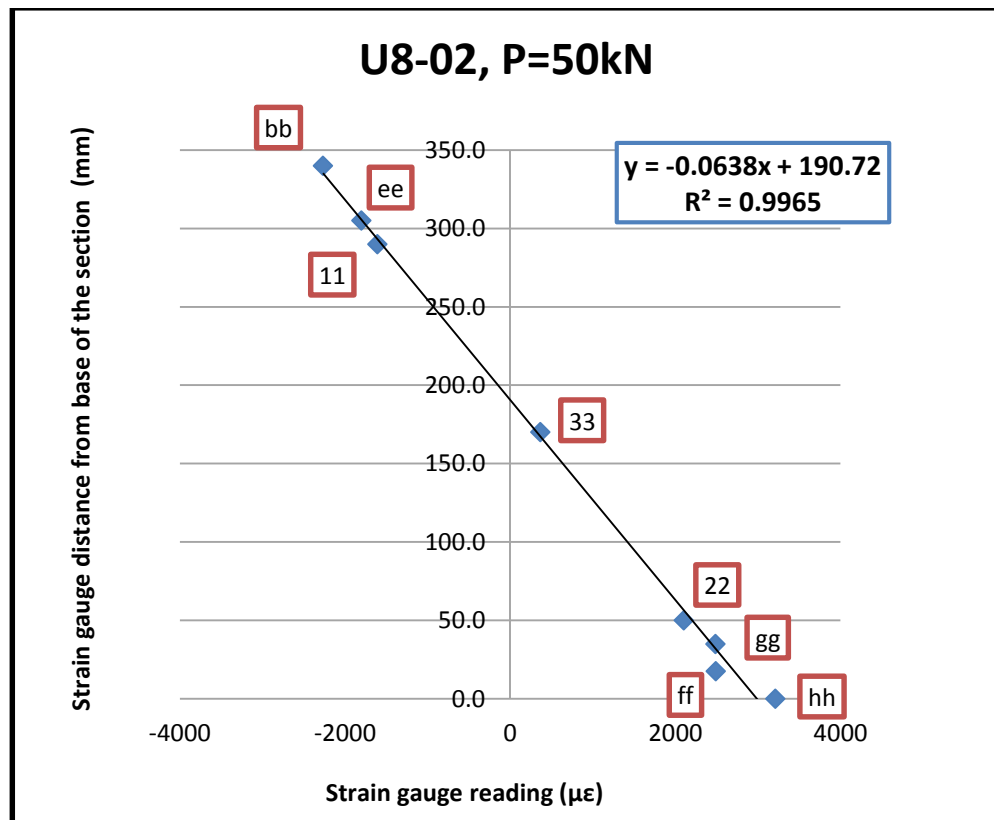

Figure C.9. Strain gauges readings vs locations of the gauges for U8-02, west web (mid-span) at P=50kN
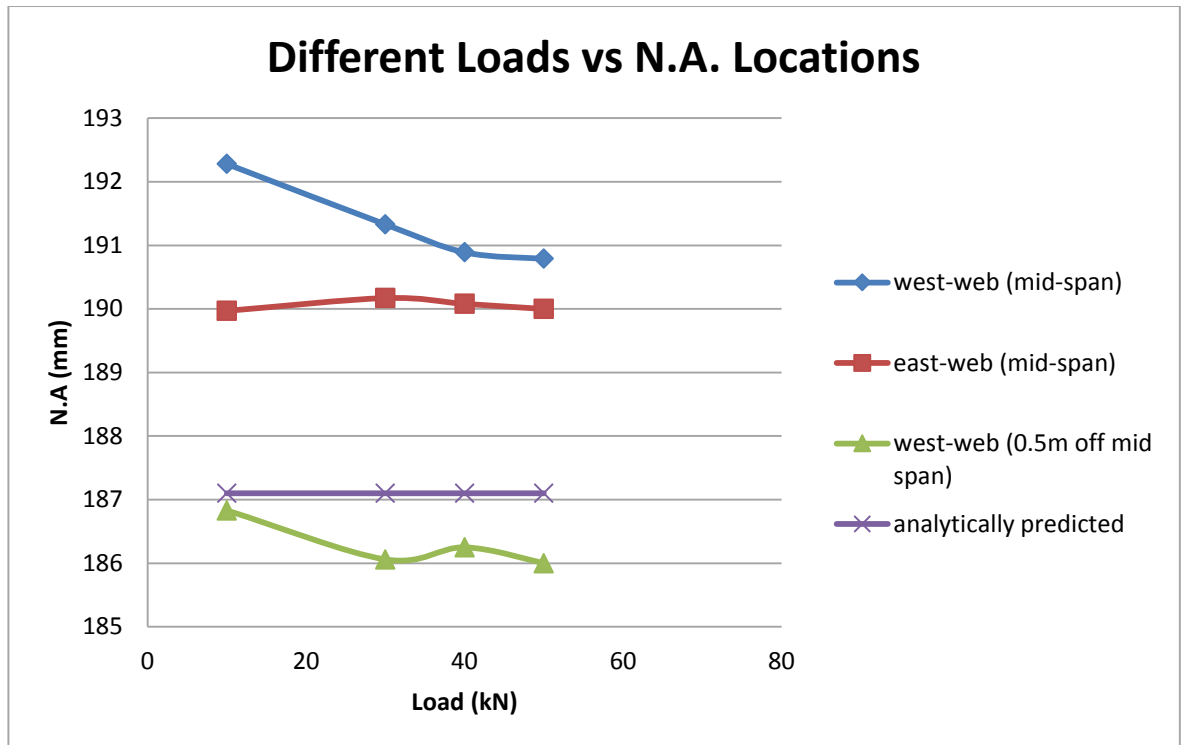
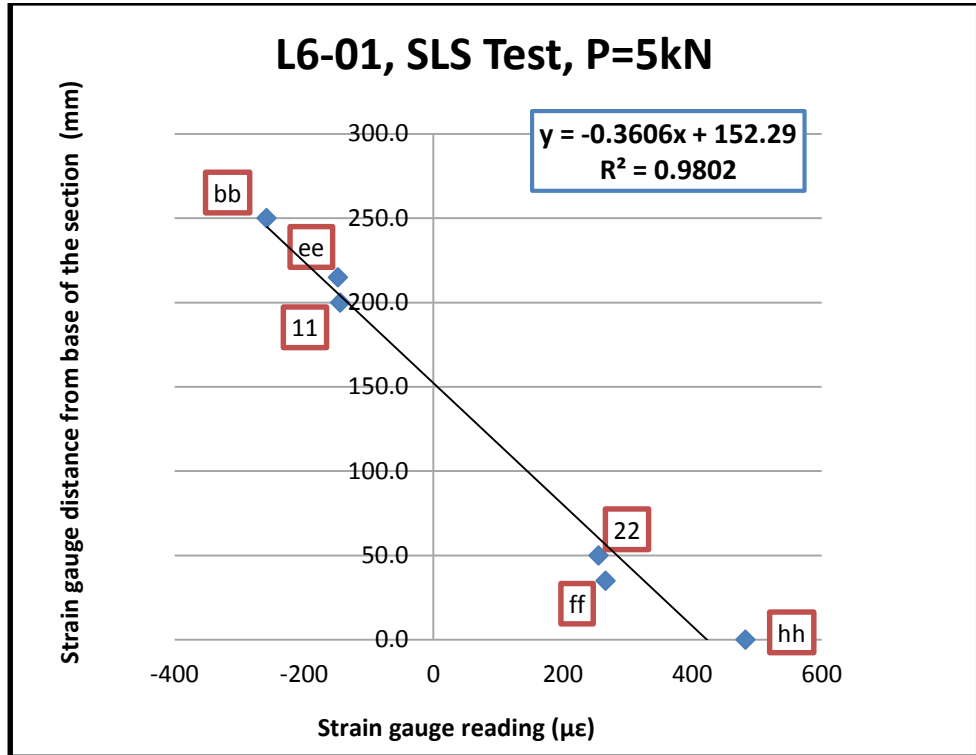Figure C.10. Location of N.A for at different load levels for U8-02

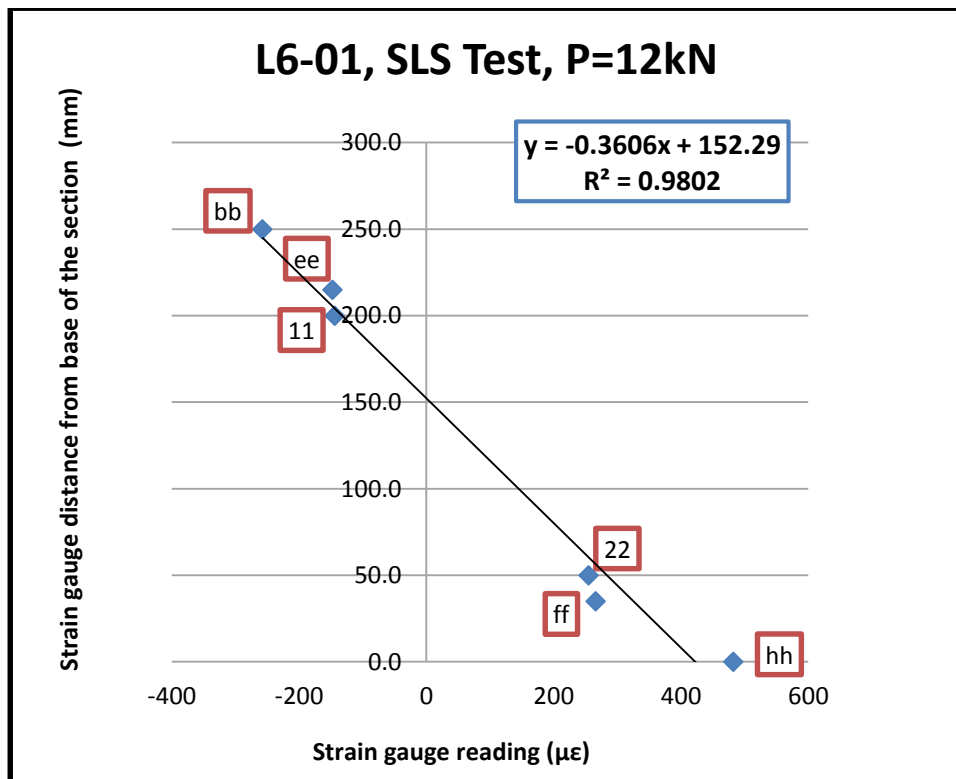Figure C.11. Strain gauges readings vs locations of the gauges for L6-01, west web (mid-span) at P=5kN

Figure C.12. Strain gauges readings vs locations of the gauges for L6-01, west web (mid-span) at P=12kN

Figure C.13. Strain gauges readings vs locations of the gauges for L6-02, west web (mid-span) at P=5kN

Figure C.14. Strain gauges readings vs locations of the gauges for L6-02, west web (mid-span) at P=12kN
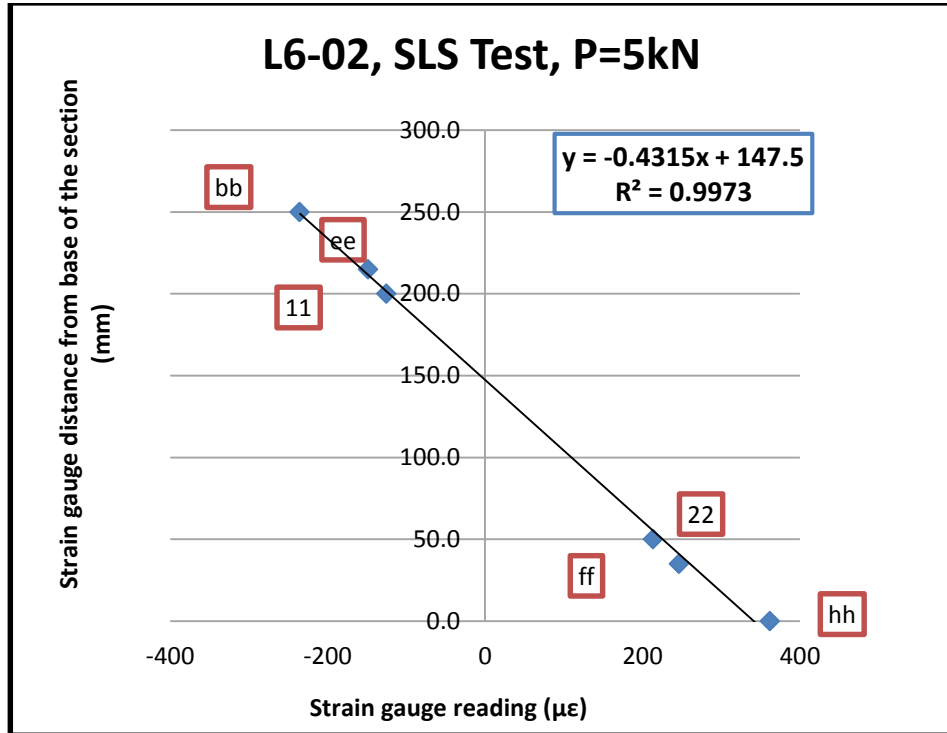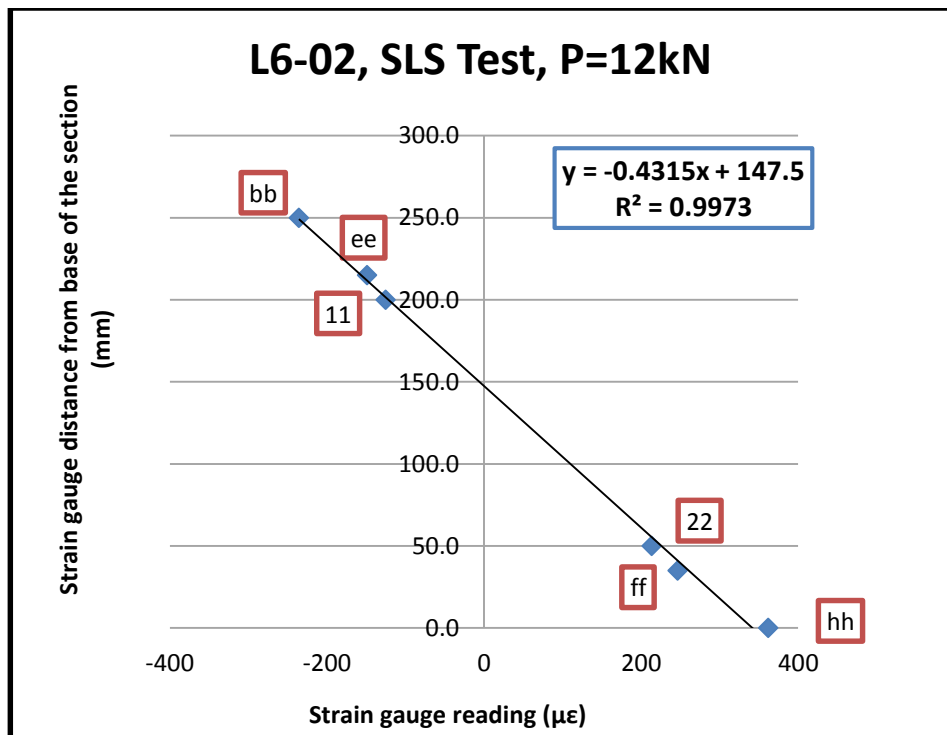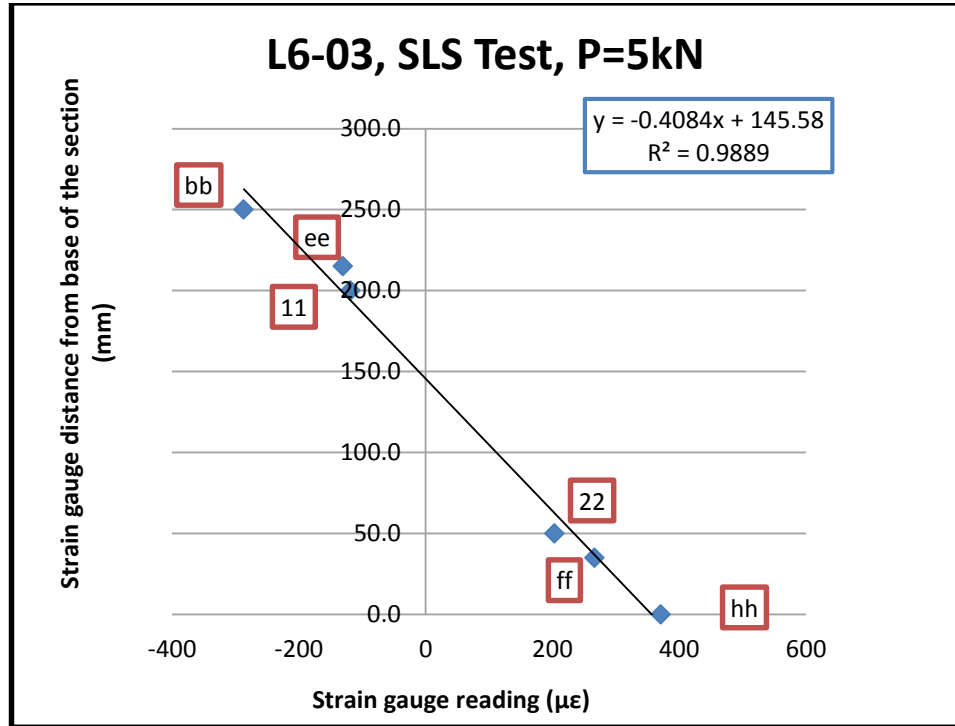
Figure C.15. Strain gauges readings vs locations of the gauges for L6-03, west web (mid-span) at P=5kN
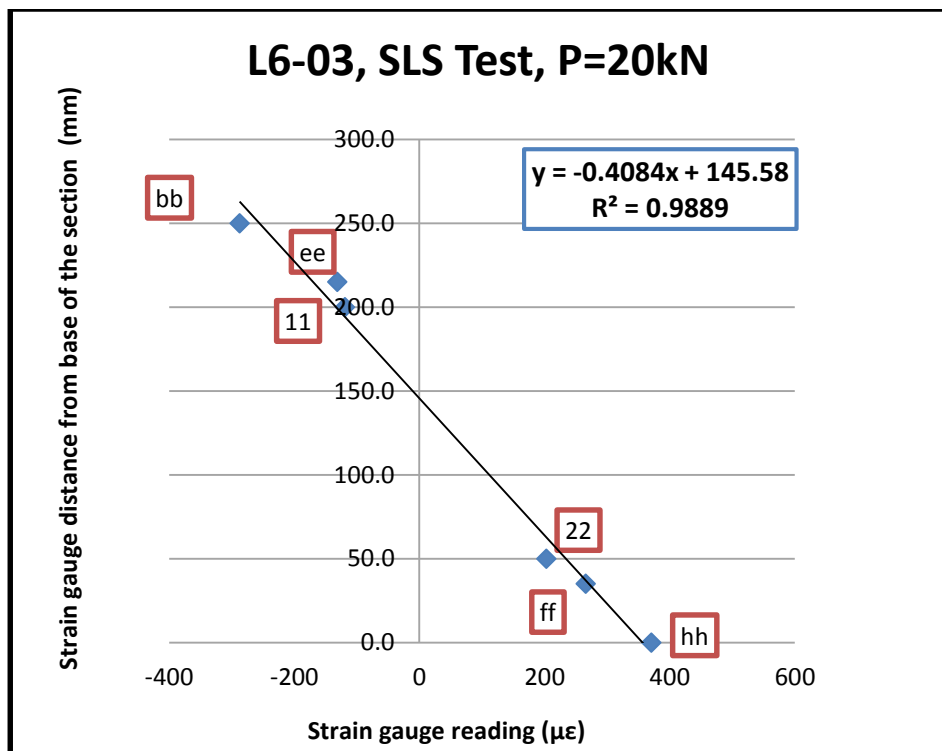

Figure C.16. Strain gauges readings vs locations of the gauges for L6-03, west web (mid-span) at P=20kN

Appendix D: Calculation of Mean and 5th Percentile value

According to AS/NZS 4357.3 (2006), the mean value ($\bar{m}$), 5th percentile value ($m_{05[75]}$), and coefficient of variation (V) of the test values m_1, m_2, …, m_n shall be calculated from the following equation:

$$\bar{m} = \exp(\bar{y} + \frac{S_y^2}{2}) \qquad\qquad \text{Eq D.1}$$

$$m_{05[75]} = \exp(\bar{y} - k_s S_y) \qquad\qquad \text{Eq D.2}$$

$$V = \sqrt{\exp(S_y^2) - 1} \qquad\qquad \text{Eq D.3}$$

Where

$$\bar{y} = \frac{1}{n} \sum_{i=1}^{n} \ln m_i \qquad\qquad \text{Eq D.4}$$

$$S_y = \sqrt{\frac{1}{n} \sum_{i=1}^{n} (\ln m_i - \bar{y})^2} \qquad\qquad \text{Eq D.5}$$

Values of k_s confidence coefficient for estimating $m_{05[75]}$ for n test specimens, are given in Table D.1.

TABLE D.1
k_s for 5TH PERCENTILE VALUE—
75% CONFIDENCE

Number of Specimens (n)	k_s
30	1.87
35	1.85
40	1.83
45	1.82
50	1.81
70	1.78
100	1.76
200	1.72
500	1.69
1000	1.68
3000	1.66
∞	1.645

NOTE: Intermediate value may be obtained using interpolation.

The mean values ($\bar{m}$) and 5th percentile values (m$_{05[75]}$) of LVL material properties are calculated according to Equations D.1 to D.5, and the results are presented in Table D.2.

Table D.2 The mean value ($\bar{m}$), 5th percentile value (m$_{05[75]}$) of the LVL material properties

Component Name	Top flange cross-banded LVL (Flat-wise tests)	Webs hySpan-Project LVL (Edge-wise tests)	Bottom flanges, hySpan-Project LVL (Flat-wise tests)
($\bar{m}$): Flexural MOE, E$_x$ (GPa)	9.6	13.3	13.1
(m$_{05[75]}$)**:** Flexural MOE, E$_x$ (GPa)	7.7	12.2	10.2
($\bar{m}$):Bending strength, f$_b$ (MPa)	52.4	65.3	72.6
(m$_{05[75]}$)**:** Bending strength, f$_b$ (MPa)	40.2	54.7	54.5
($\bar{m}$):Tension strength, f$_t$ (MPa)	34.1	37.4	37.4
(m$_{05[75]}$)**:** Tension strength, f$_t$ (MPa)	30.1	32.2	32.2
($\bar{m}$):Compression strength, f$_c$ (MPa)	42.1	51.3	51.3
(m$_{05[75]}$)**:** Compression strength, f$_c$ (MPa)	36.0	43.9	43.9
($\bar{m}$):Shear strength, f$_v$ (MPa)	5.1	6.7	5.8
(m$_{05[75]}$)**:** Shear strength, f$_v$ (MPa)	4.4	6.2	4.3

Appendix E: Accuracy of Measurement Kit

Table E.1 The measurement accuracy of the experimental appliance is as follows:

	Type	Accuracy
Strain Gauges	PL-60-11	$\pm 0.000 \, \mu\varepsilon$ output
150 kN load cells	STS Avoirdupois Load Cell	± 0.000 N and 3 mv/v output
LVDTs (± 300mm and ± 400mm)	Temposonics® R Series	± 0.000 mm output
LVDTs (± 25mm)	LDC 1000A	± 0.000 mm output
LVDTs (± 12.5mm)	LDC 500A	± 0.000 mm output

LVDT: Linear Variable Differential Transformers